Investigation of Cooperativity between Statistical Rebinding and the Chelate Effect on DNA Scaffolded Multivalent Binders as a Method for Developing High Avidity Ligands to target the C-type Lectin Langerin

Dissertation
Zur Erlangung des akademischen Grades
doctor rerum naturalium (Dr. rer. nat)
im Fach Chemie

eingereicht an der
Mathematisch-Naturwissenschaftlichen Fakultät
der Humboldt Universität zu Berlin

von Gunnar Bachem

Präsidentin der Humboldt Universität zu Berlin
Prof. Dr. -Ing. Dr. Sabine Kunst

Dekan der Mathematisch-Naturwissenschaftlichen Fakultät
Prof. Dr. Elmar Kulke

Gutachter/in:
Prof. Dr. Oliver Seitz
Prof. Dr. Anna Bernardi
Prof. Dr. Christoph Rademacher

Tag der mündlichen Prüfung: 19.03.2021

Investigation of Cooperativity between Statistical Rebinding and the Chelate Effect on DNA Scaffolded Multivalent Binders as a Method for Developing High Avidity Ligands to target the C-type Lectin Langerin

Dissertation
to obtain the academic degree
doctor rerum naturalium (Dr. rer. nat)
in Chemistry

submitted to
The Faculty of Mathematics and Natural Sciences
Humboldt Universität zu Berlin

by Gunnar Bachem

President of Humboldt Universität zu Berlin
Prof. Dr. -Ing. Dr. Sabine Kunst

Dean of Faculty of Mathematics and Natural Sciences
Prof. Dr. Elmar Kulke

Reviewers:
Prof. Dr. Oliver Seitz
Prof. Dr. Anna Bernardi
Prof. Dr. Christoph Rademacher

Date of viva voce: 19.03.2021

The work presented in this dissertation was conducted between February 2015 and November 2019 at the Department of Chemistry of the Humboldt-Universität zu Berlin under the supervision of Prof. Dr. Oliver Seitz.

Acknowledgements

First, I would like to thank Prof. Dr. Oliver Seitz for the chance to carry out my PhD in his laboratories and in such a wonderful team. I thank him for the exciting topic, his scientific mentoring, and all those controversial discussions.

I am deeply grateful for all the years spent with so many great colleagues, scientists, and friends in the Seitz lab. I was never alone with any problems - scientific or not - and learnt most things I know from them. For our beautiful runs to the lab and the fruitful discussions on the way I would like to thank Dr. Robert Zitterbart, Dr. Katharina Gröger, and Henrik Petszulat. Yogilates and crêpes in the company of life-surfers Dr. Jasmine Chamiolo and Dr. Margherita di Pisa will always be remembered with great fondness. I would like to thank the coffee room for providing such a delightful location for discussions of all sorts. Those best remembered are morning coffees with Georgie Gavins and Tim Billborough but also all those debates and laughs with Olaf Fuchs, Dino Gluhacevic, Yannic Altrichter and Sophie Schöllkopf. I would also like to thank Richard Houska and Chistian Richter as the go to people for synthesis problems. A special thanks goes to Sophie Neuber for her support with the flow cytometry experiments under time pressure. I could not have done it without her. Unforgotten is Kevin Höhne´s enthusiasm while he supported me with the synthesis during his apprenticeship. It made it worthwhile.

Many collaborators contributed to this work and supported me with invaluable advice. Prof. Dr. Christoph Rademacher granted me access to his laboratory and was always available for discussion. I would like to thank his co-workers Dr. Eike-Christian Wamhoff, Mareike Rentsch, Felix Fuchsberger, Nina-Louisa Efrém, Dr. Dongyoon Kim, Hengxi Zhang and Hannes Baukmann for their help with the ^{19}F-NMR assay, flow-cytometry, microscopy and a steady supply of protein. Especially the time spent working and discussing science with Dr. Eike-Christian Wamhoff was very inspiring and motivating. Furthermore, I would like to express my gratitude to Dr. Jens Dernedde and Dr. Kim Silberreis for their help with the SPR experiments, Prof. Dr. Kevin Pagel and Xiao Jakob Schmitt for our attempts in native MS with the langerin ECD, and Dr. Knut Rurack and Dr. Estela Climent Terol for access to their flow cytometer.

For proof-reading my dissertation, I would like to thank Tim Billborough, Georgie Gavins and Dr. Dominic Gröger, Alke Dannenberg for sponsoring the special editions and Paulina Metzscher for help formatting this work. Finally, I thank all my friends

especially Dr. Cornelius Gropp and Roland Wedekind for starting the chemistry adventure with me and my family for their never-ending support.

Abstract

Targeting the C-type lectin (CTL) langerin has received increasing attention as a novel immunotherapy strategy due to the capacity of Langerhans cells, which express langerin, to endocytose and cross-present antigens to T-cells. Langerin recognizes pathogens such as viruses, which present carbohydrates in a multivalent fashion to increase avidity as the monovalent carbohydrate ligands only display low affinity for langerin. Inspired by nature, multivalency has therefore been a key tool for overcoming the low affinities of CTL-carbohydrate interactions. In contrast to highly multivalent ligand presentation with undefined arrangements this work strove to optimize ligand economy by designing bivalent ligands that take the distance between the binding sites of the homotrimeric langerin into consideration by precise arrangement of ligands on DNA-based scaffolds. Studying the multivalent mechanisms at work led us to the design of ligands that take both statistical rebinding and the chelate effect into account. The rebinding effect was recognized as a tool that not only increases ligand avidity at a single binding site but in addition can be exploited to amplify the chelate effect. This method provides a solution for overcoming the low or non-existing multivalency effects when bivalently presenting low affinity ligands on a rigid scaffold if high affinity ligands are unavailable. A combination of this arrangement strategy with the development of a first langerin selective glycomimetic ligand led to the most potent molecularly defined langerin binder to date (IC_{50} = 300 nM). The glycomimetic-PNA-DNA ligands were selectively internalized by langerin expressing model lines at nanomolar concentrations and constitute a delivery platform for the future transport of cargo such as vaccination agents or cytotoxic compounds to Langerhans cells.

Kurzzusammenfassung

Aufgrund der Fähigkeit von Langerhans Zellen, welche den C-Typ Lektin (CTL) Rezeptor Langerin exprimieren, Antigene zu internalisieren und T-Zellen zu präsentieren, wurde Langerin als attraktives Ziel für neue Immunotherapien erkannt. Langerin kann Pathogene wie z.B. Viren erkennen, die zur Erhöhung der Avidität Kohlenhydratliganden multivalent präsentieren, da die monovalenten Kohlenhydratliganden nur niedrige Affinitäten für Langerin aufweisen. Die natürlichen monovalenten Kohlenhydratliganden besitzen nur niedrige Affinitäten für Langerin. Inspiriert durch die Natur stellt Multivalenz eine Strategie zur Überwindung der schwachen CTL-Kohlenhydrat-Wechselwirkung dar. Im Gegensatz zur hochmultivalenten Präsentation von Liganden mit undefinierter Anordnung hat sich diese Arbeit zum Ziel gesetzt auch die Ökonomie der Liganden zu optimieren, indem Liganden auf einer DNA Gerüststruktur so präsentiert wurden, dass sie die Distanz zwischen den Bindungstaschen des Homotrimers Langerin wiederspiegeln. Eine Untersuchung der relevanten multivalenten Bindungsmechanismen führte zu einer Anordnung der Liganden, die sowohl statistisches Rebinding als auch den Chelate Effekt einbezog. Der Rebinding Effekt wurde als Mittel erkannt, dass nicht nur die Avidität des Liganden an einer Bindungstasche erhöht, sondern auch ausgenutzt werden kann, um den Chelate Effekt zu amplifizieren. Diese Methode stellt eine Möglichkeit dar niedrige oder nicht vorhandene Multivalenzeffekte bei der bivalenten Präsentation von Liganden zu überwinden, wenn hochaffine Liganden nicht zur Verfügung stehen. Eine Kombination dieser Strategie mit der Entwicklung eines neuen selektiven Liganden für Langerin führte zu dem stärksten bekannten Langerinbinder (IC_{50} = 300 nM). Die Glycomimetic-PNA-DNA Liganden wurden selektiv von Langerin exprimierenden Modellzelllinien bei nanomolaren Konzentrationen internalisiert und stellen ein System dar, welches in Zukunft für den zielgerichteten Transport von Beladungen, wie z.B. Impfstoffe oder zytotoxische Stoffe Anwendung finden könnte.

Contents

1 Introduction

Carbohydrate-protein interactions drive important biological recognition processes such as the binding of viruses and bacteria to cell membranes. The affinities between monovalent carbohydrates and their sugar binding receptors, lectins, are typically in the millimolar range; too weak to trigger biological effects. In nature, a multitude of concerted carbohydrate-protein interactions between two binding partners help overcome this problem. Multivalent carbohydrate-protein interactions increase the binding affinity and even allow for the tuning of protein selectivity. Hence multivalency is a key tool for developing compounds that target C-type lectins. The multivalent presentation of carbohydrates on various scaffolds e.g. polymers[2], liposomes[3], nanoparticles[4] and carbon nanotubes[5-6] have to lead to impressive increases in affinity. While brute force presentation of many ligands on large scaffolds can lead to extremely strong potencies the challenges of selectivity and ligand efficiency are not addressed with this approach. A more economical approach to designing multivalent ligand systems is the presentation on structurally and stoichiometrically defined scaffolds such as dendrimers[7], calixarenes[8], carbohydrates[9], cyclodextrines[10] and peptides[11-12]. Another such scaffold is DNA, which has particularly unique properties.[13] The fairly rigid DNA double helix structure has a persistence length of approximately 600 Å and forms a double helix structure by self-assembly.[14] The characteristics of the helical structure are well understood allowing for precise positioning of ligands. What makes DNA-based scaffolds particularly convenient is that the sequence based self-assembly makes a multitude of multivalent arrangements accessible with limited synthetic efforts. Full control over the valency and distance between modified nucleotides makes DNA-based ligand systems ideal for optimising ligand efficacy. [13, 15-21]

In this study, multivalent DNA-based ligands were applied to examine the efficient multivalent targeting of langerin, a trivalent lectin receptor found on Langerhans cells. The targeted delivery of tumour-associated antigens to Langerhans cells has been identified as a novel cancer vaccination strategy.[22] A method for optimising avidity is presented by rationally designing molecularly defined multivalent ligand systems that take both the geometry of the target protein and the strength of the interaction at a single binding site into account. The rebinding effect was identified as tool that can work cooperatively with the chelate effect amplifying multivalency and ligand efficacy. The results will help to understand the underlying principles for designing efficient multivalent systems and may deliver tools for the development of highly

potent and selective therapeutics even when only weak monovalent ligands are available.

2 Theoretical Background

2.1 Multivalency

Multivalency is comprised of multiple noncovalent and typically weak interactions between two or more binding partners. The use of multivalency is widespread in nature e.g. pathogens such as viruses are coated with a multitude of oligosaccharides for these purposes. The type of carbohydrates, their orientation and the distances between the carbohydrate ligands create information, which allows the virus to interact with its surroundings. Only when the sugar pattern of the pathogen is recognized by the receptor of a host cell do they interact. Lectins (carbohydrate binding proteins) represent a group of receptors that recognise carbohydrate structures. As monovalent carbohydrate – lectin interactions are often very weak, multivalency is exploited to afford the necessary affinity.[23-24] Oligosaccharides on the virus surface act as a multivalent carbohydrate ligand that can bind to a multivalent receptor. The multivalency effect describes the observed increase in binding affinity between multivalent interaction partners in comparison to the affinity of the monovalent interaction. To quantify this, Whitesides *et al.* introduced the β – factor (Table 1, Formula 1), which describes the relationship between the binding constant of the binding of a multivalent system with the monovalent binding constant.[25] A large β - factor is equal to a large affinity increase between binding partners. Although the β - factor is often used in the literature to illustrate affinity improvements due to multivalency, this factor does not consider concentration effects due to valency. If information on the valency of the interaction is available, this can be inserted into the equation to attain a normalized parameter β/n (Table1, Formula 2). The β/n-value describes the affinity enhancement per ligand. A truly multivalent interaction requires a β/n-value > 1. However, as multivalent systems do not always provide information on the number of ligands in the multivalent system (e.g. in the case of polydisperse polymers) the β – factor is still widely used for comparison instead of β/n.

The multivalency effect should not be mistaken with cooperativity. The cooperativity effect is a term describing how the binding of one ligand with e.g. a multivalent receptor influences the binding strength of a second ligand to the same receptor. It is

possible and common for a multivalent system to exhibit negative cooperativity and a positive multivalency effect. [26] The α-value (Table 1, Formula 3) is a measure of the degree of cooperativity and describes the relationship between the strength of the first and second binding process.[25] Positive cooperativity corresponds to an α-value > 1 and means the binding of a second ligand is stronger than the first. Negative cooperativity means the α-value is < 1.

Table 1 Cooperativity effect and Multivalency effect[25-26]

Multivalency effect	Valency corrected multivalency effect	Cooperativity effect
Formula 1	Formula 2	Formula 3
$\beta = \frac{K(multi)}{K(mono)}$	$\beta/n = \frac{K(multi)}{K(mono) * n}$	$\alpha = \frac{\lg K\ (multi)}{\lg K(mono)\text{^}n}$

The most well-known example of a positive cooperativity effect is the binding of four oxygens to tetrameric hemoglobin, which is important for hemoglobin´s remarkable ability to release and uptake oxygen.[27] An example illustrating negative cooperativity but a positive multivalency effect was described by Karulin et. al, who studied the interaction between bivalent rabbit antibodies and antigens sites found on Bacillus sp. bacterial cells.[28] The binding constant of the monovalent Fab fragment was determined to be $K^{(mono)} = 3.6*10^9\ M^{-1}$. According to Formula 3 (Table 1) for the α-value to be >1, K^{multi} has to be larger than $K^{(mono)2} = 3.6*10^{18}\ M^{-}1$. Instead, the bivalent binding constant was determined as $K^{multi} = 1\ 10^{11}\ M^{-1}$, which was only 30 times higher than the monovalent binding. [28] The α-value is < 1 and the binding is therefore negatively cooperative. The multivalency effect described by the β/n-value = K(multi) / (K(mono)*n) = $10^{11}\ M^{-}1$/ ($3.6\ 10^9$ *2 M^{-1}) is > 1. (The valency of an antibody = 2.) Although the affinity increase does not fit the criteria for positive cooperativity (α > 1), the multivalency criteria β/n > 1 is met. Hence, this interaction shows negative cooperativity but a multivalency effect.

2.2 Thermodynamics of Multivalency

A full thermodynamic description of multivalent binding remains complex due to the number of participants and several overlaying effects.[29-30] A simple consideration of a model bivalent system consisting of two ligands on a scaffold and a bivalent receptor (Figure 1) will allow for some general conclusions, about which factors influence multivalency and therefore should be considered when designing a multivalent ligand.

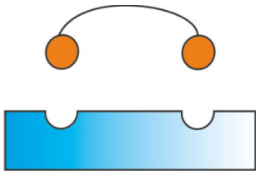

Figure 1. Model System consisting of a bivalent receptor (blue) and a bivalent ligand system.

According to the Gibbs-Helmholtz equation ($\Delta G = \Delta H - T\Delta S$) the binding affinity between the ligand and the receptor are defined by the change in enthalpy and entropy during the binding process. Simplified, the change in enthalpy can be considered as the sum of the individual enthalpies. The change in entropy is largely defined by the change in conformational entropy. The loss of entropy during the binding process is smaller for pre-organized systems. In other words, the more rigid the scaffold holding the ligands of a multivalent system, the smaller the entropy penalty upon binding. For example, Bandlow *et al*. compared the bivalency effect using a rigid DNA core and a flexible PEG linker as scaffolds when targeting hemaglutinin. Although the flexible PEG linker assures optimal binding enthalpy, the bivalency effect was 75-fold stronger when applying the more rigid DNA scaffold. [17, 31-32] Too rigid a scaffold may however prevent bivalent binding altogether. A flexible scaffold on the other hand will ensure optimal binding enthalpy of both ligands but the loss in entropy will be higher. Effective molarity (EM) and effective concentration (C_{eff}) are two terms that have also been used to understand multivalent interactions. C_{eff} describes the probability that two reactive groups or binding partners will react/bind based on the "real concentration" of one of the binding partners as experienced by its counterpart. In the model bivalent system, the binding of the first ligand is an intermolecular process, whereas the binding of the second ligand is an intramolecular process. It is easy to visualize that the second ligands degrees of freedom are limited by scaffold length and flexibility. A rigid scaffold, with exactly the right distance to bridge the receptor binding sites, brings the

second ligand and the second binding site into proximity, and therefore increases the C_{eff}. However, a very rigid tether and an incorrect distance may mean that the C_{eff} of the second ligand as experienced by the binding site is lower than the concentration of the free ligand. In this case intermolecular binding will be favoured over intramolecular binding. Hence, a rigid tether is advantageous to increase the $C_{eff,}$ but some degree of scaffold flexibility is necessary to make sure the intramolecular interaction can take place. The closely related EM is an empirical term defined as the ratio between the first-order rate constant of an intramolecular reaction and the second-order rate constant of the corresponding intermolecular reaction.[33] While C_{eff} is calculated or estimated from the physical properties of the multivalent ligand, EM is determined empirically. In a model bivalent ligand-receptor system Krishnamurthy *et al*. were able to measure that the intramolecular binding process was most favoured over the intermolecular binding process when the tether length was optimal for bivalent binding.[33] Von Krbek *et al*. investigated the EM between a divalent [18]crown-6 host with a rigid core and its association to bivalently presented primary ammonium ions. The scaffold between the ions was altered in distance and a flexible (alkyl spacer) or rigid (aryl/alkynl spacer) core implemented. The flexible spacer led to a high EM even when the match between the divalent host and guest was not optimal. In contrast, the rigid aryl/alknyl linker system was much more sensitive and a small deviation from the optimal distance led to a much reduced EM. [34]

In conclusion, these concepts guide the design of multivalent ligands and suggest that for an optimal bivalency effect a rigid scaffold is superior provided the binding of the ligands is not prohibited by the rigidity. Of course, as a perfect fit between multivalent ligands and multimeric receptors is near to impossible, in practice it is advisable to maintain some scaffold flexibility when designing a multivalent system. Regardless of the scaffold and ligand, every multivalent system will also require a linker connecting the scaffold and ligands. The effect of the linker on the binding affinity and binding mechanism is often neglected. A longer and more flexible linker can help overcome conformational shortages between ligand and receptor. However, conversely, it undermines the precise positioning of ligands on a rigid scaffold and the entropic

penalty during the binding process is increased. Again, a compromise between these two effects is necessary.

2.3 Multivalent Binding Mechanisms

Besides the thermodynamic principles that underpin multivalency it is also necessary to understand the molecular mechanisms between multivalent binding partners. In fact, the macroscopic multivalency effect described by the β-effect is associated with different microscopic mechanisms of interaction that even compete against one another. These different mechanisms are classified as the intramolecular non-aggregative mechanism (chelation), the intermolecular aggregative mechanism (cross-linking), statistical rebinding and steric shielding. [35] For simplicity the same model system (Figure 1) consisting of a bivalent receptor and a bivalent ligand will be assumed in the following explanations, but these mechanisms also apply to multivalent systems with higher valency.

Intramolecular Chelation. The chelation binding mechanism (Figure 2A) describes a system where the two binding sites of a bivalent receptor interact with two carbohydrates of a ligand in a 1:1 binding mode. Once one ligand interacts with a binding site the second ligand can either bind to a second binding pocket in an intramolecular fashion or bridge two receptors intermolecularly. In most cases the intramolecular process is favoured due to the higher effective molarity and entropic advantage. This mode of action has received the most attention in our group and others due to great affinity enhancements achieved by this source. [15, 17-19]

Intermolecular Aggregation (Cross-linking). If the effective concentration of the second ligand of a bivalent ligand in a bivalent-ligand-receptor system as perceived by the receptor, is lower than the free ligand concentration intermolecular binding is favoured over intramolecular binding. (Alternatively, the bivalent ligand may also bind to the bivalent receptor monovalently.) This process can lead to cross linking of receptors by the bivalent ligand and is called intermolecular aggregation or cross-linking (Figure 2B). Recent work by Dubel et. al illustrated the importance of the monovalent affinity for cross linking to take place. Interestingly, a weaker monovalent ligand affinity reduced the concentration threshold for crosslinking. [36] Rohse *et al*. provided evidence that ligand valency can influence the dominant binding mechanism. While the examined bivalent glycopeptides bound to the tetravalent lectin Wheat Germ Agglutinin in an intramolecular non-aggregative manner, the tetravalent glycopeptides

cross-linked several tetravalent lectins to form a 3:3 multimers. [37] Gestwicki *et al*. examined the effect of structural diversity on the binding mechanism. To this end, a series of multivalent mannose ligand with different scaffold shapes and sizes, valency, and ligand density were synthesized. As expected, high molecular weight polymers with high valency bound many copies of the lectin ConA by crosslinking. [38] Cross-linking is relevant for the triggering of receptor mediated signalling pathways. Receptors can diffuse through the membrane and cluster around a multimeric ligand, which in turn mediates downstream signalling. [39-40]

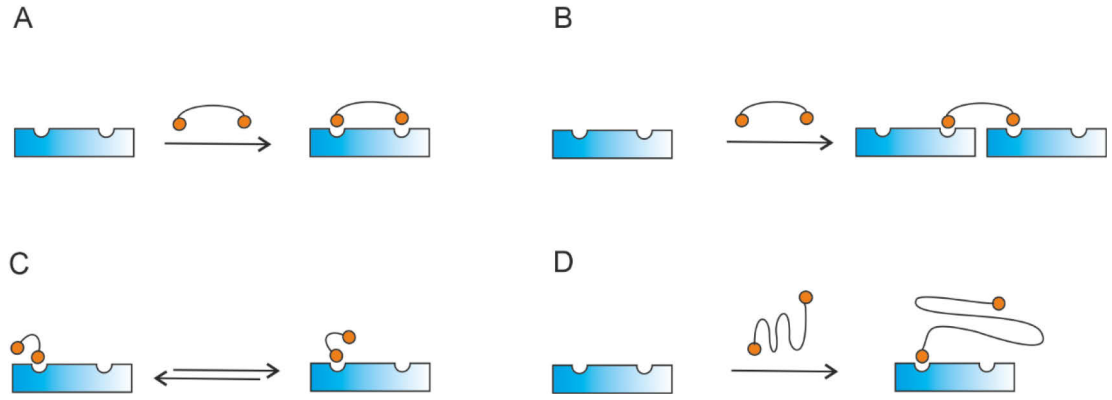

Figure 2. A) Intramolecular / Chelation mechanism: Bivalent ligand bridges the two binding sites of the trivalent receptor (blue). B) Aggregative mechanism/ Cross-linking: Intermolecular interaction between bivalent ligand (orange) and trivalent receptor (blue). C) Statistical Rebinding: Two ligands (orange) of a bivalent binder interact with the same binding site of a trimeric receptor (blue), quickly replacing each other. D) Steric shielding: Bivalent ligand binds to the trivalent receptor (blue) and blocks of the binding sites for other ligands.

Statistical Rebinding. In some cases where bivalent ligands are not able to bridge the distance between two binding sites or in cases with monovalent receptors multivalent ligands may nevertheless display a multivalency effect ($\beta/n>1$). The statistical rebinding effect (*Figure 2*C) is due to a mechanism where one ligand, bound to the receptor, brings another ligand, attached to the same scaffold, into proximity of the same binding site, thereby increasing the effective ligand concentration.[30, 35] Mangold *et al*. examined the statistical rebinding effect by investigating the affinity of mannose-equipped PAMAM dendrimers to monomeric Concanavalin A (Con A), a well-studied plant lectin in multivalent research. Impressively, a dendrimer with 16 mannose units displayed a 3-fold affinity enhancement per sugar ($\beta/n = 3$), which was attributed to the statistical rebinding effect.[41]

Steric Shielding. Although steric shielding (Figure 2D) itself is not multivalency it is an effect often mentioned in the context of multivalency as it can be caused by large multivalent scaffolds. In this case the binding of a large multivalent ligand to the receptor blocks off any further binding sites of the receptor. Hence, this mode of action does not actually increase the affinity of the multivalent ligand (although unspecific binding of the scaffold may also play a role) but rather prevents accessibility for competitive binders. In a thorough investigation Vonnemann *et al*. found that the steric shielding effects on the IC_{50} value was minor in comparison to multivalency effects in their model system. [42]

2.4 C-type Lectines

Oligosaccharides on cell surfaces and pathogens serve as a recognition code for the sugar-binding proteins known as lectins. The C-type lectins (CTLs) form a family of calcium dependent carbohydrate binding proteins. CTLs expressed by dendritic cells can detect pathogens and activate adaptive and innate immune answers. [43] The carbohydrate binding sites are highly solvent exposed and hydrophilic. Affinities of mammalian CTLs with monosaccharides are typically in the millimolar range.[44] The carbohydrate recognition domains (CRDs) of the CTLs fall into two groups, each containing highly conserved residues. The EPN (Glu-Pro-Asn) motif, which binds to mannose type ligands, or the QPD (Gln-Pro-Asp) motif, responsible for galactose-type ligand binding. This is due to the fact that the primary interaction is between the non-reducing end of the carbohydrates and the receptor binding pocket. EPN containing binding pockets prefer the equatorial spatial conformation of the 3- and 4-OH groups, present in mannose. Binding pockets with the QPD motif prefer the equatorial 3-OH, and axial 4-OH conformation as found in galactose. [45] Secondary binding interactions can cause selectivity for additional or more complex glycans.[46] However, CTLs are often able to bind several mono- and oligosaccharides, thanks to the flat and hydrophilic binding site. Importantly, many CTLs form multimeric structures enabling multivalent interactions with oligosaccharides. [47]

The membrane-bound C-type lectins can be categorised in type I and type II C-type lectins depending on the orientation of the N-terminus. Type 1 C-type lectins have an N-terminus that points outwards and contains several CRDs. The N-terminus of type II C-type lectins points into the cytoplasm of the cell and possess a single CRD at the C-terminus.[48]

2.4.1 Langerin

The research presented here focuses on langerin, a trimeric type II transmembrane CTL found on Langerhans cells. Langerhans cells are found in the epidermis and interpret the appropriate immune response when encountering pathogens. 49 Each langerin protein is comprised of a cytoplasmic domain, a transmembrane region, and an Extra Cellular Domain ECD. The ECD consists of an α-helical neck domain and a

carbohydrate recognition CRD containing one Ca2+ ion. Due to interactions between the CRDs and neck domains the ECD forms a rigid trimer (hereafter named only ECD) with the three carbohydrate binding pockets separated by 42 Å. (Figure 3)

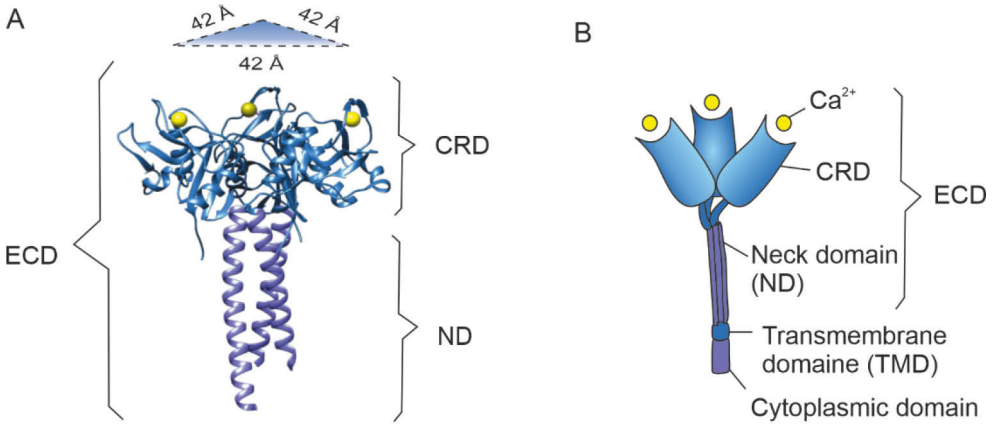

Figure 3. A) Crystal structure of langerin ECD PDB= 3KQG B) Cartoon of the whole langerin protein

Langerin contains the EPN motif and therefore displays a preference for mannose and fucose type glycans. Additionally, glucosamine and 6-sulfo-galactose have been reported to bind langerin.[50] The binding is largely defined by the coordination of the Ca^{2+} ion with two vicinal, equatorial hydroxyl groups (Figure 4). Evidence for a second calcium independent mannose binding site on the CRD, which was originally reported in the literature, has been withdrawn. [51-54] Skerra *et al*. determined the affinity of the langerin CRD for mannose (K_D = ca. 6.1 mM) and Man(a1–2)Man (K_D = 4.2 mM). This highlights the typical millimolar affinity for carbohydrates and the absence of secondary interactions with the CRD. A good overview of the typically millimolar affinities of the natural ligands was reported by Stambach *et al*. Man (K_I = ca. 2.3 mM), Fuc (K_I = ca. 2.6 mM), GlcNAc (K_I = ca. 2.8 mM), Gal-6-OS (K_I = 3.0 mM) and $Man_9GlcNAc_2$ (K_I = 0.2 mM).[50] A submillimolar affinity was also measured for a heparin-derived trisaccharide (K_D = ca. 0.5 mM) in a dependent manner.[55] Additionally, a heparin-based hexasaccharide was reported to bind only to the full langerin ECD trimer via a calcium-independent binding site.[55-56]

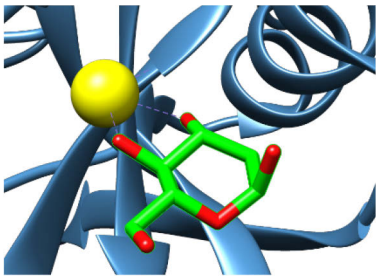

Figure 4. Crystal structure of mannose(green/red) binding to Ca2+ (yellow), which is embedded in the CTL langerin (blue). pdb =3P7G

Langerin can bind pathogens such as the human immunodeficiency virus (HIV) and mediate internalization of the pathogens in Birbeck granules (specific to langerin) as well as presenting antigens to T-cells. Therefore langerin is involved in the innate as well as in the adaptive immune response.[43] Only recently have langerin expressing Langerhans cells been identified as a promising immunotherapy target due their ability to present antigens and stimulate T-cell response, and their localisation in the epidermis. This approach is comprised of delivering an antigen to Langerhans cells immunizing through the skin (termed epicutaneous immunisation), a simple and cheap alternative to conventional DC immunotherapy, which relies on loading DCs with antigens in vitro before injecting back into the patient[22] Previous research has shown that the the efficacy of immune responses can be enhanced when the antigen is not only injected into the skin but rather selectively delivered (targeted) to a receptor expressed by immune cell e.g. by conjugating the antigen to a receptor specific antibody.[49, 57-58] Alternatively, the use of glycan-modified liposomes as delivery platoform was reported as a means for lectins targeting.[59-60] Therefore, the development of selective high affinity langerin binders has become an interesting target with the potential for application immunotherapy. [47, 61]

2.4.2 Langerin vs. DC-SIGN

DC-SIGN is a C-type lectin present on dendritic cells and enables the interaction of dendritic cells with T cells by binding to ICAM-3.[52] The DC-SIGN ECD forms a tetramer with each CRD harbouring a calcium ion, which are between 40 and 95 Å apart (Figure 5).[51, 62] Like langerin DC-SIGN binds to mannose type ligands (K_D (mannose) = 3.5 mM) with comparable affinity. In contrast, the affinity for Man(a1–2)man (K_D = ca. 0.9 mM) is considerably higher indicating that unlike langerin the

DC-SIGN CRD does not only interact with terminal mannose but also internal mannose residues.[54, 62-63] Remarkably, despite their overlapping carbohydrate specificity and similar roles in the first level immune response, langerin and DC-SIGN have very different roles in HIV infection. Unlike DC-SIGN, which mediates the transmission of HIV to T cells, langerin internalises and degrades HIV, thereby inhibiting the infection.[64] Hence the selective inhibition of DC-SIGN while maintaining langerin function has received considerable attention in the literature.[65-66] Furthermore, from a multivalency perspective the comparison between DC-SIGN and langerin is equally interesting. As mentioned, both CTLs bind the same high mannose-type ligands such as the HIV glycoprotein gp120. However, langerin and DC-SIGN form two distinct multimeric structures with defined distances between the binding sites. The langerin ECD forms a trimer and the three biding sites are each 42 Å apart.[51] The DC-SIGN ECD forms a tetramer and the distance between the binding sites range between 40 and 95 Å (Figure 5). [62] The similarities in monovalent binding affinities and selectivity raises the question whether selectivity may be induced by a smart multivalent presentation of ligands. If the ligands of a multivalent system can be arranged in such a way that the presentation matches the binding sites of one lectin but not the other, this should lead to elevated affinities for one of the lectins. If the multivalent effect can be tuned to promote significant increases in affinity for a precise multivalent conformation a selective and very effective inhibition of the lectins will be achieved.

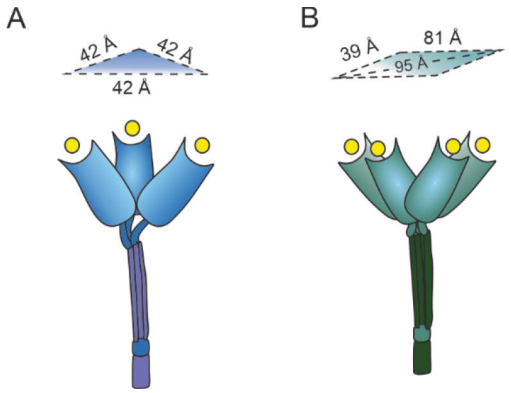

Figure 5. Comparison of trimeric langerin ECD (A) and tetrameric DC-SIGN ECD (B) with Ca^{2+} (yellow)

Hence the key to achieving multivalency based selective inhibitors is the development of multivalent systems that make the precise spatial arrangement of ligands and high avidity possible.

2.5 Multivalent Presentation of Carbohydrates

The efficient targeting of lectins is necessary in order to learn about their biological role, inhibit their function, when they play a role in diseases, or even deliver cargo to antigen presenting cells as an immunotherapy. Therefore, the development of ligands with higher affinity for their target lectin than the canonical carbohydrates has received much attention. One approach to succeed in increasing affinity is by learning from nature and applying the benefits of multivalency. To investigate the multivalent presentation of carbohydrate ligands for affinity enhancement many different scaffolds including nanoparticles[4, 67], dendrimers, capsid proteins[68], fullerenes[69-70], polymers[71], calixarenes[8], DNA[13, 72] and liposomes[3, 47, 60] have been equipped with ligands.[24, 73] The following chapter will highlight recent strategies applied for multivalent CTL inhibition focusing on examples addressing the CTLs langerin and DC-SIGN.

Tabarani *et al*. examined the affinity of multivalently presented mannose on dendrimers Figure 6A). The ability of the multivalent ligand to inhibit the interaction between gp120 and DC-SIGN was measured. The glycoprotein gp120 found on the surface of HIV contains several high mannose N-glycan structures and has an affinity for DC-SIGN in the nano-molar range. The binding of HIV to DC-SIGN is crucial for the T-cell infection as the dendritic cells, which express DC-SIGN, present virus to the T-cells in the lymph nodes. Interestingly, the presentation of 16 mannose units was not sufficient to achieve a stronger binding than the background signal. A total of 32 mannose units were needed to achieve a multivalent effect and an IC_{50} = 50 µM calculated was measured. Hence, the IC_{50} per mannose ligand (1.6 mM) was still in the millimolar range. This example shows how difficult it is to achieve a multivalency effect with a very poor monovalent ligand.[74]

Penadés *et al*. prepared multivalent gold glyconanoparticles (Figure 6B), which presented oligomannosides, and tested their ability to inhibit the gp120-DC-SIGN interaction.[75]Goldparticles with an average diameter of 1.3 nm and roughly 40 mannosides lead to an already remarkable affinity increase and full inhibition of the gp120-DC-SIGN interaction at 20 µM. The mannoside-goldnanoparticle was therefore roughly 1000-fold more potent than free methyl-α-D-mannopyrannoside, which displayed full inhibition at only 25 mM. However, the affinity per ligand for

full inhibition remains in the nearly millimolar range, approximately 800 µM. Interestingly, they found that the use of Manα 1-2Manα units instead of mannose produced much stronger DC-SIGN inhibitors. The most efficient nanoparticle was equipped with 25 diamannosides and showed a 20,000 fold improved affinity (full inhibition at 115 nM) in comparison to the free Manα 1-2Manα (full inhibition at 2.2 mM). This corresponds to a 750 fold affinity improvement per ligand and an affinity of 2.9 µM per mannoside. This example clearly demonstrates two principles. First, the multivalency effect often becomes larger when increasing the number of ligands as the 32mer mannose-dendrimer by Tabarani *et al*. showed affinity of 1.6 mM per mannoside in comparison to 0.8 mM in the 40 mer developed by Penadés *et al*. monovalent ligand. Second, the use of a more potent monovalent ligand (Manα 1-2Manα was 11-times more potent than methyl-α-D-mannopyrannoside) led too much higher multivalency effect (20,000 fold vs 1000 fold). Critically, the authors also found that the gold nanoparticles themselves were able to interact with gp120 at a submicromolar level. The 25 dimannoside-gold nanoparticle displayed a K_D = 0.2-1.0 µM for gp120. Naturally, this raises many questions as to how the gold nanoparticles are inhibiting the gp120-DC-SIGN interaction. Even if the nanoparticles and DC-SIGN are not binding to gp120 via the same binding sites, as the authors suggest, once the gold nanoparticles bind to gp120, it will be shielded off from interacting with DC-SIGN. Steric shielding, therefore, almost certainly influences the measured affinities in this case and the real affinities may be much lower.

Becer *et al*. investigated the potential of mannose and galactose containing glycopolymers, with a number-average degree of polymerisation of 58, (Figure 6C) to inhibit the interaction between the HIV glycoprotein gp120 and DC-SIGN. Unsurprisingly, the best binder contained only mannose and no galactose units, as DC-SIGN is known to bind specifically to the equatorial 3-OH and 4-OH groups of mannose. The glycopolymer containing only galactose did not bind to DC-SIGN. The polymannoside with approximately 58 (100%) mannose units showed an IC_{50} =37 nM corresponding to 2 µM per mannoside. In comparison the polymannoside with only 25 % mannose and 75 % galactose was found to display and IC_{50} of 1.45 µM, meaning

22 µM per mannoside. Hence the affinity improvement per mannoside for the 100 % mannose glyopolymer was over 10-fold stronger than the 25 % mannose glyopolymer.

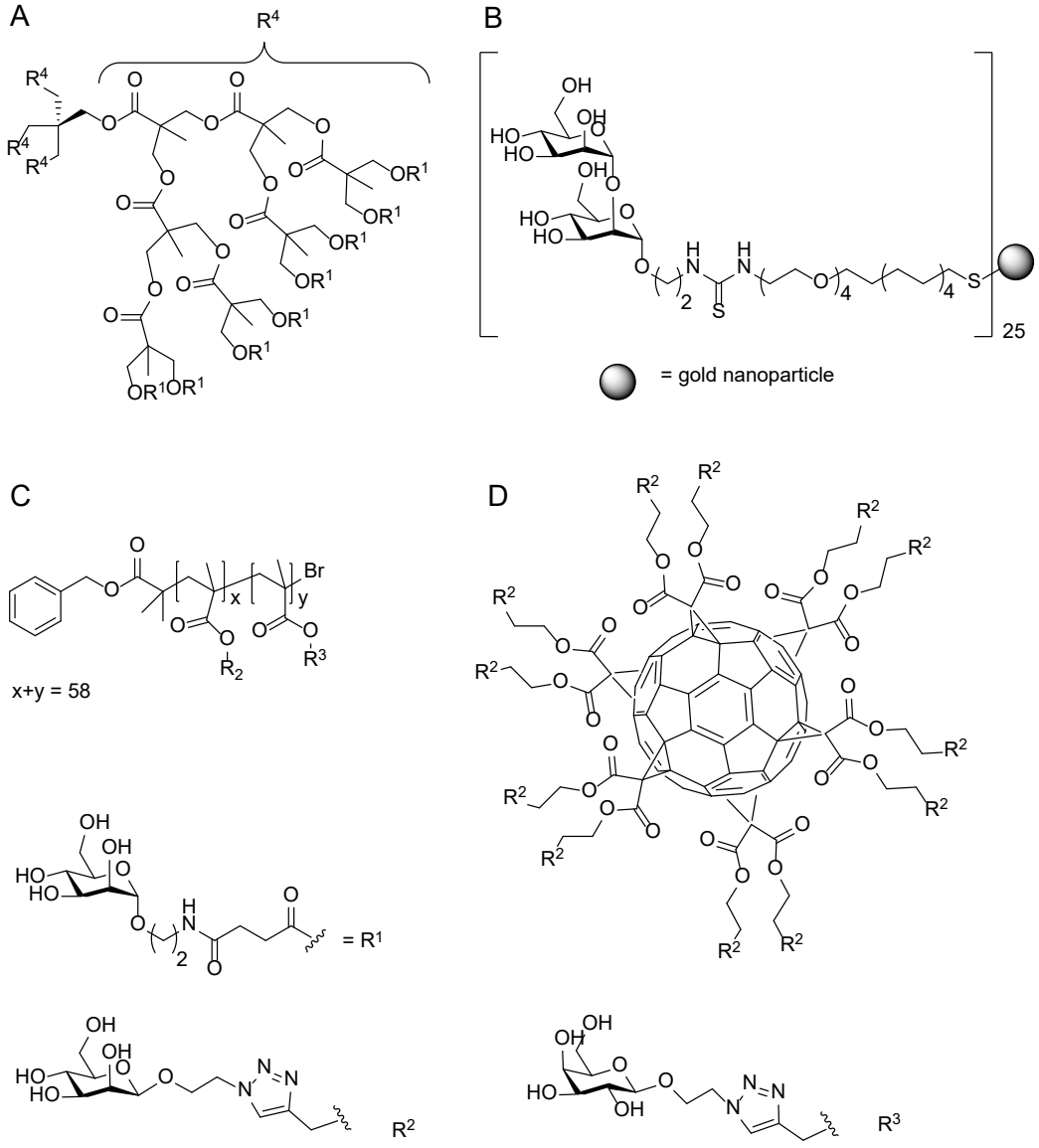

Figure 6 A. Mannose-dendrimer[74]; B. Manα 1-2Manα-goldparticle[75]; C. Mannose-Galactose-polymers [71]; D. Galactose-Fullerence[69]

This result again stresses the high number of carbohydrates necessary to gain a strong multivalency effect with a low affinity monovalent ligand and an undefined arrangement.[71]

Another interesting scaffold, which makes use of its rigid spherical shape and allows for precise functionalisation in a 3D fashion are fullerenes. Although typically suffering from low solubility Rojo and his group showed that by employing the

Copper-catalysed click reaction to functionalise C60 fullerenes with 12 or 36 sugar moieties gave water-soluble molecules of non-amphiphilic character.[70] The ability of these multivalent mannose-equipped fullerenes (Figure 6D) to inhibit the DC-SIGN mediated Ebola viral infection was examined. The Ebola virus glycoprotein (the pseudovirus in this transfection model) is fully dependent on DC-SIGN, which was expressed on Jurkat cells, for viral entry and infection. While a control galactose-equipped fullerene was not able to inhibit the infection, a C_{60} fullerene with 12 mannose units showed an IC_{50} = 2 μM. Surprisingly, the glycofullerene with 36 mannosides displayed a 34-fold lower potency and an IC_{50} = 68 μM. The introduction of a longer spacer between the fullerene core and the 32 mannose moieties increased the potency again 200-fold to IC_{50} = 0.3 μM corresponding to an affinity of 11 μM per mannoside. Evidently, this example highlights that not only ligand valency influences the multivalency effect but also the accessibility of the ligand to interact with the binding pocket, which may have been compromised in the shorter linker system. Impressively, a multivalent effect was achieved with only 12 mannose units. However, the Ebola pseudovirus transfection assay generally resulted in much lower IC_{50} values than the inhibition of the gp120-DC-SIGN interaction, examined by Surface Plasmon Resonance (SPR), in the previously mentioned examples. For example the 32 mannoside-dendrimer reported by Tabarani *et al*. and mentioned above showed an IC_{50} = 337 nM in the Ebola pseudovirus transfection assay although the IC_{50} in the SPR assay was only 50 μM.[74, 76]

Bernardi and her group presented fundamental work by tethering four different monovalent ligands, with respective affinites for DC-SIGN, to dendrimers.[77] This allowed the group to examine the effect of the monovalent affinity on the multivalency effect as the valency of the glyodendrimers was gradually increased (Figure 7). The affinities were determined by measuring the ability of the glycodendrimers to inhibit the interaction between DC-SIGN and immobilised mannosylated BSA (mannose-BSA). A weak monovalent ligand, mannose (IC_{50} = 3.2 mM) and a stronger pseudo-dimannoside (IC_{50} = 1.0 mM) were compared, among others. Increasing the valency of the mannoside-dendrimer from 4 (Figure 7 A) to 6 did increase the overall affinity, but the β/n values remained at 1.1 and 0.7 respectively meaning these were only

concentration effects. A real improvement was made when the number of mannose units reached 9 (IC_{50} = 128 µM) with a 3-fold affinity improvement in comparison to the monovalent affinity (Figure *7* B). The dendrimers with 12 (IC_{50} = 67 µM) and 18 (IC_{50}=36 µM) mannose units showed even greater affinity improvements of 4- and 5-fold per mannose unit.

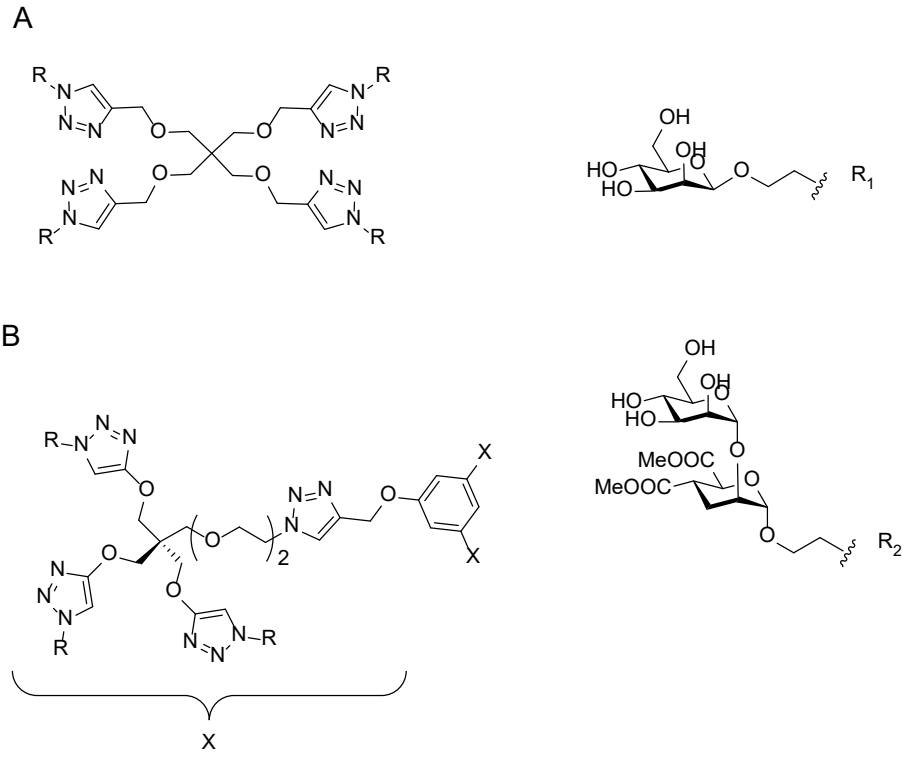

Figure 7. A) Tetravalent dendron. B) Nonavalent dendron. Bernardi and her group work increased the valency of the dendrimer from 4 (A) to 9 (B) while applying two ligands with different affinities.

In comparison, the multivalent presentation of the pseudodimannoside (Figure *7*), which was 3-fold more potent than mannose, displayed a 4-fold affinity improvement per sugar moiety when displayed tetravalently (IC_{50} = 39 µM). A dendrimer with 9 pseudo-dimannosides (IC_{50} = 14 µM) was even 8-fold more potent per ligand. Again, these results stress the difficulties in achieving a multivalency effect greater than the concentration effects (β/n>1) when applying a very weak monovalent ligand at low valencies. The more potent pseudo-disaccharide immediately leads to a much stronger multivalency effect. Interestingly Bernardi and her group also compared the application of different dendrimer cores with the same valency by attaching the pseudo-dimannoside to tetravalent Bolton type dendrimers, tetravalent pentaerythritol based dendrimers and two different hexavalent dendrimers. In both cases the structure of the scaffold had very little influence on the affinity of the multivalent ligand. The

authors suggest that therefore the shape of a multivalent ligand is less influential on their activity than the valency. However, it is worth noting that all the dendrimers applied here are so flexible that they bear very little real structural and spatial information in solution. A more rigid scaffold would be necessary to test the authors hypothesis.

Very recently, Neuhaus *et al*. described a systematic investigation of multivalent binders for langerin. Trivalent langerin inhibitors (A) were constructed by equipping a asymmetrically branched three-armed polymer with one mannose ligand each. The design was chosen to resemble the structure of the trimeric langerin ECD (Figure 8A). By varying the length of the polymer arms the authors found that the trivalent ligand with the shortest arms was most potent in inhibiting the interaction between the langerin ECD and a mannose derived reporter ligand. The measured IC_{50} = 44 μM for the best trivalent structure meant a 33 fold affinity improvement in comparison to free mannose (IC_{50} = 4.5 mM) and an affinity of 132 μM per ligand. The authors point out that a bridging of the langerin CRDs (chelate effect) can be excluded due to short length of the polymer arms, which do not allow for bridging of the binding pockets. As the affinity of the best trivalent ligand to the CRD (IC_{50} =4.3 mM) is similar to the IC_{50} of mannose, thereby excluding statistical rebinding at one binding site, the authors propose a different mode of mechanism, where the trivalent ligand sits between the three binding sites of the langerin ECD, increasing EM and avidity. However, it remains inconclusive as to why to polymers with longer arms, which should have matched the distances between the binding pockets better showed inferior potencies[78] Taniguchi equally equipped a trivalent polymer scaffold with a disaccharide (Figure 8B) containing 6-sulfated galactose, known to bind langerin selectively. Impressively, the trivalent ligand was able to inhibit the interaction between the immobilised langerin ECD and a biotinylated reporter ligand in an Elisa assay with an IC_{50} =2.7 μM. This meant a 430 fold affinity improvement in comparison to the monovalent ligand (IC_{50} =3.5 mM). The multivalent presentation of the same ligand on a linear polymer with an average of 33 units per polymer lead to a nanomolar binder (IC_{50} = 2.1 nM). However, the protein was immobilised for the Elisa type assay, which

typically leads to larger multivalency effects than solution-based assays, which may favour cross-linking if the loading of the surface is too high .

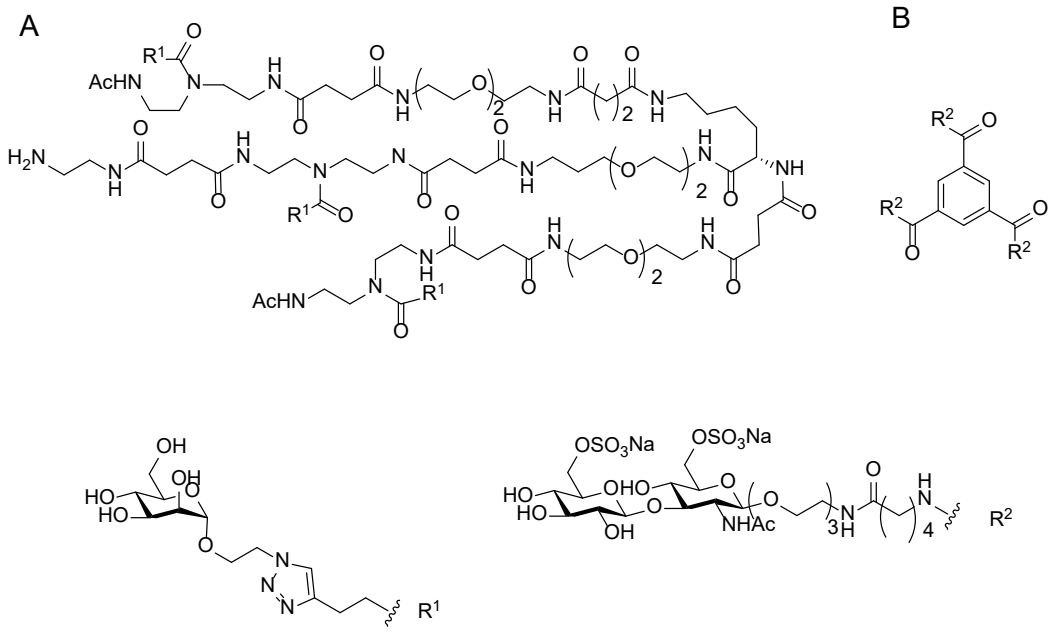

Figure 8. A) Trivalent mannose-Polymer as langerin inhibitor[78]. B) Trivalent presentation of sulphated Disaccharide as langerin inhibitor. [61]

While the mentioned multivalent constructs were often successful in increasing the total avidity, the designs paid very little attention to the spatial presentation of the multivalent ligands and sometimes even had incomplete information on the precise quantity of ligands, which is vital for optimizing ligand economy. The following examples have applied strategies that allow for a more exact quantification and exact positioning of the ligands.

Morbioli et al. prepared mannosylated calixarenes (Figure 9A) and tested their ability to inhibit the interaction between DC-SIGN and mannosylated BSA by SPR. The most rigid example displayed the best affinity (IC_{50} = 200 µM) with a relative mannose potency of 4. [79] This was much better than what was achieved with the more flexible tetravalent mannose-equipped dendrimers (IC_{50} = 700 µM). [77]Due the structure of the calixarenes the affinity increase in this case is solely due to statistical rebinding and the chelating effect can be excluded.

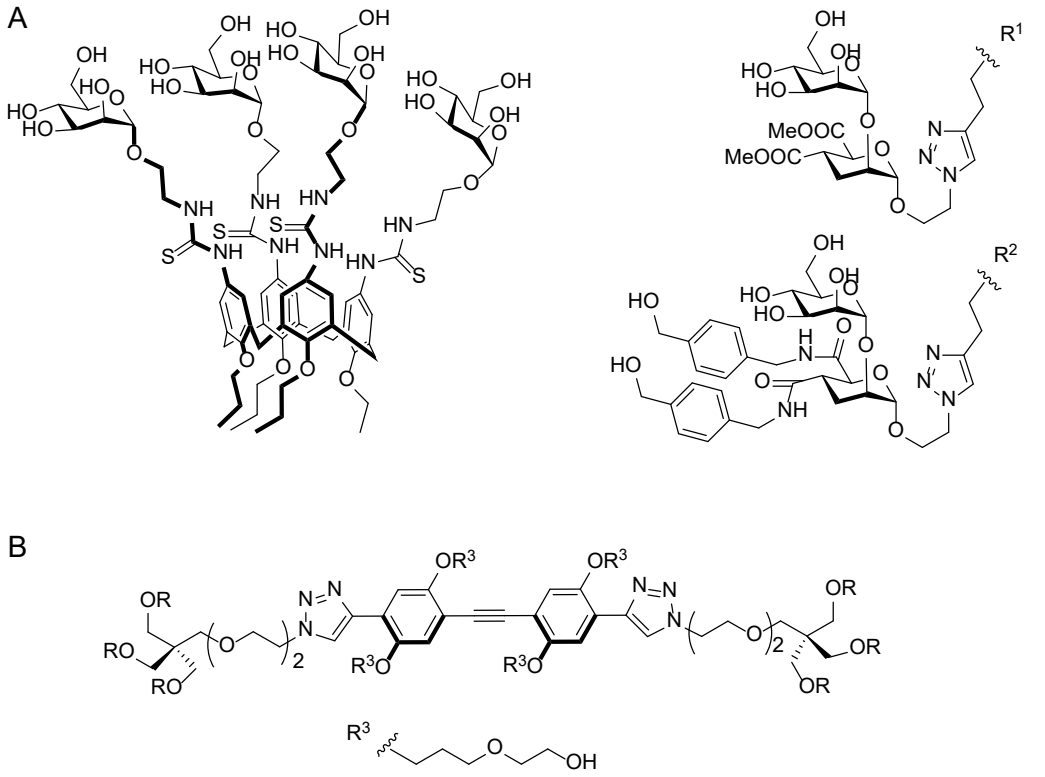

Figure 9. A) Tetravalent mannose equipped calixarene[79] B) Example of hexavalent presentation of dimannoside (R^1 or R^2) glycomimetic on rigid core. The phenylene-ethynylene spacer is shown exemplary with two phenyl units. [80]

The following examples will be making use of much larger scaffolds, which allow precise spatial control of the ligands. One of the aims of these approaches was to synthesise multivalent ligands specifically designed to be able to bridge several binding pockets of a lectin thereby making deliberate use of the chelate effect. For example, Artner *et al*. applied expanded genetic code to express a structurally well defined "pseudo-wild-type barstar" protein scaffold from *Bacillus amyloliquefaciens*, in which methionine was replaced by homopropargylglycine. Subsequently four lactose ligands were conjugated to the protein via a click reaction and the linker lengths between the ligands and the protein scaffold varied. The potency of the site specifically modified protein to inhibit the interaction between the immobilised Thomsen-Friedenreich (TF) antigen and the tetrameric lectin peanut agglutinin was measured by SPR. Interestingly, the tetravalent lactose-modified barstar protein with the medium linker in length was the most efficient inhibitor and roughly 4 times more potent than the monovalently equipped lactose-barstar protein. Although this example demonstrates the use of a very large and well defined scaffold for multivalent

inhibition it is clearly limited by the hurdles of introducing modified amino acids site specifically. [81]

In 2019 Wen *et al*. compared the presentation of tetramannose on a tetravalent polyproline scaffold (Figure 10), which was designed so that the calculated distance between the conjugation sites was 32 Å with the presentation of tetramannose on a trivalent dendrimer scaffold. The affinity for the CTLS langerin and DC-SIGN was compared. Interestingly, while the dendrimer showed a 170-fold higher affinity for DC-SIGN over langerin, the polyproline scaffold displayed increased selectivity and 4800-fold higher affinity for langerin than DC-SIGN was determined. The authors argue that the increased selectivity is induced by the oligomannose pattern. However, as both the langerin and DC-SIGN ECD have binding pockets roughly 40 Å apart this remains inconclusive.

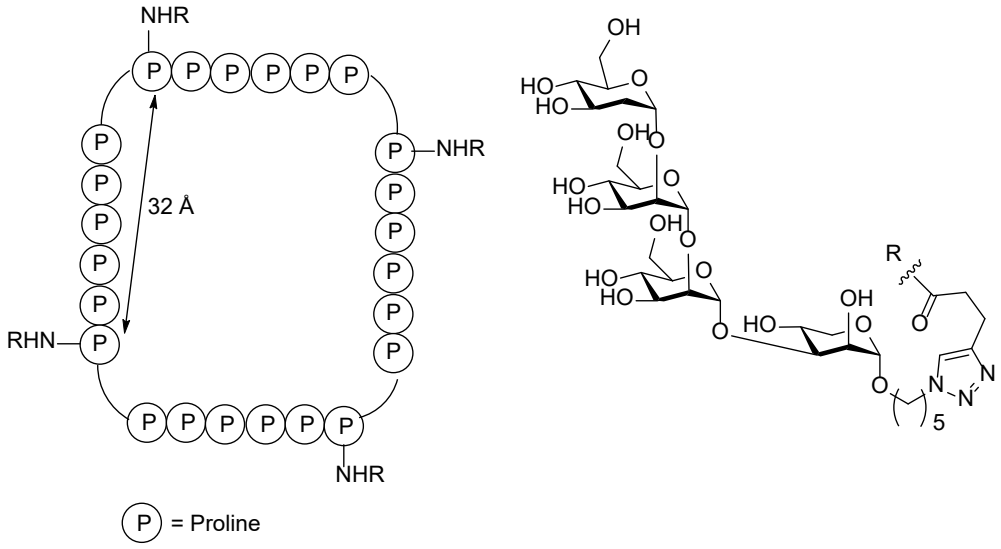

Figure 10 Tetravalent presentation of Tetramannoside on a polyproline scaffold.

Bernardi and her group reported the use of a rigid core consisting of phenylene-ethynylene units for multivalent presentation. Both ends of the scaffold, termed molecular rod by the Bernardi group, were equipped with either a single ligand or a cluster of three carbohydrates (Figure 9B). The length of the rigid spacer was varied from one phenyl group to up to three increasing the distance between the ligands at either end. By applying two different monovalent ligands with different affinities, they created a system to study the influence of monovalent affinity, valency and distance between the ligands on the multivalency effect. The ability of the ligands to inhibit the interaction between DC-SIGN and immobilised mannosylated bovine serum albumin

(mannose-BSA) was determined. The weaker ligand, a pseudo-dimannoside, had a monovalent affinity of IC_{50} = 900 μM and the more potent dibenzylamide- pseudo-dissacharide an IC_{50} = 270 μM. For the bivalent presentation of the pseudo-dimannoside the affinity to DC-SIGN increased from 175 μM to 67 to 36 μM when increasing the phenyl spacer of the rigid core from 1 to 2 to 3 units (Figure 9B). The trend for the hexavalent construct was the same with IC_{50} values decreasing from 34 μM to 25 μM to 9 μM in the same row of scaffolds. Similarly, the affinity of the bivalent dibenzylamide pseudo-disaccharide increased from 34 μM to 19 μM to 8 μM when increasing the rods length. The trend for the hexavalent presentation of the more potent ligands was less obvious as the IC_{50} stay constant between 5 and 7 μM, which may be due to the lower limit of the assay, as pointed out by the authors. In total these examples clearly picture a situation where increasing the distance between the ligands on either end of the molecular rod corresponds to a gain in affinity. Although the authors point out that even the shortest rod can bridge two binding sites of DC-SIGN (distance = 40 Å) in their most extended conformation, this was regarded an unlikely situation as the flexible linker between the core and ligands allows for folding in every direction. In fact, the more compact conformations (< 35 Å) were calculated to represent over 95 % of the sampled population when a long and flexible linker was applied. For the longest rod (three phenylene-ethynylene units) and in combination with a shorter linker the proportion of conformations long enough to bridge the DC-SIGN binding pockets was calculated to be up to 30 %, which lead to higher affinity. Hence, the more likely the ligands are able to bridge the binding pockets the more the affinity gains are not only dependent on statistical rebinding but also profit from a chelating effect. The best multivalency effect was acquired for the hexavalent presentation of the pseudisaccharide on the longest rod with a 17-fold affinity increase per ligand. However, this was an exception and is probably due to the assay limit as the more potent dibenzylamide ligand afforded better β/n values for all other distances evaluated. Furthermore, the multivalency effects also profits from the bivalent presentation of ligand clusters in comparison to the only bivalent presentation, enhancing the β/n value by a factor of at least two. Hence, this impressive study implies that the local clustering of ligands can be used to improve a chelate binding effect and was a major source of inspiration for our work presented here. At the same time the

difficulty in predicting the actual distance between the ligands when changing the core length illustrates the advantages of using a consistent. Being able to position ligands at specific positions without the need to change the scaffold would minimise scaffold-based effects. A scaffold that allows for a very high control of the space between ligands on a consistent core is DNA, which will be discussed in detail in the next chapter.

2.6 Nucleic Acids for Multivalent Presentation of Ligands

DNA does not just carry genetic information but is also comprised of a unique supramolecular structure, the DNA double helix. The DNA single strand backbone consists of a deoxyribose-phosphodiester. Every ribose unit is linked to one of the four nucleobases adenine, cytosine, guanine, and thymine. According to Watson-Crick base pairing, two complementary DNA single strands interact with each other via hydrogen bonding and π-stacking to form a double helix. The DNA duplex is an unusually rigid molecule with a persistence length of 500 - 700 Å or 150 -220 base pairs making it an ideal rigid scaffold molecule. [14]The defined sequence and modular assembly of DNA allow for site-specific modifications. Together with the well-understood structure of the double helix this enables the precise positioning of conjugated ligands. Furthermore, the introduction of nick sites or single strand regions enables tuning of the DNA rigidity. Unlike many artificial polymers, DNA also boasts an extremely good solubility in aqueous media due to the polyanionic backbone. DNA is however let down by its instability towards nucleases and acidic conditions. Therefore, DNA mimics have been developed to enhance certain characteristics. One particularly successful mimic was the invention of peptide nucleic acid (PNA) by Nielsen *et al*. The sugar phosphate backbone was replaced by a pseudopeptide backbone comprised of (2-Aminoethyl)glycin building blocks. PNA is also able to form a double helix with either complementary PNA or DNA. The structure of a PNA-DNA duplex is a mixture of A- and B-DNA with a diameter of 23 Å. One helical turn consists of 13 base pairs (42 Å) and the twist between two base pairs is 28 °.[82-83] The use of PNA has several advantages over natural oligonucleotides. The lack of negative charges on the PNA strand omits strand repulsion and leads to a higher thermal stability of the PNA-DNA duplexes. PNA is easily accessible by the highly developed solid phase peptide chemistry. PNA is much more stable towards acidic and basic conditions than DNA due to the peptide backbone. Furthermore, PNA is stable towards nucleases and proteases facilitating experiments in cells and biological environments. Interestingly PNA-DNA duplexes are also more rigid than DNA-DNA duplexes.[84] A drawback is the inferior solubility in comparison to DNA. Therefore, charged amino acids are commonly attached to PNA to increase the aqueous solubility. In order to

functionalize PNA site-specifically, the development of modified PNA monomers was necessary. L-γ-modified PNA was shown to possess superior DNA binding capacities.[85-86] Thanks to the well understood PNA-DNA double helix structure the precise positioning of ligands on the duplex is easily accessible. The calculation of the distance and orientation between ligands is straightforward. To avoid spiralization effects a nick site can be introduced by hybridizing a full-length DNA with shorter complementary PNA strands allowing for rotational freedom.[15-16]

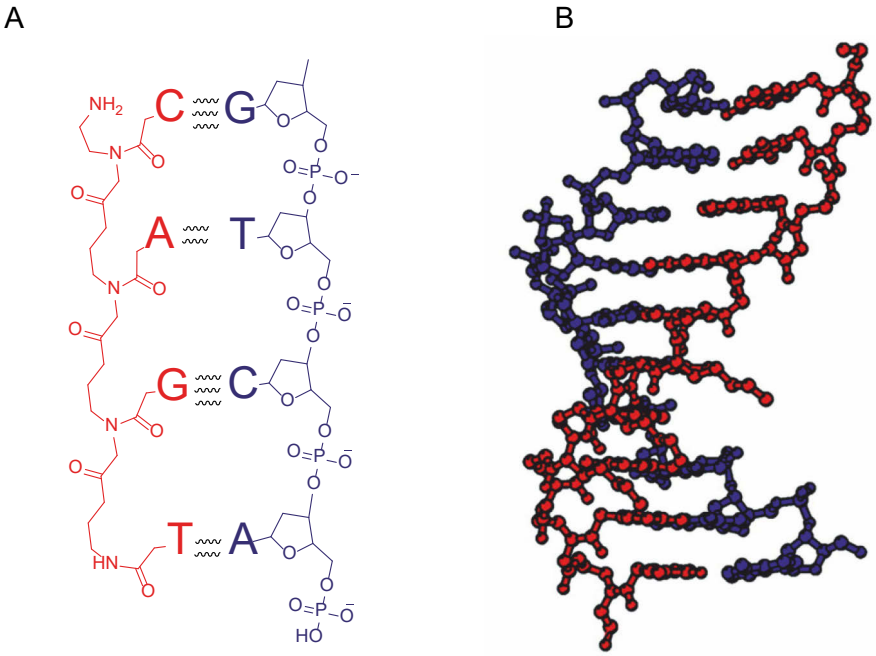

Figure 11 A) PNA (red)-DNA (black) H-bonds (wiggly lines) B) Electron density map of d-Lys-based right-handed PNA(red)–DNA(blue) double-helix structure. The pattern of the base stacking resembles that found in the B form of the DNA double helix. This image was reproduced with permission from PNAS [1]

2.7 DNA based Scaffolds for Carbohydrate Presentation

The use of oligonucleotides to form supramolecular glycoclusters by self-assembly was largely pioneered by Kobayashi and his co-workers in 2004. A thymine phosphoramidite functionalized with galactose (Gal) was synthesised. Using automated oligonucleotide synthesis the modified thymine was incorporated into a DNA single strand between 18 and 20 bases in length. Hybridization of several Gal-DNA oligonucleotides with a large template strand enabled the multivalent presentation of the carbohydrates on a DNA duplex (Figure 12A). The examination of the binding of these constructs to Ricinus-communis_Agglutinin 120 (RCA_{120}) revealed that the density and the twist of the galactose ligands influenced the lectin recognition.[87]

In 2009 Gorska *et al*. coupled a pair of α-1,2-dimannosides covalently tethered by an 11-atom linker to the N-terminus of one PNA strand and the C-terminus of another PNA oligomer. By hybridisation of both PNA strands with suitable DNA templates, the distance between the pair of dimannosides was varied (Figure 12B). Binding experiments to 2G12, a HIV antibody, by SPR gave valuable insights into the optimal multivalent presentation of the carbohydrates for 2G12 binding. The two binding sites of 2G12 are known to be roughly 30 Å apart. The number of nucleotides between the two pairs of ligands was increased from 0, to 10, to 20 and to 30. The potency decreased in the same order from 4 μM , to 8 μM, to 17 μM, and to 89 μM. This was perhaps not the expected result as a spacer of 10 nucleotides corresponds to distance of 32 Å resembling the space between the binding sites of 2G12. Surprisingly, the authors argue that the shortest distance complex (0 nt between the ligands) corresponds to a maximum distance of 38.5 Å between the carbohydrate ligands if the linkers are in their most stretched out conformation. However, as pointed out by Bernardi and her group in the previous example, flexible linkers are very unlikely to be in their most stretched out conformation.[80] Statistical rebinding should therefore be considered as an alternative explanation for the advantageous affinity. In contrast, the heterobivalent distance screening of a dimannoside on one strand and a pair of dimannosides on the other for the same target found that the complex with a 10 nt spacer was the most potent inhibitor. Indeed, it strikes as rather bizarre that the author initially chose the

DNA based approach, which allows for the exact spatial positioning of the ligands on this rigid scaffold, if they believe this can also be achieved by a flexible linker.

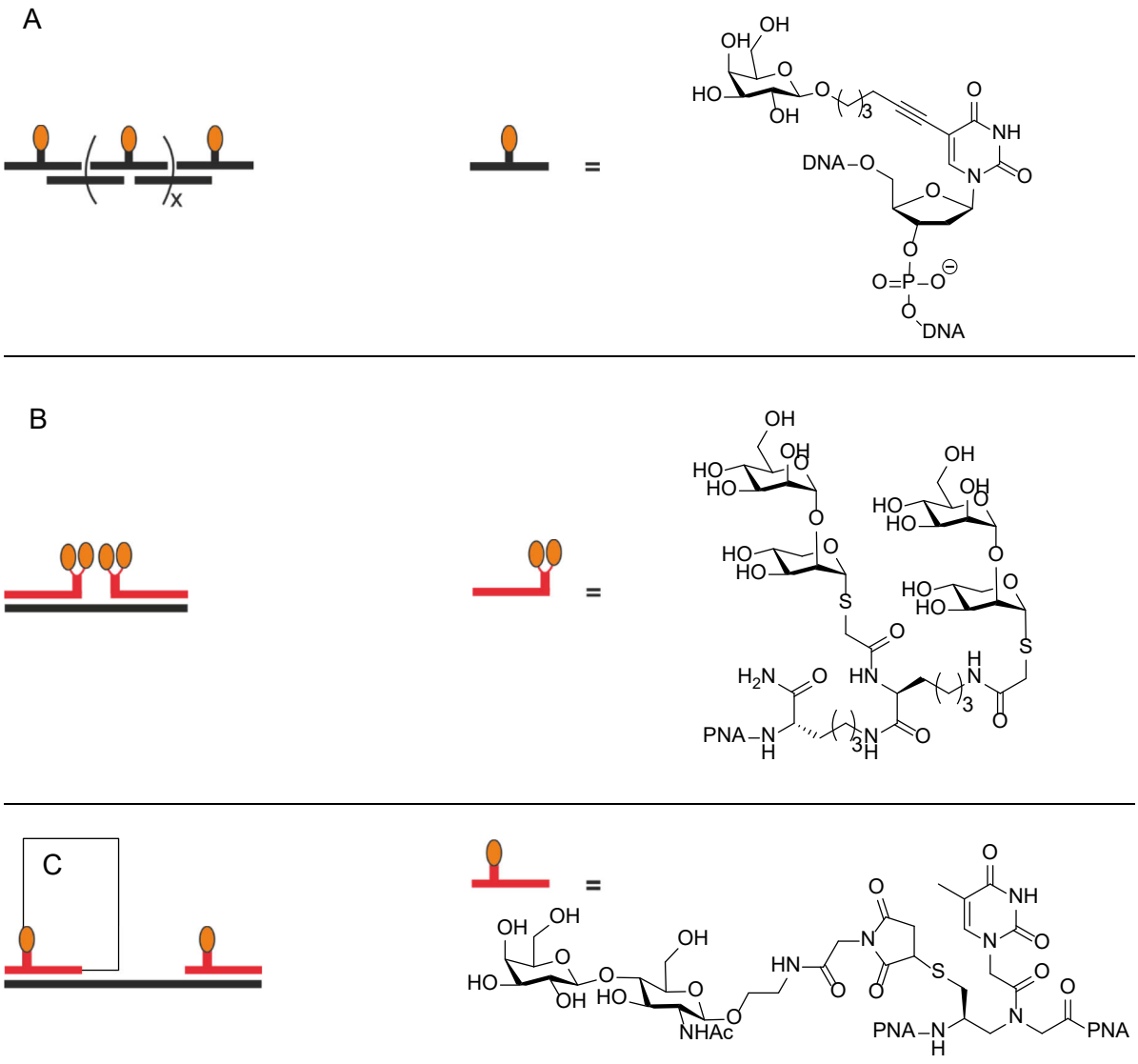

Figure 12 ▬▬ = DNA single strand, ▬▬ = PNA single strand, ● = carbohydrate ligand A) Kobayashi et al. equipped DNA with galactose to form supramolecular glycoclusters [87] B) Gorska et al. equipped a PNA-DNA double helix with mannoside clusters.[88] C) Scheibe et al. ligated LacNAc to a PNA-DNA duplex and examined the binding effects to ECL when increasing the flexibility of the scaffold by introducing a single strand region.[15]

Additionally, a whole range of further mannoside clusters were presented bivalently on DNA and the tether length between the disaccharides varied. Only the mentioned complexes, with the 11-atom linker between the disaccharides, showed any binding to the antibody. Hence, this publication does teach that the linker can have a major impact

on the binding capacity and adjacently presented ligands can achieve surprising results. Unfortunately, no coherent answers are delivered to explain these phenomena.

Scheibe *et al*. constructed bivalent LacNac-PNA-DNA duplexes in 2010 that were able to bind the bivalent Erythrina cristagalli lectin (ECL). A γ-thiol modified PNA thymine monomer was developed allowing for site specific modification. The thiol-modified PNA strand was conjugated to a maleimide functionalized ligand. By hybridizing two LacNac-PNA sequences to a series of DNA templates the position of the LacNac ligands was adjusted. This simple building block system facilitated the Angstroem scale precise positing of ligands on a PNA-DNA scaffold, termed a molecular ruler. A distance-affinity screening revealed the optimal distance between the ligands for binding to ECL, which correlated well with distance between the binding pockets established from the crystal structure. [15] Interestingly, when increasing the flexibility of the PNA-DNA duplex by introducing a single strand region the affinity was further increased (Figure 12C). The authors argue that this allowed the molecular ruler to adapt to the concave structure of ECL. Overall, an 80-fold affinity increase per monovalent carbohydrate was achieved.

Bandlow *et al*. bivalently presented 2,6 sialy-LacNac bivalently on a PNA-DNA system which enabled an up to 50 fold affinity enhancement per ligand to trimeric hemagglutinin (HA) in comparison to Sialyl-LacNac.[17] Not only was the optimal distance (59 Å) for the bivalent inhibition of the trimeric hemagglutinin (HA) determined but the spatial screening also revealed a secondary carbohydrate-binding site. A comparison between the rigid DNA based scaffold and a flexible polyethylene glycol (PEG) revealed the necessity of a rigid core for a strong bivalency effect (Figure 13A). By applying rolling circle amplification (RCA) Bandlow *et al*. synthesised long sequence-repetitive DNA templates allowing for the oligomerisation of the distance-optimized bivalent binders. The most successful constructs were 1000-fold more effective per carbohydrate than the monovalent ligand.

In 2012 Matsui *et al*. reported a trigonal DNA based inhibitor designed to bridge three of the four binding sites of tetrameric Concanavilin A (ConA). DNA was equipped with either three, six or twelve maltose ligands on the 3′ terminus. Three

oligonucleotides, with carefully chosen sequences, hybridized to form a three-way junction with ligands on either all three, two, one or none of the ends. While the number of ligands per arm had little effect on the affinity, increasing the number of ligand-equipped arms drastically increased ligand potency. The best binder had an over 700 times higher affinity to ConA than monovalent mannose (38 fold affinity enhancement per ligand). [89] Interestingly, a degree of flexibility was necessary for optimal binding, which was introduced by keeping the end of each arm a single strand region. The same group also equipped the trigonal DNA scaffold with three 2,3-sialyllactose ligands per arm (Figure 13B). The nonavalent ligand was designed to bridge the distance between the sialic acid binding sites on the HA trimer leading to an 80,000 fold affinity increase (K_I = 0.25 μM) in comparison to 2,3 sialyllactose (K_I = 20 mM). The affinity of the nonavalent complex was compared with the potency of the same scaffold equipped with just one ligand per arm ((K_I = 1 μM) and the scaffold equipped with equipped with three ligands on only one arm (K_I = 2 μM). The results suggest that the 80,000-fold potency increase of the nonavalent 2,3 sialylllactose was due to both a statistical rebinding effect and a chelating effect. [90] In 2017 Machida *et al* reported a first example of dynamic cooperativity in multivalent lectin inhibiton. The bacterial Ralstonia solanacearum lectin (RSL) comprises six fucose binding sites (K_D=2μM) that are each 20 Angstroem apart. Winssinger and his group conjugated a fucose ligand to a short 4 mer PNA strand via a short PEG linker. The PNA strand was designed to be self-complementary, thereby forming a bivalent fucose ligand. Due to the low melting temperature (TM < 15 °C, at 2 μM) the PNA strands were assumed to remain in the dissociated form at concentration under 1 μM. However, in the presence of RSL the PNA duplex was stabilized as the effective concentration of PNA was increased by the fucose ligands binding to the lectin and vice versa (Figure 13C). A K_D=83 nM was determined by SPR, which corresponds to a 25-fold affinity increase in comparison to the monovalent fucose.

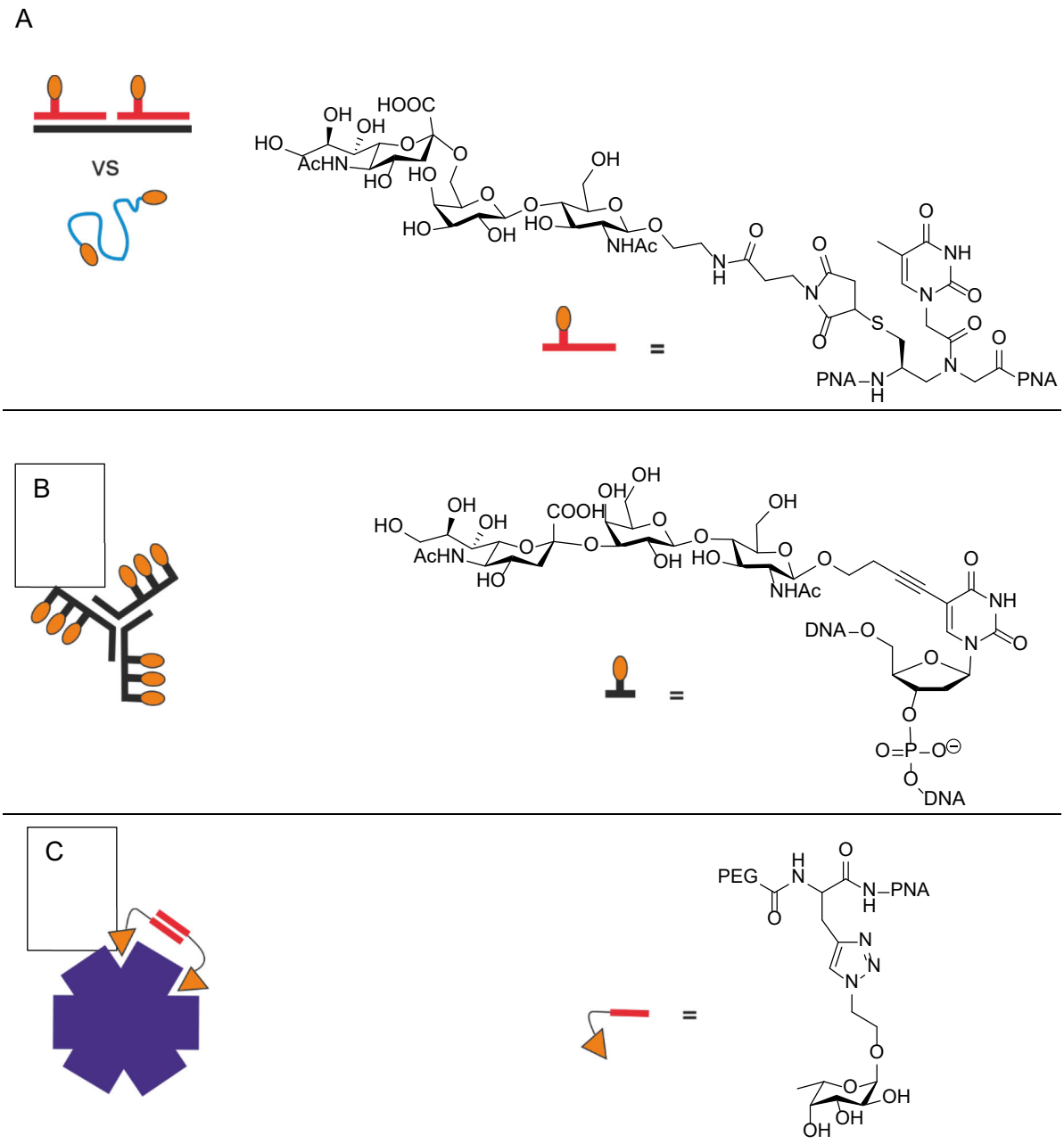

Figure 13 ▬ = DNA single strand, ▬ = PNA single strand, ~ = PEG, ● / ▲ = carbohydrate ligand A) Bandlow et al. compared the multivalency effects when bivalently presenting 2,6 sialy-LacNac on a rigid PNA-DNA duplex and a fexible PEG linker.[17] B) Matsui et al designed a trivalent DNA based scaffold and presented ligand clusters at each end to match the C3 symmetry of ConA.[89] C) Machida et al. reported dynamic cooperativity for multivalent lectin inhibition. The binding of the ligand to RSL and the formation of the duplex effectively support each other.[91]

The authors argue this was due to the positive cooperativity effect, which enabled multivalency.[91]In summary, a whole range of cores have been used to present carbohydrate ligands multivalently. The use of DNA as a scaffold has proven to be particularly advantageous, as it allows to present the ligands in a precise spatial conformation matching the target geometry and valency leading to optimised ligand

economy. Many of the examples clearly highlight that a stronger monovalent ligand leads to a larger multivalency effect. The example described by Gorska *et al*. highlights that the role of the linker between ligand and scaffold should not be underestimated. The use of statistical rebinding and the chelation effect has been described in many cases here, however only the Ebara and Bernardi groups describe systems that help understand how both effects influence each other, which was a major part of the work described here.

2.8 Glycomimetics

A common approach to develop lectin ligands with higher affinity and selectivity than the natural carbohydrate binders is the development of glycomimetics. Glycomimetics are designed to mimic the canonical ligands and function analogously. Carbohydrate based glycomimetics are assumed to retain their canonical binding mechanism. Non-carbohydrate ligands merely mimic the structure of the carbohydrate. It is very difficult to predict whether non-carbohydrate glycomimetics bind to a lectin in a canonical fashion. The rational design of glycomimetic ligands for CTLs is generally challenging. One reason are the shallow binding pockets. A deep binding pocket possesses more options for additional interaction between a modified ligand and the binding pocket. Furthermore, the canonical ligands often have multiple calcium dependent binding modes with the binding sites, which makes it difficult to predict the effect of ligand modifications.[92] Finally, off-target effects can be generated due to the cross-recognition of carbohydrate ligands between CTLs.[65]

As very few specific langerin inhibitors have been published, the focus will lie on glycomimetics designed to discriminate between DC-SIGN and langerin. Although both CTLs are related, DC-SIGN is considered to promote HIV infection while langerin can eliminate the virus by Birbeck granule formation. The design of glycomimetics that can select between both proteins has therefore received much interest from a biomedical standpoint.

Wamhoff *et al*. synthesized a range of of 2-deoxy-2-carboxamido-α-mannoside analogs and screened their affinity for langerin via a newly developed ^{19}F NMR assay. Perhaps disappointingly for the authors the mannose derivatives - except for one - afforded reduced langerin affinities in comparison to mannose. The introduction of a sulfate group at the 6 position afforded a roughly 3-fold higher affinity than mannose. This was not surprising, as 6-sulfo-galactose was previously known to be a slightly more potent langerin ligand than mannose.[93] Porkolab *et al*. carried out a detail study on the binding of acetylated glucosamine (GlcNAc) derivatives to DC-SIGN and langerin.[65] Bernardi and her co-workers were able to show how certain modifications induce langerin or DC-SIGN selectivity. In accordance with the work by the Rademacher group above, they discovered that the introduction of a sulfate group at

the position 6 of GlcNac drastically increased affinity for langerin and decreased affinity for DC-SIGN (selectivity factor roughly 600). Replacing Lysine313 for an alanine residue was shown to remove the affinity gain for langerin, highlighting the importance of K313-sulfate-interaction. By replacing the 6-position of a pseudodimannoside with a positively charged amine they were able to induce inverse selectivity. Repulsion between both positive charges is responsible for a decrease in langerin affinity. As the affinity for DC-SIGN of this amine-modified pseudomannoside is increased simultaneously (unfortunately no structural explanation is delivered), a selectivity factor of seven is achieved. [65]

Andreini *et al*. synthesised derivatives of fucose using a common fucosylamide anchor. SPR testing of their affinity for DC-SIGN and langerin gave high selectivity of these ligands for DC-SIGN. This effect was explained by the similarity of the binding mode of these fucosyl amides to Lewis X, a known inhibitor of DC-SIGN but not langerin.[66]

Apart from the exemplary discussed carbohydrate based glycomimetic approaches non-carbohydrate glycomimetics have also been developed. For example, Garber *et al*. synthesized derivatives of the natural product shikimic acid to able to mimick the 3- and 4- OH hydroxyl groups of mannose, which are essential for binding of mannose to langerin/DC-SIGN. Subsequently, they showed that their glycomimetic ligand had a slightly higher affinity for DC-SIGN than ManNAc. Furthermore, the multivalent presentation of this glycomimetic ligand on polymers synthesized by ring-opening metathesis polymerization afforded micro molar inhibitors.[94] Critically, very little is known about the binding mode of this glyomimetic ligands. While carbohydrate-based ligands are generally assumed to bind in a canonical fashion, the same assumption cannot be made for non-carbohydrate glyomimetics. A lack of knowledge about the binding site of a ligand makes the rational design of multivalent ligands impossible. The use of carbohydrate-based ligands for multivalent lectin inhibition is therefore generally assumed favourable.

Although the combination of glycomimetics and multivalency seems like an ideal tool to afford selective and very potent ligands the reality can be more complex. Carbohydrate based glycomimetics may have different binding modes than the natural

ligands. Furthermore, the mode of binding may also have an influence on the multivalency effect. In one example, Sutkevciate *et al*. examined the multivalency effects of two glycomimetics they had previously developed. Two mannose-based glycomimetics DC-SIGN inhibitors, a pseudomannobioside (IC_{50}=1.19 mM) and a linear pseudomannotrioside (IC_{50}=0.16 mM) were presented on a tetravalent dendrimer core and subsequently on full dendrimer containing 32 ligands each. Surprisingly, the tetravalent assembly afforded a similar affinity for the pseudomannobioside (IC_{50}=227 μM, β/n = 1.3) and the pseudomannotrioside(IC_{50}=120 μM, β/n = 0.3) . Infact, only the tetravalent bimannoside displayed a β/n-effect >1. On a 32-dendrimer the difference in β/n-effect was even more pronounced. The bimannoside had an 18-fold higher affinity per ligand, while the trimannoside only had a 4-fold affinity increase per ligand.[95] By combining ITC, micro calorimetry, analytical ultracentrifugation and dynamic light scattering the DC-SIGN – ligand interaction was studied and the authors revealed that the monovalent pseudomannotrioside was able to cluster DC-SIGN. However, it presumably loses this ability once presented on a multivalent scaffold.[96] These results illustrates that while it is commonly known that a higher monovalent affinity also leads to a higher multivalency effect and β-effects, this may not be the case for glycomimetics if the binding mode is changed.

3 Objective

Antigen presenting cells such as Langerhans cells play an important role in first level immune response by recognising and presenting foreign antigens to T-cells thereby activating the immune system. Langerhans cells express the receptor langerin, which can recognize pathogens by their carbohydrate surface. Because of this role, langerin is receiving increasing interest as an immunotherapy target. [22]

Despite its well-known trivalent structure[51], no molecularly defined multivalent ligands able to bridge the binding pockets have been developed. The chelate effect should lead to superior multivalency and ligand efficacy. However, a systematic investigation on the optimal multivalent ligand presentation to target langerin is pending. Neuhaus *et al*. designed trivalent flexible polymers of different lengths and equipped with one mannose unit per arm. [78] However, this led to only micromolar binders and the authors acknowledged that the optimised trivalent ligand was not able to bridge the carbohydrate binding pockets. As Bandlow *et al*. have shown that flexible polymers are inferior scaffolds for designing multivalent ligands due to a lack in rigidity, we sought to apply nucleic acid architectures as rigid scaffolds known to allow for Ångström scale precise positioning of ligands along the rigid helix. [17]

The objective of this work was the development of multivalent and selective ligands for the trimeric lectin langerin. Based on previous work in the Seitz lab we aimed to explore whether carbohydrate-PNA-DNA complexes could be applied to develop high affinity multivalent ligands for targeting langerin. We aimed to combine the development of a selective glycomimetic langerin ligand with a systematic examination of multivalent ligand arrangement to optimise not only overall avidity but also ligand efficacy. Therefore, the first aim was the development of a novel glycomimetic ligand for langerin with improved affinity and selectivity in comparison to the natural ligand mannose. Next, a DNA programmed spatial screening was to be carried out to characterize the optimal bivalent ligand presentation for langerin targeting. To this end, the distance between the ligands positioned on the DNA-based scaffold was altered to investigate the structure-activity relationship and determine the optimal ligand positioning for the chelate effect.

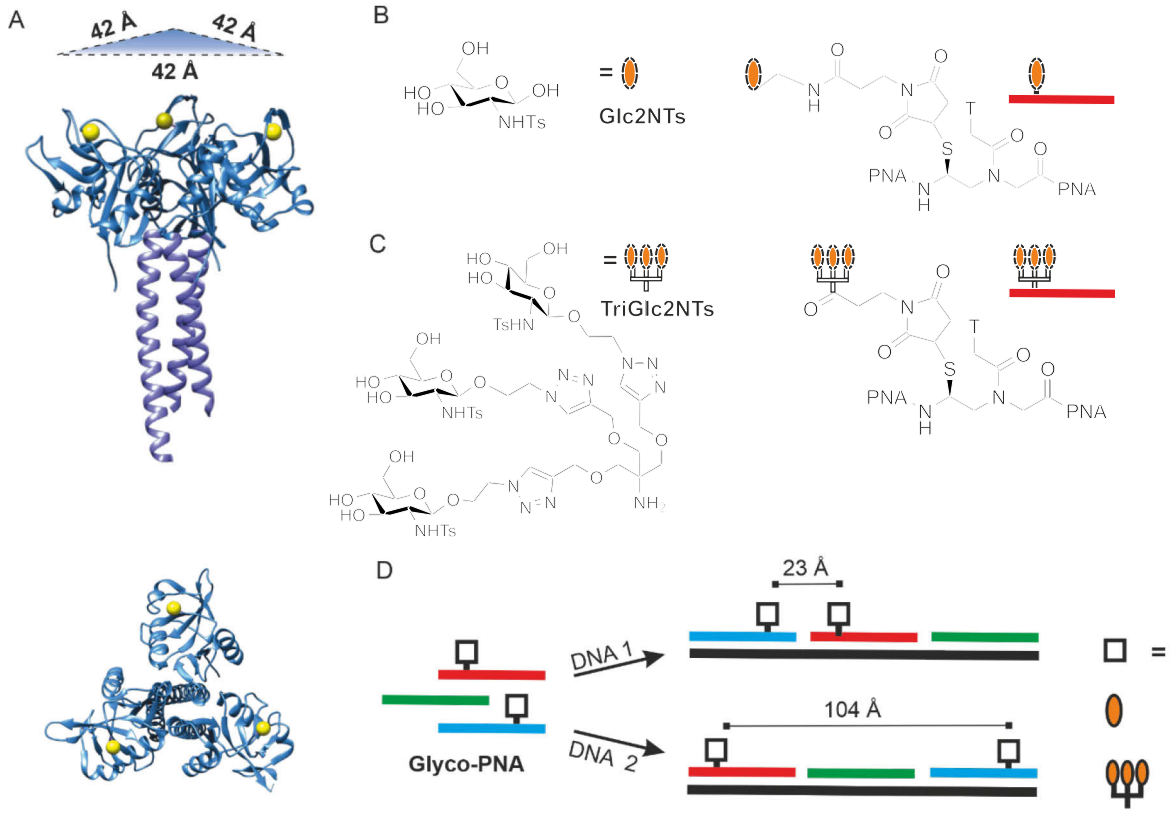

Figure 14. A) Crystal structure of the trimeric langerin extracellular domain (PDB: 3kqg) with Ca^{2+} ions (yellow) embedded in the CRD (blue) from a side view and from the top).B Glc2NTs ligand and Glc2NTs-PNA conjugates C)TriGlc2NHTs and TriGlc2NTs-PNA conjugates. D) Hybridization of modified (blue, red) and unmodified (green) peptide nucleic acid (PNA) oligomers with DNA templates (black) affords bivalent Ligand-PNA-DNA complexes with different distances between the ligands.

Next, we strived to develop a general tool for overcoming the limitations of weak monovalent ligands. It has been shown that a stronger monovalent ligand induces greater chelate multivalency effects.[36] However, in the case of mammalian C-type lectins often only weak millimolar binders are available leading to very low or no bivalency effect. Brute force approaches such as multivalent polymers[71] and liposomes[47] to overcome the weak monovalent affinities are not able to address ligand efficiency, a key advantages of precise bivalent-DNA based approaches. Therefore, the cooperativity between the statistical rebinding effect and the chelate effect was to be investigated as a strategy for improving the avidity effect. To this end a DNA based scaffold was equipped with two clusters of carbohydrate ligands and a DNA-programmed spatial screening was to be carried out. Ideally, this approach would generate greater multivalency effects without losing the structure-activity information of the DNA-based scaffolds.

Finally, we wanted to examine the selectivity of our ligands by testing the binding and internalisation capability of the optimised bivalent ligands to cells expressing either of the related mannose binding receptors langerin and DC-SIGN. The evaluation of the multivalent ligands required the development of suitable assays for these systems. We therefore explored several competitive assays. A newly developed ^{19}F-NMR assay was to be established for the spatial screening of bivalent ligands. SPR was to be established as an orthogonal assay to the 19 F-NMR. Furthermore, to detect the selectivity of the ligands on the cellular level two cell-based assays using flow cytometry for the read out were to be applied to our multivalent systems.

Based on previous work by Scheibe *et al*. a building block block system, comprised of a long DNA template and three short complementary PNA strands and allowing for the formation of multivalent Ligand-PNA-DNA complexes, was to be employed. The formation of multivalent carbohydrate-PNA-DNA complexes made the synthesis of functionalised PNA oligomers necessary. Thiol-modified and azide-modified PNA monomers were to be synthesised and incorporated in PNA oligomers. Several different carbohydrate-ligands were to be investigated as candidates for multivalent langerin binding. Hence, the development of the synthesis routes of the maleimide- or alkyne-modified ligands was necessary. Furthermore, to implement the use of ligand clusters, trivalent carbohydrate ligands clusters were to be synthesised, that could equally be conjugated to the PNA oligomers.

4 Results and Discussion

4.1 Synthesis

The objective of this work was to use DNA based scaffolds for the multivalent ligand presentation. The use of PNA-DNA scaffolds has previously been established in the Seitz lab.[15, 97] In short PNA strands with the desired modification at defined positions were synthesized by SPPS, the ligands conjugated to the PNA strands and subsequently hybridized to a long DNA strand. By varying the template and the PNA strands the distance between the ligands could easily be adjusted via this building block system. The application of the PNA-DNA double helix as a molecular ruler made the site-specific conjugation of a ligand to the PNA necessary. Several different PNA backbone modifications, which allow for post synthesis conjugation are known in the literature.[98] The Seitz lab has established the use of thiol modifications in the γ -position, allowing for thiol-maleimide conjugation. Alternatively, we also report the use of a γ-azido-modified PNA building block and the use of the the Copper catalyzed Alkyne-azide Click reaction.

4.1.1 PNA Monomer Synthesis

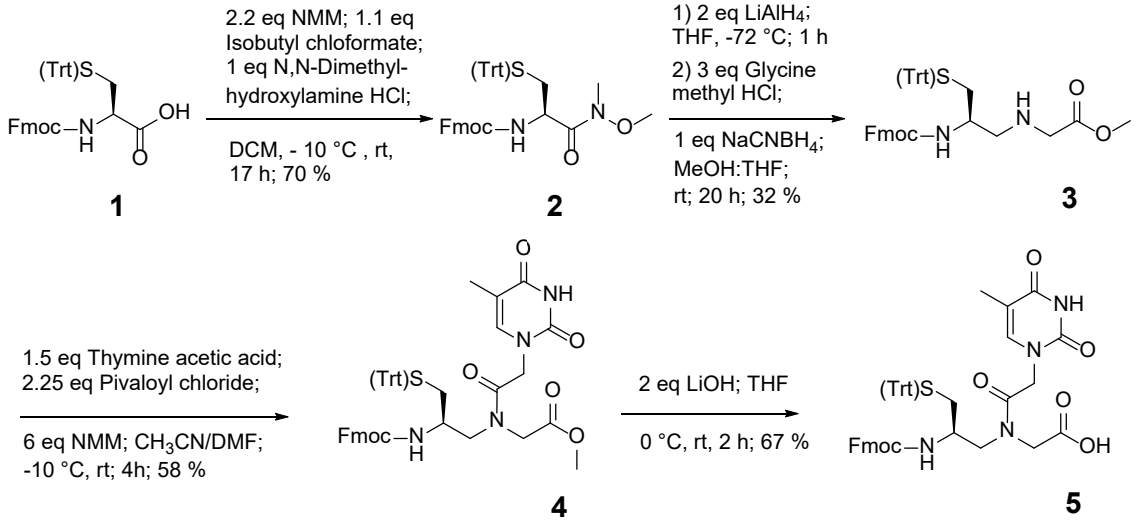

Scheme 1. Synthesis of thiol-modified PNA monomer for the thiol-maleimide conjugation strategy.[15]

According to a procedure by Scheibe *et al*. a thiol-modified PNA building block **5** (Scheme 1) was synthesized starting from Fmoc-Cysteine(Trt) **1**.

Likewise, we synthesized an azide-modified PNA building block (Scheme 2) with Fmoc-Lysine(Boc) **6** as starting material. In a first step, Fmoc-Lysine(Boc) **6** was converted to the Weinreb amide **7**. After activation of the acid with isobutyl chloroformate, N,O-dimethylhydroxylaminehydrochloride attacks the activated acid under basic conditions. The Weinreb amide **7** was selectively reduced to the aldehyde with lithium aluminum hydride at −72 °C. Without purification, the aldehyde was converted to an imine with glycine methylester and reduced to the amine **8**, which forms the PNA backbone, in a one pot reaction. Thymine acetic acid was activated with pivaloyl chloride and coupled to the amine **8** to give the intermediate product **9**.

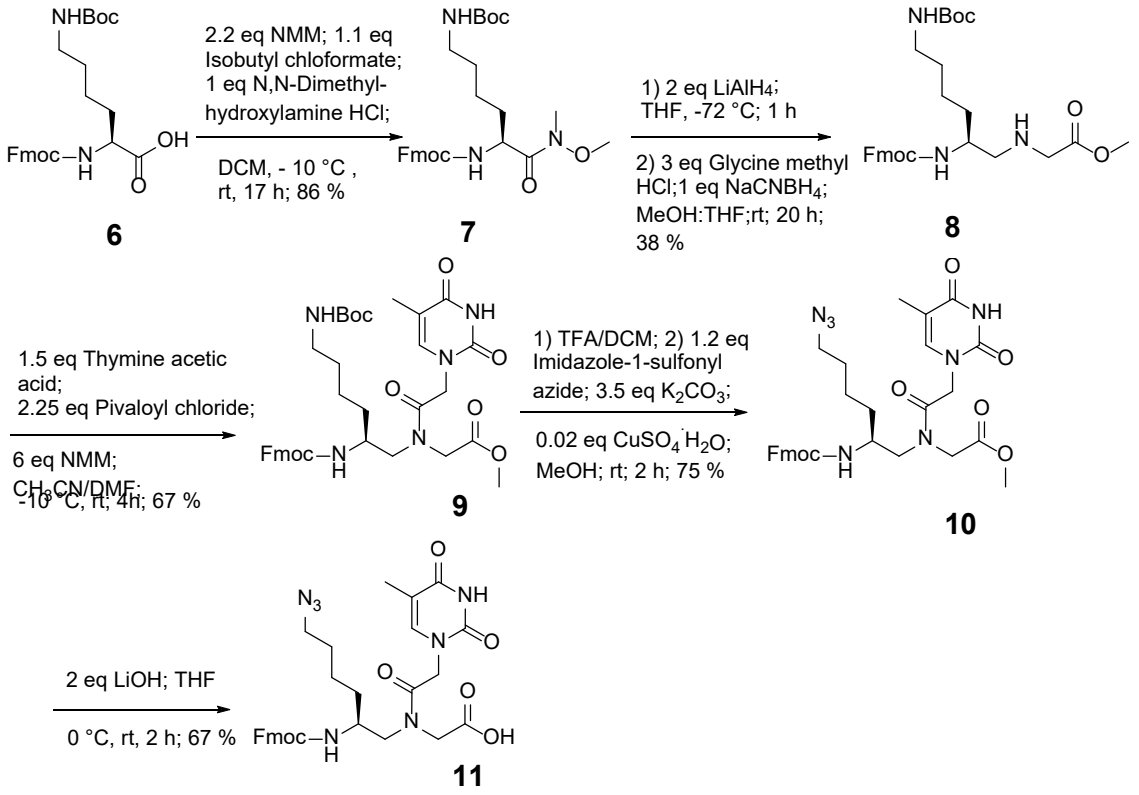

Scheme 2. Synthesis of azide-modified PNA monomer for the alkyne-azide click conjugation strategy. This work was partially conducted by Kevin Höhne (apprentice Humboldt) under my supervision.

Thereafter, the Boc group was removed under acidic conditions and the amine function transferred to an azide by reacting with the azide transfer reagent imidazole-1-sulfonyl azide under basic conditions to give **10**. Finally, acid **10** was deprotected by adding two equivalents of lithium hydroxide to yield the azide modified PNA-monomer **11**.

4.1.2 Ligand Synthesis

Depending on the conjugation chemistry required the investigated ligands were functionalized with either a maleimide- or alkyne-modification. Three ligands able to bind to the C-type lectine langerin were synthesised and functionalized. In addition, all three ligands were also synthesized as trimeric clusters. To obtain the clusters, azido functionalized ligands were synthesized, and three ligands attached covalently to a trialkyne scaffold via a copper click reaction. The reasons behind the development of these ligands will be discussed in the chapter 4.2 while the synthesis of these carbohydrate derivatives will be discussed in this chapter.

4.1.2.1 Glc2NHTs Ligands

The first ligand synthesized for this work was a tosylated glucosamine derivative. A linker was introduced via a glycosylation reaction at the anomeric centre. Both the maleimido- and the azido-functionalized derivative were utilised. In both the case of DC-SIGN and langerin the vicinal equatorial hydroxyl groups 3-OH and 4-OH of D-mannose are mainly responsible for binding to the Ca^{2+} ion, which is central in the lectin-sugar interaction.[52, 99] Modifying the reducing end of D-glucosamine therefore presumably retains the native binding mode. For the synthesis of the maleimido-functionalised Glc2NHTs ligand **23** (Scheme 3)**,** D-glucosamine hydrochloride **12** was initially converted with p-anisaldehyde to form the imine **13**. After acetylation of the alcohol groups with acetic anhydride to give the protected sugar **14** the imine was removed under acidic conditions and the amine **15** reprotected with a trichloroxycarbonyl-(Troc) protecting group. The Troc protected derivative **16** enables a strong neighbouring group participation, which allowed for the anomerically controlled glycosylation reaction with ethanethiol in the presence of borane trifluorid as activator. Subsequently, a second glycosylation with N-Cbz-amino ethanol using Dimethyl(methylthio)sulfoniumtri-fluormethansulfonate (DMTST) to activate the thioglycoside **17** lead to the formation of the β-anomer acetal product **18**. Treatment of the Troc protected glucose amine derivative **18** with zinc in acetic acid led to the reduction and removal of the Troc group.

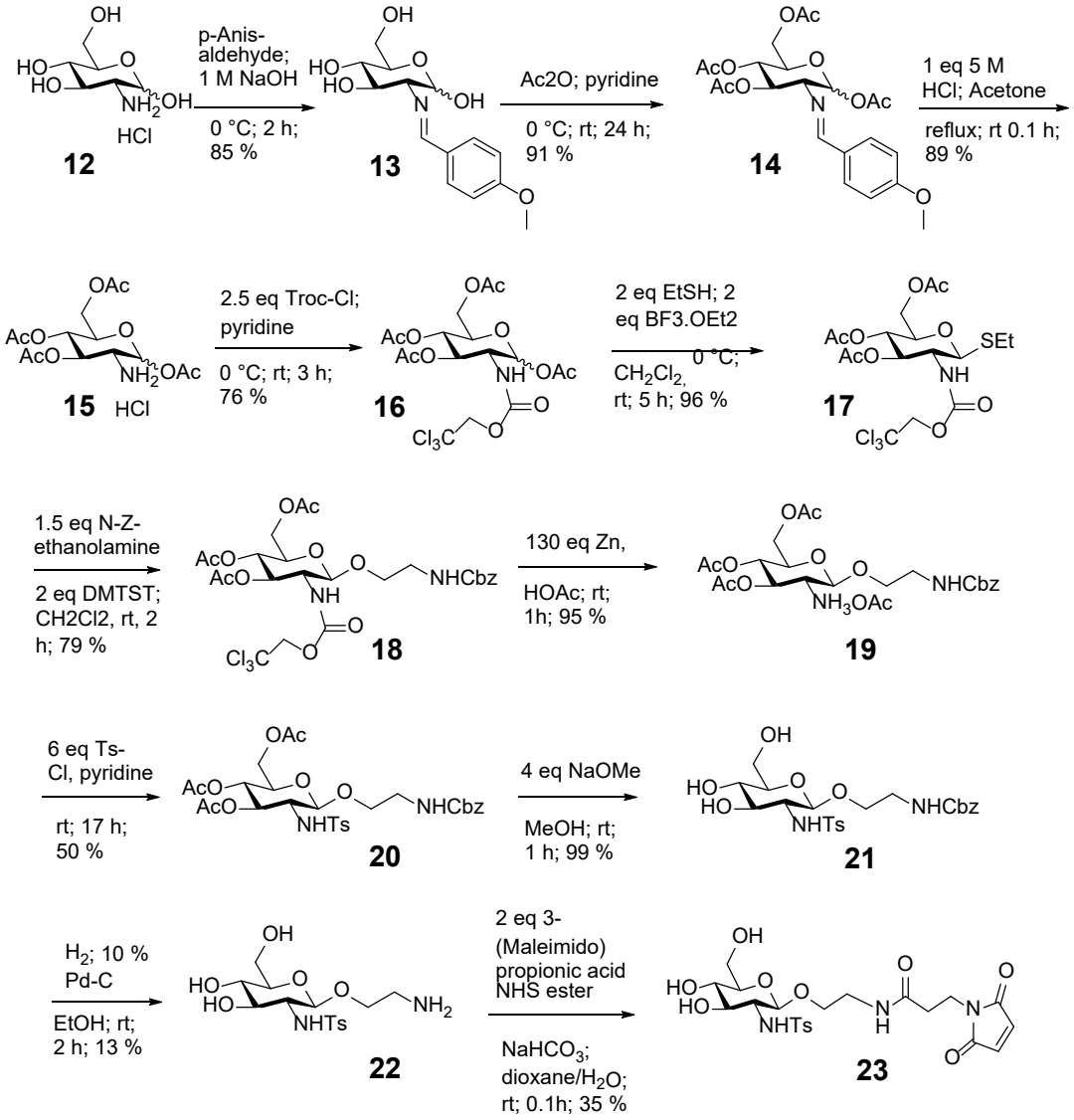

Scheme 3. Synthesis of the maleimide linker modified Glc2NHTs ligand by introducing a 2-aminoethyl-linker at the C-1 position and subsequently introducing the maleimide functionalization.

After extensive drying of the residue to remove any remaining acetic acid molecule **19** was dissolved in pyridine and six equivalents of tosyl chloride added. Although this led to the desired sulfonamide product **20,** both UPLC and TLC control showed the formation of a second product, which was identified as the acetylated amine. It was believed that the acetate counter ion may be activated by the tosyl chloride and then in a second step acetylate the amine. The procedure was optimized by dissolving molecule **19** in ethyl acetate after Troc removal and deprotonating the amine with saturated sodium hydrogen carbonate solution, which led to improved yields (50 % vs 20 %). In the final steps the acetate protecting groups were removed by addition of sodium methoxide (**21)** and the Cbz group was removed by hydrogenation to give the

amine functionalised Glc2NHTs derivative **22**. Under mildly basic conditions, the amine was converted to the desired maleimide **23** by addition of 3-(Maleimido) propionic acid) N-hydroxysuccinimide ester.

An alkyne modified version of Glc2NHTs was synthesised following a similar procedure (Scheme 4). The Troc-protected sugar **16** was converted with propargyl alocohol in the presence of boron trifluoride as activator to yield the alkyne-modified sugar **24**. The Troc protecting group was removed and the amine converted to the sulfonamide **25** by reacting with six equivalents of tosyl chloride. The removal of the acetate-protecting groups under basic conditions led to the desired alkyne functionalized Glc2NHTs **26.**

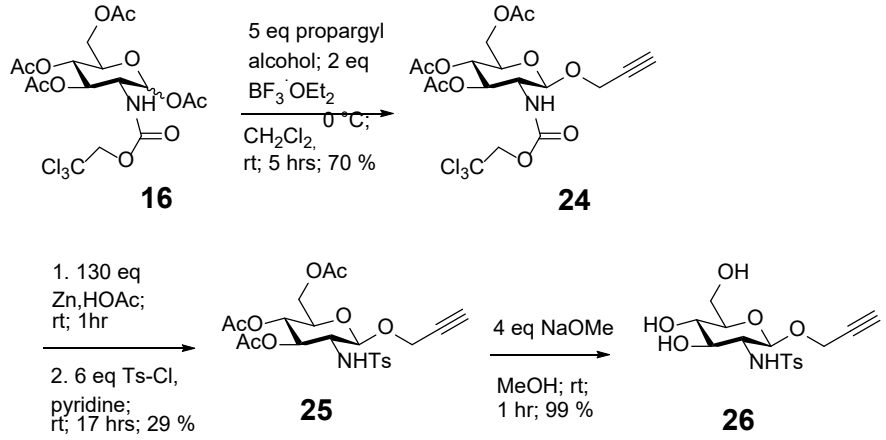

Scheme 4. Synthesis of the alkyne- modified Glc2NHTs ligand.

The synthesis of a trivalent version of Glc2NHTs (TriGlc2NHTs **31**) required a small trivalent alkyne scaffold **30** and the azide functionalized ligand **29**. The trialkyne **30** was synthesised according to a literature procedure from Tris(hydroxymethyl)aminomethane (TRIS) by reacting N-Boc-protected TRIS with propargyl bromide before deprotecting the amine under acidic conditions. The azide modified Glc2NHTs **29** was synthesised (Scheme 5) by functionalising the Troc-protected sugar **16** with bromoethanol in the presence of boron trifluoride as activator. The Troc protecting group was removed and the amine tosylated as described before. Subsequent substitution of the bromide with an azide and the removal of the acetate-protecting groups under basic conditions led to the desired azide functionalized Glc2NHTs **29** (Scheme 5).

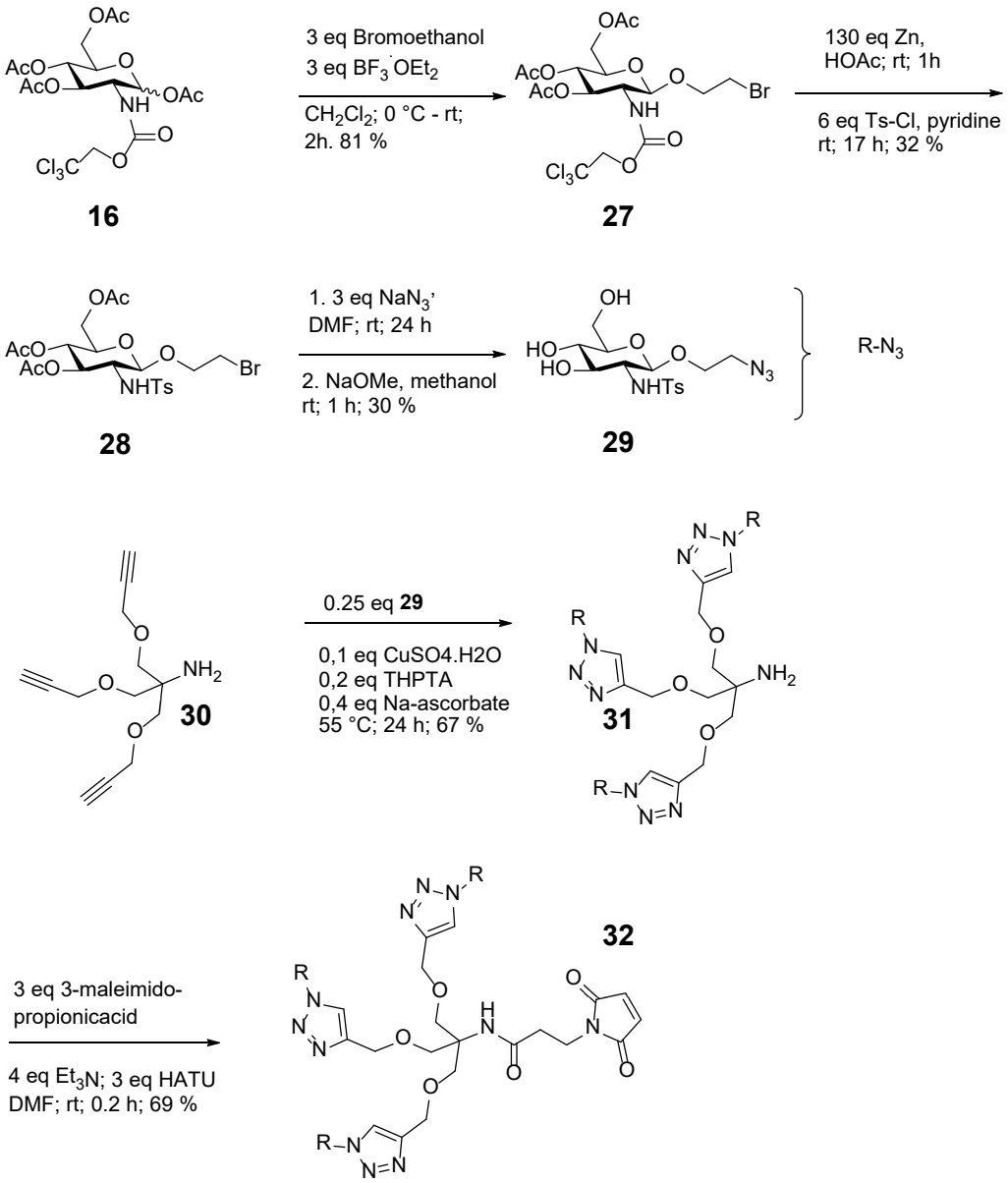

Scheme 5. Synthesis of TriGlc2NHTs. Three azide modified Glc2NHTs ligands were attached to a trivalent alkyne scaffold via a click reaction.

Three azide modified ligands were attached to the trialkyne scaffold **30** via a click reaction (Scheme 5). The reaction of **31** with 3-(Maleimido) propionic acid N-hydroxysuccinimide ester was not successful, presumably due to the steric hindrance of the trivalent scaffold. Instead, 3-maleimdo propionic acid was activated with HATU before addition to the amine **31** , which led to maleimido-functionalised TriGlc2NHTs **32**.

4.1.2.2 Mannose Ligands

The functionalization of mannose (Scheme 6) was achieved by introducing a linker at the anomeric center according to a procedure by Scheibe *et al.*[100] D-mannose **33** was acetylated with acetic anhydride under basic conditions to give the protected sugar **34**. A glycosylation reaction with bromo ethanol gave the α-glycoside **35**. The bromide **35** was converted to the azide **37** by reacting with sodium azide. The azide **37** was subsequently reduced to the amine **38** under hydrogenation conditions. Finally, the maleimido-moiety was introduced to yield the maleimido-functionalised mannose **39**.

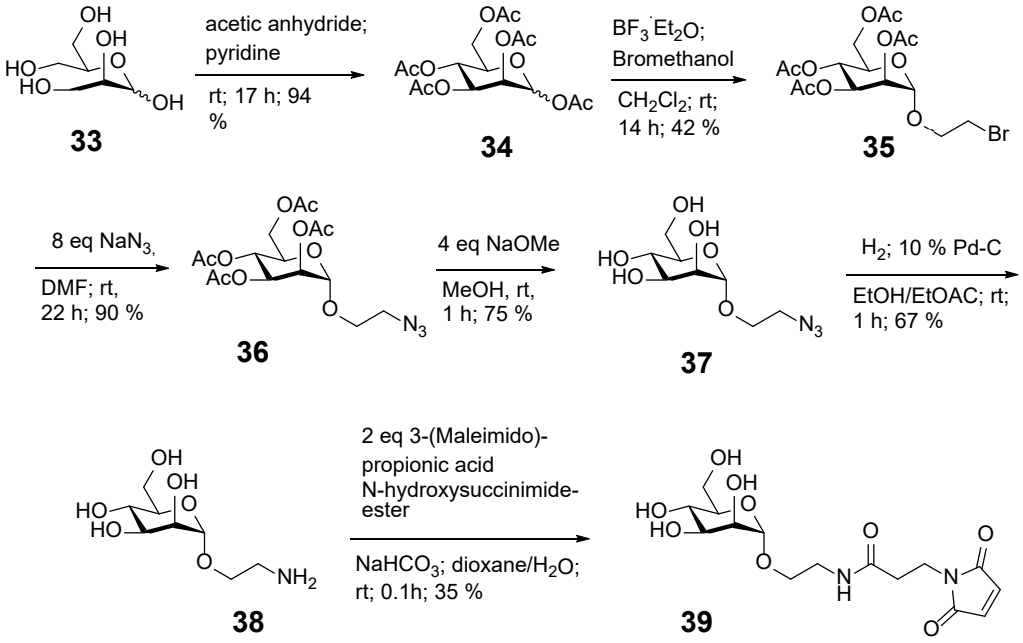

Scheme 6. Synthesis of the linker modified mannose ligand by introducing a 2-aminoethyl-linker at the C-1 position and subsequently introducing the maleimide functionalization.[15]

A trivalent mannose ligand, TriMan **40,** was synthesized (Scheme 7) according to the same procedure as for TriGlc2NHTs starting from the azide modified mannose **37** and the trivalent alkyne scaffold **30**. As before, TriMan **40** was converted to the maleimeido-functionalised TriMan **41** by reacting with 3-Maleimdo propionic acid using HATU.

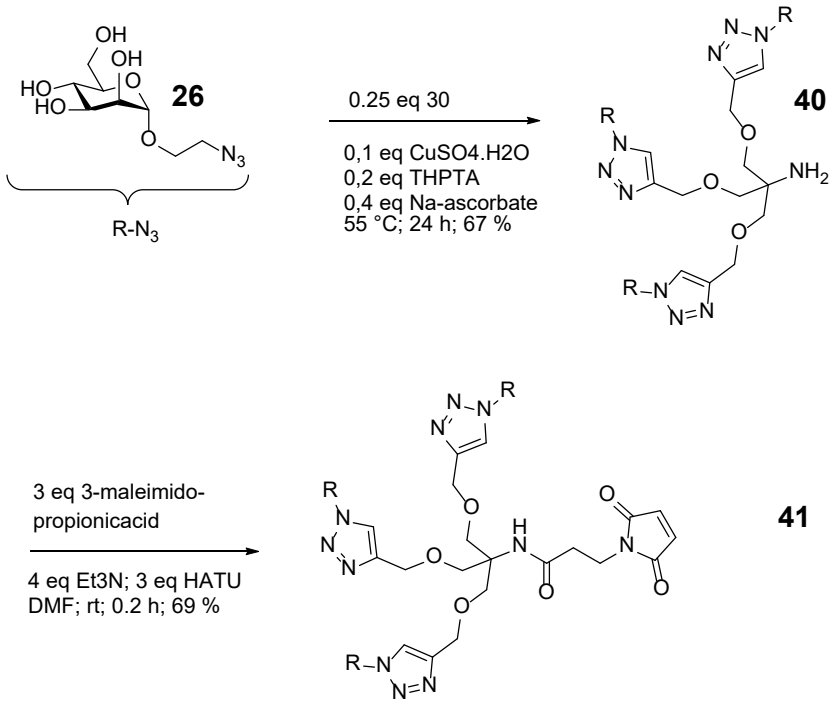

Scheme 7. Synthesis of TriMan. Three azide modified mannose ligands were attached to a trivalent alkyne scaffold via a click reaction.

4.1.2.3 BiPhMan Ligands

A biphenyl derivative of mannose, BiPhMan **49**, previously discovered by Eike Wamhoff was synthesized. Unlike for Glc2NHTs and mannose the linker was attached via the 6-OH. This was due to the design of the ligand, which had been modified with a biphenyl group at the anomeric centre. The biphenyl group was important for binding of the BiPhMan ligand to the CRD as shown in STD NMR experiments by Eike Wamhoff.92 The synthesis route applied by Wamhoff was comprised of a total of 14 steps (from mannose to the amine functionalized BiPhMan ligand 49). 92 Therefore, a novel synthesis route (Scheme 8) that reduced the total number of steps to only 10 was developed. This work was partially conducted by Gary Domeniconi (École polytechnique fédérale de Lausanne) during his research internship under my supervision. To begin, the 6-OH of mannose **33** was tosylated under basic conditions before an excess of acetic anhydride was added to protect the remaining alcohol groups. Afterwards, the tosylate group of the protected sugar **42** was substituted with

sodium azide at elevated temperatures.

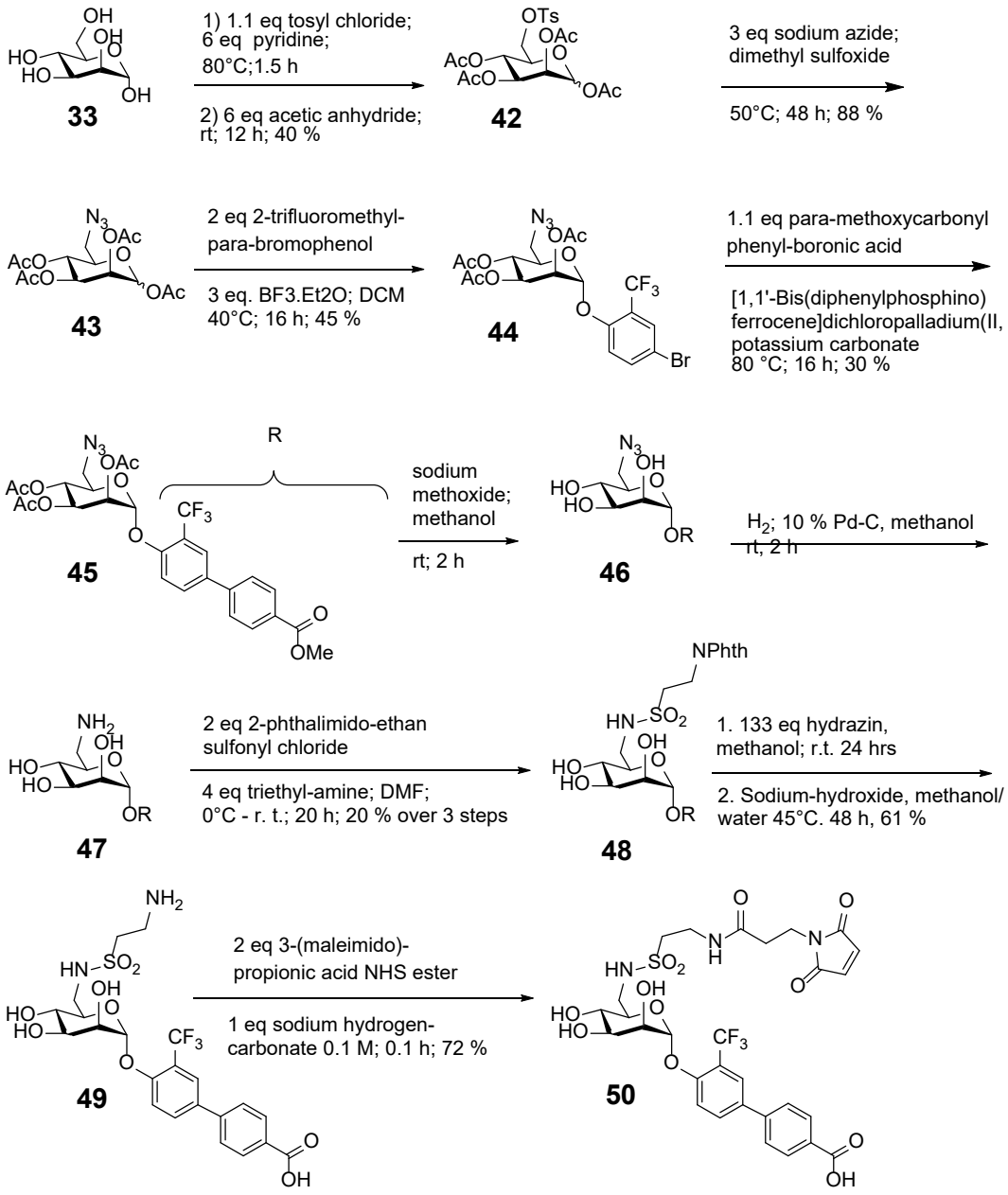

Scheme 8. Synthesis of Maleimide functionalized BiPhMan ligand starting from mannose. This synthesis was partially conducted by Gary Domeniconi during his internship under my supervision.

By replacing DMF with DMSO as solvent the yield for product **43** improved dramatically from 14 to 88 %. Next, the glycosylation reaction with the phenol in the presence of boron trifluoride selectively afforded the acetal **44**. In a Suzuki type reaction the biphenyl derivative **45** was formed by coupling the bromophenyl glycoside with the para-methoxycarbonylphenyl-boronic acid. Thereafter, the acetate groups were removed addition of sodium methoxide in dry methanol to avoid deprotection of the acid. Subsequent hydrogenation of the azide **46** afforded the amine

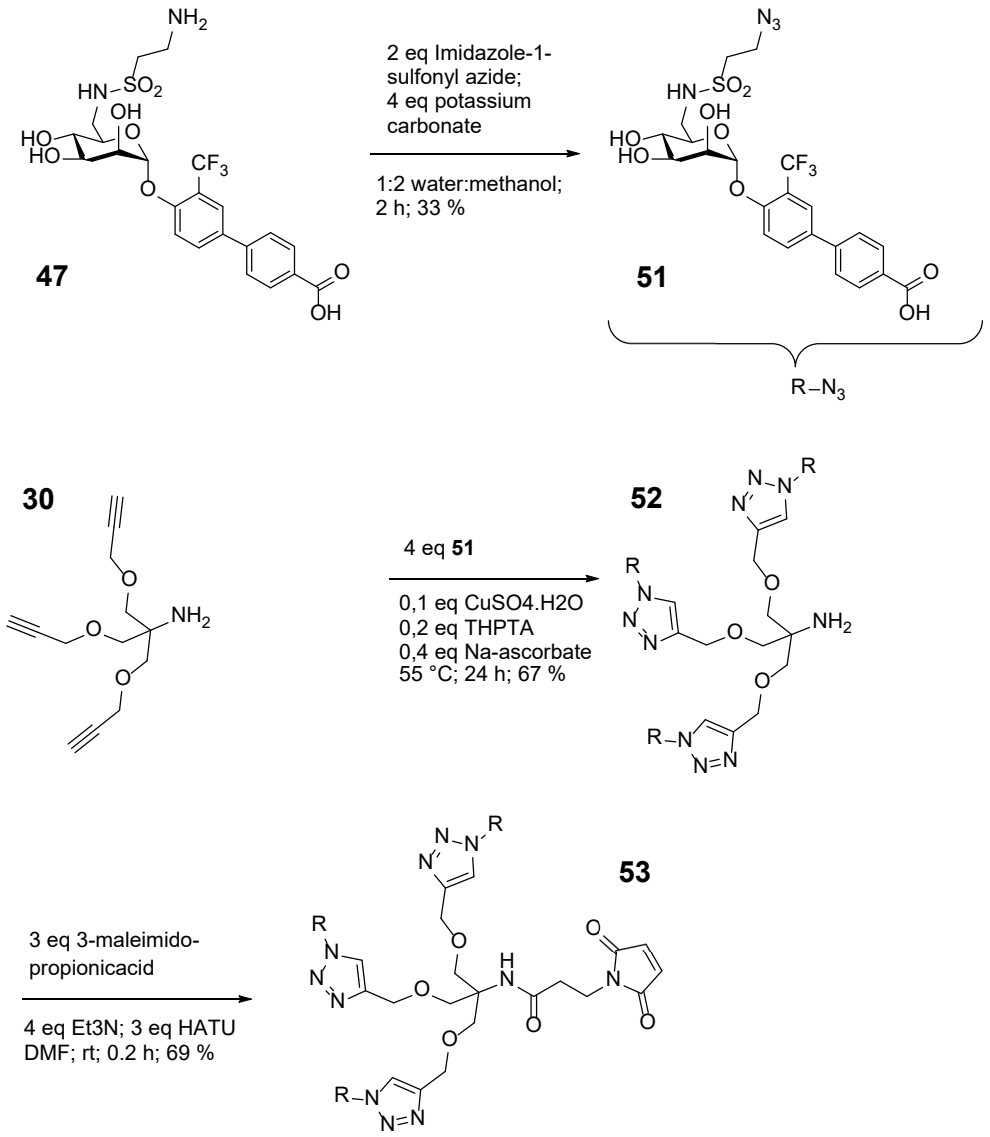

Scheme 9. Synthesis of TriBiPhMan. Three azide modified TriBiPhMan ligands were attached to a trivalent alkyne scaffold.

47. The amine was converted with 2-phtalimidoethanesulfonyl chloride to introduce the desired sulfonamide function and linker. The phthalimide **48** was deprotected by the addition of hydrazine monohydrate before deprotecting the acid by adding lithium hydroxide, water and elevating the reaction temperature to 45 °C. As previously the amine functionalized ligand **49** was converted to the maleimide **50** by adding maleimidopropionic acid NHS ester under mildly basic conditions .It should be noted that Gary Domeniconi discovered that replacing the first two steps (tosylation, acetylation) by a slightly longer route gave higher yields due to a much easier isolation of the desired compounds. Mannose was first tritylated and subsequently acetylated. Next the trityl-protecting group was removed under acidic conditions and the free

alcohol group tosylated under basic conditions. The cleaner product is presumably due to the much higher selectivity of the 6-OH for tritylchloride than tosylchloride. Despite the additional steps the overall yield for azide **44** was therebye increased from 35 to 66 %.

In order to synthesise the TriBiPhMan ligand **52** an azide moiety was introduced to molecule **49** via an azide transfer reaction. Three azide functionalized ligands **51** were attached to the same trialkyne scaffold **30** to afford the TriBhMan ligand **52** using the established azide-alkyne cycloaddition (Scheme 9). The maleimide-functionalised BiPhMan **53** was introduced by coupling 3-maleimido propionic acid to the amine of the scaffold.

4.1.3 PNA-Oligomer Synthesis

The PNA-oligomers required in this work were synthesized by automated SPPS using a Fmoc/Bhoc strategy. To increase the solubility each of the 13 nucleotides long PNA strands were equipped by an additonal lysine (C-terminus) or one additional lysine (C-terminus) and two additional aspartates (N-terminus). The coupling of all monomers including the thiol- and azide-modified PNA monomers was carried by the following a SPPS coupling method (Scheme 10) as demonstrated by Scheibe *et al*. [15] The solid phase consisted of Fmoc TentaGel® R Ram rink amide resin. HOBt was added to the coupling conditions of the amino acids to avoid racemization. First the Fmoc protected N-terminus was deblocked with 20% piperidine (DMF). Then the carboxylic acid of the PNA building block was preactivated with HCTU and NMM and added to the resin. The cycle was completed by capping any unreacted amines with a solution of acetic anhydride:lutidine:DMF 5:6:89. A double coupling was applied to the first amino acid and all building blocks after the tenth position. Nine different PNA sequences (Table 2) were synthesized in this work. One PNA strand was left unmodified. Unmodified PNA was cleaved with a solution of TFA:TIS 95:5. Five PNA strands included a thiol modification at the positions 4(2x), 10 (2x), 6. One PNA strand was modified with two thiols at the positions 4 and 9. Thiol modified PNA **54** was cleaved with a solution of TFA:EDT:TIS 95:3:2 to avoid disulfide formation. Two azide modified PNA strands were synthesized with azido-modified thymine at the

positions 4, and 4 and 10. The azide-modified PNA strands **55** were not cleaved from the resin but first conjugated to the ligand on the resin in the next step.

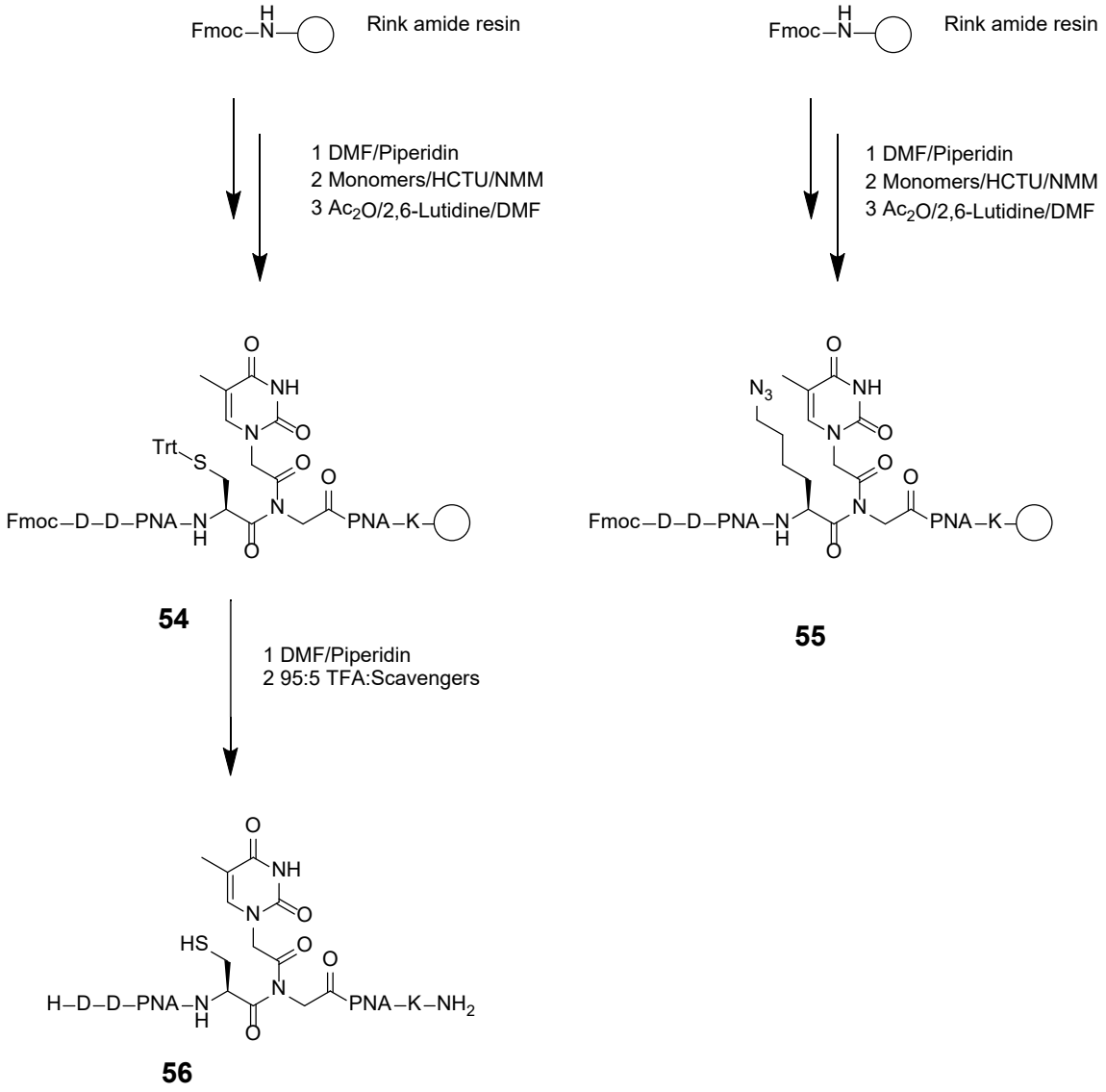

Scheme 10. A) SPPS of thiol-modified PNA B) SPPS of azide-modified PNA. The azide-modified PNA was not cleaved from the resin before the ligation step.

Table 2. Overview of synthesized PNA oligomers t* = thiol modified thymine t$^{\#}$= azide modified thymine

PNA-Oligmer	Position of modification	Sequence
S1	-	tcatcgccttcta
S2	4	actt*acttcacgc
S3	4	acct*atggacttt
S4	10	aactcctact*cct
S5	10	atgctacgtt*gac
S6	6	atacat*ccaacac
S7	4, 9	tcat*tcact*cggc
S8	4	acc t$^{\#}$at gga cttt
S9	4; 9	tcat$^{\#}$tcact*cggc

4.1.4 Ligand-PNA Conjugates

The previous chapter explained the synthesis of maleimide- and alkyne-functionalized ligands as well as the synthesis of thiol- and azide-modified PNA. In a next step, these building blocks were used to afford the desired ligand-PNA conjugates. The thiol-maleimide reaction (Scheme 11) was carried out at pH=6.5 in a phosphate buffer. At pH=6.5 the maleimide is stable towards hydrolysis but readily attacked by the nucleophilic thiol. Although pH = 6.5 should prevent disulfide formation, 0.3 mM TCEP was added as a reducing agent. A two-fold excess of ligand was added to the thiol-modified PNA and the conversion monitored by UPLC. Usually, the reaction was complete in a matter of minutes. The conjugates were purified by HPLC. This method was applied to all thiol modified PNA strands. Typical yields lay in the range of 40-80 % for the conjugation step and were limited by the product loss during HPLC purification.

4.1.4.1 Synthesis of Ligand-PNA Conjugates by Thiol-Maleimide Conjugation

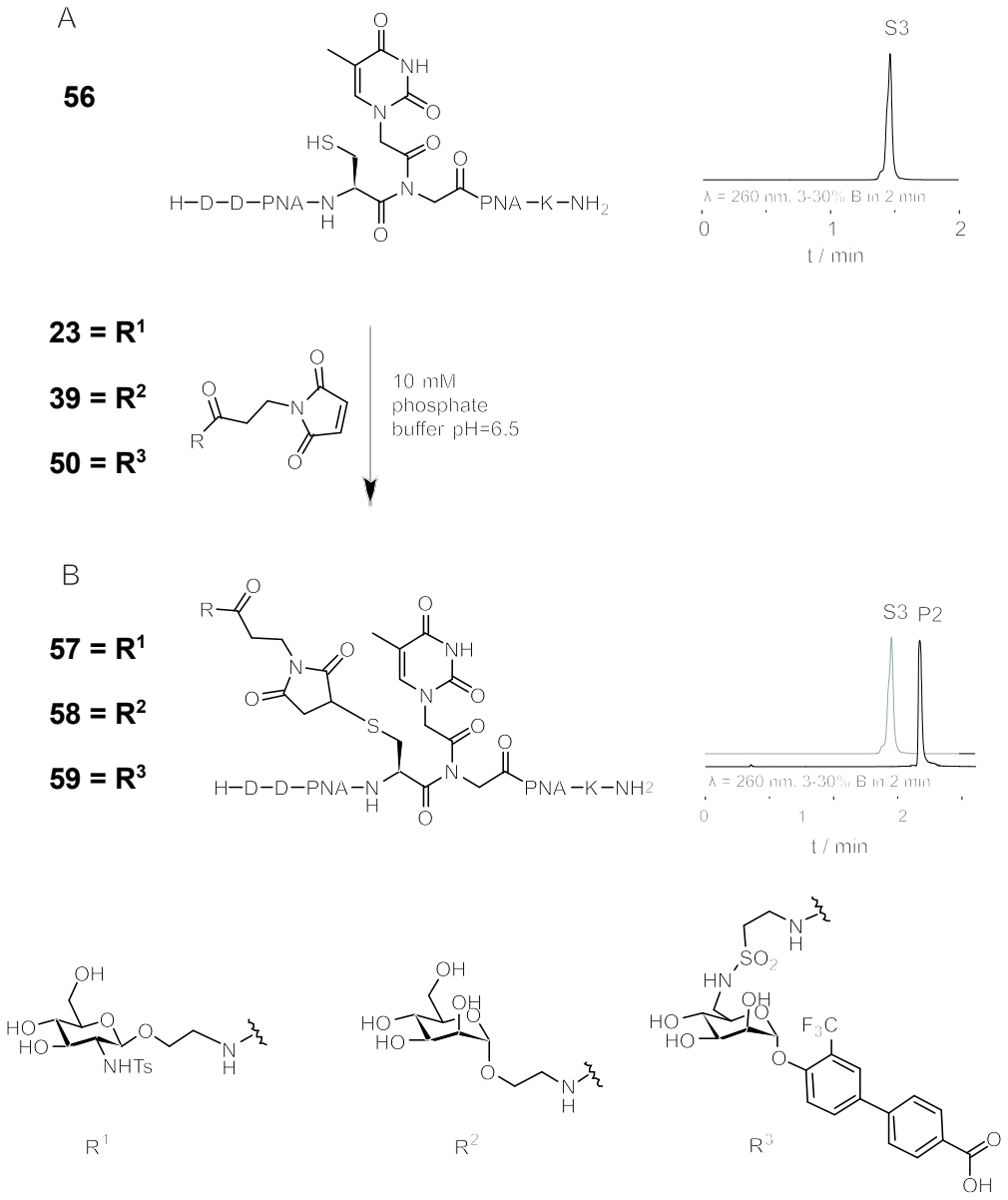

Scheme 11 Synthesis of Ligand-PNA conjugates via thiol-maleimide conjugation. A) Structure of thiol-modified PNA and exemplary HPLC trace (Absorption at λ = 260 nm, 03-30 %B in 2 min, then 90 %B) of starting material PNA S3. B) Structure of thiol-maleimide conjugation product and exemplary HPLC trace (Absorption at λ = 260 nm, 03-30 %B in 4 min) of unpurified product PNA P13 (black) and starting material S3(grey). Conditions: 2 eq. Ligand-maleimide (10 mM) **56** was added to a solution of thiol-modified PNA (100 µM) in phosphate buffer (10 mM, pH = 6.5).

Table 3. Overview of Glc2NHTs-PNA and TriGlc2NHTs-PNA conjugates synthesised via thiol-maleimide ligation. t^G = Glc2NHTs-modified thymine base; t^M = mannose-modified thymine base, t^B = BiPhMan-modified thymine base.

PNA	Structure	Position of modification	Sequence
P1		-	tcatcgccttcta
P2		4	acc t^Gat gga ctt t
P3		4	actt^{G}acttcacgc
P4		10	atgc tacg tt^{G}ga c
P5		10	aactcctact^{G}cct
P6		6	atac at^{G}cc aaca c
P7		4, 9	tcat^{G}tcact^{G}cggc
P8		4	acc t^Mat gga ctt t
P9		10	atgc tacg tt^{M}ga c
P10		4	acc t^Bat gga ctt t
P11		10	atgc tacg tt^{B}ga c

4.1.4.2 Synthesis of Glc2NHTs-PNA Conjugates by Alkyne-Azide cycloaddition

The Seitz lab has experienced no to very low yields when applying the copper catalyzed alkyne-azide cycloaddition reaction to PNA in solution, which is most probably due to coordination of the copper by PNA. The strained alkyne-azide cycloaddition reaction is a commonly applied alternative.[101] However, this would have had a large influence on the size of the linker between the PNA and ligand, which was not desired. Instead, the click reaction was carried out on solid phase (Scheme 12). *The* resin, equipped with the azide-modified PNA, was swollen in a solution of DMF saturated with Copper iodide and an excess of DIPEA added. After adding 4 equivalents of the alkyne functionalized ligand the reaction vessel was shaken overnight or longer. The progress of the reaction was

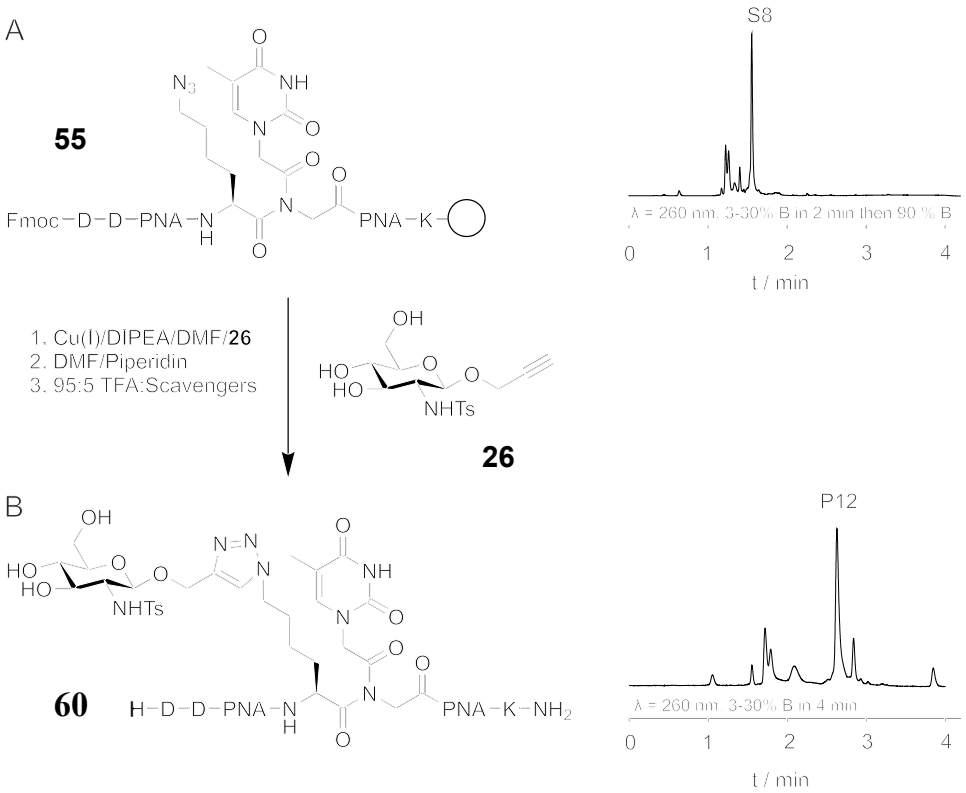

Scheme 12. Synthesis of Glc2NHTs-PNA conjugates via Copper cataylsed Alkyne-Azide Cycloaddition. A) Structure of starting material (on resin) and exemplary HPLC trace (Absorption at λ = 260 nm, 03-30 %B in 2 min, then 90 %B) of starting material PNA S8. B) Structure of azide-alkyne cycloaddition product and exemplary HPLC trace (Absorption at λ = 260 nm, 03-30 %B in 4 min) of unpurified product PNA P12. Conditions: Resin with azide-modified PNA **55** (resin loading: 2µmol) was swollen in 100 µL DMF and 4 eq. (8 µmol, 3 mg) Alkyne-modified Glc2NHTs **26** (dissolved in 50 µL DMF) added.

followed by mini cleavages and UPLC monitoring. If the conversion took longer than 48h fresh Copper iodide/DMF solution was added. The conjugates were purified by HPLC. This method was applied to synthesize two different PNAs with ligands at the position 4, and positions 4 and 9. Typically, yields of 10-20 % were achieved with this method (based on the initial loading of the resin). A drawback of this method was the much higher quantity of ligand necessary. The conjugates and complexes constructed by this method will be marked with the addition “short”, as the distance between the PNA backbone and the ligand is considerably shorter than with the thiol-maleimide ligation, as will be discussed later.

Table 4. Overview of Glc2NHTs-PNA conjugates synthesized via copper catalysed azide-alkyne cylcoaddition $t^{G\text{-}Short}$ = Glc2NHTs modified thymine base.

Number	Structure	Position of modification	Sequence
P12		4	acc $t^{G\text{-}Short}$at gga ctt t
P13		4, 9	tcat$^{G\text{-}Short}$tcact^{4}cggc

4.1.4.3 Synthesis of TriLigand-PNA Conjugates

Conjugations were carried out analogously to the thiol-maleimide strategy applied previously to monoligand-PNA conjugates.

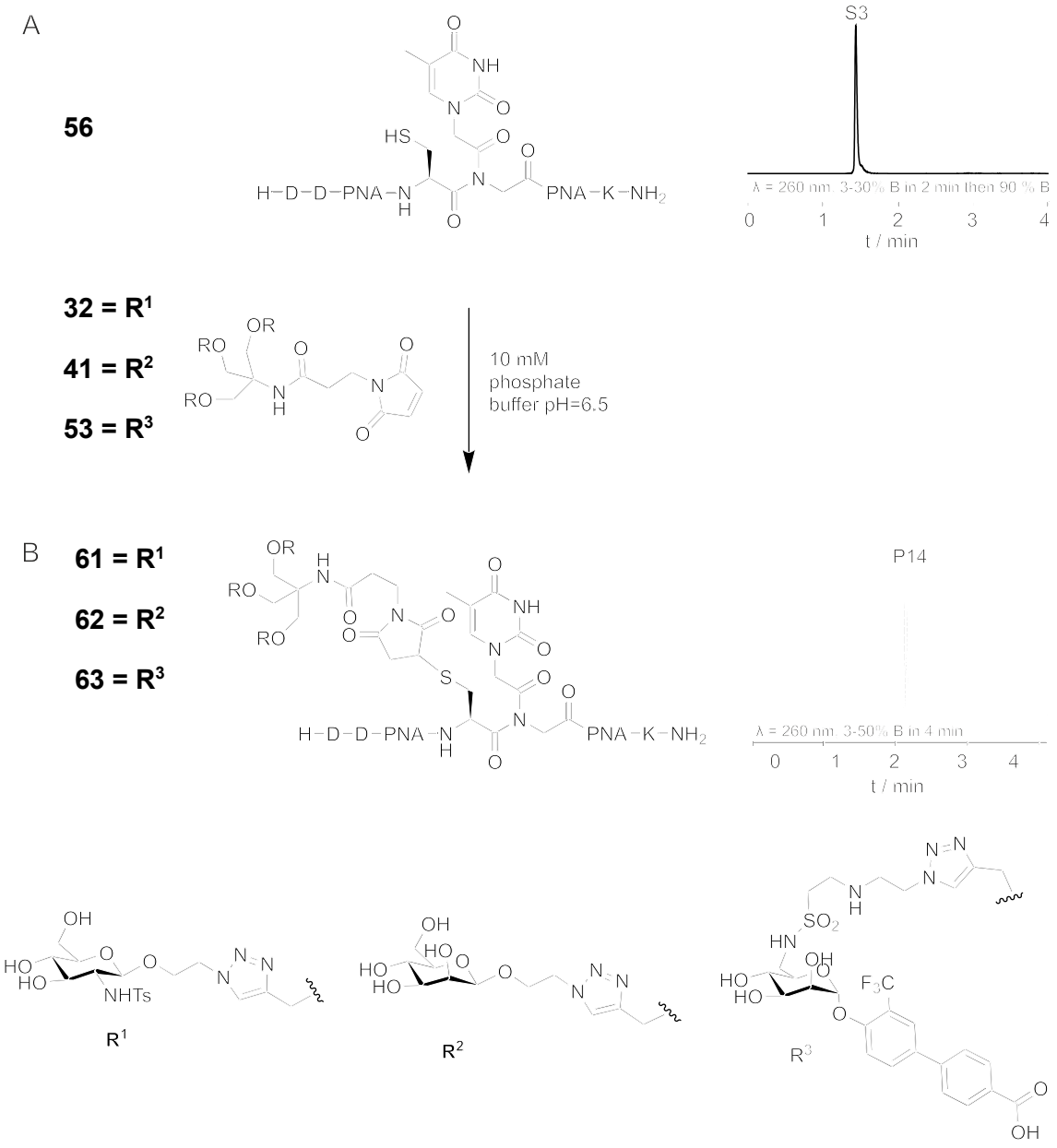

Scheme 13. Synthesis of TriLigand-PNA conjugates. Thiol-maleimide conjugation. A) Thiol-modified PNA and exemplary HPLC trace (Absorption at λ = 260 nm, 03-30 %B in 2 min, then 90 %B) of starting material PNA S8. B) Structure of azide-alkyne cycloaddition product and exemplary HPLC trace (Absorption at λ = 260 nm, 03-30 %B in 4 min) of unpurified product PNA P12. Conditions: 2 eq. TriLigand-maleimide (10 mM) was added to a solution of thiol-modified PNA (100 µM) **56** in phosphate buffer (10 mM, pH = 6.5)

At pH = 6.5 a three-fold excess of maleimide-functionalized ligand was added to the thiol-modified PNA and the conversion monitored by UPLC (Scheme 13). Usually, the reaction was complete in a matter of minutes. The conjugates were purified by HPLC.

Table 5. Overview of Triligand-PNA conjugates synthesised via thiol-maleimide ligation t^{TriG} = TriGlc2NHTs-modified thymine base; t^{TriM} = TriMan-modified thymine base; ; t^{TriB} = TriBiPhMan-modified thymine base.

PNA	Structure	Position of modification	Sequence
P14		4	actt^{TriG}acttcacgc
P15		10	aactcctact^{TriG}cct
P16		4	acc t^{TriM}at gga ctt t
P17		10	atgc tacg tt^{TriM}ga c
P18		4	acc t^{TriB}at gga ctt t
P19		10	atgc tacg tt^{TriB}ga c

4.1.5 Ligand-PNA-DNA Complex Formation

The synthesis of ligand-PNA strands by two different conjugation methods has been described. The PNA strands were modified site specifically and hence bore the ligands at defined positions. The addition of a DNA template with 39 nucleotides allows for the positioning of up to three PNA-oligomers in a defined order. By making use of different DNA templates, bivalent ligand complexes with a defined space between the ligands can be obtained. Due to the known helical structure of the PNA-DNA duplex and the defined distance between the nucleotides the distance between the ligands can easily be estimated. The melting temperatures (Table 6) of the presented ligand-PNA-DNA complexes were measured to ensure the stability of the complexes for their use under assay conditions (Figure 15). In general, the PNA-DNA complexes were found to have sufficiently high and very similar melting temperatures between 62 and 66°C meaning the duplexes were stable for use in nanomolar concentrations.[102] A

comparison between PNA strands of the same sequence but with different ligands found that the ligand modification has very little influence on the duplex stability. As some experiments were later performed at 10 % DMSO conditions for better solubility the influence of DMSO on the melting temperature was also examined. It was found that the melting temperature drops by roughly 3 °C for 10 % DMSO and 6 °C for 20 % DMSO. Hence, the complexes were also deemed stable in a 10 % DMSO/ buffer solution. Due to the helical structure of the duplexes the ligands are not only in a defined distance to one another but also in a defined angle. To reduce the influence of this angle the complexes were designed with nick sites between the modified PNA strands, which allows for rotational freedom. Additionally, the linker between the PNA backbone and the ligand should allow for some flexibility. However, it should be noted that P7 and P13 bear two ligands on one PNA strand. Therefore, there is no nick site between the ligands when these PNA strands were used.

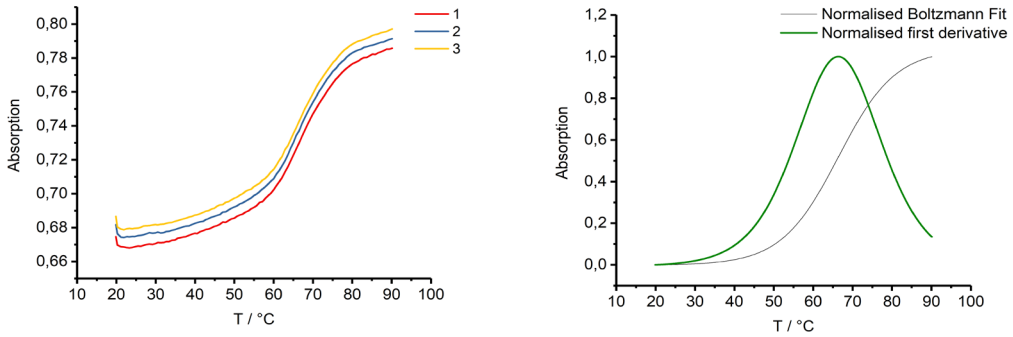

Figure 15. UV melting curves (red, blue, yellow), normalized Boltzmann Fit (black) and normalized first derivative(red) for a bivalent (G-104) PNA-DNA-complex shown exemplary. Conditions: 1 µM complex, 10 mM NaH_2PO_4, 100 mM NaCl, pH 7.0.

Table 6 lists the complexes formed in this work. The naming follows a scheme: The first letter determines the ligand (G = Glc2NHTs, M = mannose, B = BiPhMan, TG = TriGlc2NHTs, TM = TriMan, TB = TriBiPhMan). The number after the first dash is the estimated distance between the ligands. Complexes with only one ligand bear the word Mono instead of a number. Complexes with no ligand are abbreviated with nL. In some cases, additional information is given after a second dash. G-42-S describes the ligand conjugated to the PNA by the copper click cycloaddition (S = short). G-42-O means the DNA has a 10mer single strand DNA overlap. G-42-F3 refers to complexes with added flexibility. F3 corresponds to a single strand region of three nucleotides between the ligands. G-42-Cy5 uses Cyanine 5 tagged DNA.

Table 6 List of ligand-PNA-DNA duplexes. The complex name is comprised of: Ligand Abbreviation-Estimated Distance between two ligands based on 3.25 Å average rise per base pair in a DNA·PNA duplex.-Additional information. Ligand Abbreviations are as follows: G:Glc2NHTs, TG:TriGlc2NHTs, M:mannose, TM: TriMan, B:BiPhMan, TB:TriBiPhMan. The abbreviations for additional information after the second dash are defined as: S= short, O = DNA overlap, FX =Flexibility(X = number of single strang nucleotides between the ligands), Cy5 = Cyanine 5 tagged DNA, Atto = Atto647N tagged DNA. nL = complex with ligand.

Complex	Structure	Ligand	Distance [Å]	T_M [°C]
nL-Cy5		No ligand		n.d.
G-Mono		Glc2NHTs	Mono	62
G-16		Glc2NHTs	16	64
G-23		Glc2NHTs	23	66
G-29		Glc2NHTs	30	63
G-42		Glc2NHTs	42	64
G-42-Cy5		Glc2NHTs	42	65
G-49		Glc2NHTs	50	64
G-62		Glc2NHTs	62	62
G-84		Glc2NHTs	84	68
G-104		Glc2NHTs	104	66
G-16-S		Glc2NHTs-S	16	64
G-42-S		Glc2NHTs-S	42	64
G-29-F1		Glc2NHTs	23	n.d.
G-29-F3		Glc2NHTs	30	n.d.
G-29-F5		Glc2NHTs	42	n.d.
G-42-F1		Glc2NHTs	50	n.d.
G-42-F3		Glc2NHTs	62	n.d.
G-42-F5		Glc2NHTs	84	n.d.
nL-O-Cy5		No Ligand	-	n.d.
G-Mono-O		Glc2NHTs	-	63
G-23-O		Glc2NHTs	23	63

Complex	Structure	Ligand	Distance [Å]	T_M [°C]
G-42-O		Glc2NHTs	42	61
G-42-O-Cy5		Glc2NHTs	42	n.d.
G-84-O		Glc2NHTs	84	66
G-104-O		Glc2NHTs	104	64
TG-Mono		TriGlc2NHTs	Mono	65
TG-23		TriGlc2NHTs	23	66
TG-42		TriGlc2NHTs	42	64
TG-42-Cy5		TriGlc2NHTs	42	n.d.
TG-84		TriGlc2NHTs	84	68
TG-104		TriGlc2NHTs	104	66
M-Mono		mannose	Mono	62
M-42		mannose	42	65
M-62		mannose	62	62
M-84		mannose	84	62
M-104		mannose	104	64
TM-Mono		TriMan	Mono	63
TM-23		TriMan	23	64
TM-42		TriMan	42	67
TM-84		TriMan	84	64
TM-104		TriMan	104	65
TM-8x-Cy5		TriMan	42-294	n.d.
B-42		BiPhMan	42	62
B-104		BiPhMan	104	63
TB-Mono		BiPhMan	Mono	65
TB-23		TriBiPhMan	23	64
TB-42		TriBiPhMan	42	61
TB-104		TriBiPhMan	104	61

4.2 Langerin Affinity Measurements

4.2.1 Development of a Selective Langerin Ligand

The binding affinities of the ligands were measured by a ^{19}F-NMR assay (Figure 16), in collaboration with the Rademacher group (MPIKG). [93] This assay requires a small reporter molecule 2-deoxy-2-trifluoroacetamido-α-mannoside. As the reporter is labelled with a fluorine atom, ^{19}F -NMR of the compound displays a single resonance for the reporter molecule with an optimal signal to noise ratio. The Ca^{2+}-dependent interaction between the reporter molecule and langerin can be quantified via the observed relaxation rate ($R2,_{obs}$) using the CPMG pulse sequence. In the presence of the langerin ECD, the ^{19}F NMR resonance of the trifluoroacetamido group displayed line broadening (Figure 16). This made a direct measurement of K_D values for the reporter molecule (7.9 ± 0.7 mM) possible. In turn, the affinity of an arbitrary ligand can be determined based on its ability to displace the reporter ligand from langerin. The ^{19}F-NMR competitive assay was set up with a langerin concentration of 50 μM, a reporter concentration of 0.1 mM and five or more competitor concentrations of the langerin ligands. Subsequently, we measured the relaxation rate $R2,_{obs}$ was plotted against the ligand concentrations allowing for IC_{50} value calculation. The IC_{50} value is defined as the inhibitor concentration necessary for half inhibition of a protein. The inhibition constant, $K_{I,}$ describes the equilibrium constant of the dissociation of the protein-inhibitor complex. The K_I values of the monovalent ligands were determined as described by Wamhoff et al. and will be used to compare the monovalent affinities.[93] The K_I values were calculated with the assumption of a one to one binding mode between inhibitor and protein. As the multivalent ligands also made other binding modes possible the affinities of the multivalent inhibitors were characterised by their IC_{50} values. Where available both the K_I values and the IC_{50}s of the monovalent ligands will be noted to enable comparison with the IC_{50}s of the bivalent ligands. To achieve the goal of multivalent selective langerin inhibition the first objective was the development of a suitable langerin ligand. This ligand should possess a considerably higher affinity than mannose (KD ≈ 5mM) and N-acetylglucosamine (KD ≈ 4 mM), two potent natural monovalent langerin binders. Furthermore, a selectivity for langerin over other mannose-type-binding CTLs such as DC-SIGN was necessary. Mannose

and N-acetylglucosamine can bind both langerin and DC-SIGN with comparable affinities. The increase in affinity was deemed as vital because the affinity has a crucial influence on the multivalent effect.[36]

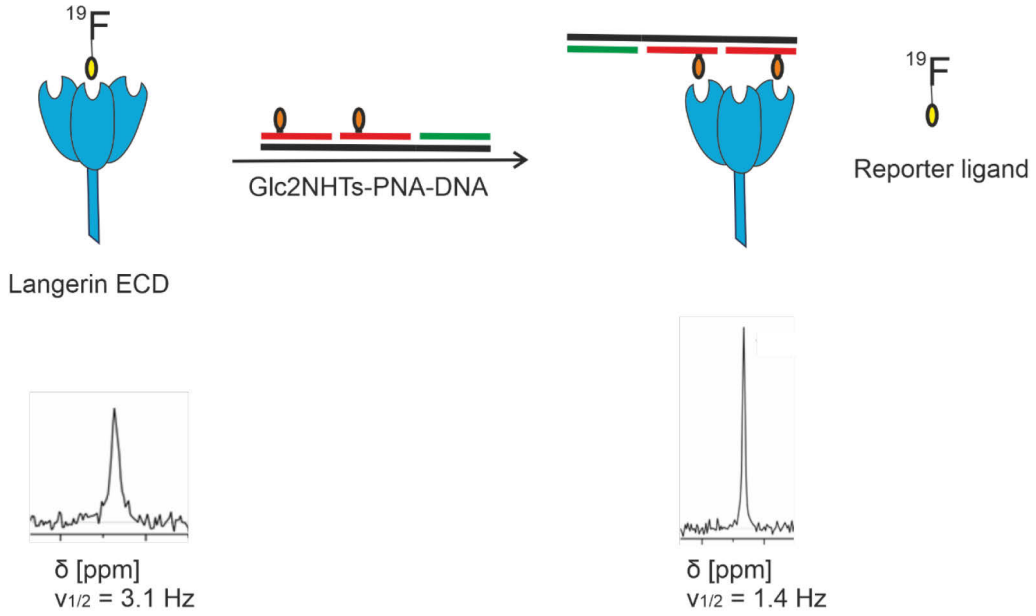

Figure 16. Setup of ^{19}F-NMR assay. A ^{19}F-marked mannose derivative binds to the trivalent langerin ECD. The bivalent ligand-PNA-DNA duplex displaces the 19F-marked mannose derivative. Bound to the langerin ECD, the ^{19}F NMR resonance of the trifluoroacetamido group displayed line broadening.

Previous results in the Rademacher group had shown that sulfated glucosamine e.g. GlcNS had a 4 times higher affinity for langerin than GlcNAc, a langerin binder with a similar affinity to mannose. A comparison with the X-ray crystal structure suggested this could be due to interaction between the sulfate and K299 or K313. It was assumed that the positive effect on binding affinity could be mimicked by a sulfonamide group. Additionally, small aromatic substitutions at the C2 position were proposed to enable cation-π interactions with K313 and H-π interactions with F315 and P310, respectively. Therefore, a small range of GlcNS analogs (Figure 17) was synthesised. The lead compound **72** was synthesised by myself and the synthesis of further compounds (**69**-**71**, **73**) was conducted by Eike Wamhoff (MPIKG, Potsdam) and David Hartmann (University of Cambridge/MPIKG). The synthesised ligands **69-72** were evaluated by Eike Wamhoff (MPIKG) and revealed increased affinities for all the glucosamine derivatives in comparison to GlcNAc (Table 7). The tosylated

glucosamine (Glc2NHTs, **72**) proved to be the most potent candidate with an affinity of $K_I = 0.32 \pm 0.05$ mM.

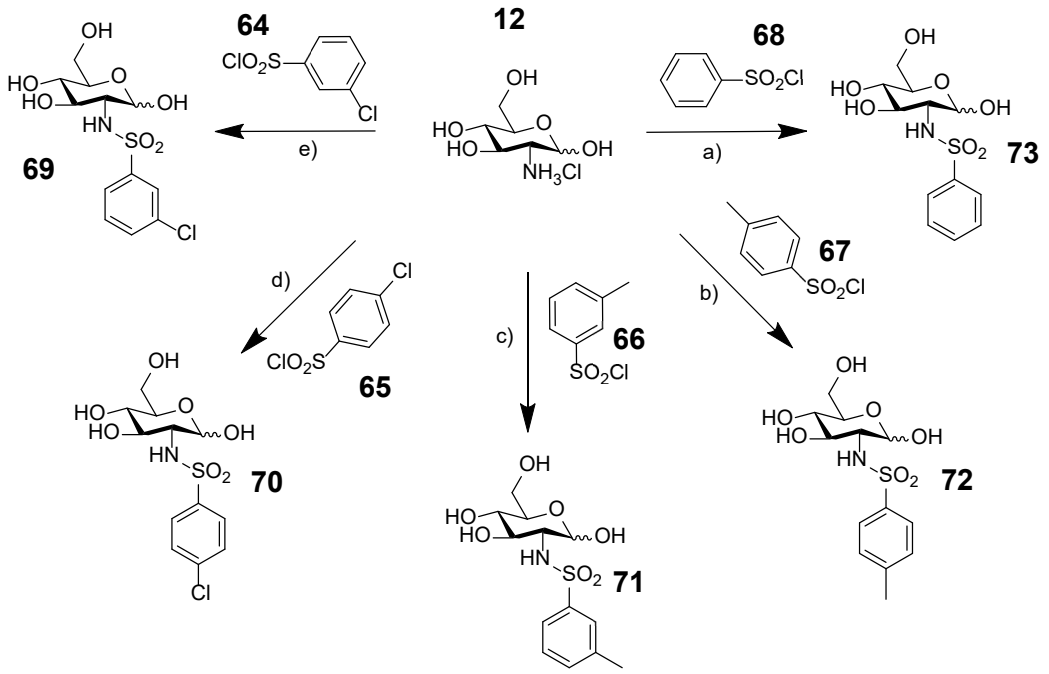

Figure 17. Synthesis of GlcNS derivatives. Reactions conditions for the synthesis of glucosamine derivatives: a) Et_3N, anhydrous MeOH, 0°C to rt, b) sodium hydroxide, acetone, rt, c) DIPEA, anhydrous methanol rt. Yields between 7 and 90 %.[47] This work was conducted by Eike Wamhoff (MPIKG), David Hartmann (University of Cambridge/MPIKG) and myself.

The methyl group at para position does not seem to form any favorable interaction with the protein as demonstrated by the very similar affinity of the phenyl derivative **73**. However, replacing the para-methyl group by meta-substituents on the phenyl ring led to an increase in K_I values. Substituting the methyl group with a chloride function decreased the affinity, which may be due to steric hindrance, solvation effects or the change in electronic character of the phenyl ring. Based on the structure activity relationship (SAR) it was assumed that the phenyl ring forms a positive interaction with K299, P310 or F315 of langerin.[47] Next, the selectivity of the newly designed ligand was tested by comparing the affinity to langerin and DC-SIGN (Table 8). Interestingly Glc2NHTs exhibits a 14-fold stronger affinity for langerin than mannose. The affinity for DC-SIGN was shown to be 6-fold lower than affinity of mannose for DC-SIGN. Evidently, this was a very encouraging result. The remarkable 54-fold selectivity of Glc2NHTs for langerin was a striking achievement. A rational approach to further improve the langerin affinity and selectivity would have been the introduction of a negative charge on the C6 position. Porkolab *et al*. demonstrated a

10 fold affinity improvement by introducing a sulfate at the C6 position (GlcNac-6-OS). [65] However, this makes the ligand synthetically much more laborious and an addition of both effects (toluene sulfonamide at C2 and sulfation at C6) can only be assumed if the same binding modes apply for GlcNAc6S and Glc2NHTs.

Table 7. Binding affinities of GlcNS derivatives for langerin[47] Conditions: complexes incubated with langerin (50 μM) and 0.1 mM ^{19}F-marked reporter ligand in 25 mM Tris/HEPES with 10 % DMSO, 10% D2O, 150 mM NaCl, 0.05 mM TFA and 5 mM CaCl2 at pH 7.8 and 25° C. The measurements were conducted by Eike Wamhoff (MPIKG).

Compound	K_I [mM]	IC 50 [mM]	Rel. potency (based on GlcNAc)
GlcNAc	4.1 ± 0.7	3.8 ± 0.7	1
73	0.37 ± 0.04	0.34 ± 0.2	11
72 Glc2NHTs	0.32 ± 0.05	0.37 ± 0.3	13
71	0.56 ± 0.09	0.55 ± 0.2	7
70	0.60 ± 0.02	0.59 ± 0.2	7
69	0.59 ± 0.06	0.62 ± 0.8	7

The ligation of the newly developed ligand to PNA made the introduction of a linker to Glc2NHTs necessary. Based on the binding mode of mannose and GlcNAc to langerin (the non-reducing end coordinates the Ca^{2+} ion in the binding pocket) we were confident that the effect of an aminoethyl-linker at the C-1 position (Scheme 3) should be minimal. The linker was further functionalised with a maleimide to be conjugated to the thiol-modified PNA. The effect of introducing a linker was examined next. As a maleimide moiety could interact cysteine present in langerin the maleimide-functionalized ligand was unsuitable for this measurement. Neither was the amine functionalized ligand an ideal candidate as we were wary of the influence a positively charged amine could have. Therefore, the amine **22** was acetylated, and the affinity of this compound determined. As the amine functionalised ligand **22** is equally acetylated to introduce the maleimide moiety, the acetylated aminoethyl-glycoside **75** (Table 8) resembles the actual ligand composition when bound to the PNA-DNA ruler.

Table 8. Monovalent Ligand Affinities determined by ^{19}F-NMRAssay. [a] The affinity for DC-SIGN was divided by the affinity for langerin to determine the selectivity value.[47] Conditions: complexes incubated with langerin (50 μM) and 0.1 mM ^{19}F-marked reporter ligand in 25 mM Tris/HEPES with 10 % DMSO, 10% D2O, 150 mM NaCl, 0.05 mM TFA and 5 mM CaCl2 at pH 7.8 and 25° C. The measurements were conducted by Eike Wamhoff (MPIKG).

Ligand	Langerin (K_I (IC_{50})	DC-SIGN (K_I (IC_{50})	Selectivity [a]
mannose (33) 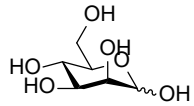	4,500 ± 500 μM (5,000 ± 500 μM)	3,000 ± 300 μM	0.66
mannose-1-O$(CH_2)_2$NHAc (74) 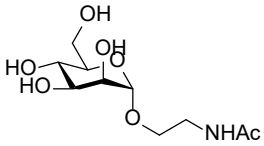	10,000 ± 1000 μM (10,000 ± 800 μM)	2,700 ± 300 μM	0.27
Glc2NHTs (72) 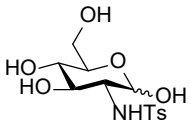	318 ± 50 μM (368 ± 28 μM)	17,000 ± 1000 μM	53.5
Glc2NHTs-1-O$(CH_2)_2$NHAc (75) 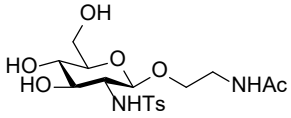	242 ± 31 μM (267 ± 19 μM)	15,000 ± 3000 μM	62.0

Thankfully, the introduction of the linker had no negative effect on the ligand affinity and even increased the affinity to K_I = 0.24 ± 0.03 mM. (Table 8) As a comparison, we also examined the influence of introducing the same linker at the C1 position of mannose (Table 8). Mannose and glucose possess the opposite stereochemistry at the C-2 position leading to opposite neighbouring group effects during the glycosylation reaction. The linker-modified Glc2NHTs ligand was therefore synthesised as β-anomer while the linker-modified mannose was synthesised as an α-anomer. Interestingly, locking the anomeric centre in the α-position demonstrated by molecule **74** had a slightly positive influence on the affinity for DC-SIGN (K_I = 2.7 mM vs 3.0 mM) but reduced the affinity for langerin (K_I = 4.5 mM vs. 10.0 mM). In contrast, locking the anomeric centre in the β-position as done for Glc2NHTs marginally increased the affinity for langerin (K_I =0.24 vs 0.32 mM) and DC-SIGN (K_I = 15 vs 17 mM). Hence

introducing a linker via an α glycoside increases the selectivity of mannose for DC-SIGN.

In summary a novel ligand was developed for langerin, with a 15-fold higher affinity than mannose and an 81-fold gain in selectivity for langerin. Modification of the ligand with aminoethyl-linker retained the favourable affinity and selectivity towards langerin. Although we were aware of potential further improvements, the affinity was considered sufficient to progress to multivalent binders.

4.2.2 Investigation of Bivalent Complexes via ^{19}F-NMR

4.2.2.1 ^{19}F-NMR Assay: Spatial Screening applying Bivalent Glc2NHTs-PNA-DNA Complexes

The langerin ECD forms a trimeric receptor with the three carbohydrate binding pockets. Feinberg *et al*. determined the distance between the CRDs of the human langerin to be 42 Å by solving the crystal structure. [51] To probe the optimal bivalent ligand presentation a DNA programmed spatial screening of langerin applying the newly developed langerin ligand was carried out. The synthesis and characterization of Glc2NHTs-PNA-DNA complexes has been described previously. In short, three PNAs, of which two were functionalized with a ligand, were hybridized with a DNA template. The building block system made the tuning of the distance between the ligands easily accessible. In collaboration with Eike Wamhoff the affinities of the bivalent complexes were measured via the established ^{19}F-NMR Assay in the laboratories of the Rademacher group. We tested a small library of complexes with distances between the ligands ranging from 16 to 84 Å. We expected the most potent binders to be those where the spatial arrangement of the ligands allows for bridging of two binding pockets. When the spatial arrangement of the trimeric lectin and the bivalent ligands are in good agreement a strong chelate effect should produce a strong langerin binder. The better the match between receptor and bivalent ligand, the greater the gain in affinity.

The binding affinity of the monovalent Glc2NHTs-PNA-DNA complex **G-Mono** (273 ± 32 μM) was in good agreement to the affinity of the Glc2NHTs-1-O$(CH_2)_2$NHAc **75** (267 ± 19 μM) implying that the DNA ruler does not have a negative impact on the

binding mechanism. The results for the bivalent ligand presentation (Table 9) revealed an optimal distance between the ligands of 16-49 Å. The 42 Å complex, **G-42,** revealed the highest potency (23 ± 2 μM) corresponding to a 12 fold higher affinity than the monovalent case. At distances above 62 Å the binding affinity decreases and the affinity of complex **G-84** (198 ± 42 μM) approaches the monovalent binding affinity (273 ± 32 μM). For distances under 42 Å we expected the same effect as the bivalent ligands would not be able to bridge the binding pockets of the receptor anymore. Surprisingly, when we decreased the distance between the ligands below 42 Å the affinities did not significantly deteriorate. The first set of experiments (82, 62, 42 Å) were performed at a protein concentration of 50 μM. As we were using a competitive assay to determine IC_{50} values the upper limit of accurate affinity determination was at half the protein concentration. It was suspected that the correct IC_{50} for the 42 Å complex may be considerably lower as we had reached the theoretical assay limit. We therefore changed the setup of the assay to a protein concentration of 25 μM. If the measured IC_{50}s were being constrained by the assay limit, we predicted that IC_{50} for **G-42** with the new set up would be reduced and possibly limited again by the new assay limit of 12 μM. However, a comparison of **G-42** with the 50 μM and 25 μM setup gave the same IC_{50} value 25 ± 1 μM and 23 ± 2 μM, respectively. Nevertheless, complexes **G-16**, **G-23** and **G-49** were measured at 25 μM protein concentration, as we were interested in measuring affinities below 25 μM.

Table 9. Distance Affinity Relationship for Bivalent Glc2NHTs-PNA-Duplexes to the langerin ECD determined by ^{19}F-NMR. [a] Estimated distance between the ligands based on 3.25 Å average rise per base pair in a DNA·PNA duplex. Conditions: complexes incubated at varied concentration with langerin (50 µM or 25 µM) and 0.1 mM 19F-marked reporter ligand in 25 mM Tris/HEPES with 10 % DMSO, 10% D2O, 150 mM NaCl, 0.05 mM TFA and 5 mM CaCl2 at pH 7.8 and 25° C. [a] based on 3.25 Å average rise per base pair in a DNA·PNA duplex. The ^{19}F-NMR assay was conducted by Eike Wamhoff (MPIKG) and myself.

Structure	Compound	Distance[a]	IC_{50} [µM]	β/n-Value
	Glc2NHTs	-	361 ± 28 *	1
	G-Mono	-	273 ± 32 #	1.3
	G-16	16 Å	35 ± 8 #	5.2
	G-23	23 Å	37 ± 9 #	4.8
	G-29	30 Å	25 ± 3 #	7.2
	G-42	42 Å	25 ± 1*; 23 ± 2 #	7.8
	G-49	49 Å	36 ± 4 #	5.0
	G-62	62 Å	126 ± 22*	1.4
	G-84	84 Å	198 ± 42*	0.9

[langerin] = 25 µM, * [langerin] = 50 µM

In summary, the spatial screening had successfully led to the discovery of an optimal distance between the ligands for binding to the langerin ECD. The best bivalent ligand displayed a 16-fold higher affinity than Glc2NHTs **72,** with a corresponding β/n value = 8. Satisfyingly, the experimentally determined optimal distance was in accordance with the theoretical distance (42 Å) between the CRDs measured by Feinberg *et al.* However, due to the large error of the measurements an optimal region between G-16 and G-49 is more precise. This may be due to the ability of langerin to sample a larger conformational space in solution. To date no reports on the minimal and maximal distance between the binding sites is available Additionally, bivalent ligands unable to bridge the distance between the CRDs showed much stronger potencies than expected and was cause for further investigations. Two possible explanations came to mind: The strong affinities of **G-16, G-23 and G-29** could be due to a strong statistical rebinding effects as described by Ebara and his co-workers when they placed three ligands

adjacently on a DNA scaffold.[90] Another consideration was the influence of the linker connecting ligand and scaffold, which may be able to bridge two CRDs at these small distances. Winssinger and his co-workers argued when they placed two mannose clusters adjacently on a DNA based scaffold the linkers were able to bridge the 30 Å distance the arms of the bivalent antibody 2G12.[88]

4.2.2.2 ^{19}F-NMR Assay: Investigation of the Linker Length

When applying the described thiol-maleimide ligation strategy the tether between the PNA backbone and the anomeric oxygen was comprised of 12 single bonds (Figure 18), which corresponds to an maximum theoretical distance of 18 Å (single bond is estimated at 1.5 Å). Two adjacent linkers could therefore theoretically span 36 Å. If these 36 Å are added to the 16 Å distance between the ligands of **G-16**, the bivalent complex would be able to bridge two CRDs. It is therefore possible that we may have reached the lower distance limit of these Ligand-PNA-DNA constructs. However, as mentioned in the introduction, Bandlow *et al*. have shown in detail that a PEG scaffold is not able to produce the same bivalency effects as the much more rigid PNA-DNA duplex. [17] The same must be assumed for the linkers. The linkers mainly consist of single C-C bonds and therefore represent a much more flexible tether than the DNA scaffold. The scenario in which both linkers are spread out in opposite directions bridging a large distance is an extreme and unlikely case. Interestingly, while Bernardi and her group concluded that the probability of spread out linkers from a rigid core is very low and hence had little effect on the avidity of their multivalent ligands, Winssinger and his group used the theory of the linkers crossing space to explain their results.[80, 88] We therefore devised an experiment to shed light on the influence of the linker length. [80, 88]

To investigate the influence of the linker length we shortened the distance between the PNA backbone and the sugar ligand. The use of the azide-alkyne cycloaddition chemistry is a very established ligation method. Figure 18 illustrates the design of our novel linker system.

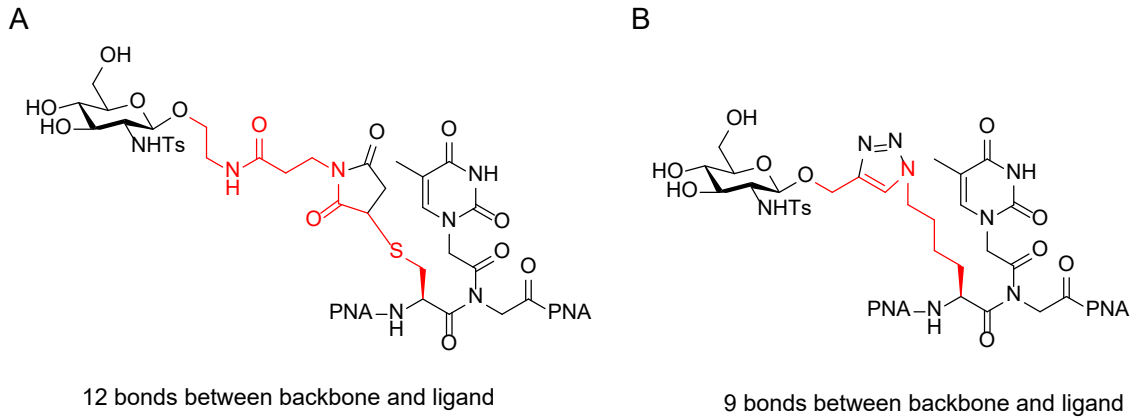

Figure 18. A) Design of the Glc2NHTs-PNA conjugates applying thiol-maleimide chemistry B) Design of the Glc2NHTs-PNA conjugates applying copper catalyzed azide-alkyne click chemistry chemistry. The red bonds illustrate the length between PNA backbone and ligand.

The distance between the PNA backbone and the anomeric oxygen of the sugar was reduced to eight single bonds and one double bond. The maximum theoretical distance therefore corresponds to only 13 Å (every bond length estimated at 1.5 Å). The previous design using thiol-maleimide chemistry consisted of 12 single bonds between the PNA backbone and the anomeric oxygen corresponding to a theoretical distance of 18 Å – 50 % longer than the new design. Furthermore, the shorter ligand should make the overall system more rigid. To implement the click chemistry approach a novel PNA building block with an internal azide functionalization and the alkyne modified Glc2NHTs ligand were synthesized as previously described. Having successfully acquired the building blocks for our click strategy these were in turn used to manufacture the ligand modified PNA. The same PNA sequences as those with the thiol modified PNA monomer were synthesized via SPPS and the ligands attached as previously described. As expected, these complexes had identical melting temperatures to the thiol maleimide conjugates and the desired ligand-PNA-DNA complexes were constructed in the same fashion.

The 16 Å and 42 Å complexes containing the copper-click ligation approach will hereafter be referred to as **G-16-S** and **G-42-S,** respectively**;** S standing for the short linker. We examined the influence of the short linker on the 42 Å and 16 Å complexes, as complex **G-42** was the best binder and **G-16** the shortest examined distance (Table 10). In both cases the affinities remained the same independent of the linker. This result indicated that the length of the linkers is not responsible for the strong affinities at very

short distances (<42 Å). If this had been the case, we would have observed a decrease in affinity for **G-16-S** in comparison to **G-16**. If the 16 Å of the duplex are added to twice the theoretical distance of the linkers (13 Å) the theoretical span of the ligands on **G-16-S** adds up to only 42 Å. Bearing in mind that it is not only impossible that the linkers stretch out in a perfectly straight line but that also the sterical hindrance of the DNA scaffold reduces the conformational freedom of the linkers, we were able to conclude that the span of the linkers was not responsible for the increased affinity of **G-16** and **G-23.** The need for flexibility to allow the ligand to bind and the theoretical advantage of a rigid scaffold is a classical trade-off.

Table 10. Comparison of the binding affinities to the langerin ECD for the standard thiol-maleimide approach and the short azide-alkyne click approach determined by ^{19}F-NMR. Conditions: complexes incubated with langerin (25 µM) and 0.1 mM 19F-marked reporter ligand in 25 mM Tris/HEPES with 10 % DMSO, 10% D2O, 150 mM NaCl, 0.05 mM TFA and 5 mM CaCl2 at pH 7.8 and 25° C. [a] based on 3.25 Å average rise per base pair in a DNA·PNA duplex. The ^{19}F-NMR assay was conducted by Eike Wamhoff (MPIKG) and myself.

Structure	Compound	Distance[a]	IC_{50} [µM]	β/n-Value
	Glc2NTs	-	361 ± 28*	1.0
	G-16	16 Å	35 ± 8#	5.2
	G-16-S	16 Å	38 ± 5#	4.8
	G-42	42 Å	23 ± 2#	7.8
	G-42-S	42 Å	16 ± 3#	11.2

[langerin] = 25 µM, * [langerin] = 50 µM

As both the previous thiol-maleimide and and the click-chemistry approach resulted in identical IC_{50}s it was assumed that the level of flexibility delivered by the linkers was already in the optimum range considering the tradeoff situation. Additional evidence that the span of the linker was not responsible for the increased affinity of **G-16**, **G-23** and **G-29** comes from comparing the affinity of **G-62** and **G-16**. If the span of linker effectively enabled **G-16** to extend the distance between its ligands the same should apply conversely for the **G-62** complex, which should then be able to similarly reduce the distance between the ligands. However, the affinity of **G-62** = 126 µM was nearly 4-fold lower than the affinity of **G-16**.In summary, the use of an orthogonal conjugation strategy confirmed our previous results and gave evidence that the linker

was not responsible for the low IC_{50}s measured for very short distance complexes (<42 Å). As the synthetic effort of this strategy was very large and the results identical it was not further pursued to examine the linker lengths influence on the affinity of the remaining complexes.

4.2.2.3 ^{19}F-NMR Assay: Investigation of Statistical Rebinding

Next, we examined the possibility that statistical rebinding was causing the unexpected results obtained for the small distance molecular rulers. Therefore, the affinities of the Glc2NHTs-PNA-DNA complexes to the trivalent langerin ECD and the monovalent langerin CRD were compared. While the CRD is monovalent, containing one carbohydrate binding site, the ECD forms a trimer containing three CRDs. If the bivalent ligands were able to bridge the sugar binding epitopes (chelation) of the ECD, then the affinity for the monovalent CRD should be greatly decreased, as the chelation effect would become non-existent. If a strong rebinding effect was causing the multivalency effect, this affinity gain should be retained for the monovalent CRD. As before, we examined the **G-16** and **G-42**.

Interestingly, we obtained different effects for both complexes under investigation. In the case of **G-42** the affinity decreased 5-fold from 23 ± 2 µM (ECD) to 120 ± 20 µM (CRD). The affinity of **G-42** to the langerin CRD was roughly 2-fold higher than the affinity of **G-Mono** (273 ± 32) and can be regarded as a concentration effect ($\beta/n = 1$), as the bivalent complex carries twice as many ligands. In contrast, the affinities of **G-16** to the ECD (35 ± 8 µM) and CRD (60 ± 20 µM) are the same when including the errors. The affinity of the of **G-16** to the CRD is 2-fold stronger than the affinity of **G-42** to the CRD. Additionally, the affinity of the **G-16** to the CRD is 4-fold higher than **G-Mono**. Hence, a β/n value > 1 is retained. These comparisons provide us with a strong indication that while **G-42** can bridge the two CRDs of the ECD, the improved affinity of **G-16** is due to a rebinding effect. Unsurprisingly, the rebinding effect is much stronger for the very short 16 Å complex, **G-16**, than for the 42 Å complex, **G-42**. **G-16** brings both ligands in proximity to one binding site. The linkers provide additional flexibility for both ligands to bind to the same CRD. In the case of **G-42**, the scaffold holds the ligands apart preventing statistical rebinding.

Table 11. Comparison of the binding affinities to the trimeric langerin ECD and the monomeric langerin CRD for the 42 Å and 16 Å complexes determined by ^{19}F-NMR. Conditions: complexes incubated with langerin (25 µM) and 0.1 mM 19F-marked reporter ligand in 25 mM Tris/HEPES with 10 % DMSO, 10% D2O, 150 mM NaCl, 0.05 mM TFA and 5 mM CaCl2 at pH 7.8 and 25° C. [a] based on 3.25 Å average rise per base pair in a DNA·PNA duplex. The ^{19}F-NMR assay was conducted by Eike Wamhoff (MPIKG) and myself.

Structure	Compound	Distance[a]	Target	IC_{50} [µM]	β/n-Value
	G-16	16 Å	ECD	35 ± 8#	5.2
	G-16	16 Å	CRD	60 ± 20*	3.0
	G-42	42 Å	ECD	23 ± 2#	7.8
	G-42	42 Å	CRD	120 ± 20*	1.5

[langerin] = 25 µM, * [langerin] = 50 µM

In conclusion, the **G-16** complex holds the two ligands in a position that makes statistical rebinding efficient, **G-42** holds the two ligands in a position that makes chelation efficient. The rebinding effect will be further investigated by examining a molecule where three ligands are covalently attached in such a way that cross-linking of the ECD binding sites is impossible. It should be noted that G-16 is the only complex with two ligands conjugated to one PNA strand. There is no nick site between the ligands to reduce helical stress.

4.2.2.4 ^{19}F-NMR Assay: Investigation of Scaffold Flexibility

Scheibe *et al*. showed that increased flexibility of bivalent ligand-PNA-DNA complexes can increase the affinity of these bivalent complexes by improving their capacity to adjust to the form of the protein surface.[15] Although we had considerable evidence that the surface of the langerin ECD is flat and easily accessible, we wanted to assess the introduction of flexibility to the PNA-DNA scaffold for potential improvement of the affinity and efficacy of the bivalent ligands.[103]

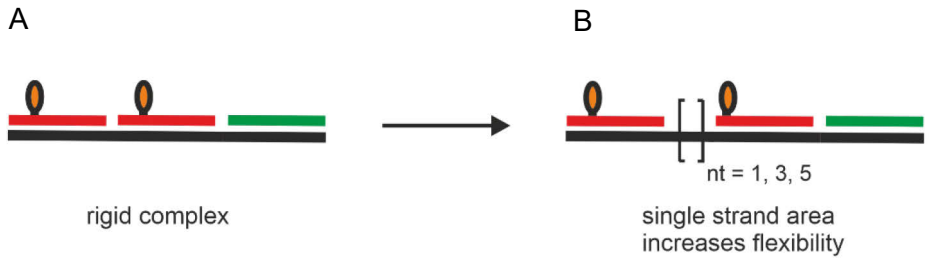

Figure 19. A) Rigid Glc2NHTs-PNA-DNA duplex without single strand region. B) Flexible Glc2NHTs-PNA-DNA duplex by adding a DNA template with a single strand region 1,3 or 5 nucleotides in length.

To increase the flexibility of the molecular rulers a single strand DNA area was introduced to the PNA-DNA duplexes. The identical PNA strands were hybridized to a DNA template strand with one, three or five unpaired nucleotides between two PNA strands (Figure 19). The single strand region will cause a large increase in the flexibility of the duplexes. However, it should not be forgotten that even the introduction of a single strand region will influence the distance between the ligands. We tested the introduction of flexibility for two different distances 29 and 42 Å and slowly increased the flexibility by increasing the number of unpaired nucleotides from one to three to five (Table 12). The complexes with increased flexibility due to single strand DNA are labelled with FX, where X corresponds to the number of single strand nucleobases. For example, G-42 with a single strand region of three nucleobases is given the name G-42-F3. Notably, none of the complexes with increased flexibility showed a better affinity than the rigid complexes. The addition of one nucleobase for the 42 Å complex (**G-42-F1**) led to a roughly threefold decrease in affinity (68 ± 15 µM) in comparison to the rigid **G-42** (23 ± 2 µM). However, the addition of further nucleobases increased the affinity and an additional five nucleobases (**G-42-F5**) was nearly as potent (36 ± 2 µM) as the rigid case. In the case of the 29 Å complex the addition of one nucleobase also led to a roughly threefold decrease in affinity (64 ± 15 µM) in comparison to the rigid **G-29** (25 ± 3 µM). The use of a three base single strand region (**G-29-F3**) showed a greatly decreased affinity (147 ± 58 µM) while **G-29-F5** showed a similar affinity (61 ± 22 µM) as **G-29-F1**. These results are difficult to interpret as there is no obvious pattern and two different binding modes (chelate binding and statistical rebinding) have to be taken into consideration. The IC_{50} for complex **G-29-F3** was much higher than any of the other values, which may give

reason to assume the **G-29-F3** result was an artefact. The ^{19}F-NMR measurements were only devised as single measurements due to the high quantities of complex and protein needed for every titration. However, those experiments that were repeated e.g. **G-42** and the use of two different conjugation strategies provided us with evidence that the method was generally robust.

Table 12. Flexibility-affinity relationship for bivalent Glc2NHTs-PNA-DNA-duplexes G-29 and G-42 determined by ^{19}F-NMR. A single strand region between the ligands of 1,3 or 5 nucleotides in length was added. Conditions: complexes incubated with langerin (25 µM) and 0.1 mM 19F-marked reporter ligand in 25 mM Tris/HEPES with 10 % DMSO, 10% D2O, 150 mM NaCl, 0.05 mM TFA and 5 mM CaCl2 at pH 7.8 and 25° C. [a] based on 3.25 Å average rise per base pair in a DNA·PNA duplex. The ^{19}F-NMR assay was conducted by Eike Wamhoff (MPIKG) and myself.

Structure	Compound	Distance[a] + single strand nucleotides	IC_{50} [µM]	β/n-Value
	Glc2NHTs	-	361 ± 28*	1.0
	G-29	29 Å	25 ± 3#	7.2
	G-29-F1	29 Å+1	64 ± 15#	2.8
	G-29-F3	29 Å+3	147 ± 58#	1.2
	G-29-F5	29 Å+5	61 ± 22#	3.0
	G-42	42 Å	23 ± 2#	7.8
	G-42-F1	42 Å + 1	68 ± 15#	2.7
	G-42-F3	42 Å + 3	41 ± 6#	4.4
	G-42-F5	42 Å + 5	36 ± 2#	5.0

[langerin] = 25 µM, * [langerin] = 50 µM

One interpretation of the measured affinities for the 42 Å complexes when increasing the flexibility may be that two different phenomenas were taking place. While an increase in flexibility may have generally reduced the affinity of the constructs when considering the chelating effect, it may at the same time have facilitated the rebinding effect, which had been shown to be low for the rigid 42 Å complex, **G-42**. This could be a possible explanation of why the initial introduction of flexibility first lead to a loss in potency and further flexibility reduces the potency loss, as rebinding becomes efficient. A similar hypothesis can be made for the 29 Å complexes. The initial

introduction of flexibility lead to a first decrease in affinity, which may be due to a weaker chelate effect. However, in this case, due to the presumably already strong influence of the rebinding effect on the binding affinity at this short distance, a further introduction of flexibility does not facilitate rebinding and the potency remains weak when the flexibility is increased further. In total, there is not enough evidence to prove these explanations. Further experiments to investigate the matter are difficult to design as it is impossible to separate the two multivalency mechanisms (chelate binding and statistical rebinding). Furthermore, increasing the single strand region will always have a small influence on the distance between the ligands, which was neglected in this discussion. As the potency of the more flexible constructs was not increased in comparison to their rigid counterparts it was assumed that the trade-off situation between flexibility and rigidity was advantageous in the rigid system for this flat and easily accessible protein surface.

4.2.2.5 ^{19}F-NMR Assay: Multivalent Glc2NHTs Constructs

Although the bivalent screening had led to an increase in affinity, **G-42** was only 22-fold more potent than Glc2NHTs. We were interested in developing a general approach for further amplifying the avidity of the multivalent ligands. It is known that a higher monovalent affinity leads to a larger bivalency effect.[36] Instead of implementing a more potent ligand, we envisioned exploiting both the statistical rebinding effect, we had measured, and the chelating effect cooperatively, ideally without losing either ligand efficacy or the distance affinity relationship we had discovered. To confirm the rebinding effect a trivalent ligand **31** unable to bridge the distance between the CRDs of langerin was designed and evaluated. Three azide modified Glc2NHTs ligands **29** were therefore covalently attached on a trialkyne scaffold **30** to form TriGlc2NHTs **31**. TriGlc2NHTs was additionally modified with a maleimido-function so that the same thiol-maleimide chemistry could be applied as before. Initially, the affinity of TriGlc2NHTs to langerin was examined in the ^{19}F-NMR assay in collaboration with Hannes Baukmann (MPIKG). As expected, this new compound exemplified the strong statistical rebinding effect we had previously encountered. TriGlc2NHTs displayed an IC_{50} of 12 ± 2 μM, a 30-fold affinity enhancement over Glc2NHTs.

Table 13. Distance affinity screening of TriGlc2NHTs-PNA-DNA duplexes determined by ^{19}F-NMR. Conditions: complexes incubated at varied concentration with langerin (25 µM) and 0.1 mM ^{19}F-marked reporter ligand in 25 mM Tris/HEPES with 10 % DMSO, 10% D2O, 150 mM NaCl, 0.05 mM TFA and 5 mM CaCl2 at pH 7.8 and 25° C. [a] based on 3.25 Å average rise per base pair in a DNA·PNA duplex. The ^{19}F-NMR assay was conducted by Hannes Baukmann, Nina-Louisa Èfrem (both MPIKG) and myself.

Structure	Compound	Distance [a]	IC_{50} [µM]
	Glc2NHTs (72)	-	361 ± 28*
	TriGlc2NHTs (31)	-	10 ± 2#
	TG-23	23 Å	2,1 ± 4,7#
	TG-42	42 Å	11,9 ± 6,5#
	TG-84	84 Å	8,5 ± 2,4#
	TG-104	104 Å	6,4 ± 6,0#

[langerin] = 25 µM, * [langerin] = 50 µM

The examination of the bivalent TriGlc2NHTs molecular rulers in the ^{19}F-NMR assay was investigated in collaboration with Nina-Louisa Èfrem (MPIKG) and led to statistically identical IC_{50}s values (Table 13) for all the distances (23, 42, 82, 104 Å). As the measured IC_{50}s were substantially under the lower assay limit (12.5 µM) the errors became nearly as large as the values themselves. This indicated that we had reached the limit of the ^{19}-F NMR assay due to a langerin concentration of 25 µM making the establishment of a second assay with a lower limit, necessary.

In conclusion, the initial spatial screening and subsequent experiments with the bivalent Glc2NHTs constructs presented us with several astonishing results. The optimal distance between two ligands appears to corresponded with the calculated distance between two binding sites in the crystal structure, 42 Å. Adding additional flexibility to our ruler did not increase the affinity implying that the fit of the ruler and protein surface is already ideal. The length of the linker did not influence the binding affinity, which also indicated that the chosen maleimide linker system represents a good compromise between the entropic advantage of a rigid system and the practical necessity of flexibility in the linker system to ensure the ligand can adjust to the binding pocket. Additionally, we provided evidence that a strong rebinding effect takes place when two or more ligands are placed in proximity but unable to bridge the langerin binding sites. This formed the idea of bivalently presenting a cluster of ligands to magnify the chelate effect but could not be evaluated due to the limits of the ^{19}F-NMR assay.

Although the ^{19}F-NMR had proved valuable for our spatial screening of langerin it also possessed a number of draw backs. These included the high material consumption (every titration point was performed in a 180 µL NMR tube), the high assay limit at 12.5 µM (25 µM protein concentration) and that the assay was only established to reliably determine multivalent ligands for langerin. A comparison with other lectins to explore selectivity was therefore not possible. Due to the drawbacks of the ^{19}F-NMR assay, we were interested in establishing an orthogonal assay to overcome these limitations and verify our results.

4.2.3 Investigation of Bivalent Complexes via SPR

Surface Plasmon Resonance (SPR) is a widely used tool to measure the binding of protein-protein and ligand-protein interactions. The benefits of SPR (Figure 20) include that it is a label free method, no fluorophore or radioactive marker is necessary, very little compound is needed and the kinetics of the binding (k_{on} and k_{off}) can often be directly determined from the measurement. The SPR measurements were conducted by Kim Silberreis (Dernedde group, Charité) and evaluated by myself. There were two possibilities regarding the immobilisation onto the chip. The first possibility was to immobilize the protein on the chip, and then measure the binding of the ligands to the immobilized protein directly. This has the advantage that the K_D can be measured directly and typically much less compound is necessary.[71] The drawbacks are that the immobilization works via a peptide bond formation between a carboxylic acid function on the chip and a lysine of the protein.

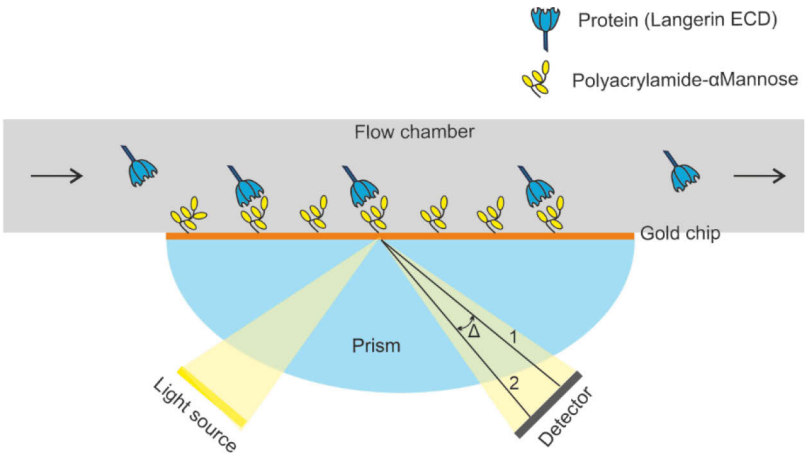

Figure 20. Competititve SPR assay. Gold chip borders to a flow chamber on the one side and circular prism on the other side. Polarized light is emitted through the prism and reflected under conditions of total internal reflection. The angle of the surface plasmon resonance wave is dependent on the refractive index of the material, which in turn is sensitive to mass changes on the gold surface. The binding of an interaction partner e.g. a protein to the ligand in the chamber therefore directly correlates to a change in SPR angle. The change in SPR angle is marked here by 1 and 2.

As langerin contains lysine in the carbohydrate recognition domain some langerin would become inactive. Additionally, the difference in SPR signal for very small ligands such as our free sugar molecules would not be detectable, as this is sensitive to a change in mass on the chip surface. Furthermore, immobilisation of the protein on the chip makes crosslinking of the proteins much more likely. Instead, biotin-polyacrylamide-αmannose was immobilized on a streptavidin functionalized dextran

chip. In this competitive set up the ability of the ligands to inhibit the binding of the protein to polyacrylamide-αmannose is determined. The advantages of this assay set up are that both protein and ligand are in solution and crosslinking is therefore less likely than for prearranged immobilised interactions partners. Furthermore, the analysis of small ligands is unproblematic as the large protein binding to the chip causes a clear shift in SPR angle. Additionally, a competitive assay is usually more robust, especially towards unspecific binding. The disadvantages are that considerably more compound is needed, and complete inhibition is difficult. Moreover, langerin can bind to dextran. Therefore, the surface of the gold chip had to be loaded very densely to prevent binding of langerin to dextran. However, minor binding of langerin to the dextran should not be detrimental as this is also specific to the carbohydrate recognition domain. The determined affinity of langerin for the chip may therefore be a combined affinity for the immobilised Polyacrylamid-mannose and surface available dextran. As the SPR chip can easily be regenerated, this afore mentioned error should be identical in all measurements.

Gratifyingly, we were able to establish a SPR assay for langerin in collaboration with the Dernedde group. Langerin was determined to bind to the Polyacrylamide-αmannose-functionalised chip with a K_D = 1.5 µM. The SPR assay required only 35 µL per titration point and the assay was optimized for a protein concentration of 500 nM dramatically decreasing the assay limit to 250 nM. For the competitive set up the ligands were incubated with the protein and the solutions injected over the measuring channel (polyacrylamide-α-D-mannose) and a reference channel (polyacrylamide-α-D-galactose). Galactose does not bind to langerin. For evaluation, the reference channel values were subtracted from the measuring channel values. Corrected response values were calculated by dividing the values by the langerin baseline and used for determining the IC_{50}s.

4.2.3.1 SPR Assay: Bivalent Glc2NHTs-PNA-DNA ligands

We determined the affinities of a small library of bivalent Glc2NHTs-PNA-DNA complexes to langerin to verify the previously measured results and the discovered distance affinity relationship. To begin with a single point inhibition assay allowed us to perform a spatial screening at a fixed ligand concentration (10 µM) in three independent replicates (Figure 21). Clearly, the 42 Å complex showed the strongest inhibition of the langerin-chip interaction in each replicate. An Anova test proved that the differences in inhibition were statistically significant.

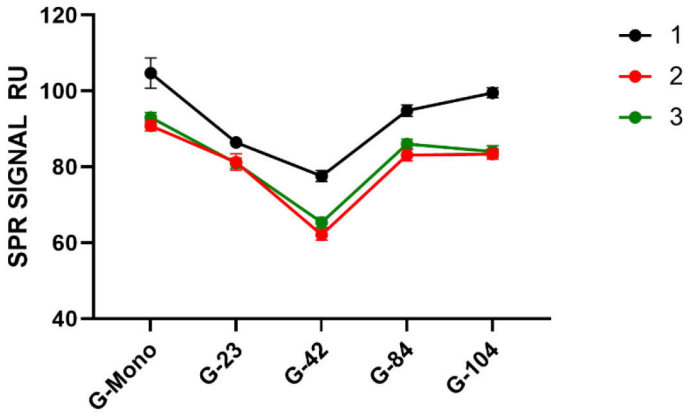

Figure 21. Residual langerin-chip-interaction at 10 µM ligand concentration in response units (RU). Errors are the SD of technical duplicates.1,2 and 3 represent three independent replicates. Values from the same SPR run are marked with identical colors. Conditions: Before injection, the protein sample (500 nM) and the complexes were incubated for 5 min at rt in 25 mM HEPES buffer with 150 mM NaCl and 5 mM CaCl2 at pH 7.8 and 25° C. The samples were injected over a reference, and α-D-mannose–polyacrylamide chip and the residual langerin binding measured. The SPR assay was conducted by Kim Silberreis (Charité) and evaluated by myself.

Thereafter, a serial dilution of the ligands in order to calculate the IC_{50}s was examined (Table 14). The IC_{50} of the Glc2NHTs **72** was determined to be 347 ± 11 µM, which was in good agreement with the IC_{50} value determined in the ^{19}F-NMR assay (361 µM). The monovalent Glc2NHTs-DNA-PNA complex, **G-Mono**, showed a 3-fold higher affinity of 105 ± 44 µM. An increase in affinity upon attachment of the ligand to the PNA-DNA scaffold was also measured with the ^{19}F-NMR. This is partly due to locking the ligand in the β-anomer conformation. However, similar effects have been observed for other ligand-PNA-DNA systems and may be explained by steric shielding.[17, 42, 104] The examination of the bivalent ligand-PNA-DNA complexes revealed a distance affinity relationship regarding the presentation of the ligands. **G-23** and **G-104** showed the lowest affinities of the bivalent complexes with 52 ± 2 µM

and 40 ± 14 µM, respectively. The highest affinity was measured for **G-42** with an affinity of 16 ± 1 µM. In contrast to the ^{19}F-NMR assay the 84 Å complex, **G-84,** displayed an only slightly lower affinity (21 ± 2 µM) than **G-42**. The optimized complex **G-42** was 22 times more potent than the Glc2NHTs ligand and showed a 7-fold enhanced affinity over **G-Mono**. Impressively, the experimentally determined optimal distance was therefore in good accordance with the result obtained from the ^{19}F-NMR assay and the Euclidian distance between the canonical carbohydrate binding sites (PDB: 3kqg). The surface of the langerin ECD is known to be flat and easily accessible making the agreement between the crystal structure and the experimentally determined distance feasible.[103] As expected, a very long distance between the ligands (104 Å) led to greatly reduced potency. The IC_{50} of **G-104** (40 ± 14 µM) is roughly half of **G-Mono** (105 ± 44 µM) and merely a concentration effect. Interestingly, we needed a slightly longer distance to achieve this reduction in potency than in the ^{19}F-NMR assay, where **G-84** had been a significantly weaker binder. Another difference between the two assays was that the statistical rebinding effect seems to be weaker in the SPR assay. In the SPR assay the potency of **G-42**, which has a chelate mechanism, is 3.25-fold higher than the potency of **G-23**, which presumably has a statistical rebinding mechanism. In the ^{19}F-NMR assay **G-42** was only 1.6-fold more potent. A close look at the assays may help resolve this difference. Both assays are competitive systems and therefore the properties of the displaced ligands have a large influence on the IC_{50}s. In the ^{19}F-NMR assay a monovalent mannose derivative is being displaced (KD = 8 mM) while for the SPR system a polyvalent mannose derivative (KD = 1.5 µM), itself capable of statistical rebinding, is being displaced. It is therefore reasonable that the statistical rebinding has a larger effect on inhibitor potency in the ^{19}F-NMR assay. In summary, we had successfully established an orthogonal assay and verified the 42 Å complex, **G-42**, as the optimised bivalent Glc2NHTs-PNA-DNA ligand. When comparing the ^{19}F-NMR and SPR assay the large uncertainties should be pointed out. Due to the substantial amount of ligand and protein required, the 19F-NMR measurements were performed as single experiments and the errors of this previously validated assay depend largely on the goodness of the fit (single experiments).[93] The SPR experiments were conducted as duplicates and the statistical significance of the differences in inhibition potency

confirmed by the triplicate measurement at a single concentration. Both assays and distance affinity screenings resulted in a trend regarding the bivalent presentation of Glc2NHTs. The good agreement between these orthogonal assays provide the robustness of the results and confirmed **G-42** as the optimal bivalent Glc2NHTs ligand.

4.2.3.2 SPR Assay: Multivalent Glc2NHTs-PNA-DNA ligands

Next, we revisited the bivalent presentation of TriGlc2NHTs clusters on the PNA-DNA scaffolds, as we had envisioned this as a tool for magnifying multivalency effects. However, the NMR assay was not able to determine the potency of this method due to the lower concentration limit of the assay. Gratifyingly, the SPR assay led to more conclusive results for the bivalent presentation of TriGlc2NHTs (Table 14). The affinity of TriGlc2NHTs **31** (IC_{50} = 50.5 μM) was determined to be 7-fold higher than Glc2NHTS (IC_{50} = 347 μM). The rebinding effect leads to 2.3 -fold affinity enhancement (β/n) per ligand. However, this was considerably lower than the 10-fold β/n-value measured for TriGlc2NHTs in the ^{19}F-NMR assay. As discussed before the ^{19}F-NMR assay appears to lead to stronger rebinding effects, which may be due to the different competitive system. As experienced for Glc2NHTs, the attachment of the TriGlc2NHTs ligand to the scaffold led to a first increase in affinity (IC_{50} = 10.5 ± 2.2 μM). The relative increase is slightly higher than for Glc2NHTs **72**, which may be due to the positively charged free amine of TriGlc2NHTs. Positive charges near the binding site are known to reduce langerin affinity by interacting with a lysine of the binding site.[65] Therefore attaching TriGlc2NHTs to the scaffold will additionally profit from removing this negative interaction. Remarkably, the distance affinity relationship shows the same profile as for the bivalent presentation of Glc2NHTs.

TG-42 proved to be the most potent langerin binder. The IC_{50} of **TG-42** (0.3 ± 0.02 μM) corresponds to a 35-fold higher affinity than the **TG-Mono** (10.5 ± 2.2), a 168-times higher affinity than TriGlc2NHTs and 1156-fold more potent than Glc2NHTs. Complex **TG-23** afforded a decrease in affinity (0.8 ± 0.1 μM). Increasing the distance between the ligands to 84 Å equally led to a large decrease in inhibitory potency (1.0 ± 0.06). A further increase in distance to 104 Å reduced the affinity even

further(IC_{50}=1.8 ± 0.7 µM). However, **TG-104** retains more than twice the potency of the monovalent complex. As the length of the rigid scaffold makes chelation very unlikely it is possible that crosslinking is causing this increase in affinity.

Table 14. Affinities measured for the bivalent presentation of Glc2NHTs and TriGlc2NHTs determined by SPR. The relative potencies based on Glc2NHTs and TriGlc2NHTs and the corresponding valency corrected β/n-value are compared. Conditions: 5 min incubation of complexes with 500 nM langerin in 25 mM HEPES, 150 mM NaCl, 5 mM CaCl2, pH 7.8, 25° C followed by determining binding of residual langerin to an α-D-mannose–functionalized SPR chip. [a] based on 3.25 Å average rise per base pair in a DNA·PNA duplex. The SPR assay was conducted by Kim Silberreis (Charité) and evaluated by myself.

Structure	Compound	Distance [a]	IC_{50} [µM]	Rel. Potency based on Glc2NTs (β/n-value)	Rel. Potency based on TriGlc2NTs (β/n-value)
	Glc2NHTs	-	347 ± 11	1 (1)	-
	G-Mono	-	105 ± 44	3 (3)	-
	G-23	23 Å	52 ± 2	7 (3.5)	-
	G-42	42 Å	16 ± 1	22 (11)	-
	G-84	84 Å	21 ± 2	17 (8.5)	-
	G-104	104 Å	40 ± 14	9 (4.5)	-
	TriGlc2NHTs	-	50.5 ± 0.5	7 (2.3)	1 (1)
	TG-Mono	-	10.5 ± 2.2	33 (11)	4.8 (4.8)
	TG-23	23 Å	0.8 ± 0.1	434 (68)	63 (31.5)
	TG-42	42 Å	0.30 ± 0.02	1157 (193)	168 (84)
	TG-84	84 Å	1.0 ± 0.1	347 (58)	50.5 (25.3)
	TG-104	104 Å	1.8 ± 0.7	192 (32)	28 (14)

To investigate the possibility of cross-linking further studies such dynamic light scattering would be necessary. These results not only demonstrated the capability of DNA based molecular rulers to harness both the power of the chelating and the statistical rebinding effect simultaneously but also made some very fundamental comparisons possible. As previously elaborated, extensive research in the Seitz and has shown that a more potent ligand generally leads to a stronger chelate effect.[36] A fundamental question therefore arises whether the application of ligand clusters capable of statistical rebinding can amplify chelate effects in the same fashion. To answer this question the relative potencies of bivalent Glc2NHTs-PNA-DNA and TriGlc2NHTs-PNA-DNA complexes in comparison to Glc2NHTs and TriGlc2NHTs,

respectively, were plotted in Figure 22, solid lines. The bivalent presentation of TriGlc2NHTs amplified the distance affinity response. The bivalent presentation of TriGlc2NHTs in **TG-42** led to a 168-fold avidity enhancement in comparison to TriGlc2NHTs **31**. In comparison bivalent presentation of the weaker Glc2NHTs only increased the relative inhibitory potency of G-42 22-fold. This proves that, like the relationship between the strength of a ligand and the chelate effect, statistical valency can be exploited to increase chelate bivalency effects. Furthermore, to compare the overall efficiency of the ligands the β/n-values were additionally calculated based on the affinity of Glc2NHTs(Table 14). The β/n value is calculated by dividing the measured IC_{50} value by the number of ligands.

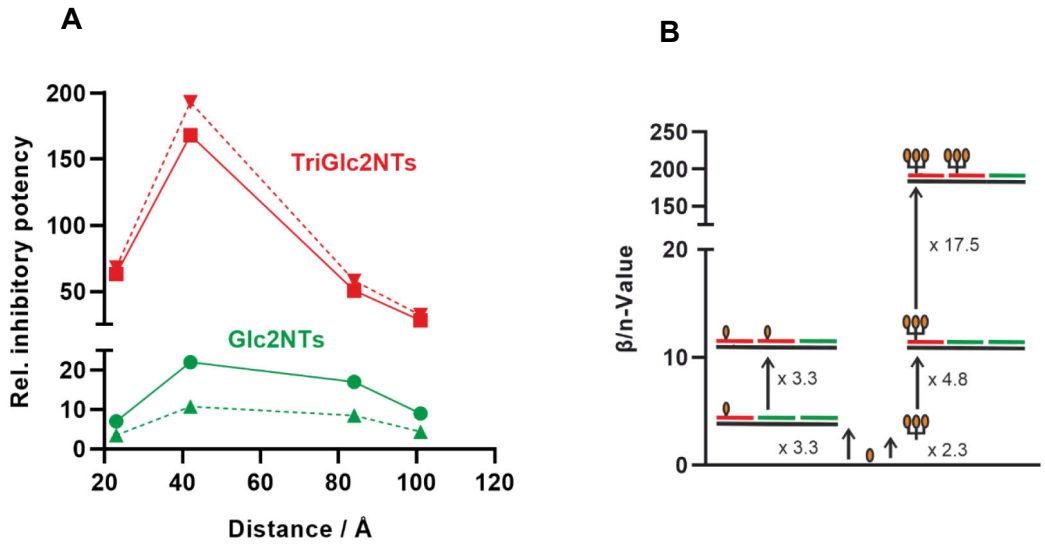

Figure 22. A) Distance dependence of relative inhibitory potency for the bivalent presentation of Glc2NTs (green) or TriGlc2NTs (red) as multiples of Glc2NHTs (green solid line) or TriGlc2NHTs (red solid line). Dashed lines show the valency corrected β/n-values based on the number of Glc2NTs ligands. B) β/n-value (based on Glc2NHTs) for Glc2NHTs, TriGlc2NHTs, G-Mono, G-42, TG-Mono and TG-42 illustrating the x-fold increases in β/n-value.

The optimised TriGlc2NHTs ligand, **TG-42,** showed a 193-fold affinity enhancement per Glc2NHTs moiety in comparison to the only 11-fold affinity enhancement per ligand displayed by **G-42** (Figure 22, dashed lines). Hence, making use of the statistical rebinding effect to enhance the chelate effect improved the overall ligand economy. A detailed analysis of the factors contributing to the 1156-fold affinity enhancement is illustrated in Figure 22 B. The ligand cluster TriGlc2NHTs (IC_{50} = 51 µM) is 2.3-fold more potent per ligand than Glc2NHTs (IC_{50} = 347 µM). Attaching TriGlc2NHTs to the DNA based scaffold led to an 4.8-fold enhancement of ligand efficiency (IC_{50} **TG-Mono** = 10.5 µM vs IC_{50} TriGlc2NHTs = 50 µM), as previously

discussed. By comparing the monovalent (IC_{50} **TG-Mono** = 10.5 μM) and bivalent (IC_{50} **TG-42** = 0.3 μM) presentation of the TriGLc2NHTs, a 17.5-fold affinity enhancement can be contributed to the chelate effect, which has the strongest impact and moves the affinity into the nanomolar range. However, the chelate effect very much depends on the strength of the interaction at the carbohydrate binding site and optimising the distance between the ligands. Hence, the bivalent Glc2NHTs complex, **G-42,** bearing the weaker ligand only exhibits a chelate dependent affinity enhancement per ligand of 3.3. The non-optimally arranged bivalent TriGlc2NHTs complex, **TG-104**, only displays a chelate dependent affinity enhancement of 2.9.

One more comparison between the bivalent presentation of Glc2NHTs and TriGlc2NHTs can be made. As the DNA-based ligands are ideal for probing the distance between two binding sites (e.g. when no crystal structure is available) a sensitivity factor can be calculated for the match and mismatch case. As shown by the distance affinity relationships the ligands **G-42** and **TG-42** showed the best match for the known 42 Å distance between the binding sites of langerin. The 104 Å complexes (**G-104** and **TG-104**) present the worst match, as the distance between the ligands is more than twice as long as the distance between the binding sites. (A comparison with **G-23** and **TG-23** would also be possible. However, as the rebinding effect plays such a large role in these short complexes the affinities do not describe the ligands abilities to bridge the binding sites.) To calculate a sensitivity factor, the affinity of the mismatch case is divided by the affinity of the match. For Glc2NHTs the selectivity factor calculated from **G-42** and **G-104** is therefore 2.5. In comparison the selectivity factor for TriGlc2NHTs (**TG-104** vs. **TG-42**) is enhanced to 6. This result is surprising as one could assume that the bivalent Glc2NHTs complexes are more precise at probing the distance between two binding sites than bivalently presenting ligand clusters. However, in both cases a flexible linker was used to conjugate the ligands to the duplex. Presumably, the linker has a larger effect on the sensitivity than the use of clusters. The advantageous sensitivity factor for the bivalent presentation of TriGlc2NHTs further promotes the idea of using bivalent clusters on DNA-based scaffolds when constructing ligands designed to match the target geometry.

Overall, the presentation of the Glc2NHTS on our multivalent PNA-DNA scaffolds

resulted in extraordinarily potent ligands with up to nanomolar affinities and an over 1000-fold improved affinity in comparison to Glc2NHTs. This method should represent a general solution for amplifying the affinity of multivalent DNA based ligands or making chelate effects possible when the monovalent ligands are too weak. It is important to put these results into the context of previously done research to evaluate our strategy of designing well defined ligands with optimised ligand economy for the targeting of langerin. In comparison, Hartmann and her co-workers designed a trivalent polyamide-based langerin ligands (Figure 8A), which resulted in an only 35-fold potency increase per ligand.[78] However, Hartmann and her co-workers applied the much weaker ligand mannose. Taniguchi was able to attain a 1000-fold potency gain by equipping a C-3 symmetric scaffold with 6-sulfo-Galβ4(6-sulfo-GlcNAc) as illustrated in Figure 8B.[61] However, Taniguchi *et al*. applied an Elisa assay immobilising langerin on the surface, which can be manipulated by cross-linking if the protein density is too high. A comparison with DNA based ligand approaches can also be made. The 700-fold affinity improvement for ConA described by Ebara and his co-workers when presenting a total of 18 maltose units on a trivalent DNA based scaffold corresponds to a 38-fold potency enhancement per ligand (Figure 13B).[89] Bandlow *et al*. reported a up to 50-fold affinity enhancement per ligand for the bivalent display of sialyl LacNac to inhibit hemagglutinin (Figure 13A). [17]Scheibe *et al*. reported a 33-fold potency improvement per ligand when bivalently presenting LacNac to inhibit ECL (Figure 12C).[15] These comparisons highlight the power of combining statistical rebinding with a distance optimised chelate effect, which led to a 193 fold affinity enhancement per ligand. However, the compared examples started with a millimolar binders therefore the comparison is not concise. A comparison with the bivalent presentation of a cluster of three modified mannose ligands on a rigid molecular rod presented by Bernardi and her group is perhaps more feasible as they began with a monovalent affinity (IC_{50} = 270 μM) comparable to the affinity of Glc2NHTs (347 μM). [80]The optimised scaffold led to an IC_{50} = 5 μM, which corresponds to a relative potency enhancement per ligand β/n = 9. (The authors point out this may be limited due to lower limit of the assay). The spatial screening with PNA-DNA, which led to an enhanced affinity per ligand β/n = 193, therefore demonstrates the power of these high precision DNA-type scaffolds.

4.2.3.3 SPR Assay: Multivalent Mannose-PNA-DNA ligands

We were further interested in the use of ligands, which did not exhibit a selectivity for langerin over other CTLs. This would allow answering the question whether such a selectivity could be achieved purely by the spatial arrangement of the ligands. As mentioned, mannose is one of the most potent natural langerin inhibitors and also binds to other C-type lectins such as DC-SIGN. Therefore, the multivalent presentation of mannose should allow to compare the binding to langerin and DC-SIGN. However, the affinities are in the millimolar range for both targets. [54] A screening with bivalent mannose complexes M-42, M-62, M-84, M-104 using an Ella type plate assay against langerin and DC-SIGN did not lead to any results (not shown) as the bivalency effects were not strong enough to measure at a synthetically feasible concentration. Additionally, the complexes showed poor solubility in the millimolar range. A single measurement of **G-42** vs langerin with the ^{19}F-NMR assay did not show any multivalency effect despite applying the previously established optimised bivalent presentation. However, based on the impressive results achieved by combining statistical rebinding and chelate effect the same approach was envisioned for mannose. The Trimannose ligand **40** (TriMan) was initially tested in the ^{19}F-NMR assay (conducted by Nina-Louisa Èfrem) against langerin (Table 15). TriMan (IC_{50} = 0.3 ± 0,1 mM) was 10-fold more potent than mannose (IC_{50} = 5.1 ± 1.3 mM). Interestingly, TriMan **40** showed a 6-fold affinity enhancement per ligand in comparison to mannose, which is slightly lower than the 10-fold affinity gain per ligand achieved for TriGlc2NHTs. Evidently, the lower affinity of mannose to langerin leads to a smaller rebinding effect. However, the trivalent mannose ligand reported by Hartmann and her co-workers showed affinities for langerin up to an IC_{50} = 44 µM.[78] Interestingly, Hartmann reported that their trivalent polyamide with the shortest arms was the strongest inhibitor. However, TriMan **40** has considerably shorter arms than the best inhibitor reported by Hartmann. As neither the Hartmann ligands nor the TriMan ligand are able to bridge the langerin binding sites these results may imply that there is an optimal arm length for statistical rebinding.

In the SPR assay neither mannose nor TriMan were able to able to inhibit the langerin-chip interaction by 50 % up to a final concentration of 5 mM (Table 15). Therefore,

no IC_{50} was calculated. At 5 mM ligand concentration the residual langerin Binding was 83 ± 2 % and 65 ± 2 % for mannose and TriMan, respectively. As previously mentioned, the rebinding effect appears to be stronger in the ^{19}F-NMR assay, this may be due to the difference in the competitive systems. While TriMan is quite capable of displacing the monovalent ^{19}F-mannose derivative due to its rebinding advantage, it has no such advantage when competing against the highly multivalent Polyacrylamid-mannose-functionalised-chip. The same small library of bivalent TriMan-PNA-DNA complexes (**Tm-Mono**, **Tm-23**, **TM-42**, **TM-84**, **TM-104**) was examined via the SPR assay to determine their affinity to langerin (Table 16). Because of expected low inhibition capacities, instead of a titration the inhibition of the langerin chip interaction was monitored at a single high concentration (220 µM) in single measurements. The residual langerin-chip interaction was measured. A more potent ligand prevents the langerin-chip interaction more effectively. The monovalent TriMan-PNA-DNA complex, **TM-Mono**, was able to reduce the protein-chip interaction to 56 %. The bivalent complexes revealed the same distance affinity relationship that had been uncovered with the Glc2NHTs ligand. The 42 Å, **TM-42**, complex reduced the protein-chip-interaction to only 20 % and was the strongest inhibitor.

Table 15. Affinity of mannose and TriMan for langerin determined by ^{19}F-NMR and SPR. [a] Conditions: complexes incubated with langerin (50 µM) and 0.1 mM ^{19}F-marked reporter ligand in 25 mM Tris/HEPES with 10 % DMSO, 10% D2O, 150 mM NaCl, 0.05 mM TFA and 5 mM CaCl2 at pH 7.8 and 25° C. [b] Conditions: 5 min incubation of complexes (5mM) with 500 nM langerin in 25 mM HEPES, 150 mM NaCl, 5 mM CaCl2, pH 7.8, 25° C followed by determining binding of residual langerin to an α-D-mannose–functionalized SPR chip. The ^{19}F-NMR assay was conducted by Nina-Louisa-Èfrem (MPIKG) and the SPR assay by Kim Silberreis (Charité) and evaluated by myself.

Compound	IC 50 ^{19}F-NMR [a]	β/n	Residual Langerin Binding at 5mM Ligand Concentration [b]
mannose	5.1 ± 1.3 mM	1	83 ± 2 %
TriMan	0.3 ± 0,1 mM	3.4	65 ± 2 %

The bivalent complexes revealed the same distance affinity relationship that had been uncovered with the Glc2NHTs ligand. The 42 Å, **TM-42**, complex reduced the protein-chip-interaction to only 20 % and was the strongest inhibitor. **TM-23** displayed only minorly reduced inhibitory power (22 % interaction remaining). **TM-84** and **TM-104** had reduced potency with 27 % and 33 % interaction remaining,

respectively. Hence, the bivalent presentation of TriMan was nearly 3-fold more potent than the monovalent complex. Again, the attachment of the ligand onto the DNA scaffold had an advantageous effect on ligand affinity as observed for Glc2NHTs and TriGlc2NHTs. Unfortunately, no direct comparison with TriMan **40** can be made as the ligand did not show any inhibition at 220 µM concentration. However, based on the determined remaining protein-chip-interactions an $IC_{50} > 5$ mM for TriMan and an $IC_{50} < 220$ µM for **TM-42** can be assumed. This correlates to an affinity enhancement of at least 3.7 per mannose ligand. In summary, the experiments with mannose-based ligands displayed the difficulties of working with very low affinity ligands and the advantages of combining statistical rebinding and chelating effect. The application of TriMan as a means to increase ligand affinity (TriMan vs mannose) at one binding site provided multivalency effects when presented bivalently that could not be achieved with the bivalent presentation of mannose. A further examination and comparison to other mannose binding lectins would be highly interesting. Therefore, a future aim is the establishment of the SPR assay for DC-SIGN to compare the binding of the ligands to this CTL.

Table 16. Distance affinity screening for TriMan-PNA-DNA duplexes determined by SPR. The residual langerin binding to the SPR chip was monitored at a single inhibitor concentration (220 µM). Conditions: 5 min incubation of complexes with 500 nM langerin in 25 mM HEPES, 150 mM NaCl, 5 mM CaCl2, pH 7.8, 25° C followed by determining binding of residual langerin to an α-D-mannose–functionalized SPR chip.The experiments were carried out as single measurements; therefore, no error was calculated. [a] based on 3.25 Å average rise per base pair in a DNA·PNA duplex. The SPR assay way conducted by Kim Silberreis (Charité) and evaluated by myself.

Structure	Compound	Distance[a]	Langerin Binding at 220 µM Ligand
	TM-Mono	-	56 %
	TM-23	23 Å	22 %
	TM-42	42 Å	20 %
	TM-84	82 Å	27 %
	TM-104	104 Å	33 %

4.2.3.4 SPR Assay:Multivalent BiPhMan-PNA-DNA ligands

As working with a millimolar affinity ligand was tedious and the expected multivalency effects much lower than for a more potent ligand, a more powerful ligand that targets both langerin and DC-SIGN was necessary. Wamhoff *et al*. had recently discovered a Biphenyl modified-mannose glycomimetic (BiPhMan **49**) with improved affinity for langerin (K_I = 0.25 ± 0.07 mM) as well as DC-SIGN (K_I = 0.8 mM).[105] As the previously developed synthesis route by Eike Wamhoff was extremely long, a new route was composed and successfully used to attain the ligand. This work was partially carried out by Gary Domenico (exchange student EPFL, Lausanne) under my supervision. Additionally, to further verify the advantages of the bivalent Triligand presentation a trivalent TriBiPhMan **52** was synthesized. With the previous results in hand, the application of the novel BiPhMan and TriBiPhMan seemed very promising. Both ligands **49** and **52** were attached to PNA applying thiol-maleimide chemistry and a small range of bivalent BiPhMan-PNA-DNA and TriBiPhMan-PNA-DNA complexes constructed. BiPhMan **49** was measured to have an IC_{50} = 435 ± 98 μM by SPR for langerin, which was in the same range as Wamhoff *et al*. had measured using the ^{19}F-NMR assay (K_I = 250 ± 70 μM). Disappointingly, both **B-42** (IC_{50} = 277 ± 20 μM) and **B-104** (IC_{50} = 232 ± 18 μM) were only roughly twice as potent as the ligand **49 (**Table 17**).** In fact, the weak multivalency effects were most likely concentration effects (β/n<1). This was very surprising as the potency of BiPhMan (IC_{50} = 435 ± 98 μM) for the langerin ECD is comparable to Glc2NHTs (IC_{50} = 347 ± 11 μM). A similar monovalent affinity should make similar multivalency effects possible. It is conceivable that the binding orientation of BiPhMan **49** and mannose to langerin are not the same. The linker for BihPhMan was introduced at the C-6 position unlike for mannose and Glc2NHTs, where the linker was introduced at C-1. Even though the linker was shown to not directly negatively impact the binding of a single BiPhMan ligand to langerin it may prohibit optimal multivalent binding, by forcing the ligand into an orientation where the linker points towards the protein.[105]

Gratifyingly, the implementation of the TriBipHMan **52** showed multivalency effects (Table 18). The TriBiPhMan ligands were measured at a maximum concentration of 50 μM.

Table 17. Distance affinity screening for BiPhMan-PNA-DNA duplexes determined SPR. Conditions: 5 min incubation of complexes with 500 nM langerin in 25 mM HEPES, 150 mM NaCl, 5 mM CaCl2, pH 7.8, 25° C followed by determining binding of residual langerin to an α-D-mannose–functionalized SPR chip. [a] based on 3.25 Å average rise per base pair in a DNA·PNA duplex. The SPR assay way conducted by Kim Silberreis (Charité) and evaluated by myself.

Structure	Compound	Distance[a]	IC_{50} [μM]	β/n- Value
	BiPhMan	-	435 ± 98	1
	B-42	42 Å	277 ± 20	0,64
	B-104	104 Å	232 ± 18	0,76

The monovalent **TB-Mono** was only able to inhibit 13 % of the langerin-chip interaction at this concentration making an IC_{50} calculation impossible. As in the previous spatial screenings the 42 Å complex, **TB-42**, (IC_{50} = 4,7 ± 0,2 μM) was the best binder and nearly 100 times more potent than the BiPhMan ligand. The ligands **TB-23** (IC_{50} = 25.3 ± 4.3 μM and **TB-104** (IC_{50} = 44.0 ± 7.0 μM) showed reduced affinities for langerin. An up to 15-fold affinity improvement per BiPhMan moiety was calculated for **TB-42**. In comparison, **TB-104** only exhibits a relative potency increase per ligand of 1.6. The results prove that the joint strategy of rebinding and chelate effect lead to superior multivalency effects and yet illustrate how crucial an optimal presentation of the binders remains for ligand economy.

In conclusion, these results further supported the bivalent presentation of trivalent ligands on the DNA scaffold and demonstrated the optimised distance in the spatial screening = 42 Å. Complex **TB-42** is roughly two orders of magnitude more potent than the BiPhMan ligand. However, this gain falls 10-fold short of the affinity improvement of 1000 achieved for the **TG-42** in comparison to Glc2NHTs. This supports the assumption made for the BiPhMan ligand that, possibly due to the binding orientation and position of the linker, the multivalency effects are smaller for this ligand. Having successfully established a spatial screening on langerin, with a ligand that binds both to DC-SIGN and langerin, with synthetically feasible IC_{50} values in the low micromolar range the next goal will be to test the same compounds against DC-SIGN. Hopefully, distinct structure-affinity relationships will be established, which

will help in understanding how selectivity based on the spatial orientation of multivalent ligands can be generated.

Table 18. Distance affinity screening for TriBiPhMan-PNA-DNA duplexes determined by SPR. Conditions: 5 min incubation of complexes with 500 nM langerin in 25 mM HEPES, 150 mM NaCl, 5 mM CaCl2, pH 7.8, 25° C followed by determining binding of residual langerin to an α-D-mannose–functionalized SPR chip. [a] based on 3.25 Å average rise per base pair in a DNA·PNA duplex. The SPR assay way conducted by Kim Silberreis (Charité) and evaluated by myself..

Structure	Compound	Distance[a]	Langerin Binding at 50 µM Ligand	IC_{50} [µM]	β/n-Value
	BiPhMan	-	95 ± 3 %	435 ± 98	1
	TB-Mono	-	87 ± 2 %	n.d.	-
	TB-23	23 Å	23 ± 5 %	25,3 ± 4,3	3
	TB-42	42 Å	3 ± 2 %	4,7 ± 0,2	15
	TB-104	104 Å	29 ± 1 %	44,0 ± 7,0	1.6

In summary, we developed two *in vitro* assays (^{19}F-NMR and SPR) which successfully enabled the determination of the optimal multivalent ligand presentation for langerin. Satisfyingly, we achieved the same optimal distance of 42 Å when applying both assays and different ligands. The results showed that different multivalency mechanisms play a role (statistical rebinding and chelating). Furthermore, the combination of both effects generally led to more potent and more efficient multivalent ligands. In fact, in the cases of mannose and BiPhMan only the bivalent presentation of the TriMan and TriBiPhMan made the determination of the binding affinities possible and afforded multivalency effects. Furthermore, the results with the BiPhMan and TriBiPhMan ligand suggest that not only the binding affinity but also the binding orientation and linker may influence the multivalency effects.

4.3 Affinity for Langerin overexpressing Cells

4.3.1 Competitive Cell Assay

Although the bivalent Glc2NHTs-PNA-DNA complexes were potent binders for the langerin ECD protein in both the NMR and SPR assay it remained to be shown that this was also possible for a cellular system. For the further evaluation of the bivalent Glc2NTs-PNA-DNA, we advanced to testing the bivalent ligands against langerin and DC-SIGN expressing cells. Furthermore, by comparing the affinity between langerin and DC-SIGN overexpressing cells, selectivity could be evaluated. We collaborated with the AG Rademacher, who were able to provide Raji cells modified to stably overexpress langerin or DC-SIGN.[47] The cellular assay was conducted by Felix Fuchsberger (MPIKG) and myself to examine the affinity of ligand-PNA-DNA duplexes based on a previously established assay in the Rademacher group to test the binding of ligand equipped liposomes to langerin.[47, 60]

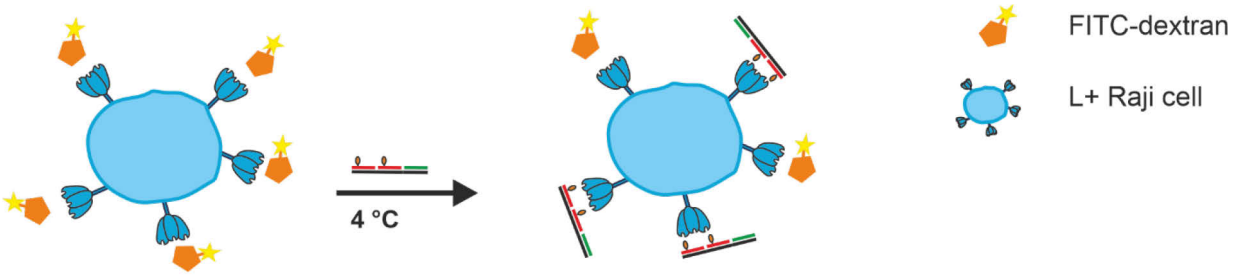

Figure 23. Competitive 96 well plate cell assay step up. Bivalent ligands displace FITC-dextran bound to langerin expressing cells. The remaining MFI is read out by flow cytometry. Cartoon portrays a single well in the assay.

Langerin or DC-SIGN overexpressing Raji cells were counted and 50,000 cells added per well to a 96 well plate in cell media (RPMI). The cells were incubated with the ligands and a competitive reporter ligand for 60 min at 4°C. The reporter ligand was comprised of a fluorophore marked polysaccharide, FITC-dextran (2,000kDa), which binds to both langerin and DC-SIGN (Figure 23). Upon incubation the applied ligands bind to their target protein and displace FITC-dextran to varying degrees. After washing, cells were fixed with paraformaldehyde and resuspended in cell media. The fluorescence at wavelength 666 nm, which is proportional to the remaining FITC-dextran bound to the cell, was detected via flow cytometry. Mean fluorescence Intensity (MFI) was plotted against the ligand concentration and the IC_{50}s calculated.

As an internal control, every 96 well plate included mannose as one of the ligands tested. Each individual experiment included 3 technical triplicates. The assay had previously been established for liposome-based ligands using Hanks Balanced Salt Solution (HBSS), a phosphate buffer modified with sodium bicarbonate. The poor solubility of the Glc2NTs-PNA-DNA complexes in HBSS made the addition of DMSO necessary. To ensure the cells viability a maximum DMSO concentration of 4 % was possible . As the solubility of the complexes in HBSS with 4% DMSO remained poor, another strategy was needed to enhance the solubility. Therefore, we adjusted the design of our complexes by adding a DNA overlap of 10 nucleobases, which improved the solubility substantially by adding negative charges. The complexes containing the DNA overlap are marked with an "O" e.g. G-42-O.

Table 19 shows the results measured in three independent replicates. Four bivalent complexes G-23-O, G-42-O, G-82-O, G-104-O, and the monovalent complex G-Mono-O were examined. On average the calculated IC_{50}-values for mannose were in the range of 5 to 6 mM. However, in the first distance affinity screening (Replicate 1) the values for mannose varied greatly (3-14 mM). A comparison of the measured values for the bivalent Glc2NHTS-PNA-DNA complexes is difficult if a similar fluctuation is assumed as for the values acquired in the mannose control experiments. In the second and third replicates, the obtained IC_{50}s of the mannose control were much more stable and comparable to previously obtained results in the Rademacher group (5-6 mM). Furthermore, the results of the second and third row showed good agreement, while the values of the first replicate differentiate. The further evaluation will therefore concentrate on the values gained in the second and third independent replicates. Disappointingly, the obtained IC_{50}s to do not show any distance affinity relationship (all IC_{50}s = 4-7 μM). The second and third replicates show that all the bivalent complexes have the same capacity of displacing dextran from the langerin expressing cells regardless of the distance between the ligands. However, the bivalent complexes are all roughly ten-fold more potent than Glc2NHTs (IC_{50} = 57 μM). An explanation of these results remains difficult. No information on the langerin expression rates on the cells was available. Furthermore, it is not known how the langerin ECDs are positioned to one another e.g. clustering effects and whether this

changes after adding bivalent ligands. The closely related C-type lectin DC-SIGN forms nanometre sized clusters on the cell surface.[39] If clustering takes place in the case of langerin this could explain, why the measured affinities were highly enhanced but no distance affinity relationship was evident.

Table 19. Competitive Cell Assay: Distance Affinity Relationship for Bivalent Glc2NHTS-PNA-DNA constructs with DNA overlap. Conditions: Raji cells were incubated with ligands and FITC-dextran (0.025 mg/mL in HBSS (4% DMSO) for 60 min at 4 °C, resuspended in cell media, fixed with paraformaldehyde, resuspended in fresh media and analysed by flow cytometry. The Errors are the SD of technical triplicates. [a] based on 3.25 Å average rise per base pair in a DNA·PNA duplex. The assay was conducted by Felix Fuchsberger (MPIKG) and myself.

Structure	Compound	Distance[a]	IC_{50} [µM] Replicate1	IC_{50} [µM] Replicate 2	IC_{50} [µM] Replicate 3
	mannose	-	13 600 ± 600	5900 ± 400	6100 ± 200
	mannose		2700 ± 1000	5200 ± 500	5400 ± 400
	Glc2NHTs		-	-	57 ± 10
	G-Mono-O	-	40.9 ± 4.8	-	-
	G-23-O	23 Å	5.4 ± 1.0	6.5 ± 0.6	6.0 ± 0.8
	G-42-O	42 Å	57 ± 4	4.6 ± 1.0	4.5 ± 0.9
	G-84-O	84 Å	21.7 ± 3.5	4.9 ± 0.6	4.8 ± 1.3
	G-104-O	104 Å	147 ± 10	6.0 ± 0.4	7.0 ± 1.4

Cross-linking of the receptors by the bivalent ligands could be influencing the binding affinities. Cross-lectin binding may even lead to similarly strong affinity increases as the one to one binding between the bivalent ligands and the langerin ECD. Subsequent work with the cell internalisation assay, which will be discussed in the following chapter, revealed that the DNA overlap could interfere with affinity measurements by causing unspecific binding. Although the competitive nature of the assay makes it rather robust against the influence of unspecific binding the assay was repeated without the DNA overlap. The initial problem of poor solubility in the HBSS buffer was overcome by using HEPES buffer, which generally has much better solubility properties for PNA-DNA duplexes than phosphate buffers. The use of 4 % DMSO as previously was not necessary. The range of bivalent Glc2NHTs ligands was re-examined and their affinity for the langerin expressing Raji cells characterized.

The results are listed in Table 20. The mannose control experiment delivered an IC_{50} (4.5 ± 0.77 mM) comparable to the previous experiments. All the Glc2NHTs-PNA-

DNA complexes showed greatly increased affinities in comparison to Glc2NHTs. Disappointingly, we were not able to identify a distance affinity relationship. As before, the bivalent complexes all showed the same affinities when taking the errors into account. Notably, the monovalent complex **G-Mono** showed the same affinity as the bivalent complexes **G-23, G-42, G-84, G-104** and was roughly 100 times more potent than free ligand **72**. Furthermore, the affinity increase was much larger than the previously determined affinity increases when using complexes without DNA overlap.

Table 20 Competitive Cell Assay: Distance Affinity Relationship for Bivalent Glc2NHTS-PNA-DNA constructs. Conditions: Raji cells were incubated with ligands and FITC-dextran (0.025 mg/mL in 10 mM HEPES, 150 mM NaCl, 3 mM EDTA, pH 7.4 for 60 min at 4 °C, resuspended in cell media, fixed with paraformaldehyde, resuspended in fresh media and analysed by flow cytometry. The Errors are the SD of technical triplicates. [a] based on 3.25 Å average rise per base pair in a DNA·PNA duplex The assay was conducted by Felix Fuchsberger (MPIKG) and myself

Structure	Compound	Distance[a]	IC_{50} Langerin	IC_{50} DC-SIGN
	mannose	-	4500 ± 770 µM	3700 ± 400 µM
	Glc2NHTs (72)	-	23 ± 43 µM	-
	G-Mono	-	0.27 ± 0.28 µM	-
	G-23	23 Å	0.21 ± 0.04 µM	> 150 µM
	G-42	42 Å	1.09 ± 0.97 µM	> 150 µM
	G-84	84 Å	0.28 ± 0.10 µM	> 150 µM
	G-104	104 Å	0.54 ± n.d. µM*	> 150 µM

* Error not determinable due to an unsuccessful fitting process

A final experiment compared the different conditions that had been used in the assay, to determine their influence on the measured affinities. We tested the influence of 4 % DMSO and the influence of the DNA overlap (Table 21). As shown in Table 21 the use of 4 % DMSO and the DNA overlap could not explain the differences of the measured IC_{50} values. In addition the bivalent complexes **G-Mono, G-23, G-42, G-84** and **G-104** were also tested against DC-SIGN expressing Raji cells but no inhibition of the dextran-cell interaction was detected up to a concentration of 150 µM. This experiment proved that the Glc2NHTs-PNA-DNA duplexes were selective langerin binders. This result was not unexpected as the monovalent ligand Glc2NHTs **72** showed a 53-fold selectivity for langerin over DC-SIGN in the ^{19}F-NMR assay.

Table 21 Competitive Cell Assay: Comparison with and without DNA overlap; buffer =HBS (HEPES buffered solution) or 4 % DMSO/HBS. Performed as single experiments. The assay was conducted by Felix Fuchsberger (MPIKG) and myself.

Structure	Compound	Buffer	IC_{50} [uM]
	mannose	HBS	5800 ± 1000
	mannose	4% DMSO	6600 ± 1000
	Glc2NHTs	HBS	18 ± 1
	Glc2NHTs	4% DMSO	25 ± 5
	G-84	HBS	0,26 ± 0,06
	G-84	4% DMSO	0,15 ± 0,02
	G-84-O	HBS	0,20 ± 0,01
	G-84-O	4% DMSO	0,20 ± 0,03

In summary, although trends in IC_{50} values remained the same between complexes measured on the same day, the competitive cell assay did not provide reliable results. The large distribution in determined IC_{50} values for the mannose control experiment and the bivalent complexes on different measuring days or different plates made a comparison of the affinities difficult. The comparison of different conditions ensured this was not due to small variations in the assay setup. The differences could therefore be biological errors. As previously mentioned, very little information about the amount and distribution of the receptors on the cell was known and how this varies over time, which may be influencing the binding affinities. While the obtained values resulted in more questions than answers a positive aspect remains that we had again demonstrated the successful application of DNA based scaffolds for designing extremely potent multivalent inhibitors. The bivalent Glc2NHTs-PNA-DNA complexes were up to 100-fold more potent than Glc2NHTs and showed an up to 21 000-fold higher affinity than mannose for langerin expressing cells. Furthermore, Glc2NHTs-PNA-DNA complexes were not able to displace FITC-dextran from DC-SIGN overexpressing cells, proving the selectivity of the ligands.

4.3.2 Affinity Cell Assay

Although the previous experiments had shown the potency of the bivalent ligands to inhibit the interaction between dextran and langerin expressing cells the assay results were regarded as unreliable due to the discussed problems. Therefore, a gain-of signal assay was designed to evaluate the selectivity of the ligands.

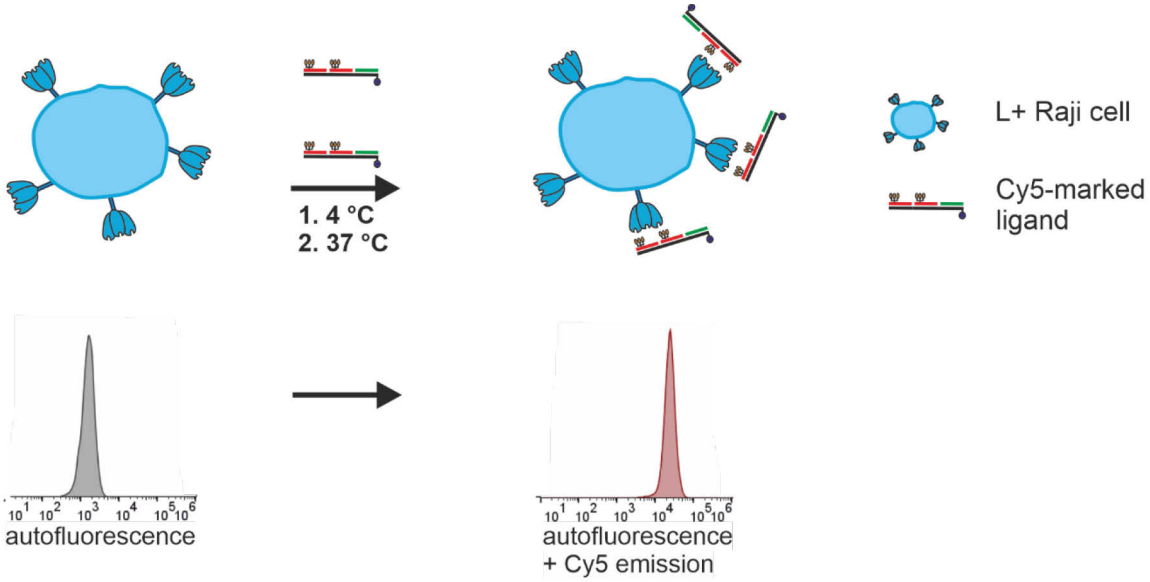

Figure 24. Cell Internalization assay set up: Langerin expressing Raji cells are incubated with bivalent ligands at 4 °C and 37 °C. The Cy5 emission was subsequently read out by flow cytometry.

Targeting L^+ cells selectivity has been difficult to achieve. Duinkerken *et al*. applied branched PAMAM dendrimers to present the Lewis Y trisaccharide multivalently, which bound to both langerin and DC-SIGN expressing cells.[106] Furthermore, the potential advantages of the improved bivalent TriGlc2NHTs ligand in a biological environment was to be examined. To demonstrate the selectivity of optimised bivalent ligands **G-42** and **TG-42**, their binding and internalisation capacity to langerin overexpressing (L^+) Raji cells was compared to DC-SIGN overexpressing cells (DCS^+) and wild type (wt) Raji cells. The wt Raji cells do not express langerin or DC-SIGN receptors natively. The DCS^+ and wt cells therefore act as negative controls. Additionally, the L^+ cells should be able to discriminate between PNA-DNA complexes that contain the Glc2NHTs and no-ligand bearing duplexes (nL). This would prove that complex binding and potential uptake is ligand dependent. In the previous competitive cell assay, cells were incubated with ligands at 4° C to ensure that the measured effects were purely binding effects. At higher temperatures receptor

mediated internalization can take place. For this assay clathrin-mediated endocytosis was deliberately taken into account. The assay measured the ability of ligands to bind to the receptors and be internalised. 50 000 langerin-, DC-SIGN overexpressing or wild type Raji cells were incubated with fluorophore marked ligands at a final concentration of 660 or 66 nM. The bivalent ligand complexes were marked with a fluorophore by introducing Cyanine 5 (Cy5) conjugated DNA strand as the template strand, which is a commercially available. Fluorophore tagged complexes are indicated e.g. Cy5 tagged G-42 is named G-42-Cy5. After 45 min of incubation at 4°C, the cells were resuspended in fresh media and incubated for 60 min at 37 °C to allow for internalization. Prior to analysis cells were centrifuged, aspirated and resuspended in fresh media.

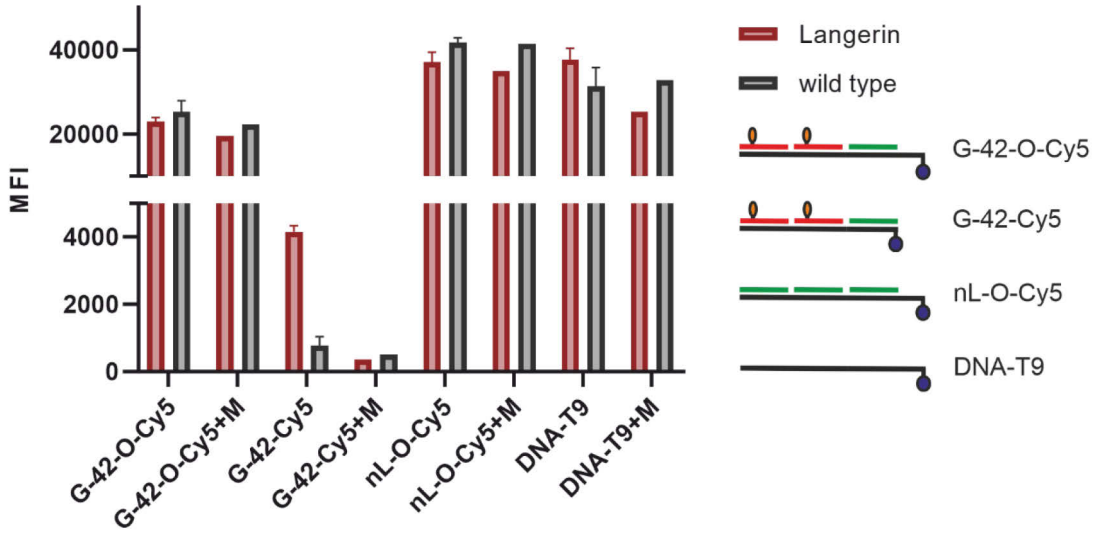

Figure 25. Affinity cell assay: G-42-O-Cy5, nL-O-Cy5 and DNA-T9 binds to both L^+ and wt Raji cells. G-42-Cy5 binds selectively to L^+ cells. Incubation of cells with G-42-Cy5 and Mannan (+M) leads to MFI on the background level. Conditions: Raji cells were incubated with ligands in cell media for 45 min at 4 °C (660 nM), resuspended in fresh media, incubated for 60 min at 37 °C, resuspended in fresh media and analysed by flow cytometry. The Errors are the SD of three independent experiments. The preliminary experiments were conducted by Felix Fuchsberger (MPIKG) and myself

Dr. Knut Rurack (Bundesanstalt für Materialforschung und -prüfung) kindly provided access to flow cytometry, which was used to determine the mean fluorescence intensity (MFI) of the cell population. The results were corrected by subtracting the autofluorescence background MFI, defined as the MFI readout from Raji L^+ cells without DNA or ligand treatment. In the first method the final concentration of the ligands was 660 nM. In a second alternative method the final concentration of the

ligands was 66 nM. Treating with 10-fold lower concentration it was deemed that an extra washing step prior to analysis was not required, therefore in the second method cells were measured by flow cytometry directly after incubation at 37°C. The results achieved with method 2 will be specifically pointed out as such. In both methods described, a negative control was achieved by incubating the cells with the Glc2NHTs ligands and Mannan (e.g. Figure 25: G-42-Cy5+M). Mannan is a very potent langerin and DC-SIGN inhibitor and therefore should be able to displace the Glc2NHTs-protein interaction. As Mannan binds specifically to the receptors, it will only eliminate canonical binding of the bivalent ligands to the receptors. Another negative control was introduced to rule out nonspecific binding and internalisation of the DNA-fluorophore conjugate; a Cy5-conjugated PNA- DNA duplex **nL-Cy5**.

An initial experiment was carried out in collaboration with Felix Fuchsberger (MPIKG) comparing Cy5-marked DNA **T9-Cy5**, **G-42-O-Cy5,** and the same complex but without DNA overlap **G-42-Cy5.** Binding and subsequent internalization to L^+ and wt cells was examined, applying method 1 as described.This experiment gave some very surprising results. In the case of the L^+ Raji cells all the tested ligands showed a mean fluorescence intensity (MFI) substantially higher than the autofluorescence background readout (MFI readout from the Raji cells without ligand treatment). Typically, the autofluorescence background level MFI was between 1500 and 2000. However, incubating wild type Raji cells with the same ligands revealed that these results can be partially attributed to unspecific binding. **G-42-O-Cy5, nL-Cy5** and **DNA-T9** showed the same elevated MFIs for the L^+ and wt cells. **G-42-Cy5** on the other hand, which did not contain a DNA overlap, revealed a strong MFI increase for L^+ cells, which was 4-fold larger than the MFI measured for wt cells (background). This demonstrates that only **G-42-Cy5** specifically binds to the langerin receptor. Single strand DNA appears to unspecifically bind to the cell and therefore cannot discriminate between the L^+ and wild type cells. As a further control we added Mannan to **G-42-Cy5** during incubation, which led to a reduction of the MFI to a similar level as the MFI for the wt cells, confirming that **G-42-Cy5** binds canonically to langerin on L^+ cells. The addition of Mannan to the other compounds did not lead to MFI reduction (Figure 25). To eliminate the ‘stickiness’ of the DNA to the Raji cell surface

the cells were incubated with 10% DNA blocking buffer (0,1 mg/mL Salmon sperm DNA, 0,2 % BSA in PBS) prior to use. Although this had been successfully implemented in the Seitz lab when faced with unspecific binding of DNA it did not improve the results for the complexes with DNA overlap. Based on these preliminary results all further experiments, which were carried out with the help of Sophie Neuber (Humboldt University) utilised complexes without a DNA overlap. The MFI level measured when incubating the ligands without DNA overlap with wt cells will be named the background binding level from here on. The ability of the 42 Å Glc2NHTs complex, **G-42-Cy5**, the 42 Å TriGlc2NHTs complex, **TG-42-Cy5,** and a PNA-DNA duplex without ligand functionalization **nL-Cy5** to bind/internalize to L^+ , DCS^+ and wt Raji cells were compared. Figure 26 A shows the results obtained for method 1. As can be seen the MFI is elevated in the case of the L^+ cells for both the **G-42-Cy5** and **TG-42-Cy5**. Upon addition of Mannan, a strong canonical langerin inhibitor, the MFI signal fell to the background binding level. The remaining MFI is due to residual unspecific binding to the cell (background). As a further control experiment **nL-Cy5** was incubated with L^+ cells leading to a background level MFI - comparable to the Mannan control, previously. In the case of the **nL-Cy5** the addition of Mannan did not decrease the MFI signal proving that this is residual unspecific binding. In comparison the incubation of the **G-42-Cy5** and **TG-42-Cy5** with DCS^+ and wt Raji cells did not lead to an MFI increase above the background level. Adding Mannan retained the background binding background MFI value for DCS^+ and wt Raji cells. Clearly, the residual MFI signal was due to unspecific binding (background). Evidently, **G-42-Cy5** and **TG-42-Cy5** bind to the L^+ cells canonically and the PNA-DNA scaffold does not interfere with the ability of the receptor to internalise. For the TriGlc2NHTs complex, **TG-42-Cy5,** the MFI of L^+ cells was 9-fold higher than for wt Raji cells (signal to noise). In comparison the signal to noise for the Glc2NHTs complex **G-42-Cy5** under identical conditions was only 4. This result was consistent with the 53-fold higher affinity of **TG-42** than **G-42** for langerin (Table 14). Previously, the Rademacher group had incubated the same cell lines with mannose equipped liposomes (M-liposome) to evaluate whether the DC-SIGN expressing Raji cells were in fact capable

of canonical binding, as recently published [47]

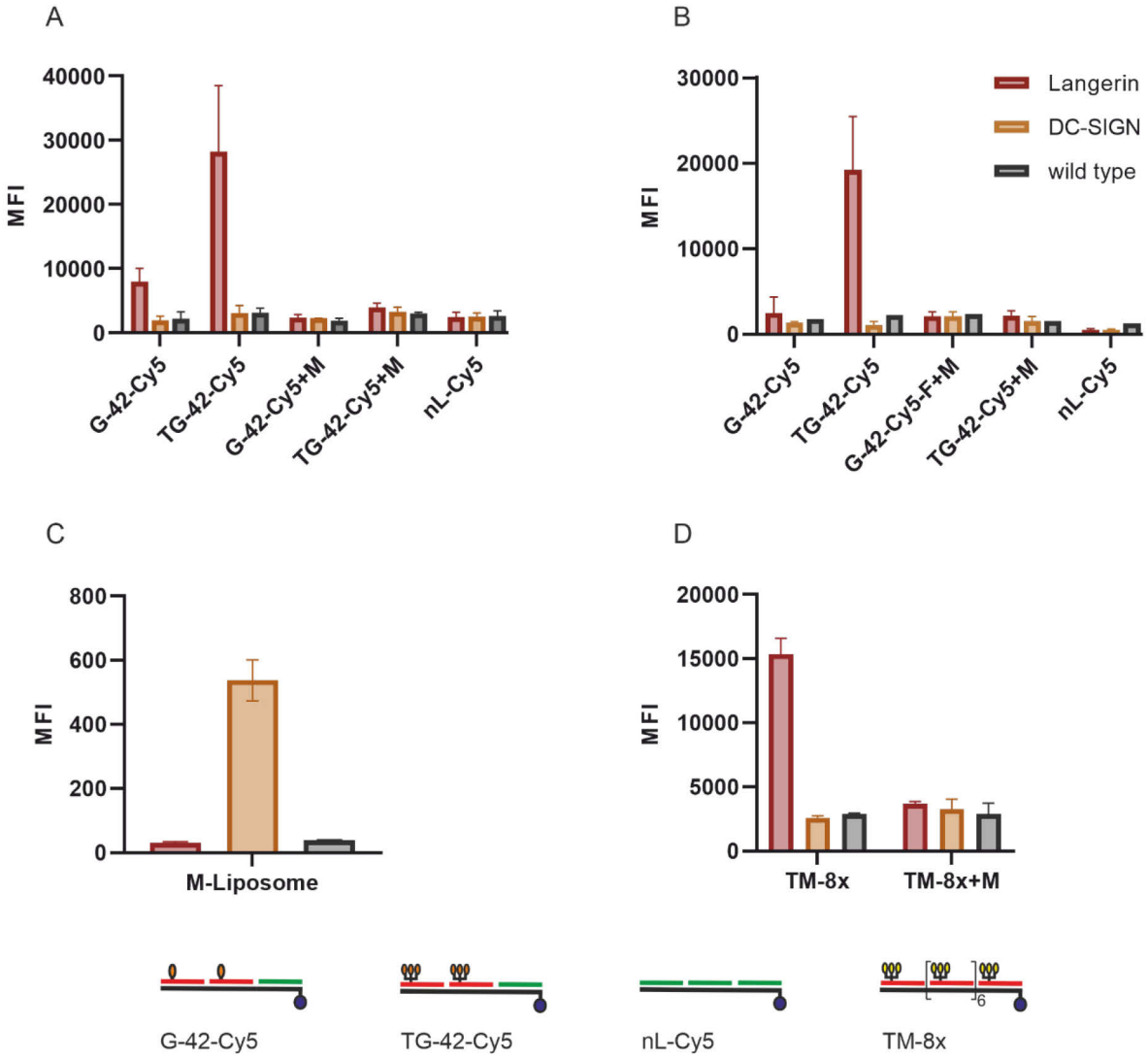

Figure 26 Affinity cell assay: Comparison of binding/internalization of A) nL-Cy5, G-42-Cy5, TG-42-Cy5; method 1 B) nL-Cy5, G-42-Cy5, TG-42-Cy5; method 2 C) mannose equipped Liposome (M-Liposome); method 3. D). TM-8x; method 1. The addition of Mannan is abbreviated by +M. Conditions: Method 1 and 2: Raji cells were incubated with ligands in cell media for 45 min at 4 °C (method 1 = 660 nM,; method 2 = 66 nM), resuspended in fresh media, incubated for 60 min at 37 °C, resuspended in fresh media (only method 1) and analysed by flow cytometry. Method 3: Raji cells were incubated with liposomes (16 µM) and incubated for 60 min at 4 °C, reuspended in fresh media and evaluated by flow cytometry. Experiments with DNA-based ligands were partly conducted by Sophie Neuber (Humboldt University) under my supervision. Experiments with mannose equipped liposomes were designed and conducted by Mareike Rentzsch (MPIKG). The errors are the SD of three independent experiments.

In this similar experiment devised and conducted by Mareike Rentsch (MPIKG), Raji cells were incubated with liposomes (16 µM) and incubated for 60 min at 4 °C, reuspended in fresh media and evaluated by flow cytometry. Astonishingly, although mannose shows similar affinities for both DC-SIGN and langerin, the multivalent mannose-liposomes were selective for DC-SIGN (Figure 26 C). This illustrates how

unique the selective binding capability for langerin, demonstrated by **G-42-Cy5** and **TG-42-Cy5**, is. Notably, we were not able to confirm these results by presenting mannose multivalently on the PNA-DNA duplex. Eight PNA strands, 13 nucleotides in length and modified with TriMan, were hybridised with a 104-nucleotide long DNA strand (**TM-8x**). The mannose-PNA-DNA duplex carrying a total of 24 mannose units was incubated with L^+ , DCS^+ and wt Raji cells applying method 1 but surprisingly only the L^+ cells displayed increased MFI values above the unspecific binding level (Figure 26D). This was unexpected as the experiments by the Rademacher group had led us to expect DCS^+ cells to be targeted most strongly by high mannose ligands. A direct comparison of the MFI values obtained for M-lipsome and TM-8x is not valid as different flow cytometers were used and the MFI value unitless. It cannot be excluded that the multivalent presentation of mannose on liposomes or DNA leads to different selectivity effects. Indeed, Fehres et al compared the internalisation of Lewis-Y, which is recognised by both langerin and DC-SIGN, when presented on synthetic long peptides (SLP) or liposomes. Remarkably, they found that langerin only internalised the glycan-modified-peptides into the cells efficiently. In contrast DC-SIGN internalised the glycan-modified liposomes but not the glycan-modified-SLP.[58] Importantly, no information on the quantity and the density of the mannose units on the liposome is available. The clustering of DC-SIGN on the cell surface may favour multivalent mannose-liposome structures. An evaluation of the cells using fluorescence microscopy did indeed show the DCS^+ cells were expressing DC SIGN-(fluorescent protein) at the cell membrane, as expected. However, further experiments should be carried out to examine the availability of DCS^+ Raji cells for canonical binding.

To demonstrate the additional value of the improved **TG-42-Cy5** ligand the same internalisation assay was carried out with a lower concentration of ligand (66 nM); described earlier as the second method. This time the second washing step after incubation at 37°C was eliminated. The second washing step was deemed unnecessary and could potentially weaken the signal. Additionally, since a 10-fold lower concentration of ligand was used, it was likely that the nonspecific binding to the cell surface would be less prominent, improving the signal to noise ratio. The results

(Figure 26 B) shows that incubation with **TG-42-Cy5** elevated the MFI 9-fold over the background level of the wt cells. Adding Mannan reduced the signal. As expected, the MFI for incubation with DCS^+ and wt cells was not elevated. In contrast to method 1, **G-42-Cy5** did not lead to elevated MFI above the unspecific binding background level upon incubation with L^+ cells at 66 nM concentration (method 2). Based on the SPR experiments complex **TG-42** is 53-fold more potent than the complex **G-42**. In conclusion the advantages of the combining statistical rebinding and chelation to increase the potency of the ligands are clearly apparent in the cellular context, where low concentrations play an important role due to toxicity and to limit nonspecific binding.

In summary a competitive assay and an internalisation/binding assay were developed to examine the binding and internalisation of the bivalent Glc2NHTs and TriGlc2NHTs ligands in a cellular system. Satisfyingly, both the **G-42** and **TG-42** were bound and internalized by L^+ cells at nanomolar concentrations. The bivalent TriGlc2NHTs presentation provided superior langerin targeting properties. Furthermore, the selectivity for L^+ cells over another mannose binding C-type lectin DC-SIGN was shown. Unfortunately, a distance affinity relationship could not be detected on the cell system, which may be due to clustering of the receptors. Furthermore, the loss-of-signal read out proved to be unreliable in the competitive cell assay.

5 Summary and Outlook

5.1 Summary

The trimeric receptor langerin is found on Langerhans cells, which have received increasing interest as an immunotherapy target. [22, 51] Langerhans cells can internalise antigens via langerin and stimulate T-cell response by presenting the antigens. Selectively targeting C-type lectins such as langerin is a challenging task as lectins with different physiological roles (e.g. langerin and DC-SIGN) do not show preference for a single carbohydrate and the affinities of the monovalent carbohydrate ligands are typically in the millimolar range. Highly multivalent ligand systems have been applied to increase avidity on a range of different scaffolds such as polymers[71], dendrimers[7] and liposomes[47]. In contrast to such brute force strategies our approach focused on improving ligand economy by rationally designing molecularly defined multivalent ligands and optimising avidity. The objective of this work was to develop high affinity multivalent ligands that selectively bind the C-type lectin (CTL) langerin. The method of choice was combining the development of selective glycomimetic langerin ligand with the advantages of multivalent ligand presentation on DNA based scaffolds. DNA-based scaffolds possess unique properties allowing precise positioning of ligands on highly defined rigid scaffold easily accesible via self-assembly.[15, 18-19, 97] Full control over the distance between the ligands allows to optimise the match (meaning the distance between two ligands corresponds to the distance between two binding sites) between the multivalent ligand system and the multimeric target protein. In particular, the design of ligands able to bridge two carbohydrate binding sites of langerin (chelate effect) was of interest to us. The chelation effect has been shown to provide superior binding affinities for the bivalent inhibition of lectines.[15, 80] Previous research has shown that the strength of the chelate effect is highly dependent on the affinity of the monovalent ligands.[36] However, monovalent affinities for C-type lectines are often in the millimolar range and developing high affinity glycomimetic remains challenging. We therefore envisioned a strategy for amplifying the chelate effect and optimising ligand efficacy. The rebinding effect, which can increase avidity at a single binding site, was to be combined with the chelate effect (bridging two binding sites) as a method to mimic the advantages of a high affinity ligand.

Based on rational design a glycomimetic langerin ligand, Glc2NHTs **72** (Figure 27C), was developed which displayed a 13-fold increase in affinity in comparison to mannose. Strikingly, Glc2NHTs revealed a 53-fold selectivity for langerin over DC-SIGN. Mannose binds both langerin and DC-SIGN with roughly the same millimolar affinity displaying marginal 1.4-fold selectivity for DC-SIGN. Bivalent DNA based Glc2NHTs ligands (Figure 27) were characterised as langerin binders by two orthogonal assays. In the case of the ^{19}F-NMR assay the ability of the ligands to displace a fluorine-tagged mannose derivative from interacting with langerin was measured. The SPR assay detected the ligands´ ability to inhibit the interaction between langerin and an SPR chip functionalised with α-D-mannose–polyacrylamide.

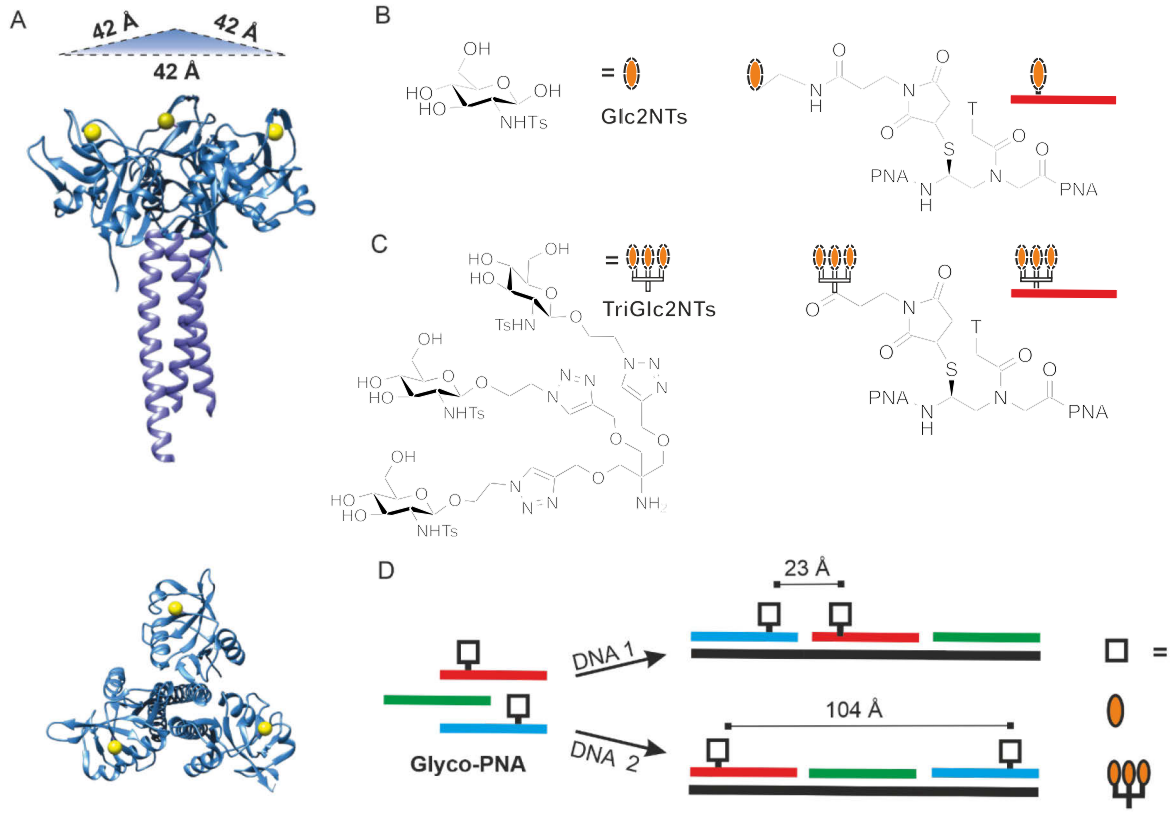

Figure 27 A) Crystal structure of the trimeric langerin extracellular domain (PDB: 3kqg) with Ca^{2+} ions (yellow) embedded in the CRD (blue) from a side view and from the top).B Glc2NTs ligand and Glc2NTs-PNA conjugates C)TriGlc2NHTs and TriGlc2NTs-PNA conjugates. D) Hybridization of modified (blue, red) and unmodified (green) peptide nucleic acid (PNA) oligomers with DNA templates (black) affords bivalent Ligand-PNA-DNA complexes with different distances between the ligands.

A spatial screening of the interaction between bivalent Glc2NHTs-PNA-DNA duplexes and langerin suggested that bivalent **G-42,** with ligands 42 Å apart, was optimal for increasing the bivalency effect (Figure 28). **G-42** was 16-fold more potent than the monovalent Glc2NHTs in the ^{19}F-NMR. Moreover, the distance of 42 Å was

in agreement with the distance between the carbohydrate-binding pockets, determined from the crystal structure. [51] This result highlighted the value of the DNA based molecular ruler approach for probing the distance between two binding pockets. Experiments that increased the flexibility of the DNA scaffold by introducing a single strand region between the ligands and an investigation of the linker influence by decreasing the length of the tether between ligands and PNA backbone led us to the conclusion that an optimal trade-off between flexibility and rigidity had already been achieved when targeting the flat and easily accessible protein surface of langerin. Although increasing the distance between the ligands beyond 42 Å gradually decreased the affinity of the bivalent ligands as expected, reducing the distance between the ligands surprisingly only marginally affected ligand affinities. **G-42** (IC_{50}=23 μM) was barely more potent than **G-16** (IC_{50} = 35 μM). This was surprising, as the distance between the ligands in complex **G-16** should be too short to bridge the distance between the CRDs of langerin. By comparing the affinities of the complexes **G-16** and **G-42** for the trimeric ECD and the monomeric CRD we found that the affinities of the bivalent binders were being affected by both the chelate and the rebinding effect. The results implied that the affinity enhancement of complex **G-16** relies on the statistical rebinding effect. The complex **G-16** holds two ligands in proximity of one binding site. The affinity of **G-16** for the ECD and CRD was therefore nearly identical. The bivalency effect of 42 Å complex **G-42** was found to be predominantly due to the chelation effect as the affinity to the ECD (23 μM) was 5-fold higher than to the CRD (120 μM). To verify the statistical rebinding effect three Glc2NHTs ligands were attached to a Tris(hydroxyethyl)aminomethane core. The trivalent cluster TriGlc2NHTs (Figure 27C) is unable to bridge the langerin CRDs. Binding experiments with the ECD revealed a 30-fold affinity enhancement in comparison to Glc2NHTs in the ^{19}F-NMR assay confirming that statistical rebinding is responsible for the affinity enhancement.

Aiming to magnify the potency of the multivalent ligands, we designed bivalent TriGlc2NHTs-PNA-DNA complexes exploiting both the chelation and the statistical rebinding effect. The same DNA based scaffold system was applied to characterize the distance affinity relationship of the bivalent presentation of TriGlc2NHTS. As we had

reached the IC_{50} limit of the ^{19}F-NMR assay (half protein concentration = 25 µM) an orthogonal SPR assay (IC_{50} limit = 250 nM) was necessary to determine the affinities of these high avidity langerin inhibitors. Evaluation of the bivalent Glc2NHTs-PNA-DNA complexes with the SPR assay confirmed the 19F-NMR assay results and G-42 as the superior langerin ligand (Figure 29A). Impressively, the bivalent presentation of TriGlc2NHTs led to high nanomolar ligand affinities.

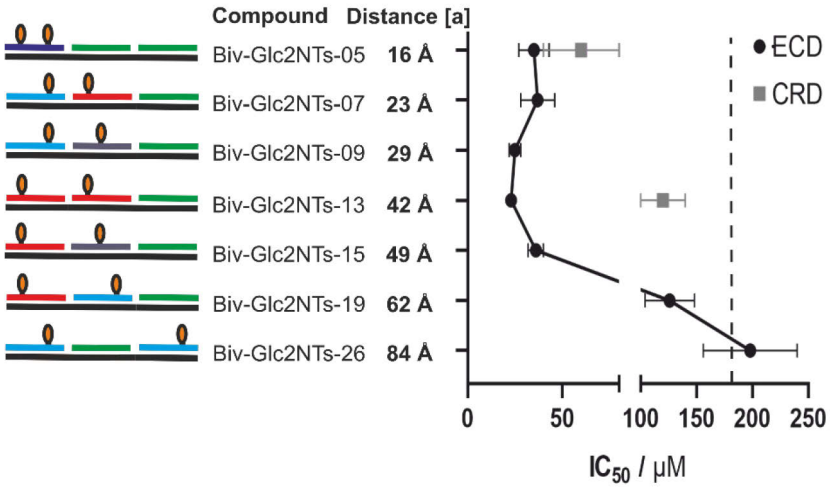

Figure 28 Distance dependent binding of bivalent Glc2NTs-PNA-DNA complexes to the langerin ECD determined by a ^{19}F NMR assay. IC_{50} values below the vertical dashed line (= IC_{50} (Glc2NTs) / 2) can be due to bivalency enhanced interactions. Grey squares mark values for binding of the langerin CRD. [a] based on 3.25 Å average rise per base pair in a DNA·PNA duplex. Conditions: complexes incubated at varied concentration with langerin (50 µM or 25 µM) and 0.1 mM.^{19}F-marked reporter ligand in 25 mM Tris/HEPES with 10 % DMSO, 10% D2O, 150 mM NaCl, 0.05 mM TFA and 5 mM CaCl2 at pH 7.8 and 25° C. [a] based on 3.25 Å average rise per base pair in a DNA·PNA duplex.

Importantly, the distance affinity relationship was retained, and **TG-42** was the most potent bivalent TriGlc2NHTs-PNA-DNA ligand (IC_{50} = 300 nM, Figure 29A). Previous research by Dubel *et al*. has highlighted the correlation between the affinity of the monovalent ligand and the chelate effect.[36] The stronger the affinity of the monovalent ligand the larger the bivalency-induced enhancements of affinity. By comparing the binding enhancements of bivalently presented Glc2NHTs and TriGlc2NHTs we evaluated whether this was also true when making use of a ligand cluster to mimic a higher affinity ligand (Figure 29B). The chelation-based affinity enhancement for **TG-42** vs. **TG-Mono** is 5-fold higher than for **G-42** vs. **G-Mono** as illustrated in Figure 29B. In conclusion the rebinding effect achieved by ligand clusters can be exploited to amplify the chelate effect when a more potent monovalent ligand is not available. The optimized **TG-42** (IC_{50}= 0.3 µM) was 168 times more potent than

TriGlc2NHTs, 1156 times more potent than Glc2NHTs and 22 000 times more potent than the natural ligand mannose, which strikingly highlights the achievements of our approach harnessing the power of the chelate effect, rebinding and glycomimetics on a DNA based scaffold. In the case of **TG-42** the chelate and rebinding effect join forces, leading to superior ligand economy (β/n = 192) in comparison to **G-42** (β/n = 12).

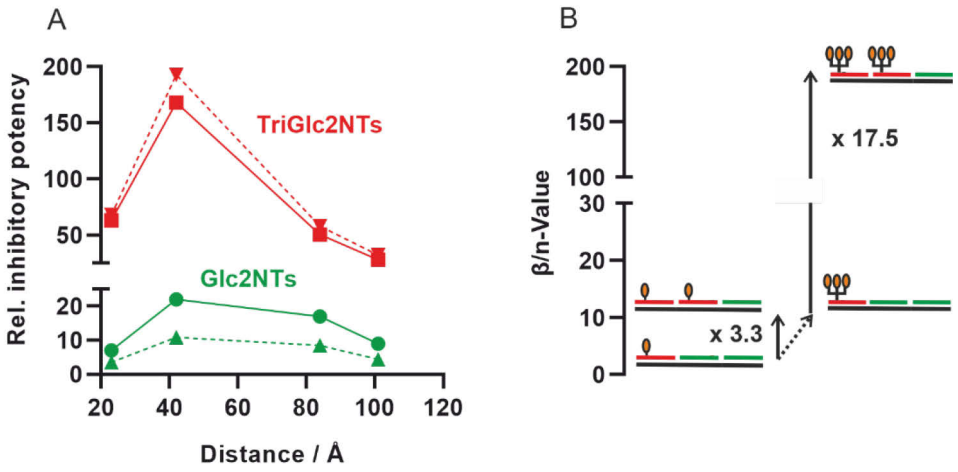

Figure 29. A) Distance dependence of relative inhibitory potency of bivalent complexes presenting Glc2NTs (green) or TriGlc2NTs (red) as multiples of the potency of unconjugated Glc2NTs (green) and TriGlc2NTs (red) ligands. The dashed line represents the valency corrected relative inhibitory potency (β/n-value) based on the number of Glc2NTs ligands (2 ligands in Biv-Glc2NTs, 6 ligands in Biv-TriGlc2NTs systems). B) β/n-Value (based on Glc2NHTs) as calculated for G-Mono, G-42, TG-Mono and TG-42.

While rebinding and chelate effect have been applied simultaneously in many examples of highly multivalent systems, the manner in which they can reinforce each other has been investigated in depth here. The lessons learnt from these experiments provide a general tool for designing multivalent ligands with improved avidity, especially when only low affinity monovalent ligands are available. Enlightened on how to design multivalent inhibitors for langerin the strategy was put to test with mannose-based ligands. Bivalent mannose-PNA-DNA ligands had not shown bivalency effects in both an Ella type and the ^{19}F-NMR assay, presumably due to the weak millimolar affinity of mannose for langerin. Therefore, this provided an ideal opportunity to evaluate the potential of combining statistical rebinding and chelation to overcome the limitations of weak monovalent ligands for multivalency. The investigation of TriMan-PNA-DNA ligands on the SPR assay displayed multivalent affinity increases, previously unachievable with bivalent Man-PNA-DNA ligands.

Despite a mannose affinity for langerin in the millimolar range (IC_{50} > 5 mM) the bivalent presentation of TriMan led to high-micromolar affinities for **TM-42** (IC_{50} < 220 μM) equivalent to an at least 4-fold affinity increase per mannose (β/n). Similarly, although the bivalent presentation of a biphenyl-modified mannose ligand, BiPhMan, (IC_{50} = 435 μM) surprisingly did not lead to a real bivalency effect for **B-42** (IC_{50} = 277 μM, β/n = 0.8), the application of both rebinding and chelation gave much more impressive results. **TB-42 (**IC_{50} = 5 μM, β/n = 15), comprised of two trivalent clusters of BiPhMan, was 87-fold more potent than BiPhMan and also 9-fold more potent than the **TB-104** (IC_{50} = 44 μM, β/n = 1.64) highlighting the retained distance affinity relationship when bivalently presenting ligands clusters on DNA-based scaffolds.

To examine the selectivity of the optimized ligands we tested the capacity of **G-42** and **TG-42** to detect langerin expressing cells. A comparison between wild type cells, langerin overexpressing and DC-SIGN overexpressing Raji cells was made. The fluorophore-marked complexes **G-42-Cy5** and **TG-42-Cy5** were incubated with the cells at nanomolar concentrations and the binding/internalization was evaluated with flow cytometry. Gratifyingly, only the cells expressing langerin were stained by the constructs. The mean fluorescence intensity of the cells expressing DC-SIGN stayed on the same level as the wild type cells. Importantly, the TriGlc2NHTs complex, **TG-42-Cy5**, was able to detect langerin expressing cells at 10-fold lower concentrations than the Glc2NHTs complex, **G-42-Cy5**. We had therefore successfully designed high affinity langerin binders able to selectively detect langerin expressing cells. While this work demonstrated the principle by attaching a fluorophore to the constructs other types of cargo such as cytotoxic agents or vaccination agents can be envisioned. Langerhans cells, which express langerin, are receiving increased attention as immunotherapy target against skin cancer. The work described here led to the first langerin selective ligands, which represents a necessary milestone to meet the high regulatory standards for a commercial application of Langerhans cell targeting.

In conclusion, we successfully demonstrated a strategy for developing selective and potent langerin binders by rationally combining glycomimetics, the statistical rebinding effect and chelate effect. Uniting the force of both multivalency mechanisms led to improved ligand economy as showcased by three different examples and

provides a tool for overcoming the limitations of weak affinities typical for monovalent lectin-glycan interactions. The optimised multivalent ligands **G-42** and **TG-42** were able to selectively detect L^+ cells at nanomolar concentrations. The rigid DNA-based scaffolds proved to be ideal to investigate the requirements for efficient ligand presentation. A comparison with recently reported molecularly defined langerin binders presenting 6-sulfo-Gal-β-4(6-sulfo-GlcNAc) (IC_{50} = 2.7 µM) and mannose (IC_{50} = 44 µM) on flexible trivalent scaffolds reveals the superior affinity of **TG-42** (IC_{50} = 0.3 µM). The most potent molecularly defined langerin binder to date.

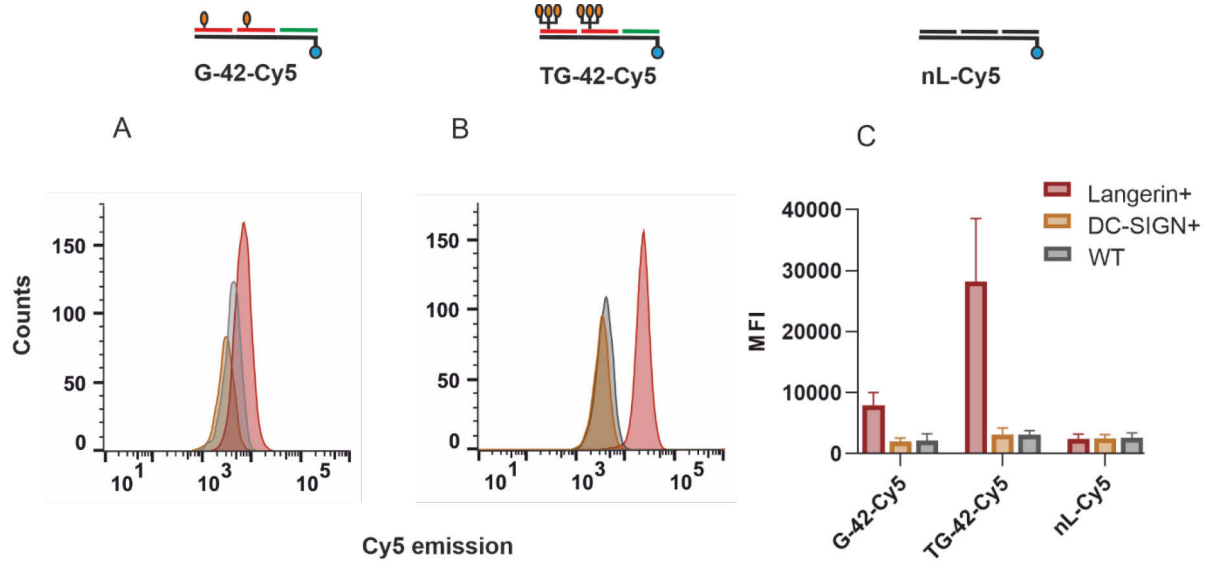

Figure 30. G-42 (A) and TG-42 (B) target Raji cells expressing langerin but not wildtype Raji cells or Raji cells expressing DC-SIGN. Histogram presentation of flow cytometry data from cells incubated with Cy5 labelled A) G-42 and B) TG-42. C) Mean fluorescence intensity (MFI) of binding/internalization of Cy5 labelled G-42, TG-42, and no ligand complex nL-Cy5 after subtraction of autofluorescence.

5.2 Outlook

We have successfully developed high avidity langerin ligands by applying a DNA-based spatial screening. By rationally combining the rebinding and chelate effect impressive multivalency effects were achieved when the arrangement of the bivalent ligand-PNA-DNA duplexes allowed for bridging of two carbohydrate binding sites. However, it remains to be shown whether a distance affinity relationship can not only be a method for optimising affinity but also a tool for creating selectivity between different multivalent targets when the monovalent ligand is non-selective (e.g. mannose and BiPhMan bind to both langerin and DC-SIGN with similar affinities). If the distance affinity screenings for two lectins lead to different optimal arrangements, selectivity can be rationally designed via the ligand arrangement. DC-SIGN and langerin make ideal candidates for a proof of principle study as both lectins bind to mannose and form multivalent structures with different distances between the binding sites (trimeric langerin 42 Å vs. tetrameric DC-SIGN 39, 81, 83, 94 Å) The next goal will therefore be examining the binding of TriMan-PNA-DNA and TriBiPhMan-PNA-DNA complexes to DC-SIGN to evaluate the optimal spatial arrangement for binding to DC-SIGN. As the SPR assay proved to be superior to the ^{19}F-NMR assay further efforts should be undertaken to establish the SPR assay for DC-SIGN. SPR has previously been used successfully to characterize DC-SIGN ligands.[80, 96, 107]. The work presented here will prove invaluable for this aim as the simple bivalent presentation of low affinity ligands did not afford large bivalency effects limiting the potential selectivity. Being able to amplify the chelate effect as described here will increase the bivalency effects and make much more significant selectivity ratios possible.

The developed DNA based ligands have been used to achieve over 1000-fold affinity (**TG-42**) increases implementing only 6 ligands. The full force of the multivalency effect is often only reached with a much greater number of ligands. However, highly multivalent strategies neglect the issue of ligand efficacy, which was addressed in this work. An interesting question therefore remains how the advantages of precise DNA-based scaffolds with superior ligand efficacy can be implemented in highly multivalent systems. Bandlow *et al* described the use of Rolling Circle Amplification (RCA) to obtain long DNA template with a repeating short DNA sequences. The DNA template

was subsequently paired with ligand modified oligonucleotides containing the previously optimised bivalent fragments to create highly multivalent DNA based ligands.[97] Although the multivalent systems containing the bivalently optimised fragments showed the highest inhibitory effect, the flexibility of the long scaffolds affected the spatial precision of the multivalent display. Thinking a step further DNA-Origami is an aspiring area of DNA research, which provides three dimensional based structures. Due their DNA based nature the structures can easily be modified to present ligands at known positions. The well-defined structure of DNA origami should be an ideal scaffold for the precise positioning of a multitude of ligands in a three-dimensional space. After a bivalent spatial screening of the target protein the optimised bivalent ligand-PNA-DNA duplex will be hybridised to a DNA origami structure via a DNA toehold thereby retaining the arrangement of the ligands and hopefully maximising ligand efficacy.

Glc2NHTs was identified as a potent and selective binder for langerin in this work and has since been applied as part of a liposomal delivery platform to deliver small molecules and encapsulated proteins to model cell lines.[47, 60] A further improvement to these delivery vehicles can be achieved by equipping liposomes with the TriGlc2NHTs-PNA-DNA ligands as the higher potency could improve the efficiency of the delivery system.

6 Experimental

6.1 General Information

PNA monomers were purchased from LGC LINK (Strathclyde, UK). Fmoc-protected lysine and Fmoc-protected aspartate were obtained from Novabiochem (Schwalbach, Germany). HCTU was purchased from Carl Roth (Karlsruhe, Germany). HOBt was obtained from Angene (Nanjing, China), DMF (low in water grade) was purchased from VWR (Darmstadt, Germany). DNA (HPLC-purified) was purchased from Biomers (Ulm, Germany). All other chemicals were provided from Acros Organics (Geel, Belgium), Sigma-Aldrich (Schnelldorf, Germany) and Merck (Darmstadt, Germany). Water was purified with a Milli-Q Ultra-Pure Water Purification System from Merck.

Column chromatography was performed with SDS 60 ACC silica gel. Silica gel 60 F254 aluminium sheets from Merck were used for **thin layer chromatography**.

1H- and 13C-NMR spectra were measured with an AVANCE II 400, Avance II 500 MHz spectrometer (Bruker) or 600 MHz spectrometer (Agilent). The signals of the protonated solvents were used as reference signals. Chemical shifts are given in ppm (parts per million).

Analytical HPLC was carried out on the UPLC-MS Waters ACQUITY UPLC System Qda as mass detector (column: ACQUITY UPLC BEH C18 1.7 µm) and solvents A (98.9% H_2O, 1% acetonitrile, 0.1% TFA) and solvents B (98.9% acetonitrile, 1% H_2O, 0.1% TFA) in a linear gradient with a flow rate of 0.5 mL/min at 50°C.

An Agilent 1100 series instrument was used to perform **semi-preparative HPLC** (column: Varian Polaris C18-A, 250 x 10.0 mm) with a flow rate of 6.0 mL/min and **preparative HPLC** (column: Macherey-Nagel VP250/21 C18 Nucleodur Gravity, 250 mm x 21 mm, 5 µm) with a flow rate of 15 mL/min, with solvents A (98.9% H_2O, 1% acetonitrile, 0.1% TFA) and solvents B (98.9% acetonitrile, 1% H_2O, 0.1% TFA) in a linear gradient.

PNA and DNA extinction coefficients Oligomers were determined by measuring the optical density on a NanoDrop ND-1000 Spectrophotometer. Molar extinction coefficients for the DNA oligomers at 260 nm were calculated with the OligoAnalyzer from Integrated DNA Technologies by the nearest neighbor method (http://eu.idtdna.com/calc/analyzer). For the PNA oligomers the molar extinction coefficients at 260 nm of the used PNA monomers were calculated via the PNA tool from PNA Bio (https://www.pnabio.com). The absorption of the mannose and Glc2NHTs ligands and the amino acid residues were neglected. ε_{260} (BiPhMan **47**) = 13.000 $L \cdot mol^{-1} \cdot cm^{-1}$.

Melting temperature analysis were measured on a Varian Cary Bio 100 UV-Vis spectrometer and Jasco V-750 spectrometer. The absorbance at 260 nm was monitored during a thermal cycle (3 cycles from 20 – 90 °C in 0.5 °C/min), the curves inflexion points were calculated and averaged over all cycles. Conditions: 1 μM complex, 10 mM NaH_2PO_4, 100 mM NaCl, pH 7.0.

6.2 Synthesis

6.2.1 Synthesis of Glc2NHTs Ligand

2-Deoxy-2-tosylamido-D-glucose(72)

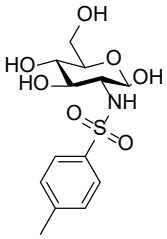

According to a literature procedure [108] *p*-toluenesulfonyl chloride (13.9 mmol, 2.65 g, 1 eq.) was dissolved in 15 mL acetone, added to glucoseamine hydrochloride (13,9 mmol, 3 g, 1 eq.) in 30 mL 1M NaOH and stirred for 4 hrs. The solvent was removed under reduced pressure and the residue purified by flash chromatography (methanol:dichloromethane 1:5) to yield the product as a white powder (4.1 g, 12.51 mmol, 90 %). The ratio of α- and β-anomer was determined to be 10:1 via ^{1}H NMR. Here, only chemical shifts corresponding to the β-anomer are documented. R_f = 0.38 with 9:1 dichlormethane:methanol. ^{1}H NMR (400 MHz, MeOD, β-anomer): δ [ppm] = 7.82 – 7.77 (m, 2 H, Ph-H), 7.37 – 7.32 (m, 2 H, Ph-H), 4.77 (d, J = 3.5 Hz, 1 H , 1-CH), 3.76 – 3.69 (m, 2 H, 6-CHa, 5-CH), 3.68 – 3.55 (m, 2 H, 6-CH6, 3-CH), 3.30 – 3.24 (m, 1 H 4-CH), 3.09 (dd, J = 10.1, 3.6 Hz, 1 H, 2-CH), 2.41 (s, 3 H, OCH_3). ^{13}C NMR (100.6 MHz, MeOD, β-anomer): δ [ppm] = 144.4 (1 C, C_q), 140.4 (1 C, C_q), 130.6 (2 C, Ph-H), 128.1 (2 C, Ph-H), 92.9 (1 C, 1-CH), 72.8 (1 C, 5-CH), 72.5 (1 C, 3-CH), 72.2 (1 C, 4-CH), 62.6 (1 C, 5-CH); 59.8 (1 C, 2-CH), 21.5 (1C, OCH_3).

1,3,4,6-Tetra-O-acetyl-2-deoxy-2-[(4-methoxyphenyl)methylidene]amino- D-glucoside (14)

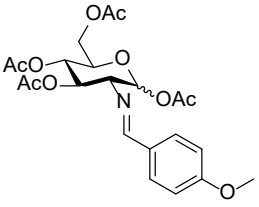

According to a literature procedure [109] glucosamine hydrochloride **12** (46.4 mmol, 10 g, 1 eq.) was dissolved in 1M aq. NaOH (47 mmol, 47 ml, 1.01 equiv.) and p-anisaldehyde (47 mmol, 6.4 g, 1.01 eq.) was added dropwise over 5 min. The reaction

mixture was left to stir at 0 °C for 2 h during which the solution solidified. The crystalline slurry was suction-filtered, rinsed with H_2O and small amounts of Et_2O to produce, after drying, a colorless solid (39.30 mmol, 11.70 g) in 85 % yield. The imine **13** (39 mmol, 11.6 g, 1 eq.) was dissolved in pyridine (60 ml), cooled to 0 °C, and acetic anhydride (30 ml) was added under continuous stirring. The cooling bath was removed and the mixture was stirred at rt over 24 h. The reaction mixture was then poured into 150 mL ice water and the precipitate suction filtered, washed with water and dried in vacuo producing a colourless solid (36 mmol, 16.7 g) with a yield of 91 % yield. Spectroscopic data were in accordance with literature values.[110] ^{1}H NMR (300 MHz, DMSO): δ [ppm] = 8.28 (s, 1H, ArC*H*=N), 7.65 (d, *J* = 8.9 Hz, 2H, Ph-*H*), 6.99 (d, *J* = 8.8 Hz, 2H, Ph-*H*), 6.07 (d, *J* = 8.2 Hz, 1H, 1-C*H*), 5.44 (dd, J=9.7 Hz, J=9.7Hz, 1H, 3-C*H*), 4.97 (dd, J=9.6 Hz, J=9.6Hz, 1H, 4-C*H*), 4.32 – 4.15 (m, 2H, 5-CH, 6-C*H*), 4.01 (d, *J* = 10.5 Hz, 1H, 6-C*H*), 3.79 (s, 3H, OCH_3), 3.44 (dd, *J* = 9.7, 8.3 Hz, 1H, 2-C*H*), 2.02, 1.98, 1.98,1.82 (4s, 3H each, 4xOAc).

1,3,4,6-Tetra-O-acetyl-2-deoxy-2-(2,2,2-trichloroethoxycarbonylamino)-D-glucoside (16)

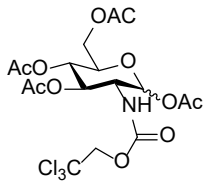

According to a literature procedure [111] the protected sugar **14** (41 mmol, 19.2g, 1 eq.) was heated to reflux in acetone, and treated with 5M HCl (41 mmol, 8.2 mL, 1 eq.). The immediately solidifying mass was cooled to rt and suction filtrated. Afterwards the crystalline mass was washed with cold diethyl ether and dried *in vacuo* to yield a colorless solid (36.5 mmol, 14 g, 89 % yield). The amine **15** (13 mmol, 5g, 1 eq.) was dissolved in 80 mL of pyridine and Troc-Cl (32.5 mmol, 4.5 mL, 2.5 eq.) was added at 0 °C. The reaction mixture was stirred for 2 h and the mixture concentrated until precipitation began. The addition of 100 mL ethyl acetate lead to complete precipitation, which was dried *in vacuo*, and yielded the desired product (9.9 mmol, 5.1 g, 76 %). Spectroscopic data were in accordance with literature values.[111] ^{1}H NMR (300 MHz, $CDCl_3$): δ [ppm] =5.74 (d, *J* = 8.8 Hz, 1H, N*H*), 5.35 (d, *J* = 9.5 Hz, 1H,

1-C*H*), 5.25 (dd, *J* = 9.3 Hz, 1H, 3-C*H*), 5.11 (dd, *J* = 9.6 Hz, *J* = 9.6 Hz,1H, 4-C*H*), 4.72 (s, 2H, Cl_3CCH_2), 4.29 (dd, *J* = 12.5, 4.5 Hz, 1H, 6-C*H*), 4.11 (dd, *J* = 12.5, 2.0 Hz, 1H, 6-C*H*), 3.96 (dd, *J* = 19.5, 9.4 Hz, 1H, 2-C*H*), 3.87-3.81 (m, 1H, 5-C*H*), 2.10, 2.08, 2.04 (3s, 3H each, 3xOAc).

Ethyl 3,4,6-tri-O-acetyl-2-deoxy-l-thio-2-(2,2,2-trichloroethoxycarbonylamino)-[3-glucoside (17)

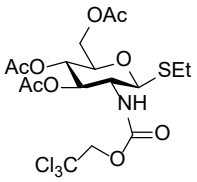

According to a literature procedure [111] the Troc-protected sugar **16** (13.8 mmol, 7.2 g, 1 eq.) and ethanethiol (193 mmol, 1.4 mL, 1.4 eq.) were dissolved in dry CH_2CI_2 (30 mL) under argon atmosphere. The mixture was cooled to 0 °C and BF_3 etherate (19.3 mmol, 2.37 mL) added over 5 min. The mixture was stirred for 40 min at 0 °C and then for 4 h at room temperature. The reaction was quenched by addition of triethylamine (1 mL), and the mixture was concentrated. Purification by flash chromatography (2:1 cyclohexane: ethylacetate) yielded the desired compound as a white powder (13.3 mmol, 7 g, 96 %). Spectroscopic data were in accordance with literature values. [111] ^{1}H NMR (500 MHz, $CDCl_3$) : δ [ppm] = 5.23 dd, *J* = 9.8 Hz, 1H, 3-C*H*), 5.18 (d, *J* = 9.3 Hz, 1H, N*H*), 5.08 (dd, *J* = 9.8 Hz, 1H, 4-C*H*) 4.80 (d, *J* = 12.1 Hz, 1H, Cl_3CCH_2),, 4.67 (d, *J* = 12.1 Hz, 1H, Cl_3CCH_2), 4.63 (d, *J* = 10.3 Hz, 1H, 1-C*H*), 4.25 (dd, *J* = 12.3, 5.1 Hz, 1H, 6-C*H*), 4.13 (dd, *J* = 12.3, 2.2 Hz, 1H, 6-C*H*), 3.78 (q, *J* = 10.1 Hz, 1H, 2-C*H*), 3.74 – 3.66 (m, 1H, 5-C*H*), 2.80 – 2.65 (m, 2H, SCH_2CH_3), 2.08, 2.03, 2.02 (3s, 3 each, 3 x Ac), 1.27 (t, *J* = 7.4 Hz, 3H, SCH_2CH_3)

(N-(Benzyloxycarbonyl)-2-aminoethyl)-3,4,6-tri-O-acetyl-N-(2,2,2-trichlorethyloxy-carbonyl)-β-D-glucoseaminide (18)

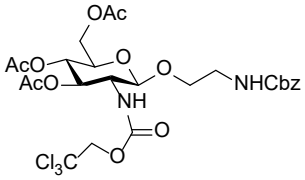

According to a literature procedure [47] under Argon atmosphere a suspension of the thioether **17** (1.9 mmol, 1 g, 1 eq.) and benzyl 2-hydroxyethylcarbamate (3.1 mmol, 0.6 g, 1.5 eq.) in 40 mL dry dichloromethane was stirred for 45 min. Dimethyl(methylthio)sulfonium tetrafluoroborate (3.8 mmol, 1 g , 2 eq.) was added as catalyst and the reaction mixture stirred for overnight at rt. After solvent removal *in vacuo* the residue was purified by flash chromatography (1:1 cyclohexane: ethyl acetate) to afford the desired compound as a white powder. Spectroscopic data were in accordance with literature values.[15] (1.5 mmol, 1 g, 79 %). R_f = 0.35 with cyclohexane:EtOAc (1:1). ^{1}H NMR (300 MHz, $CDCl_3$): δ [ppm] = 7.40 – 7.29 (m, 5H, Ph-*H*$_5$), 5.35 – 5.16 (m, 3H, N*H*-Cbz, 3-C*H*, N*H*-Troc), 5.13 – 4.99 (m, 3H, 4-CH, C*H*$_2$-Ph), 4.76 (d, *J* = 11.7 Hz, 1H, C*H*$_{2a}$-CCl_3), 4.58 (d, *J* = 8.3 Hz, 1H, 1-C*H*), 4.51 (d, *J* = 12.0 Hz, 1H, C*H*$_{2b}$$CCl_3$), 4.24 (dd, *J* = 12.3, 4.9 Hz, 1H, 6-C*H*$_{2a}$), 4.13 (dd, *J* = 12.1, 2.1 Hz, 1H, 6-C*H*$_{2a}$), 3.86 (dd, *J* = 10.1, 3.9 Hz, 1H, C*H*$_{2a}$-CH_2-NHCbz), 3.67 (m, 3H, C*H*$_{2b}$-CH_2-NHCbz, 2-C*H*, 5-C*H*), 3.53 – 3.41 (m, 1H, C*H*$_{2a}$-NH-Cbz), 3.34 (m, 1H, C*H*$_{2b}$-NH-Cbz), 2.06, 2,03, 2.02 (3s, 3H each, 3xAc).

2'-Benzyloxycarbonylaminoethyl 3,4,6-tri-O-acetyl-2-deoxy-2-(*p*-toluenesulfonylamido)-β-D-glucoside (20)

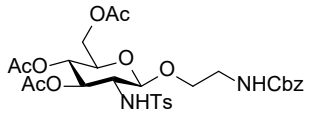

A suspension of the N-Troc-protected 2-amino-2-deoxyglucoside **18** (2 mmol, 1.1 g, 1 eq.) and freshly activated zinc (260 mmol, 20 g 130 eq.) in 60 mL acetic acid was stirred for 4 h. The reaction mixture was filtered over celite and dried *in vacuo* to yield a white solid. Under argon the solid (0.3 mmol, 165 mg, 1 eq.) was dissolved in 4 mL pyridine and 4-toluenesulfonyl chloride (0.6 mmol, 114 mg, 2 eq.) dissolved in 4 mL pyridine was added dropwise. The reaction mixture was left to stir overnight, the solvent removed *in vacuo* and the residue purified by flash chromatography (1:1 cyclohexane: ethyl acetate) to yield the desired tosylate as a white powder. (1 mmol, 640 mg, 50 %). R_f = 0.27 with methanol:dichloromethane 1:9. ESI-MS for $C_{29}H_{36}N_2O_{12}S$: $m/z(M+H^+)_{calc}$ = 637.2; $m/z(M+H^+)_{obs}$ = 637.2. ^{1}H NMR (500 MHz, $CDCl_3$): δ [ppm] = 7.64 (d, *J* = 8.2 Hz, 2H, Ph-*H*$_2$), 7.32 – 7.22 (m, 5H-Ph-*H*$_5$(Cbz)), 7.16 (d, *J* = 8.1 Hz, 2H, Ph-*H*$_2$), 5.41 (d, *J* = 8.3 Hz, 1H, N*H*-Ts), 5.25 (m, 1H, N*H*-

Cbz), 5.03 (s, 2H, CH_2-Ph), 4.95 (m, 2H, 3-C*H*, 4-C*H*), 4.27 (d, *J* = 8.2 Hz, 1H, 1-C*H*), 4.14 (dd, *J* = 12.3, 4.8 Hz, 1H, 6-CH_{2a}), 4.01 (dd, *J* = 12.3, 2.2 Hz, 1H, 6-CH_{2b}), 3.64 (m, 1H, CH_{2a}-CH_2-Cbz), 3.57 – 3.49 (m, 1H, 5-CH), 3.39 (m, 1H, 5-C*H*), 3.35 (m, 1H, CH_{2b}-CH_2-Cbz), 3.16 (d, *J* = 11.9 Hz, 1H, CH_2-CH_{2a}-Cbz), 3.11 – 3.00 (m, 1H, CH_2-CH_{2b}-Cbz), 2.29 (s, 3H, C*H*3), 1.98, 1.94, 1.81 (3s, 3H each, 3x Ac). ^{13}C NMR (126 MHz, $CDCl_3$): δ [ppm] = 171.41, 170.82, 169.45 (3s, 3xC_qAc), 156.77 ((*C*$_q$=0)Cbz), 143.51 (*C*$_q$(Ts), 138.49 (s, C_q(Ts)), 136.72 (s, C_q(Cbz)), 129.55 (2xPh-H(Ts)), 128.62 (3xPh-H(Cbz)), 128.21 (2xPh-H(Cbz), 127.27 (2xPh-H(Ts)), 101.50 (*C*1), 72.95 (*C*3), 71.85 (*C*5), 69.51 (*C*H_2-CH_2-NHCbz), 68.40 (*C*4), 66.79 (*C*H_2-Ph), 61.96 (*C*6), 58.08 (*C*2), 40.58 (*C*H_2-NH-Cbz), 26.11, 20.82, 20,72, 20.70 (3xOC=O*C*H_3).

2'-Aminoethyl 2-deoxy-2-(*p*-toluenesulfonylamido) - β-D –glucoside (22)

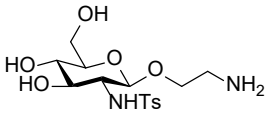

Under argon a sodium methanolate solution (0.8 mmol, 43 mg, 0.4 M, 5 eq.) was added to a suspension of acetylated sugar **20** (0.16 mmol, 100 mg, 1 eq.) in 5 mL dry methanol. After 2 hours of stirring at rt TLC control showed complete conversion. The solvent was removed in vacuo to obtain a white powder and used without further purification. The residue (0.196 mmol, 100 mg, 1 e.q.) was dissolved in degassed ethanol und 10% Pd/C added and the reaction mixture hydrogenated until the reaction was complete. The solution was filtered through a celite bed, washed with ethyl acetate and the solvent removed in vacuo. Purification by preparative HPLC (03 % to 30 % B in A within 30 min) and subsequent lypholisation gave the title amine as a white powder (0.026 mmol, 10 mg, 13 %). HR ESI-MS for $C_{15}H_{24}N_2O_7S$: m/z $(M+H^+)_{calc}$ = 377.138; m/z$(M+H^+)_{obs}$ = 377.152. ^{1}H NMR (500 MHz, D_2O): δ [ppm] = 7.75 (d, *J* = 8.4 Hz, 2H, Ph-H_2), 7.44 – 7.33 (d, *J* = 8.5 Hz, 2H, Ph-H_2), 4.41 (d, *J* = 8.4 Hz, 1H, 1-C*H*), 3.86 (dd, *J* = 12.3, 2.0 Hz, 1H, CH_{2a}-OH), 3.81 (ddd, *J* = 11.5, 8.2, 3.2 Hz, 1H, CH_{2a}-CH_2-NH_2), 3.68 (dd, *J* = 12.3, 5.4 Hz, 1H, CH_{2b}-OH), 3.47 (ddd, *J* = 11.6, 5.6, 3.5 Hz, 1H, CH_{2b}-CH_2-NH_2), 3.42-3.31 (m, 3H, 3-C*H*, 4-C*H*, 5-C*H*), 3.16 (dd, *J* = 10.0, 8.4 Hz, 1H, 2-C*H*), 3.02 (ddd, *J* = 13.6, 5.6, 3.2 Hz, 1H, CH_2-CH_{2a}-NH_2), 2.71 (ddd, *J* = 13.5, 8.1, 3.5 Hz, 1H, CH_2-CH_{2b}-NH_2), 2.40 (s, 1H, CH_3). ^{13}C NMR (126

MHz, D_2O): δ [ppm] = 144.48 (C_q), 137.61 (C_q), δ 129.59 (Ph-H), 126.49 (Ph-H), 101.17 (*C*H-1), 75.58 (*C*H-4), 73.91 (*C*H-3), 69.71 (*C*H-5), 65.65 (*C*H_2-CH_2-NH_2), 60.48 (*C*H_2-OH), 59.41 (s), 39.06 (CH_2-*C*H_2-NH_2), 20.54 (*C*H_3).

(N-(3' -Maleimidopropanoyl)--2'-aminoethyl-2-deoxy(N-(*p*-toluenesulfonylamido) - β-D –glucoside (23)

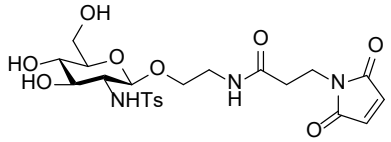

2'-Aminoethyl 2-deoxy-2-(*p*-toluenesulfonylamido) - β-D –glucoside **22** (0.24 mmol, 90,2 mg, 1 eq., 0.1M) was dissolved in 2.4 mL deionised water and added to a solution of N-succinimidyl-3-maleimido-propionat (0.36 mmol, 95, 8 mg, 1.5 eq., 0.1 M dioxane). Sodium hydrogen carbonate solution (0.1M, 2.4 mL) was added and left to shake for 1 h. After UPLC control showed completion of the reaction 5 mL water was added, the solvent removed via lypholisation and the remaining compound purified by preparative HPLC (03 % to 50 % B in A within in 30 min). Subsequent lypholisation of the product fractions gave the title maleimide as a white powder (146 umol, 77 mg, 61 %). ^{1}H NMR (500 MHz, MeOD): δ [ppm] = 7.78 (d, *J* = 8.3 Hz, 2H, Ph-*H*), 7.32 (d, *J* = 8.0 Hz, 2H, Ph-*H*), 6.80 (s, 2H, CH=CH), 4.22 (d, *J* = 8.3 Hz, 1H, 1-CH), 3.84 (dd, *J* = 11.8, 2.2 Hz, 1H, CH_{2a}-OH), 3.77 (td, *J* = 6.9, 1.3 Hz, 2H, O-CH_2-CH_2-NH), 3.66 – 3.61 (m, 2H, CH_{2b}-OH, CH_{2a}-CH_2-NH), 3.29– 3.05 (m, 7H, CH_{2b}-CH_2-NH, Cq-CH_2-CH_2-N, 2CH, 3-CH, 4-CH,5-CH), 2.47 (t, *J* = 6.9 Hz, 2H, Cq-CH_2-CH_2-N), 2.41 (s, 3H, OCH_3). ^{13}C NMR (126 MHz, MeOD): δ [ppm] = 173.13 (1C, C_q,, Maleimide), 172.24 (1C, C_q, Maleimide), 144.21 (1C, C_q,, Ph), 141.09 (1C, C_q,, Ph), 135.54 (2C, CH=CH), 130.26 (2C, Ph-H), 128.27 (2C, Ph-H), 103.33 (1C, 1-CH), 77.80 (1C, CH), 76.43 (1C, CH), 72.13 (1C, CH), 69.45 (1C, O-CH_2), 62.67 (1C, 6-CH_2), 61.27 (1C, CH), 40.32 (1C, CH_2), 35.66 (3C, CH_2, CH_2, NH-C_q-*C*H_2), 21.47 (1C, OCH3).

2'-Acetamidoethyl 2-deoxy-2-(*p*-toluenesulfonylamido) - β-D –glucoside (75)

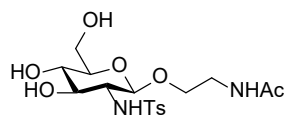

Amine **22** (9.8 mg, 26 µmol) was dissolved in MeOH (0.7 ml) and acetic anhydride (50 µl, 490 µmol) was added slowly. The reaction mixture was stirred for 72 h at room temperature, quenched with diethlyl amine and solvents were removed *in vacuo*. The residue was purified by preperative HPLC (03 % to 40 % B in A within 30 min) to yield **16** (6 mg, 14 µmol, 54%) as a white solid after lyophilization. HR ESI-MS for $C_{15}H_{24}N_2O_7S$: m/z $(M+Na^+)_{calc}$ = 441.131, m/z $(M+Na^+)_{obs}$ = 441.131. ^{1}H NMR (400 MHz, D_2O): δ [ppm] = 7.69 (d, J = 8.2 Hz, 2 H, Ph-H), 7.35 (d, J = 8.4 Hz, 2 H, Ph-H), 4.33 (d, J = 8.2 Hz, 1 H, 1-CH), 3.82 (dd, J = 1.5, 12.4 Hz, 1 H, 6-CHa), 3.64 (m, 1 H, 6-CHb), 3.60 (m, 1 H, OC$H_{2a}$$CH_2$NH), 3.38 (m, 1 H, 3-CH), 3.35 – 3.29 (m, 2 H, 4-CH, 5-CH), 3.23, m, 1 H, OC$H_{2b}$$CH_2$NH), 3.08 (dd, J = 8.4, 10.1 Hz, 1 H, 2-CH), 2.99 (ddd, J = 4.1, 5.8, 14.5 Hz, 1 H, OCH_2CH_{2a}NH), 2.80 (ddd, J = 3.9, 7.1, 14.3 Hz, 1 H, OCH_2CH_{2b}NH), 2.35, (s, 3 H, OCH_3), 1.91 (s, 3 H, COCH_3). ^{13}C NMR (100.6 MHz, D2O) : δ [ppm] = 173.84 (1 C, *C*OCH3), 144.28 (1 C, C_q, Ph), 137.64 (1 C, C_q, Ph), 129.50 (2 C, Ph-H), 126.37, (2 C, Ph-H), 101.06 (1 C 1-CH), 75.56 (1 C, 5-CH), 74.17 (1 C, 3-CH, 69.71 (1 C, 4-CH), 67.87 (1 C, O*C*H_2CH_2NH), 60.51 (1 C, 6-CH), 59.55 (1 C, 2-CH), 39.04 (1 C, OCH_2*C*H_2NH), 21.64 (1 C, CO*C*H_3), 20.53 (1 C, OCH3).

6.2.2 Synthesis of TriGlc2NTs Ligand

Tris[(propargyloxy)methyl]aminomethane (30)

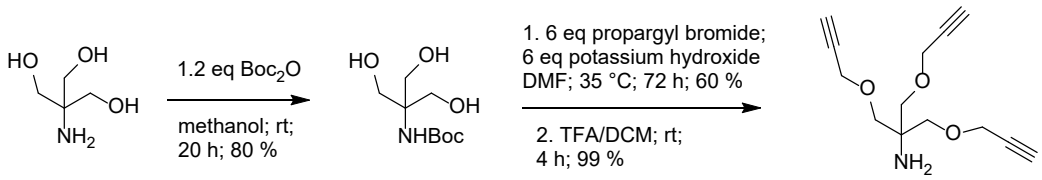

The trialkyne **30** was synthesized according to a literature procedure[112]. Spectroscopic data were in accordance with literature values.[112] ^{1}H NMR (500 MHz, MeOD): δ [ppm] = 4.23 (d, *J* = 2.4 Hz, 6H, Alkyne-CH), 3.70 (s, 6H, Cq-CH_2-O), 2.93 (dt, *J* = 7.0, 2.1 Hz, 3H, CH).

2-Bromoethyl-3,4,6-tri-O-acetyl-N-(2,2,2-trichlorethyloxy-carbonyl)-β-D-glucoside (27)

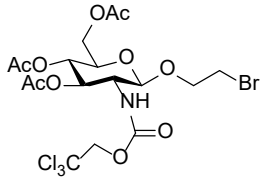

According to a literature procedure [111] under argon atmosphere a solution of the Troc-protected sugar **16** (6.2 mmol, 3.2 g, 1 eq.) and 2-bromoethanol (18.6 mmol, 2.4 mL, 3 eq.) in 40 mL dry dichloromethane was stirred for 50 min. BF_3 etherate (15.5 mmol, 1.1 mL , 3 eq.) was added dropwise at 0 °C, stirred for 15 min, slowly left to warm up to rt and the reaction mixture stir for 2 h. The reaction was quenched with 1mL trimethylamine, solvents removed *in vacuo* and the residue was purified by flash chromatography (2:1 cyclohexane: ethyl acetate) to afford the desired compound as a white powder (5.05 mmol, 2.95 g, 81 %). Spectroscopic data were in accordance with literature values.[111] ^{1}H NMR (400 MHz, $CDCl_3$): δ [ppm]= 5.31 (t, *J* = 10.0 Hz, 1H, 3-CH), 5.20 (d, *J* = 8.6 Hz, 1H, NH), 5.06 (t, *J* = 9.6 Hz, 1H, 4-CH), 4.81 – 4.62 (m, 3H, 1-CH, Cl_3CH_{2a}, Cl_3CH_{2b}), 4.27 (dd, *J* = 12.3, 4.8 Hz, 1H, 6-CH), 4.19 – 4.10 (m, 2H, 6-CH, O*C*$H_{2a}$$CH_2$Br), 3.89 – 3.79 (m, 1H, O*C*$H_{2b}$$CH_2$Br), 3.72 (dd, *J* = 9.7, 2.3 Hz, 1H, 5-CH), 3.64 (m, 1H, 2-CH), 3.50 – 3.40 (m, 2H, OCH_2C*H*$_{2a}$Br, OCH_2C*H*$_{2b}$Br), 2.09 (s, 3H, OAc), 2.03 (s, 3H, OAc), 1.42 (s, 3H, OAc).

2-Bromooethyl 3,4,6-tri-O-acetyl-2-deoxy-2-(*p*-toluenesulfonylamido)-β-D-glucoside (28)

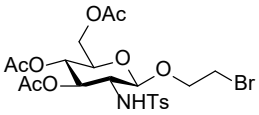

A suspension of the N-Troc protected bromoethyl glycoside **27** (2 mmol, 1.1 g, 1 eq.) and freshly activated zinc (260 mmol, 20 6, 130 eq.) in 60 mL acetic acid was stirred for 4 h. The reaction mixture was filtered over celite and dried *in vacuo* to yield a white solid. Under argon the solid (1 mmol, 1.41 g, 1 eq.) was dissolved in 15 mL pyridine. 4-Toluenesulfonyl chloride (6 mmol, 1.14 g, 6 eq.) and powdered molecular sieve were added. The reaction mixture was left to stir overnight, the solvent removed *in vacuo* and the residue purified by flash chromatography (1:1 cyclohexane:ethyl acetate) to yield the desired product as a white powder. (0,32 mmol, 170 mg, 32 %) ^{1}H NMR (500 MHz, $CDCl_3$): δ [ppm] = 7.75 (d, *J* = 8.3 Hz, 2H, Ph-H), 7.27 (d, *J* = 7.9 Hz, 2H, Ph-H), 5.40 (d, *J* = 8.5 Hz, 1H, NH), 5.07 (m, 2H, 3-CH, 4-CH), 4.42 (d, *J* = 8.2 Hz, 1H, 1-CH), 4.23 (dd, *J* = 12.3, 4.9 Hz, 1H, 6-CHa), 4.08 (dd, *J* = 12.3, 2.3 Hz, 1H, 6-CHb), 3.87 – 3.79 (m, 1H, CH2a-Br), 3.66 (m, 1H, 5-CH), 3.52 (m, 2H, CH2b-Br, 2-CH), 3.09 (ddd, *J* = 10.2, 7.4, 5.5 Hz, 1H, CH_{2a}-CH_2-Br), 3.00 (ddd, *J* = 10.2, 7.4, 6.8 Hz, 1H, CH_{2b}-CH_2-Br), 2.41 (s, 3H, OCH_3), 2.07 (s, 3H, OAc), 2.01 (s, 3H, OAc), 2.00 (s, 3H, OAc).^{13}C NMR (126 MHz, $CDCl_3$): δ [ppm] = 143.68 (1C, Cq), 138.73 (1C, Cq), 129.72 (2C, Ph-H), 127.76 (2C- Ph-H), 101.89 (1C, 1-CH), 73.20 (1C, 3-CH), 72.22 (1C, 5-CH), 70.03 (1C, CH_2-Br), 68.65 (1C, 4-CH), 62.30 (1C, 6-CH_2), 58.43 (1C, 2-CH), 29.50 (1C, *C*H_2-CH_2-Br), 21.87 (3C, OCH_3), 21.13 (6C, 2xOAc), 20.99 (3C, OAc).

Azidoethyl-N-(*p*-toluenesulfonyl)-β-D-glucoside (29)

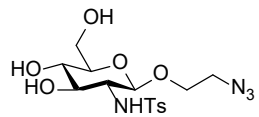

A suspension of the bromoethyl 2-deoxy-2-(p-toluenesulfonylamido)-β-D-glucoside **28** (0.32 mmol, 170 mg, 1 eq) and sodium azide (1,8 mmol, 342 mg, 6eq) in 20 mL DMF was stirred at 50°C for 22 h. Subsequently, 100 mL ethylacetate was added and the mixture washed with 0.1M HCl. After drying with magnesium sulfate, the solvents were removed in vacuo. The residue was dissolved in 10 mL methanol and sodium

methanolate solution (1.6 mmol, 86.4 mg, 0.4 M, 5 eq.) was added. After 1hr UPLC control showed full conversion, the solvent was removed in vacuo and the residue purified by (HPLC 3 % to 50 % B in A within 30 min) to afford the desired product as a white powder (0.1 mmol, 40 mg, 30%). ^{1}H NMR (500 MHz, MeOD): δ [ppm] = 7.78 (d, *J* = 8.3 Hz, 2H, Ph-H), 7.36 (d, *J* = 8.5, 2H, Ph-H), 4.25 (d, *J* = 8.3 Hz, 1H, 1-CH), 3.87 (dd, *J* = 11.9, 2.3 Hz, 1H, 6-CH2a), 3.70 (ddd, *J* = 11.0, 6.8, 4.4 Hz, 1H, C*H*$_{2a}$-CH$_2$-N$_3$), 3.66 (dd, *J* = 12.0, 6.0 Hz, 1H, 6-CH$_{2b}$), 3.38 – 3.20 (m, 4H, 5-CH,4-CH.3-CH, C*H*$_{2b}$-CH$_2$-N3), 3.13 (dd, *J* = 9.8, 8.3 Hz, 1H, 2-CH), 3.06 (ddd, *J* = 13.0, 6.2, 4.4 Hz, 1H, CH2-C*H*$_{2a}$-N3), 2.95 (ddd, *J* = 13.0, 6.8, 4.5 Hz, 1H, CH2-C*H*$_{2b}$-N3), 2.45 (s, 3H, OCH$_3$). ^{13}C NMR (126 MHz, MeOD): δ [ppm] = 143.97 (1C, Cq), 141.46 (1C, Cq), 130.27 (2C, Ph-H), 128.21 (2C, Ph-H), 103.07 (1C, 1-CH), 77.91 (1C, 4-CH), 76.72 (1C, 3-CH), 71.99 (1C, 5-CH), 68.86 (1C, *C*H$_2$-CH$_2$-N$_3$), 62.75 (1C, 6CH$_2$-OH), 61.46 (1C, 2-CH), 51.48 (1C, CH$_2$-N$_3$), 21.45 (1C, OCH$_3$).

TriGlc2NHTs (31)

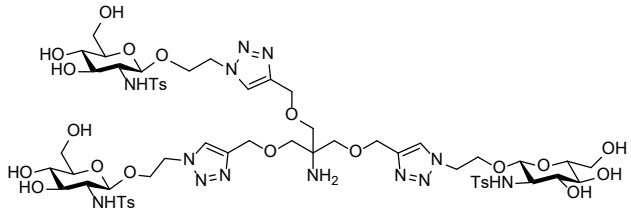

The azidoethylglycoside **29** (90 µmol, 36 mg, 4 eq) and tris[(propargyloxy)-methyl]aminomethane **30** (22.5 µmol, 7.8 mg, 1 eq) were dissolved in 500 µL water. A solution of tris(3-hydroxypropyltriazolylmethyl)amine (4.5 µmol, 2 mg, 0.2 eq), copper sulfate monohydrate (2.25 µmol, 0.5 mg, 0.1 eq) and sodium ascorbate (9 µmol, 2.8 mg, 0.4 eq) in 300 µL water was added and the reaction mixture shaken at 55°C for 24 h. After UPLC control showed full alkyne conversion, sodium hydrosulfide was added to precipitate copper. The supernatant obtained after centrifugation was purified by preparative HPLC (10 % to 40 % B in A within in 30 min) to yield the desired trivalent sugar (15.2 µmol, 22 mg, 67 %). ^{1}H NMR (500 MHz, MeOD): δ [ppm] = 8.08 (s, 3H, CH of triazole), 7.67 (d, *J* = 8.3 Hz, 6H, Ph-H), 7.22 (d, *J* = 8.0 Hz, 6H, Ph-H), 4.59 (d, *J* = 2.9 Hz, 6H, CH$_2$-Cq-N=N), 4.47 (ddd, *J* = 14.4, 7.4, 3.1 Hz, 3H, O-CH$_2$-CH$_{2a}$-N), 4.35 (ddd, *J* = 14.4, 6.1, 3.1 Hz, 3H, O-CH$_2$-CH$_{2b}$-N), 4.28 (d, *J* = 8.2 Hz, 3H 1-CH), 4.03 (ddd, *J* = 11.0, 6.1, 3.1 Hz, 3H, O-CH$_{2a}$-

CH_2-N), 3.84 (dd, *J* = 11.9, 2.1 Hz, 3H, 6-CHa), 3.67 (s, 6H, H_2N-Cq-C*H*$_2$-O), 3.64 (dd, *J* = 11.9, 5.6 Hz, 3H, 6-CHb), 3.53 (ddd, *J* = 10.8, 7.4, 3.1 Hz, 3H, O-CH_{2b}-CH_2-N), 3.29 – 3.14 (m, 12H, 2-CH,3-CH, 4-CH, 5-CH), 2.36 (s, 9H, OCH_3). ^{13}C NMR (126 MHz, MeOD): δ [ppm] = 144.73 (3C, Cq of triazole), 144.01 (3C, C_q), 141.42 (3C, C_q), 130.25 (6C, Ph-H), 128.04 (6C, Ph-H), 126.86 (3C, CH of triazole), 103.44 (3C, 1-CH), 77.92 (3C, CH sugar), 76.28 (3C, CH sugar), 72.03 (3C, CH sugar), 69.46 (3C, O-*C*H2-Cq), 68.87 (3C, O-*C*H2-CH2-N), 65.40 (3C, O-*C*H2-Cq-NH_2), 62.59 (3C, 6-CH), 61.38 (3C, N=N-C_q-*C*H_2-O), 60.23 (3C, CH sugar), 51.60 (3C, O-CH2-*C*H2-N), 21.47 (3C, OCH3).

Maleimido-TriGlc2NHTs (32)

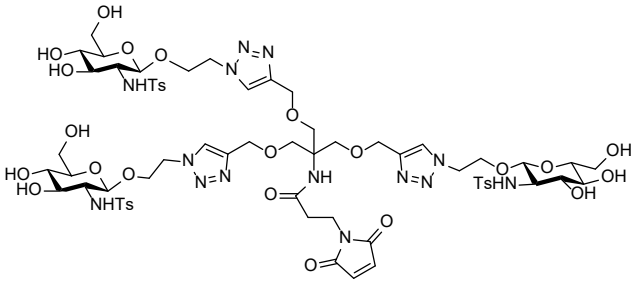

3-Maleinimidopropionic acid (21 µmol, 3.5 mg), HATU (21 µmol, 7.9 mg) and triethylamine (2.8 µmol, 4 µL) were dissolved in 200 µL DMF. After 1 min pre-activation time 126 µL of this reaction mixture was added to a solution of TriGlc2NTs **31** (4.2 µmol, 6 mg, 1 eq) in 5 mL dry DMF. UPLC control showed complete conversion after a few minutes, the solvents were removed in vacuo and the residue purified by preparative HPLC (10 % to 50 % B in A within in 30 min). Analytical HPLC: R_t = 2.7 min (10 - 50 % B in 4 min). ESI-MS: m/z $[M+2H]^{2+}_{calc}$ = 797.3; m/z $[M+2H]^{2+}_{obs}$ = 797.6. ^{1}H NMR (500 MHz, MeOD): δ [ppm] = 7.96 (s, 3H, CH of triazole), 7.68 (d, *J* = 8.2 Hz, 6H, Ph-H), 7.20 (d, *J* = 8.2 Hz, 6H, Ph-H), 6.71 (s, 2H, CH=CH), 4.59 – 4.50 (m, 6H, CH_2-Cq-N=N), 4.40 (ddd, *J* = 14.3, 7.3, 3.4 Hz, 3H, O-CH_2-CH_{2a}-N), 4.30 – 4.22 (m, 6H, O-CH_2-CH_{2b}-N, 1-CH), 3.96 (ddd, *J* = 9.7, 6.0, 3.5 Hz, 3H, O-CH_{2a}-CH_2-N), 3.83 (dd, *J* = 12.0, 2.1 Hz, 3H, 6-CHa), 3.81 (s, 6H, H_2N-Cq-C*H*$_2$-O), 3.71 – 3.60 (m, 5H, 6-CHb, C_q-CH_2-CH_2-N), 3.45 (ddd, *J* = 7.2, 6.5, 3.4 Hz, 3H, O-CH_{2b}-CH_2-N), 3.35 – 3.14 (m, 12H, 2-CH,3-CH, 4-CH, 5-CH), 2.46 – 2.38 (m, 2H, C_q-CH_2-*CH*$_2$-N), 2.34 (s, 9H, OCH_3)

6.2.3 Synthesis of Alkyne-modified-Glc2NHTs

1-O-propargyl-3,4,6-tri-O-acetyl-2-N-(2',2',2'-trichloroethoxycarbonyl)-β-D-glucoside (25)

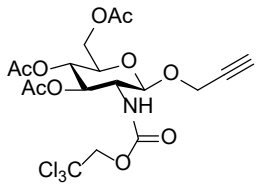

According to a literature procedure[113] the Troc protected glucosamine **16** (1.5 mmol, 0.78 g, 1 eq) was dissolved in 30 mL dry dichloromethane. A small spatula of activated molecular sieve, boron trifluoride diethyl etherate (24 mmol, 2.4 g, 16 eq) and propargyl alcohol (25.5 mmol, 1.47 mL, 17 eq) were added under argon and the reaction mixture left to stir for overnight. After TLC control showed complete conversion the reaction mixture was diluted with 200 mL ethyl acetate and ashed with a saturated solution of sodium hydrogen carbonate. The organic layer was dried over magnesium sulfate and the solvent removed in vacuo. The remaining residue was purified by flash chromatography (98:2 dichloromethane:methanol) to afford the alkyne functionalized sugar as a white solid. (1.06 mmol, 0.55 g, 70 %). R_f = 0.2 chromatography (98:2 dichloromethane:methanol). ^{1}H NMR (500 MHz, $CDCl_3$): δ [ppm] = 5.30 (t, *J* = 10.0 Hz, 1H, 3-CH), 5.15 (d, *J* = 8.7 Hz, 1H, NH), 5.09 (t, *J* = 9.6 Hz, 1H, 4-CH), 4.85 (d, *J* = 8.3 Hz, 1H, 1-CH), 4.72 (dd, *J* = 70.5, 12.0 Hz, 2H, CH_2-CCl_3), 4.42 – 4.34 (m, 2H, O-CH_2-Cq), 4.29 (dd, *J* = 12.3, 4.6 Hz, 1H, 6-CH_{2a}), 4.14 (dd, *J* = 12.3, 2.2 Hz, 1H, 6-CH_{2b}), 3.76 – 3.64 (m, 2H, 2-CH, 5-CH), 2.46 (t, *J* = 2.4 Hz, 1H, Alkyne-CH), 2.09 (s, 3H, OAc), 2.03 (s, 6H, 2xOAc). ^{13}C NMR (126 MHz, $CDCl_3$): δ [ppm] = 170.70 (1C, Cq, OAc), 170.66 (1C, Cq, OAc), 169.45 (1C, Cq, OAc), 154.14 (1C, Cq, CCl3), 98.30 (1C, 1-CH), 95.44 (1C, Cq-Alkyne), 74.50 (1C, *C*H_2-CCl_3), 71.99 (1C, 3-CH), 71.83 (1C, 2-CH), 68.47 (1C, 4-CH), 61.86 (1C, 6-CH_2), 56.07 (1C, 5-CH), 55.99 (1C, CH_2-Alkyne), 20.76 (1C, OAc), 20.64 (2C, OAc).

1-O-propargyl-3,4,6-tri-O-acetyl-2-deoxy-2-(*p*-toluenesulfonylamido)-β-D-glucoside (26)

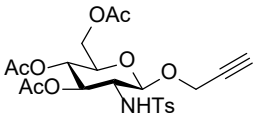

A suspension of the Troc-protected sugar **25** (4.9 mmol, 1.8 g, 1 eq.) and freshly activated zinc (140 mmol, 9 g, 29 eq.) in 50 mL acetic acid was stirred for 4h. The reaction mixture was filtered over celite and the dried *in vacuo.* The white residue was dissolved in 70 mL ethyl acetate and washed with 20 mL saturated solution of sodium hydrogen carbonate to free base the amine. After drying over magnesium sulfate, the solvent was removed in vacuo to yield the desired amine as a white foam. Under Argon the foam (2.88 mmol, 1.09 g, 1 Aq.) was dissolved in 10 mL dry pyridine and 4-Toluenesulfonyl chloride (15 mmol, 2.8 g, 5.2 eq.) was added. The reaction mixture was left to stir overnight, the solvent removed *in vacuo* and the residue purified by flash chromatography (3:2➔1:1 cyclohexane: ethyl acetate) to yield the desired product as a white foam. (0.85 mmol, 0.42 mg, 29 %). ^{1}H-NMR (500 MHz, CDCl3): δ [ppm] = 7.73 (dd, J=6.9, 5.1, 2H, Ph-H), 7.24(d, J=8.2, 2H, Ph-H), 5.34 (d, J=8.9, 1H, 2-CH), 5.12 (dd, J=19.6, 9.4, 1H, 3-CH), 5.08 - 5.01, m, 1H, 4-CH), 4.57 (d, J=8.3, 1H, 1-CH), 4.23 (dd, J=12.4, 4.7, 1H, 6-CH2a), 4.11 - 4.04, m, 6-CH_{2b}, 1-CH-O-CH2a), 3.89 (dd, J=15.9, 2.4, 1H, 1-CH-O-CH2b), 3.68 (ddd, J=9.9, 4.6, 2.4, 1H, 5-CH), 3.50 - 3.39, m, 1H, 2-CH), 2.45-2.40 (m, 1H, CH Alkyne), 2.38 (s, 3H, OCH3), 2.05 (s, 3H, OAc), 2.02 (s, 3H, OAc) , 2.00 (s, 3H, OAc). ^{13}C-NMR (125 MHz, CDCl3): δ [ppm] 171.41 (1C, Cq, OAc), 170.81 (1C, Cq, OAc), 169.46 (1C, Cq, OAc), 143.14 (1C, Cq, Ts), 138.17 (1C, Cq, Ts), 129.40 (2C, CH, Ts), 127.63 (2C, CH, Ts), 98.88 (1C, 1-CH), 78.04 (1C, Alkyne-CH), 75.85 (1C, 3-CH), 72.91 (1C, 5-CH), 68.34 (1C, 4-CH), 61.93 (1C, 6-CH2), 57.83 (1C, 2-CH), 55.98 (1C, 1-CH-O-*C*H2), 21.58 (1C, OCH3), 20.88 (1C, OAc), 20.81 (1C, OAc) ,20.69 (1C, OAc)

1-O-propargyl-2-deoxy-2-(p-toluenesulfonylamido)-β-D-glucoside (27)

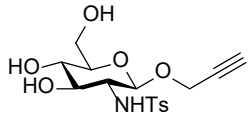

The acetylated sugar **26** (0.85 mmol, 0.42 g, 1 eq) was dissolved in methanol and sodium methanolate solution (4 mmol, 0.200 g, 0.4 M, 5 eq.). After 2 hours of stirring

at rt UPLC control showed complete conversion of the starting material. The solvent was removed in vacuo. Purification by preparative HPLC (03 % to 50 % B in A within in 40 min) and subsequent lyophilization gave the title amide as a white powder. (0.26 mmol, 0.1g, 30 %). ^{1}H NMR (500 MHz, MeOD): δ [ppm] = 7.74 (d, *J* = 8.3 Hz, 2H, Ph-H), 7.33 – 7.28 (m, 2H, Ph-H), 4.37 (d, *J* = 8.3 Hz, 1H, 1-CH), 4.05 (dd, *J* = 15.6, 2.4 Hz, 1H, CH_{2a}-Alkyne), 3.91 (dd, *J* = 15.6, 2.5 Hz, 1H, CH_{2b}-Alkyne), 3.83 (dd, *J* = 12.0, 2.3 Hz, 1H, 6-CH2a), 3.62 (dd, *J* = 12.0, 5.9 Hz, 1H, 6-CH2b), 3.34 (m, 1H, 3-CH), 3.27 (m, 1H, 4-CH), 3.19 (ddd, *J* = 9.4, 5.9, 2.3 Hz, 1H, 5-CH), 3.12 (dd, *J* = 9.8, 8.4 Hz, 1H, 2-CH), 2.76 (t, *J* = 2.4 Hz, 1H), 2.40 (s, 3H, OCH_3). ^{13}C NMR (126 MHz, MeOD): δ [ppm] = 143.99 (1C, Cq, Ts), 141.33 (1C, Cq, Ts), 130.33 (2C, CH, Ts), 128.42 (2C, CH, Ts), 100.70 (1C, 1-CH), 78.03 (1C, 5-CH), 76.70 (1C, 3-CH), 76.41 (1C, CH-Alkyne), 72.13 (1C, 4-CH), 62.82 (1C, 6-CH_2), 61.35 (1C, 2-CH), 56.17 (1C, CH_2-Alkyne), 21.63 (1C, OCH3).

6.2.4 Synthesis of Mannose Ligand

Pentaacetyl-D-mannose (34)

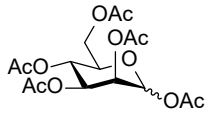

Following a literature procedure [114] a mixture of D-mannose (10.02 g, 55.7 mmol), acetic anhydride (60 mL), and pyridine (65 mL) was stirred at room temperature overnight. After 20 h, remaining acetic anhydride was hydrolyzed with 80 mL water. The aqueous solution was extracted three times with dichloromethane, and the combined organic phases were washed with saturated sodium hydrogen carbonate solution and dried with sodium sulfate. After filtration and removal of residual pyridine by azeotropic distillation with toluene, a sticky pale yellow oil (52 mmol, 20.1 g, 94 %) was isolated and used without further purification. R_f = 0.5 with cyclohexane:EtOAc (1:1).

2-Bromoethyl-2,3,4,5-tetraacetyl-α-D-mannoside (35)

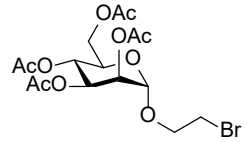

According to a literature procedure [115] boron trifluoride etherate (67.8 mmol, 8.6 mL, 3.5 eq) was added to a solution of 1,2,3,4,6-penta-*O*-acetyl-α-D-mannoside **34** (19.4 mmol, 8g, 1 eq) and 2-bromoethanol (19.75 mmol, 1.4 mL, 1 eq.) in dry CH_2Cl_2 (70 mL). The reaction mixture was stirred in the dark under argon overnight. 150 mL dichloromethane was added and the organic phase was washed with 100 mL saturated sodium hydrogen carbonate solution, 100 mL brine and 100 mL distilled water. The combined organic phases were dried over magnesium sulfate, filtered and concentrated *in vacuo*. The resulting oil was then purified using column chromatography on silica gel (ethyl acetate/hexane 1:1). The relevant fractions were collected, combined and concentrated to dryness under reduced pressure to yield the desired bromide as a pale-yellow powder. (8.8 mmol, 4 g, 42 %) Spectroscopic data were in accordance with literature values.[116] R_f = 0.6 with cyclohexane:EtOAc (1:1). ^{1}H NMR (500 MHz, $CDCl_3$): δ [ppm] = 5.35 (dd, *J* = 10.0, 3.4 Hz, 1H, 3-CH), 5.31 – 5.26 (m, 2H, 2-CH, 4-CH), 4.87 (d, *J* = 1.8 Hz, 1H, 1-CH), 4.27 (dd, *J* = 12.7, 5.9 Hz, 1H, 6-CHa), 4.16 – 4.09 (m, 2H, 6-CHb, 5-CH), 4.00 – 3.85 (m, 2H, 0-CH_2), 3.51 (t, *J* = 6.0 Hz, 2H, CH_2-Br), 2.16 (s, 3H), 2.10 (s, 3H, OAc), 2.05 (s, 3H, OAc), 2.00 (s, 3H, OAc).

2-Azidoethyl-2,3,4,5-tetraacetyl-α-D-mannoside (36)

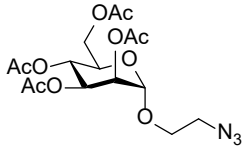

According to a literature procedure [116] mannoside **35** (6.6 mmol, 3 g, 1 eq) was dissolved in 110 mL dry dimethylformamide. Sodium azide (35.2 mmol, 4.2 g, 8 eq) was added, and the reaction mixture was stirred at 60°C for 22 h. The solvent was removed under high vacuum, the residue redissolved in 200 mL ethyl acetate, washed with 100 mL of water before removing the solvents *in vacuo.* The remaining residue was purified by column chromatography (ethyl acetate/hexane 1:1) to yield the desired azide as a colourless oil that crystallised over time (4.8 mmol, 2g, 72 %) Spectroscopic data were in accordance with literature values.[116] R_f = 0.5 with cyclohexane:EtOAc (1:1). ^{1}H NMR (500 MHz, $CDCl_3$): δ [ppm] = 5.38 – 5.26 (m, 3H, 2-CH, 3-CH, 4-CH), 4.87 (d, *J* = 1.7 Hz, 1H, 1-CH), 4.29 (dd, *J* = 12.3, 5.3 Hz, 1H, 6-CHa), 4.16 – 4.10 (m, 1H, 6-CHb), 4.05 (ddd, *J* = 9.8, 5.3, 2.4 Hz, 1H, 5-CH), 3.87 (ddd, *J* = 10.6,

7.0, 3.7 Hz, 1H, O-C*H*$_{2a}$-CH$_2$-N$_3$), 3.70 – 3.64 (m, 1H, O-C*H*$_{2b}$-CH$_2$-N$_3$), 3.47 (qdd, *J* = 13.3, 6.4, 3.6 Hz, 2H, CH$_2$-N$_3$), 2.16 (s, 3H, OAc), 2.11 (s, 3H, OAc), 2.05 (s, 3H, OAc), 1.99 (s, 3H, OAc).

2-Azidoethyl-α-D-mannoside (37)

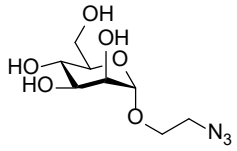

Following a literature procedure [116] protected mannoside **36** (4.8 mmol, 2g, 1 eq) was dissolved in a solution of 40 mL dry methanol and sodium methanolate (20 mmol, 1.1 g, 4 eq). After the reaction was completed the mixture was neutralised with ion-exchange resin (Levatit 1080 H), filtered, and the solvent was removed *in vacuo*. The deprotected azide mannoside was obtained as a pale-yellow syrup. (3.6 mmol, 0.91 g, 75 %) Spectroscopic data were in accordance with literature values.[116] R_f = 0.8 with *n*-PrOH:water (7 : 3). ^{1}H NMR (500 MHz, $CDCl_3$): δ [ppm] = 4.80 (d, *J* = 1.7 Hz, 1H, 1-CH), 3.93 – 3.88 (m, 1H, 3-CH), 3.85 – 3.79 (m, 2H, 4-CH, 2-CH), 3.73 – 3.67 (m, 2H, 6-CH$_2$), 3.64 – 3.53 (m, 3H, 5-CH, O-CH$_2$), 3.40 (t, *J* = 5.0 Hz, 2H, CH$_2$-N$_3$)

2-Aminoethyl- α-D-mannoside (38)

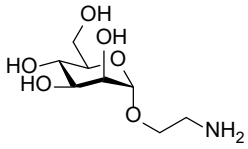

According to a literature procedure [117] the azide **37** (3.6 mmol, 0.91 g) was dissolved in 3 mL 1:1 ethyl acetate:ethanol and 0.1 mg Pd/C was added under Argon atmosphere. The flask was subsequently flushed with hydrogen, stirred for 3 h whilst product formation was monitored via TLC. Pd/C was removed by celite filtration and the solvents were removed in vacuo to give the product as a colorless syrup (2.4 mmol, 0,54 g , 67 %) Spectroscopic data were in accordance with literature values.[117] R_f = 0 with *n*-PrOH:water (7:3). ^{1}H NMR (500 MHz, MeOD): δ [ppm] = 4.77 (d, *J* = 1.6 Hz, 1H, 1-CH), 3.85 – 3.75 (m, 3H, 3-CH, 4-CH-2-CH), 3.73 – 3.65 (m, 2H, 6-CH$_2$), 3.59 (t, *J* = 9.5 Hz, 1H, 5-CH), 3.55 – 3.45 (m, 2H, O-CH$_2$), 2.89 – 2.80 (m, 2H, CH$_2$-NH$_2$).

(N-(3‘-Maleimidopropanoyl)--2-aminoethyl- α-D-mannoside (39)

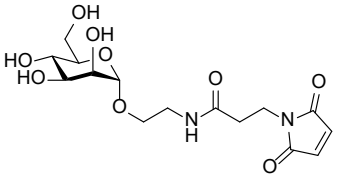

Amine **38** (480 µmol, 108 mg, 1 eq., 0.2M) was dissolved in 2400 uL deionised water and added to a solution of N-Succinimidyl-3-maleimido-propionate (720 µmol, 192 mg, 1.5 eq., 0.2 M dioxane). 2400 uL Sodium hydrogen carbonate solution (480 µmol, 180.4 mg, 1 eq., 0.2M) were added and left to shake for 1 h. After UPLC control showed completion of the reaction 5mL water was added, the solvent removed via lypholisation and the remaining compound purified by HPLC (03 % to 30 % B in A within 30 min). Subsequent lypholisation of the product fractions gave the title maleimide as a white powder (168 µmol, 61 mg, 35 %). Spectroscopic data were in accordance with literature values. [100] ^{1}H NMR (500 MHz, D_2O): δ [ppm] = 6.93 (s, 2H, CH=CH), 4.90 (d, *J* = 1.8 Hz, 1H, 1-CH), 3.97 (dd, *J* = 3.4, 1.7 Hz, 1H, 2-CH), 3.93 (dd, *J* = 12.2, 2.1 Hz, 1H, 6-CH_{2a}), 3.82 (dddd, *J* = 12.3, 10.6, 8.6, 5.2 Hz, 5H, 6-CH_{2b}, 3-CH, O-CH_{2a}-CH_2-NH, Cq-CH_2-C*H*$_2$-N), 3.70 (t (dd), *J* = 9.5 Hz, 1H, 4-CH), 3.66 (m, 1H, 5-CH), 3.60 (ddd, *J* = 10.6, 6.8, 3.9 Hz, 1H, O-CH_{2b}-CH_2-NH), 3.47 (ddd, *J* = 14.4, 6.6, 3.8 Hz, 1H, O-CH_2-CH_{2a}-NH), 3.37 (ddd, *J* = 14.4, 6.8, 4.0 Hz, 1H, O-CH_2-CH_{2b}-NH), 2.59 (dd, *J* = 7.2, 6.1 Hz, 2H, Cq-C*H*$_2$-CH_2-N).

2-Acetamidoethyl- α-D-mannoside (74)

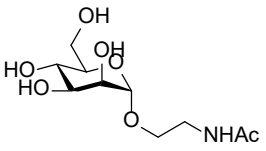

The amine functionalised mannoside **38** (23 mg, 103 µmol) was dissolved in MeOH (700 µl) and acetic anhydride (10 µl, 110 µmol) was added. The reaction mixture was stirred for 24 h at room temperature, quenched with 25 % (w/v) sodium methoxide in methanol and solvents were removed *in vacuo*. The residue was purified by reversed-phase HPLC (gradient: 0% to 10% B in a within 40 min) to yield **74** (17 mg, 26 µmol, 25%) as a white solid after lyophilization. HR ESI-MS for $C_{15}H_{24}N_2O_7S$: m/z $[M+H^+]_{calc}$ = 264.108, m/z $[M+H^+]_{obs}$ = 264.109. ^{1}-H NMR (400.1 MHz, D_2O): δ [ppm] = 4.80 (d, J = 1.8 Hz, 1H, 1-CH), 3.88 (dd, J = 1.8, 3.3 Hz, 1H, 2-CH), 3.82 (dd,

J = 2.2, 12.3 Hz, 1H, 6-CHa), 3.74 (m, 1 H 3-CH), 3.71 (m, 1 H, OC*H*$_{2a}$CH$_2$NH), 3.67 (m, 1 H 6-CHb), 3.59 (m, 1 H, 4-CH), 3.55 (m, 1 H 5-CH), 3.52 (m, 1 H , OC*H*$_{2b}$CH$_2$NH), 3.52 (ddd, J = 3.7, 7.2, 14.4 Hz, 1 H, OCH$_2$C*H*$_{2a}$NH), 3.31 (ddd, J = 3.9, 6.3, 14.4 Hz, 1 H, OCH$_2$C*H*$_{2b}$NH), 1.95 (s, 3 H, OC*H*$_3$). ^{13}C-NMR (100.6 MHz, D$_2$O): δ [ppm] = 174.17 (1 C, NH*C*OCH$_3$), 99.51 (1C, 1-CH), 72.69 (1 C, 5-CH), 70.37 (1 C, 3-CH), 69.88 (1 C, 2-CH), 66.55 (1 C, 4-CH), 65.67 (1 C, O*C*H$_2$CH$_2$NH), 60.77 (1 C, 6-CH), 38.90 (1 C, OCH$_2$*C*H$_2$NH), 21.72 (1 C, O*C*H$_3$).

6.2.5 Synthesis of TriMan Ligand

TriMan (40)

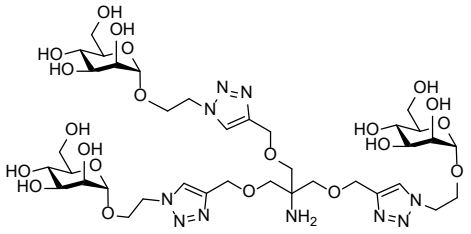

The azide modified sugar **37** (1.2 mmol, 299 mg, 8 eq) and the Tris[(propargyloxy)-methyl]aminomethane **30** (0.15 mmol, 52 mg, 1 eq) were dissolved in 500 µL water. Tris(3-hydroxypropyltriazolylmethyl)amine (30 µmol, 13 mg, 0.2 eq), copper sulfate monohydrate (20 µmol, 3.7 mg, 0,1 eq) and sodium ascorbate (60 µmol, 12 mg, 0,4 eq) were added (dissolved in 300 µL water) and the reaction mixture shaken at 55°C for 24 h. After UPLC control showed full alkyne conversion sodium hydrogen sulfide was added to precipitate copper and centrifuged. The supernatant reaction mixture was purified by preparative HPLC (3 - 20 % B in A within 30 min) and fractions lypholised to yield the desired product as a white powder (88.5 µmol, 87 mg, 59 %). ^{1}H NMR (500 MHz, MeOD): δ [ppm] = 8.03 (s, 3H, CH of triazole), 4.72 (d, *J* = 1.6 Hz, 3H, 1-CH), 4.67 – 4.62 (m, 12H, O-C*H*2-Cq-N, O-CH_2-C*H*$_2$-N), 4.12 (ddd, *J* = 10.9, 6.7, 4.2 Hz, 3H, O-CH_{2a}-C*H*$_2$-N), 3.90 – 3.83 (m, 3H, O-CH_{2b}-C*H*$_2$-N), 3.76 – 3.71 (m, 6H, 2-CH, 6CH_{2a}), 3.65 (s, 6H, Cq-C*H*$_2$-O), 3.65 – 3.52 (m, 9H, 3-CH, 4-CH, 6-CH_{2b}), 3.13 – 3.09 (m, 3H, 5-CH). ^{13}C NMR (126 MHz, MeOD): δ [ppm] = 144.96 (3C, Cq of triazole), 126.09 (3C, CH of triazole), 101.59 (3C, 1-CH), 74.95 (3C, 5-CH), 72.49 (3C, CH of sugar), 71.90 (3C, 2-CH), 69.31 (3C, H_2N-Cq-*C*H2-O), 68.35 (3C, CH of sugar), 66.67 (3C, O-*C*H_2-CH_2-N), 65.22 (3C, N=N-Cq-*C*H_2-O), 62.79 (3C, 6-CH_2), 60.64 (1C, Cq-NH2), 51.37 (3C, O-CH_2-*C*H_2-N-N).

Maleimido-TriMan (41)

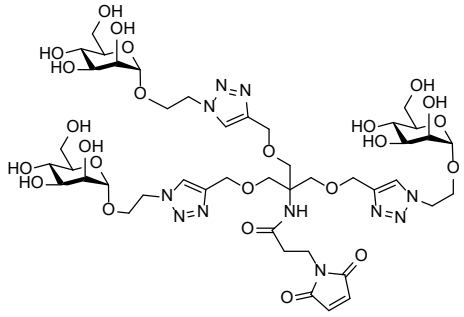

Maleimide propionic acid (21 µmol, 3.5 mg), HATU (21 µmol, 7.9 mg) and triethylamine (2.8 µmol, 4 µL) were dissolved in 200 µL DMF. After 1 min pre-activation time this reaction mixture was added to a solution of TriGlc2NHTs (4.2 µmol, 6 mg, 1 eq) in 15 mL dry DMF. UPLC control showed complete conversion after a few minutes, the solvents were removed in vacuo and the residue purified by preparative HPLC (03 – 30 % B in A within 30min) to afford the desired product as a white powder (3.5 µmol, 4 mg, 44 %). ESI-MS: m/z $[M+H]^{+}_{obs}$ = 1134.5, m/z $[M+H]^{+}_{calc}$ = 1134.4 and m/z $[M+2H]^{2+}$ = 568.0, m/z $[M+2H]^{2+}_{calc}$ = 567.7. ^{1}H NMR (500 MHz, D_2O): δ [ppm] = 8.02 (s, 3H, CH of triazole), 6.72 (s, 2H, CH of maleimide), 4.78 – 4.77 (m, 3H, 1-CH), 4.69 – 4.62 (m, 6H, O-C*H*$_2$-Cq-N), 4.55 (m, 6H, O-CH2-C*H*2-N), 4.08 (ddd, *J* = 10.8, 6.9, 3.8 Hz, 3H, O-CH_{2a}-C*H*$_2$-N), 3.91 (ddd, *J* = 11.0, 5.5, 3.8 Hz, 3H, O-CH_{2b}-C*H*$_2$-N), 3.84 (dd, *J* = 3.3, 1.7 Hz, 3H, 2-CH), 3.74 – 3.53 (m, 20H, 4-CH, 3-CH 6-CH_2, , O-CH_2-C*H*$_2$-N , Cq-C*H*$_2$-O, Cq-C*H*$_2$-CH_2), 3.06 (ddd, *J* = 9.6, 5.7, 2.3 Hz, 3H, 5-CH), 2.46 (t, *J* = 6.6 Hz, 2H, CH2-N-CO).

6.2.6 Synthesis of BiPhMan Ligand

Tetra-O-acetyl-6-O-tosy-mannoside (42)

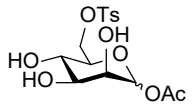

According to a literature procedure [118-119] under inert atmosphere D-mannose (19.8 g, 110 mmol, 1.0 eq.) was dissolved in dry pyridine (130 mL), and treated with tosyl chloride (23 g, 121 mmol, 1.1 eq.) while cooling (ice bath). The reaction mixture was stirred overnight. Next, the reaction was cooled down to 0°C before adding acetic anhydride (70 mL, 660 mmol, 6 eq.) Upon completion of the reaction the mixture was concentrated in vacuo and the residue dissolved in 500 mL ethyl acetate and washed

3x with saturated sodium hydrogen carbonate solution, 3 x 0.1 M hydrochloric acid and 3x brine to remove remaining pyridine. The organic solvent was removed in vacuo and the residue dried under high vacuum to give a white foam which was used without further purification. (22g, 44 mmol, 40 %). R_f = 0.4 with 1:1 ethyl acetate:cyclohexane.

2,3,4-Tetra-O-acetyl-6-azido-mannoside (43)

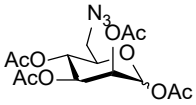

According to a literature procedure [118] 6-tosylated-per-acetylated mannose **42** (3.00 g, 6 mmol, 1.0 eq.) was dissolved in DMSO (50 mL) and treated with sodium azide (1.16 g, 17.84 mmol, 3.0 eq.). The reaction mixture was stirred for 24 hours at 50 °C and monitored by TLC. The reaction mixture was then diluted in an excess of ethyl acetate and washed 10 times with water. The collected organic phases were dried over $MgSO_4$ and the solvent was removed under reduced pressure. The product was purified using a chromatography column on silica gel (Eluent cylcohexane:ethyl acetate 1:1), to yield compound **43** in form of a pale yellow oil (88% yield). (2.0 g, 5.3 mmol, 88 %). The NMR spectrum was in accordance with literature.[120] R_f = 0.5 with 1:1 ethyl acetate:cyclohexane

1-(4-Bromo-2-(trifluoromethyl)phenoxy -2,3,4-tetra-O-acetyl-6-azido-mannoside (44)

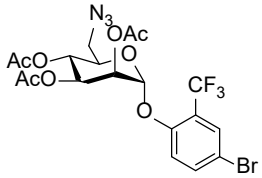

Under inert atmosphere, 6-azido-mannose **43** (5.00 g, 13.404 mmol, 1.0 eq.) was dissolved in dry DCM (130 mL) and treated with 2-trifluoromethyl-para-bromophenol (6.46 g, 26.808 mmol, 2.0 eq.). $BF_3 \cdot Et_2O$ (48 %wt., 15 mL, 3.0 eq.) was then slowly added and the reaction mixture was refluxed at 40 ºC under constant stirring for 16 hours. The reaction mixture was then quenched with water and extracted in DCM. The organic phase was dried over $MgSO_4$ and the solvent was removed under reduced pressure. The purified product was obtained through chromatography column on silica gel (Eluent cyclohexane: ethyl acetate 2:1) to the product in form of a yellow honey-

like gel (3.34 g, 6.03, 45 %). R_f = 0.7 with 1:1 ethyl acetate:cyclohexane. ^{1}H NMR (400 MHz, $CDCl_3$): δ [ppm] = 7.74 (d, *J* = 2.4 Hz, 1H, Ph-H), 7.63 (dt, *J* = 6.1, 3.1 Hz, 1H, Ph-H), 7.17 (d, *J* = 8.9 Hz, 1H, Ph-H), 5.62 (d, *J* = 1.8 Hz, 1H, 1-CH), 5.51 (dd, *J* = 10.0, 3.4 Hz, 1H, 3-CH), 5.44 (dd, *J* = 3.4, 2.0 Hz, 1H, 2-CH), 5.35 (t, *J* = 10.0 Hz, 1H, 4-CH), 4.01 – 3.93 (m, 1H, 5-CH), 3.37 (dd, *J* = 13.5, 6.6 Hz, 1H, 6-CHa), 3.25 (dd, *J* = 13.5, 2.5 Hz, 1H, 6-CHb), 2.20 (s, 3H, OAc), 2.06 (s, 3H, OAc), 2.03 (s, 3H, OAc). ^{13}C NMR (101 MHz, $CDCl_3$) δ 169.85 (1C, Cq, OAc), 169.76 (1C, Cq, OAc), 169.53 (1C, Cq, OAc), 154.63 (1C, Cq, arom), 136.19 (1C, CH arom), 130.22 (q, *J* = 3 Hz, 1C, CH arom), 122,51 (q, *J* = 242 Hz, 1C, CF_3), 121, 21 (q, *J* = 54 Hz, 1C, Cq arom), 116.83 (1C, CH arom), 114.89 (1C, Cq arom), 95.32 (1-CH), 71.48 (5-CH), 68.90 (2-CH), 68.20 (3-CH), 66.44 (4-CH), 50.86 (6-CH2), 20.75 (OAc), 20.64 (OAc), 20.56 (OAc).

1-(2-Trifluoromethyl-4-methoxycarbonyl-phenyl) phenoxy -2,3,4-tetra-O-acetyl-6-azido-mannoside (45)

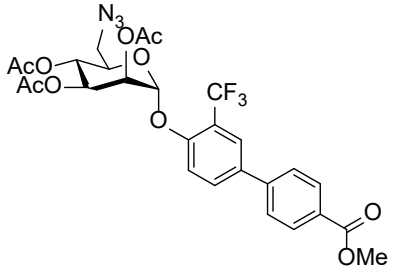

Based on a literature procedure [121] a Schlenk tube was charged with mannoside **44** (1.00 g, 1.81 mmol, 1.00 eq.), para-methoxycarbonyl-boronic acid (0.358 g, 1.99 mmol, 1.10 eq.), Pd(dppf)Cl_2·DCM (0.0443 g, 0.0542 mmol, 0.03 eq.) and K_2CO_3 (0.751 g, 5.43 mmol, 3.00 eq.). The Schlenk tube was then successively evacuated and flushed with argon multiple times. Previously degassed anhydrous DMF (20 mL) was added and the reaction mixture was stirred for 16 hours at 80 °C and monitored by TLC (Eluent cyclohexane: ethyl acetate 1:1). The reaction mixture was then cooled to room temperature, diluted with ethyl acetate, washed with water and brine. The organic phase was dried over $MgSO_4$ and the solvent was removed under reduced pressure. The purified product was obtained through a chromatography column on silica gel (Eluent cyclohexane: ethyl acetate 3:1) to yield product **45** in form of a white powder (0.72 g, 1.5 mmol, 82 %). R_f = 0.6 with 1:1 ethyl acetate:cyclohexane. ^{1}H NMR (500 MHz, $CDCl_3$): δ [ppm] = 8.11 (d, *J* = 8.6 Hz, 2H, Ph-H), 7.87 (d, *J* = 2.2

Hz, 1H, Ph-H), 7.77 (dd, *J* = 8.7, 2.3 Hz, 1H, Ph-H), 7.62 (d, *J* = 8.6 Hz, 2H, Ph-H), 7.37 (d, *J* = 8.7 Hz, 1H, Ph-H), 5.72 (d, *J* = 1.8 Hz, 1H, 1-CH), 5.56 (dd, *J* = 10.0, 3.4 Hz, 1H, 3-CH), 5.49 (dd, *J* = 3.4, 2.0 Hz, 1H, 2-CH), 5.38 (t, *J* = 10.0 Hz, 1H), 4.08 – 4.01 (m, 1H, 4-CH), 3.94 (s, 3H, OCH3), 3.39 (dd, *J* = 13.5, 6.6 Hz, 1H, 6-CHa), 3.27 (dd, *J* = 13.5, 2.5 Hz, 1H, 6-CHb), 2.22 (s, 3H, OAc), 2.07 (s, 3H, OAc), 2.04 (s, 3H, OAc). ^{13}C NMR (126 MHz, $CDCl_3$): δ [ppm] = 169.84 (1C, Cq OAc), 169.74 (1C, Cq OAc), 169.51 (1C, Cq OAc), 166.65 (1C, Cq COOMe), 152.63 (1C, Cq arom), 143.27 (1C, Cq arom), 134.46 (1C, Cq arom), 131.89 (1C, CH arom), 130.19 (2C, CH arom), 129.23 (1C, Cq arom), 126.68 (2C, CH arom), 125.98 (q, *J* = 5.6 Hz 1C, CH arom), 123.05 (q, 1C, *J* = 273.4 Hz, CF_3), 120.30 (q, *J* = 33.5 Hz, 1C, Cq arom.), 115.46 (1C, CH arom), 95.10 (1C, 5-CH), 71.34 (1C, 5-CH), 68.91 (1C, 2-CH), 68.20 (1C, 3-CH), 66.41 (1C, 4-CH), 52.10 (1c, OCH3), 50.79 (1C, 6-CH), 20.72 (OAc), 20.59 (OAc), 20.52 (OAc).

1-(2-Trifluoromethyl-4-methoxycarbonyl-phenyl) phenoxy -6-(2-phthalimido) ethylsulfonamido -mannoside (48)

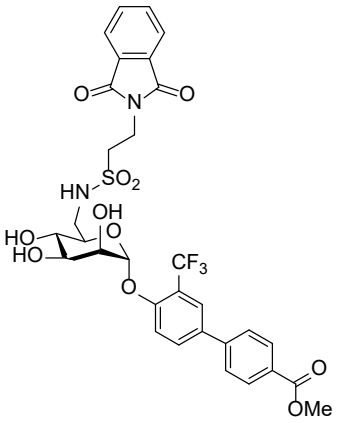

The protected azido-mannoside **45** (0.24 g, 0.5 mmol, I eq)was dissolved in 5 mL dry methanol and 25 wt % MeONa solution (500 µL) was added. The reaction mixture was stirred for 1 h at room temperature under argon and the product formation was monitored via UPLC. Thereafter the pH was neutralised using Amberlite IR120 (H+) and the solvent was removed in vacuo. Next the residue was dissolved in 3 mL 1,4-dioxane and 24 mg Pd/C was added under Argon atmosphere. The flask was subsequently flushed with hydrogen, stirred for 3 h whilst product formation was monitored via UPLC. Pd/C was removed by celite filtration and the solvents were removed in vacuo. The remaining residue (0.14 g, 0.3 mmol, 1 eq) was dissolved in

anhydrous DMF (20 mL) and ET_3N (0.17 mL 4 eq.) was added. 2-(Phtalimido)ethanesulfonyl chloride (0,6 mmol, 163 mg, 2 eq) was dissolved in 1 ml DMF and added slowly at 0°C under argon. The reaction mixture was stirred at 0°C for 20 min and then allowed to warm up to rt and stirring was continued for 24 h. The conversion was monitored by UPLC. The solvents were evaporated, and the residue purified by preparative HPLC (10 – 80 % A in B within 30min) to the product as a white powder (0.1 mmol, 67 mg, 20% over 3 steps). ESI-MS: m/z $[M+Na]^+_{obs}$ = 717.7, $[M+Na]^+_{calc}$ = 717.6. ^1H NMR (400 MHz, MeOD): δ [ppm] = 8.10 (m, 2H, Ph-H), 7.96 (dd, *J* = 8.7, 2.1 Hz, 1H, Ph-H), 7.82 (m, 5H, Ph-H, NPht), 7.71 (m, 3H, Ph-H), 5.80 (d, *J* = 1.6 Hz, 1H, 1-CH), 4.15 (dd, *J* = 3.3, 1.8 Hz, 1H, 2-CH), 4.10-3,91 (m, 6H, 3-CH, NC*H*2CH2S), 3.81-3,62 (m, 3H, 4-CH, 5-CH, 6-CHa), 3.46 – 3.27 (m, 3H, 6-CHb, $NCH_2C\mathit{H}_2S$). ^{13}C NMR (101 MHz, MeOD): δ [ppm] = 168.88 (2C CO of NPht), 168.04 (1C, Cq COOMe), 154.72 (1C arom Biphenyl), 144.49 (1C arom Biphenyl), 135.10 (2C arom of NPht), 134.44 (1C arom Biphenyl), 133.27 (1C arom Biphenyl), 132.94 (2C arom of NPht), 130.94 (2C arom Biphenyl), 129.99 (1C arom Biphenyl), 127.44 (2C arom Biphenyl), 126.15 (q, *J* = 5.4 Hz, 1C, arom BiPhenyl), 123.84 (2C arom NPht), 120.76 (q, J = 37 Hz, 1C arom Biphenyl), 117.22 (1C arom Biphenyl), 99.15 (1-CH), 74.37 (5-CH), 71.65 (3-CH), 71.36 (2-CH), 68.67 (4-CH), 52.26 (OCH_3), 50.68 ($NCH_2\mathit{C}H_2S$), 44.12 (6-CH), 33.28 ($N\mathit{C}H_2\mathit{C}H_2S$). CF_3 could not be assigned due to a low signal to noise ratio of the peak.

1-(2-Trifluoromethyl-4-carboxylate-phenyl) phenoxy -6-(2-amino)ethylsulfonamido -mannoside (49)

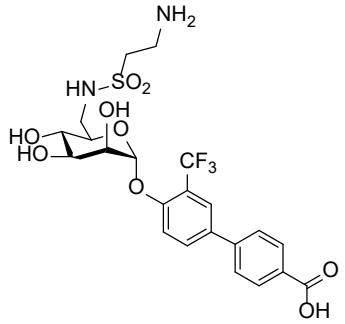

The phthalimide protected saccharide **46** (50 µmol, 34.7 mg, 1 eq) was dissolved in 5 mL dry methanol and hydrazine monohydrate (650 µmol, 31 µL, 13 eq) was added and the reaction mixture left to stir over 72 h under argon. Thereafter 200 µL 1M

NaOH was added and stirred at 45 °C overnight. UPLC control showed complete conversion of the starting material. Solvents were removed in vacuo and the residue purified by preparative HPLC (03 - 50 % B in A within 30 min) to yield the desired compound as a white powder (11.5 µmol, 8.1 mg, 23 %). ESI-MS: m/z = 551.3 $[M-H]^+_{obs}$, 551.5 $[M-H]^+_{calc}$. ^{1}H NMR (400 MHz, MeOD): δ [ppm] = 8.14 (d, *J* = 8.5 Hz, 2H, Ph-H), 7.95 (s, 2H, Ph-H), 7.76 (d, *J* = 8.5 Hz, 2H, Ph-H), 7.61 (d, *J* = 9.6 Hz, 1H, Ph-H), 5.73 (d, *J* = 1.6 Hz, 1H, 1-CH), 4.17 – 4.09 (m, 1H, 2-CH), 4.00 (dd, *J* = 9.4, 3.3 Hz, 1H, 3-CH), 3.77 (t, *J* = 9.7 Hz, 1H, 4-CH), 3.72 – 3.62 (m, 1H, 5-CH), 3.56-3.38 (m, 6H, 6-CHa, 6-CHb, CH_2-NH_2, SO_2CH_2). ^{13}C NMR (126 MHz, MeOD): δ [ppm] = 169.64 (1C, COOH), 155.31 (1C, Cq Biphenyl), 144.98 (1C, Cq Biphenyl) ,135.27 (1C, Cq Biphenyl), 133.63 (1C, CH Biphenyl), 131.65 (2C, CH Biphenyl), 131.17 (1C, Cq biphenyl), 127.90 (2C, CH Biphenyl s), 126.69 (q, *J* = 5.2 Hz, 1C, CH Biphenyl), 125.01 (q, *J* = 271 Hz, 1C, CF_3), 120.95 (q, 1C, *J* = 30.8 Hz, 1C, Cq, Biphenyl), 117.75 (1C, CH Biphenyl), 100.20 (1-CH), 74.61 (5-CH), 72.03 (3-CH), 71.77 (2-CH), 68.67 (4-CH), 50.53 (SO_2CH_2), 44.59 (6-CH), 36.01 (NCH_2).

1-(2-Trifluoromethyl-4-carboxylate-phenyl) phenoxy - -6- N-(3-maleimido-propanoyl)-2-aminoethylsulfonamido -mannoside (50)

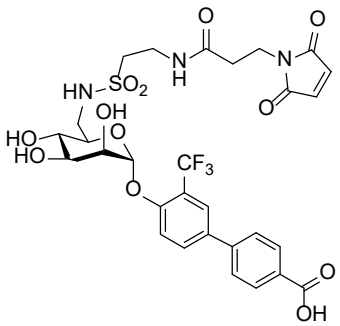

Amine **47** (4 µmol, 2.2 mg, 1 eq, 0.1M) was dissolved in 40 uL deionised water and added to a solution of N-Succinimidyl-3-maleimido-propionate (6 µmol, 1.6 mg, 1.5 eq, dioxane). 40 uL Sodium hydrogen carbonate solution (40 µmol, 1 eq, 0.1M) were added and left to shake for 1 h. After UPLC control showed completion of the reaction 2 mL water was added, the solvent removed via lyophilization and the remaining compound purified by preparative HPLC (03 % to 60 % B in A within 30 min). Subsequent lypholisation of the product fractions gave the title maleimide as a white powder (2.8 µmol, 2 mg, 70 %). ESI-MS: m/z = 702.3 $[M-H]^+_{obs}$, 701.7 $[M-H]^+_{calc.}$ ^{1}H NMR (500 MHz, MeOD): δ [ppm] = 8.03 – 7.98 (m, 2H, Ph-H), 7.84 (dd, *J* = 8.7, 2.3

Hz, 1H, Ph-H), 7.81 (d, *J* = 2.2 Hz, 1H, Ph-H), 7.67 – 7.62 (m, 2H, Ph-H), 7.54 (d, *J* = 8.7 Hz, 1H, Ph-H), 6.68 (s, 2H, CH=CH), 5.61 (d, *J* = 1.7 Hz, 1H, 1-CH), 3.98 (dd, *J* = 3.4, 1.8 Hz, 1H, 2-CH), 3.84 (dd, *J* = 9.5, 3.4 Hz, 1H, 3-CH), 3.69 – 3.58 (m, 3H, 4-CH, CH_2-N), 3.55 – 3.47 (m, 1H, 5-CH), 3.42 – 3.36 (m, 3H, 6-CHa, CH_2-NH), 3,19 (m, 1H, 6-CHb), 3.12 – 3.04 (m, 1H, SO_2-CH_2), 2.32 (t, *J* = 6.9 Hz, 2H, CO-CH_2).

1-(2-Trifluoromethyl-4-carboxylate-phenyl) phenoxy -6-(2-azido)ethylsulfon-amido-mannoside (51)

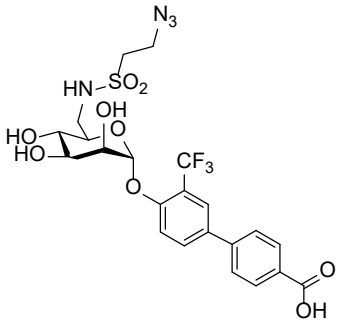

Amine **47** (26 µmol , 14.3 mg 1 eq), imidazole-1-sulfonyl azide HCL salt (52 µmol, 10.8 mg, 2 eq), potassium carbonate (91 µmol, 12.5 mg, 3.5 eq) and copper sulfate monohydrate (3.9 µmol, 0.9 mg, 0.15 eq) were added together and dissolved in 4 mL 2:1 methanol:water and left to stir for two h. Sodium hydrogen sulfide was added to precipitate copper, solvents removed *in vacuo* and the residue purified by preparative HPLC (10 - 50 % B in A within 30 min). Subsequent lypholisation of the product fractions gave the title azide as a white powder (5 mg, 6.5 µmol, 33 %). ESI-MS: m/z = 599.3 $[M+Na]^+_{obs}$, 599.5 $[M+Na]^+_{calc}$. ^{1}H NMR (500 MHz, MeOD): δ [ppm] = 8.11 (d, *J* = 8.6 Hz, 2H, Ph-H), 7.92 (m, 2H, Ph-H), 7.74 (d, *J* = 8.6 Hz, 2H, Ph-H), 7.62 (d, *J* = 8.5 Hz, 1H, Ph-H), 5.69 (d, *J* = 1.7 Hz, 1H, 1-CH), 4.08 (dd, *J* = 3.4, 1.8 Hz, 1H, 2-CH), 3.94 (dd, *J* = 9.5, 3.4 Hz, 1H, 3-CH), 3.72 (t, *J* = 9.6 Hz, 1H, 4-CH), 3.65 – 3.58 (m, 3H, 5-CH, CH_2-N_3), 3.51 (dd, *J* = 14.2, 2.5 Hz, 1H, 6-CHa), 3.29 (d, *J* = 6.6 Hz, 1H, 6-CHb), 3.23 (t, *J* = 6.7 Hz, 2H, SO_2-CH_2). ^{13}C NMR (126 MHz, MeOD): δ [ppm] = 169.55 (1C, COOH),), δ 155.07 (1C, Cq Biphenyl), 144.97 (1C, Cq Biphenyl), 135.10 (1C, Cq Biphenyl), 133.55 (1C, CH Biphenyl), 131.54 (2C, CH Biphenyl), 130.99 (1C, Cq Biphenyl), 127.82 (2C, CH Biphenyl), 126.72 (q, J = 5.4 Hz, 1C, CH Biphenyl), 126.19 (q, J = 283.5 Hz, 1C,CF_3), 121.00 (q, J = 31 Hz, 1C, Cq Biphenyl), 117.72 (1C, CH Biphenyl), 100.00 (1-CH), 74.69 (5-CH), 71.99 (3-CH), 71.66 (2-CH), 68.93 (4-CH), 52.26 (SO_2CH_2), 46.76 (CH_2-N_3), 44.77 (6-CH).

TriBiPhMan (52)

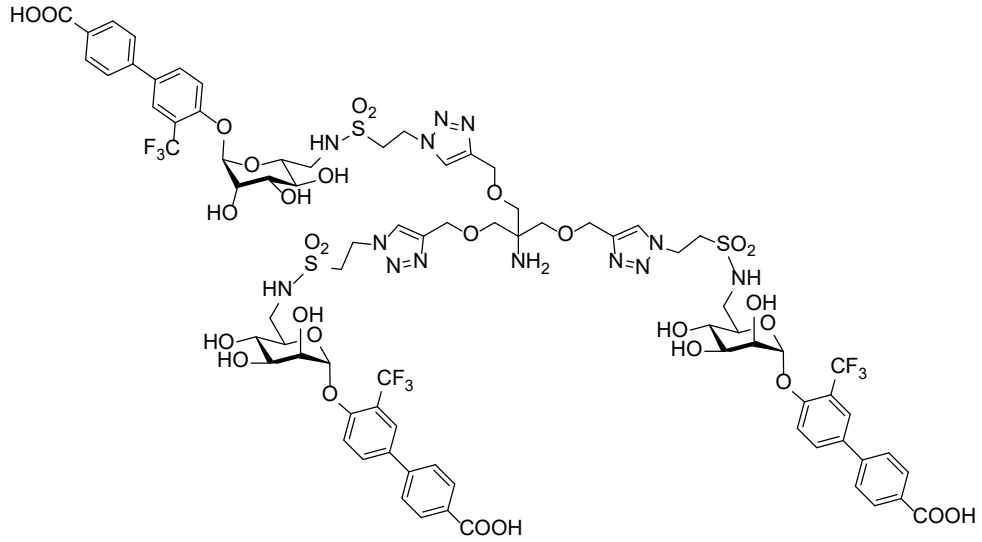

The azide modified sugar **51** (8.6 µmol, 5 mg, 4 eq) and Tris[(propargyloxy)-methyl]amino-methane **30** (2.1 µmol, 1.2 mg, 1 eq) were dissolved in 270 µL water:acetonitrile 2:1. A solution of Tris(3-hydroxypropyltriazolylmethyl)amine (0.2 µmol, 0.4 mg, 0.2 eq), copper sulfate monohydrate (0.5 µmol, 0.12 mg, 0,1 eq) and sodium ascorbate (0.84 µmol, 0.16 mg, 0,4 eq) in 15 µL water were added and the reaction mixture was shaken at 55°C for 24 h. After 24 hours a solid had precipitated, which was identified as the product by analytical HPLC and ESI-MS and was used without further purification. (2 µmol, 3.9 mg, 95 %). Analytical HPLC: R_T = 2.4 min (3 - 90 % B in A within 4 min). ESI-MS: m/z = 982.6 $[M\text{-}2H]^{2+}_{obs}$, 983.3 $[M\text{-}H]^{2+}_{calc}$.

Maleimido-TriBiPhMan (53)

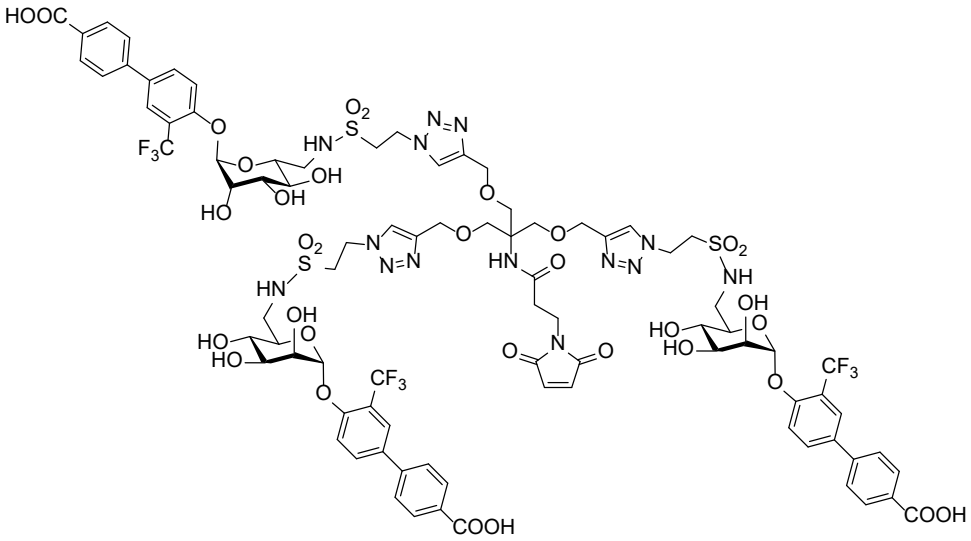

3-Maleimido propionic acid (6 µmol, 1 mg, 3 eq), HATU (6 µmol, 2.3 mg, 3 eq) and triethylamine (8 µmol, 1.1 µL, 4eq) were dissolved in 100 µL DMSO. After 1 min pre-activation time the reaction mixture was added to a solution of TriBiPhMan **50** (2 µmol, 3.9 mg, 1 eq) in 100 µL DMSO. UPLC control showed complete conversion after a few minutes, the solvent was blown off under air pressure and the residue redissolved in acetonitrile: water 1:1 before purification by preparative HPLC (10 - 60 % B in A within 40 min. Subsequent lypholisation of the product fractions gave the title Maleimdo-TriBiPhMan as a white foam. (1.5 mg, 0.67 µmol, 33 %). Analytical HPLC: R_T = 2.4 min (3 - 90 % B in A within 4 min). ESI-MS: m/z = 1058.5 $[M+2H]^{2+}$; 1058.9 $[M+H]^{2+}_{calc}$. ^{1}H NMR (500 MHz, DMSO): δ [ppm] = 8.03 (s, 3H, CH of triazole), 7.96 (d, *J* = 8.4 Hz, 6H, Ph-H), 7.92 – 7.84 (m, 6H, Ph-H), 7.76 (d, *J* = 8.4 Hz, 6H-Ph-H), 7.54 (d, *J* = 8.8 Hz, 3H, Ph-H), 7.33 (m, 3H), 6.88 (s, 2H, CH=CH), 5.63 (s, 3H, 1-CH), 4.63 (t, *J* = 7.2 Hz, 6H, O-C*H*2-Cq-N,), 4.39 (m, 6H, O-CH_2-C*H*$_2$-N), 3.88 – 2.19 (m, 23H, protons could not be assigned due to the large solvent peaks).

6.2.8 Synthesis of Mercaptomethylated PNA monomer

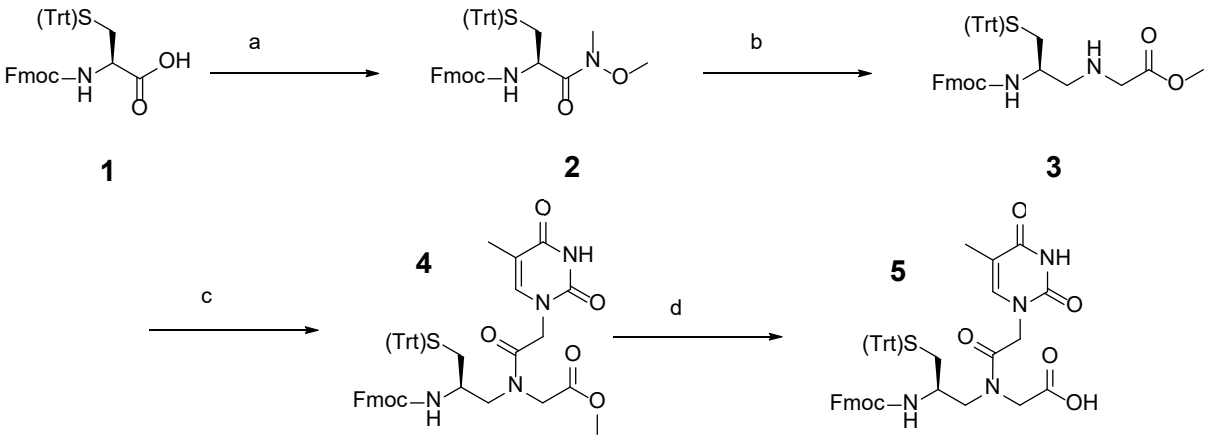

a) 2.2 eq NMM; 1.1 eq Isobutyl chloformate; 1 eq N,N-Dimethylhydroxylamine HCl; DCM, - 10 °C , rt, 17 h, 70 % b1) 2 eq $LiAlH_4$; THF, -72 °C; 1 h b2) 3 eq glycine methyl HCl; 1 eq $NaCNBH_4$; MeOH:THF; rt; 32 % c) 1.5 eq Thymine acetic acid; 2.25 eq Pivaloyl chloride; 6 eq NMM; CH_3CN/DMF; -10 °C, rt; 58 % d) 2 eq LiOH; H2O:THF, 0 °C, rt, 67 %. Synthesis and spectroscopic data were in accordance with literature.[15]

6.2.9 Synthesis of Azido-functionalised PNA-Monomer

Boc-Lys(Fmoc)-N(Me)OMe (7)

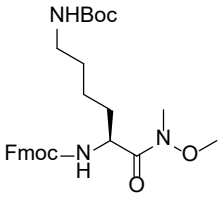

Based on a literature procedure [15] under Argon atmosphere a solution of (*R*)-*N*-Fluorenylmethoxycarbonyl-*S*-lysine(Boc) (32.01 mmol, 15 g, 1 eq) and N-methylmorpholine (70.42 mmol, 7.73 g, 2.2 eq) in 300 mL dichloromethane was cooled to -10 °C. Isobutylchloroformate (35.21 mmol, 4.8g, 1.1 eq) was added dropwise in five minutes. After 15 minutes activation time N,O-Dimethylhydroxylaminehydrchloride (32.97 mmol, 3.22 g, 1.03 eq) was added as a solid and the reaction mixture left to stir overnight at rt. The reaction mixtre was washed with 200 ml 0.2 M potassium hydrogen sulfate solution and the aqueous phase reextracted three times with 50 ml dichloromethane. After drying with magenisum sulfate the solvent was removed in vacuo and the remaining residue purified by flash chromatography (3:1 ➔ 1:1 cyclohexane:ethyl acetate) to yield the desired weinrebamide as white foam. (27.6 mmol, 4.1 g, 86 %). Spectroscopic data were in

accordance with literature values.[122] R_f 0.3 with cyclohexane:ethyl actetate 1:1. ^{1}H NMR (500 MHz, $CDCl_3$): δ [ppm] = 7.76 (dd, *J* = 7.6, 0.5 Hz, 2H, Fmoc-H), 7.60 (t, *J* = 7.4 Hz, 2H, Fmoc-H), 7.44 – 7.36 (m, 2H, Fmoc-H), 7.31 (tdd, *J* = 7.4, 3.5, 1.0 Hz, 2H), 5.57 (d, *J* = 8.8 Hz, 1H, NH-Fmoc), 4.72 (s, br, 1H, NH-Boc), 4.60 (s, br, 1H, NH-C*H*), 4.35 (d, *J* = 7.2 Hz, 2H, CH-CH_2-O), 4.21 (d, *J* = 7.1 Hz, 2H, C*H*-CH_2-O), 3.77 (s, 3H, OCH_3), 3.22 (s, 3H, N-CH_3), 3.10 (s, br, 2H, CH_2-NH Lys), 1.54 – 1.33 (m, 15H, 9H Boc, 6H, Lys side chain).

Boc-Lys(Fmoc)-PNA backbone (8)

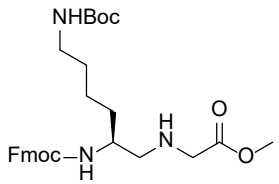

Based on a literature procedure [15] weinrebamide **7** (27 mmol, 13.8 g, 1 eq) was dissolved in 200 mL dry tetrahydrofurane under argon atmosphere and cooled to -72 °C. Afterwards a solution of lithium aluminium hydride (54 mmol, 3.5 M, 15.4 mL, 2 eq) was added dropwise to the flask. After one hour TLC control showed complete conversion of the starting material. The reaction mixture was quenched by the addition of 50 ml 0.2M potassium hydrogen sulfate solution and the three extractions with 100 mL diethylether were performed. After washing of the organic phases with saturated sodium chloride solution and one reextraction with 100 mL diethylether the combined organic fractions were combined, dried with magnesium sulfate and the solvent removed in vacuo. The remaining foam was used in the next step without further purification. Under Argon the aldehyde (18 mmol, 8.2 g, 1 eq) was dissolved in 120 mL tetrahydrofurane:methanol (3:1) and glcyinemethylester (54 mmol, 6.8 g, 3 eq) and sodiumcyanoborohydride (19 mmol, 1.2 g, 1.05 eq) were added and the reaction mixture left to stir for 4.5 hrs as UPLC control showed complete conversion of the starting material. The solvent was removed in vacuo, the remaining residue dissolved in 300 mL ethyl acetate and washed with brine and water (50 mL). After drying with magnesium sulfate the solvent was removed in vacuo and the residue prufied by flash chromatography (2:1 cyclohexane:ethyl acetate) to yield a white foam. (7 mmol, 3.7 g, 38 % over two steps). Spectroscopic data were in accordance with literature values. [123] R_f = 0.2 with 2:1 cyclohexane:ethyl acetate.^{1}H NMR (500 MHz, $CDCl_3$): δ [ppm]

= 7.76 (d, *J* = 7.5 Hz, 2H, Fmoc), 7.61 (d, *J* = 7.3 Hz, 2H, Fmoc), 7.39 (t, *J* = 7.4 Hz, 2H, Fmoc), 7.31 (t, *J* = 7.4 Hz, 2H, Fmoc), 5.08 (d, *J* = 7.6 Hz, 1H, NH-Fmoc), 4.61 (s, br, 1H, NH-Boc), 4.40 (d, *J* = 6.4 Hz, 1H, C*H*$_2$-Fmoc), 4.22 (t, *J* = 6.7 Hz, 1H, C*H*-Fmoc), 3.71 (s, 3H, OC*H*$_3$), 3.70 (s, br, 1H, NH-C*H*), 3.42 (m, 2H CH_2 glycine), 3.09 (m, 2H, Fmoc-NH-CH-C*H*$_2$), 2.70-2.60 (m, 2H, Fmoc-NH-CH-C*H*$_2$), 1.54 – 1.29 (m, 15H, 9H Boc, 6H Lys side chain)

γ-Lys(Fmoc) PNA-thymine monomer methylester (9)

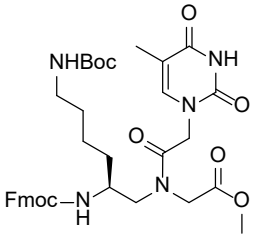

Based on a literature procedure [15] under argon thymine acetic acid (0.87 mmol, 0.16 g, 1.5 eq) was dissolved in 15 mL dimethylformamide:acetontrile and cooled to -5 °C. Pivaloyl chloride (1.31 mmol, 0.38 mL, 2.25 eq) and N-methylmorpholine (3.48 mmol, 0.38 mL, 6 eq) were added. After 20 min a solution of the PNA bachbone **8** (0.58 mmol, 0.3 g, 1 eq) dissolved in 2 mL dry dimethylformamide was added dropwise. After 1.5 hrs TLC control showed full conversion of the starting material. The reaction mixture was worked up by adding 70 mL ethylactetate, washing five times with 20 mL 0.1 M hydrochloride solution. The organic phase was dired with mageniusm sulfate and the solvent removed in vacuo. The remaing residue was purified by flash chromatography (2:1 ➔1:1 cyclohexane:ethyl acetate) to yield a white foam. (0.4 mmol, 0.21 g, 48 %) Spectroscopic data were in accordance with literature values. [123]R_f 0.1 with 2:1 cyclohexane:ethyl acetate. ^{1}H NMR (500 MHz, $CDCl_3$): δ [ppm] = 9.34 (d, *J* = 20.8 Hz, 1H, NH Thymine), 7.75 (d, *J* = 7.5 Hz, 2H, Fmoc), 7.66 – 7.50 (m, 2H, Fmoc), 7.38 (dt, *J* = 7.5, 3.9 Hz, 2H), 7.38 (dt, *J* = 7.5, 3.9 Hz, 2H, Fmoc), 7.33 – 7.27 (m, 2H, Fmoc), 6.98 (s, 1H, CH-thymine), 6.95 (d, *J* = 1.1 Hz, 1H, NH thymine), 5.61 (d, *J* = 8.0 Hz, 1H, NH-Fmoc), 5.12 (d, *J* = 7.7 Hz, 1H, NH-Boc) 4.76 – 4.60 (m, 2H, CO-C*H*$_2$-thymine), 4.51 – 4.21 (m, 3H, CH_2-CH-Fmoc), 4.21 – 4.13 (m, 2H, CH_2-glycine), 3.77 (s, 3H, OCH3), 3.71 (s, 1H, Fmoc-NH-C*H*-CH2), 3.62 – 3.50 (m, 1H, Fmoc-NH-CH-C*H*2a), 3.34 (m, 1H, Fmoc-NH-CH-C*H*2b),

3.09 (m, 2H, C*H*$_2$-NH Lys), 1.95 – 1.82 (m, 3H, CH3 thymine), 1.42 (m, 15H, 9H Boc, 6H lysine side chain).

Azide PNA monomer (11)

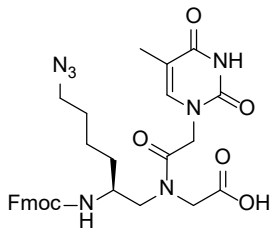

The Boc-protected PNA Monomer **9** (4 mmol, 2.1 g) was dissolved in 10 ml dichloromethane and 5 ml TFA was added. After two hours UPLC control showed complete removal of the Boc protecting group and the solvents were removed in vacuo. The remaining residue was used in the next step without further purification. The amine (1.35 mmol, 0.8 g, 1 eq) was dissolved in 15 mL methanol. Then Imidazole-1-sulfonyl azide (1.62 mmol, 0.43 g, 1.2 eq), potassium carbonate (4.7 mmol, 0.65 g, 3.5 eq), and copper sulfate mono hydrate (0.03 mmol, 0.007 g, 0.02 eq) were added and the reaction mixture left to stir at rt for 4 hrs. UPLC control showed complete conversion of the starting material, the solvents were removed in vacuo and the residue dissolved in ethylacetate. The organic fraction was washed three times with water and sodium hydrogen carbonate und then reextracted three times with ethyl acetate. The combined organic fractions were dried with magnesium sulfate, the solvents removed in vacuo. The remaining white foam was used in the next step without further purification. The azide (1.05 mmol, 0.65 g, 1 eq) was dissolved in 20 mL tetrahydrofuran and a solution of lithium hydroxide (2.1 mmol, 0.5 M, 4.2 mL, 2eq) was added dropwise at 0 °C. After 2 hrs the reaction TLC showed complete conversion. The pH of the reaction mixture was adjusted to pH=2 by adding a solution of formic acid (25%) and then extracted three times with 30 mL ethyl acetate. The combined organic fractions were washed with 30 mL brine, reextracted three times with 30 mL ethyl acetate, dried with magnesium sulfate and the solvents removed in vacuo. The remaining residue was purified by flash chromatography (dichloromethane:methanol:formic acid 84.5:15:0.5) to yield the desired PNA monomer as a white solid (0.6 mmol, 0.36 g, 60% over three steps). UPLC control showed only 60 % purity (integrated over the UPLC run at 260 nm). However, as the

coupling rate was over 80% and gave only the desired product no further efforts were made to purify this compound. ESI-MS: m/z = 604.4 $[M+H]^+_{obs}$, 604.3 $[M+H]^+_{calc}$.^{1}H NMR (500 MHz, DMSO) [2 Rotamere]: δ [ppm] = 11.28 (s, 0.5H, NH-imide), 11.26 (s, 0.5H, NH-imide), 7.89 (d, *J* = 7.5 Hz, 2H, Fmoc-H), 7.69 (t, *J* = 8.1 Hz, 2H, Fmoc-H), 7.50 – 7.26 (m, 5H, Fmoc-H, Fmoc-NH), 7.20 (d, *J* = 7.7 Hz, 1H, CH-thymine), 4.77 – 3.83 (m, 7H, CO-CH2-thymine, Fmoc-CH, Fmoc-CH-C*H*2, N-C*H*2-COOH), 3.64 – 3.19 (m, 5H, NH-C*H*-CH2-N, NH-CH-C*H*2-N, CH2-N3), 1.73 (s, 1.5H, CH3-thymine), 1.70 (s, 1.5H, CH3-thymine), 1.62 – 1.02 (m, 6H, C*H*2-C*H*2-C*H*2-CH2-N3).

6.2.10 Synthesis of PNA oligomers

Automated Solid-Phase PNA synthesis: Linear solid-phase PNA synthesis was performed by using an Intavis ResPep parallel synthesizer and Intavis microscale columns. TentaGel R RAM resin (typical loading: 0.20 mmol/g, 2μmol-scale) from Rapp Polymers (Tübingen, Germany) was allowed to swell in DMF for 30 min and then transferred to the synthesizer.

Fmoc cleavage: 250 μL DMF/Piperidine (4:1, v/v) was added to the resin over 2 min. The resin was washed with 200 μL DMF (3x). The Fmoc cleavage was repeated two times.

Coupling of amino acid: 54 μL HCTU (5.4 eq, 0.2 M in NMP), 30 μL NMM (12.0 eq, 0.8 M in NMP) and 40 μL Boc-protected lysine (6.0 eq, 0.3 M in NMP) were mixed in a pre-activation vessel. After 2 min, the pre-activation solution was transferred onto the resin. After 30 min, the resin was washed with 200 μL DMF (3x) and the coupling was repeated.

Coupling of PNA monomer: 36 μL HCTU (3.6 eq, 0.2 M in NMP), 20 μL NMM (8.0 eq, 0.8 M in NMP) and 40 μL PNA monomer (4.0 eq, 0.2 M in NMP) were mixed in a pre-activation vessel. After 2 min, the pre-activation solution was transferred onto the resin. After 39 min, the resin was washed with 200 μL DMF (3x) and the coupling was repeated.

Capping: 250 µL DMF/Ac_2O/2,6-lutidine (89:5:6, v/v/v) was added to the resin for 2 min. The resin was washed with DMF (300 µL, 5x).

Cleavage from the solid support: Non-thiol-containing PNA oligomers were cleaved by addition of a solution of TFA/ H_2O/*i*PrSiH (1 mL, 90:5:5, v/v/v) and 5 mg L-cystein methylester hydrochloride to the resin, whereas thiol-containing PNA oligomers were cleaved by addition of TFA/*i*PrSiH/EDT (1 mL, 95:3:2, v/v/v) to the resin for 90 min. The suspension was filtered and the resin was washed with TFA (250 µL, 2x). Cold diethyl ether (13.5 mL) was added to the combined filtrates. The turbid mixture was centrifugated for 15 min (4000 rpm, 4 °C). The precipitate was washed with cold diethyl ether (1 mL) and dried under an argon stream.

Purification: The crude product was dissolved in water/acetonitrile (97:3, v/v) and purified by semi-preparative HPLC (3→30 % B in 30 min). **Yields:** General yields for PNA Synthesis was between 10 and 30 %.

6.2.11 Ligand-PNA conjugation

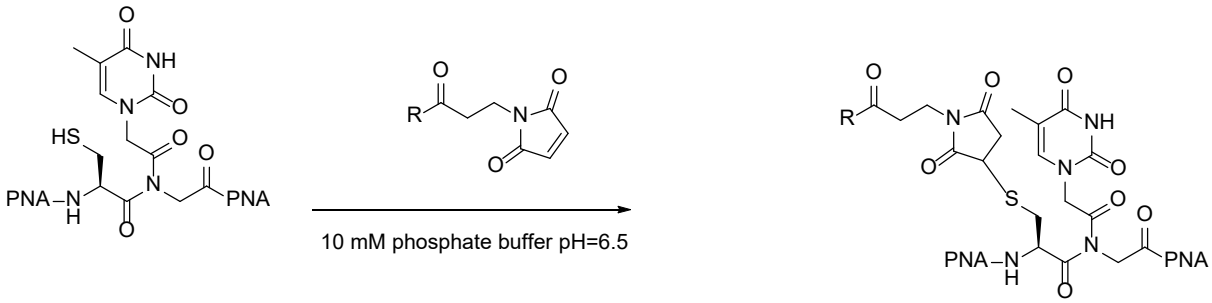

Ligand-PNA conjugation by thiol-maleimide conjugation: One equivalent of thiol methylated PNA (350 – 1000 µM in water, typical scale 200 – 400 nmol) and 2 equivalents of maleimido-Ligand (5 – 20 mM in water) were diluted to a 100 µM PNA concentration in freshly degassed sodium dihydrogen phosphate buffer (10 mM, pH 6.5) and 0.3 mM TCEP. The reaction mixture was shaken at room temperature and progress of the reaction was monitored by UPLC analysis. After complete ligation, the reaction mixture was acidified and lyophilized. The residue was dissolved in water (0.1 % trifluoroacetic acid) and purified by semi-preparative HPLC. Lyophilization afforded the product as a white powder.

Yields: 40 – 90 %

Figure 31. Thiol-maleimide ligation of maleimide-functionalized ligand to a thiol methylated PNA oligomer.

Sugar-PNA conjugation by copper-catalyzed click reaction: The resin (2 μmol loading), equipped with azide-modified PNA, was swollen in a solution of 100 μL DMF saturated with Copper iodide and an excess of DIPEA added. After adding 4 equivalents (2 μmol, 3 mg) of the alkyne functionalized ligand **26** the reaction vessel was shaken for 48 h at rt. The progress of the reaction was followed by mini cleavages and UPLC monitoring.

Cleavage from the solid support: The PNA oligomers were cleaved by addition of a solution of TFA/ H_2O/*i*PrSiH (1 mL, 90:5:5, v/v/v) to the resin for 90 min. The suspension was filtered and the resin was washed with TFA (250 μL, 2x). Cold diethyl ether (13.5 mL) was added to the combined filtrates. The turbid mixture was centrifugated for 15 min (4000 rpm, 4 °C). The precipitate was washed with cold diethyl ether (1 mL) and dried under an argon stream.

Purification: The crude product was dissolved in water/acetonitrile (97:3, v/v) and purified by semi-preparative HPLC (3→30 % B in 30 min).

Yields: Total yield of the copper-catalyzed click strategy for PNA synthesis and conjugation was between 7 and 8 %.

6.2.12 Synthesised PNA Oligomers

Unmodified PNA oligmers

P1 **H-DDtcatcgccttctaK-NH_2 (P1):** ε_{260} = 116.100 L·mol^{-1}·cm^{-1}, 2.7 µmol, 27 %, t_R (HPLC): 1.47 min (3 − 30 % B in 2 min). $C_{152}H_{199}N_{71}O_{49}$. ESI-MS: m/z = 952.4 ([M+4H]$^{4+}$, calcd.: 952.2), 762.3 ([M+5H]$^{5+}$, calcd.: 761.9), 635.2 ([M+6H]$^{6+}$, calcd.: 635.1)

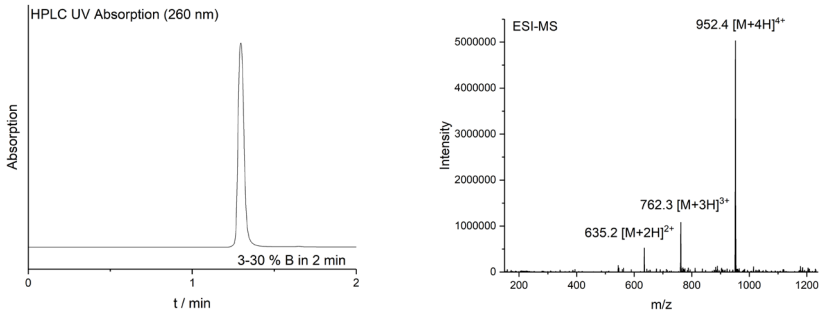

Thiol-modified PNA oligomers

S1 **H-DD acct(~CH_2SH)atggactttK-NH_2:** ε_{260} = 128.300 L·mol^{-1}·cm^{-1}, 2.2 µmol, 22 %, t_R (HPLC): 1.49 min (3 − 30 % B in 2 min). $C_{155}H_{201}N_{75}O_{48}S$. ESI-MS: m/z = 979.9 ([M+4H]$^{4+}$, calcd.: 979.5), 784.1 ([M+5H]$^{5+}$, calcd.: 783.9), 653.7 [M+6H]$^{6+}$, calcd.: 653.5)

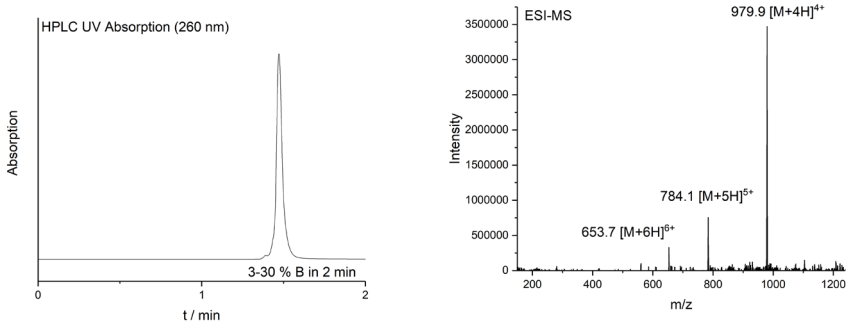

S2 **H-actt(~CH_2SH)acttcacgcK-NH_2:** ε_{260} = 121.000 L·mol^{-1}·cm^{-1}, 400 nmol, 20 %, tR (HPLC): 1.54 min (3 − 30 % B in 2 min). $C_{145}H_{190}N_{72}O_{41}S$. ESI-MS: m/z = 1210.5 ([M+3H]$^{3+}$, calcd.: 1210.9), 907.9 ([M+4H]$^{4+}$, calcd.: 908.4), 726.9 ([M+5H]$^{5+}$, calcd.: 726.9)

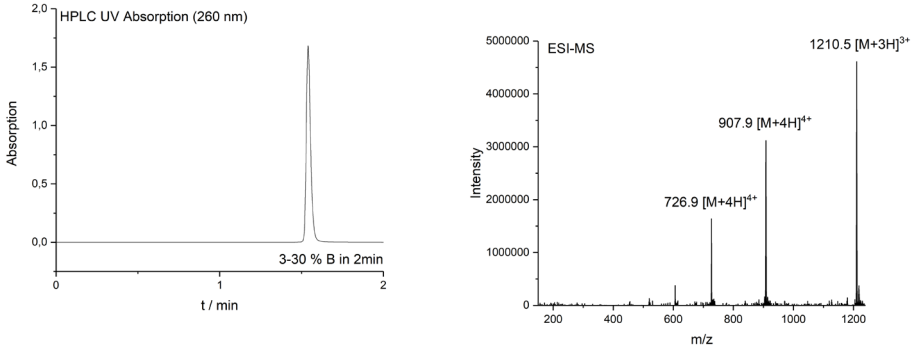

S3 **H-DDatgctacgtt(~CH_2SH)gacK-NH_2:** ε260 = 131200 L·mol^{-1}·cm^{-1}, 2.3 µmol, 23 %, tR (HPLC): 1.40 min (3 − 30 % B in 2 min). $C_{155}H_{200}N_{78}O_{47}S$. ESI-MS: m/z = 985.9 ([M+4H]$^{4+}$, calcd.: 985.5), 789.1([M+5H]$^{5+}$, calcd.: 788.9), 657.4([M+6H]$^{6+}$, calcd.: 657.6)

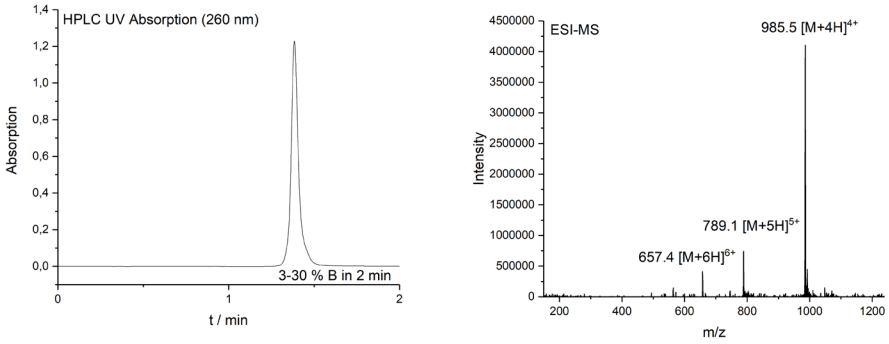

S4 **H- aactcctact(~CH_2SH)cct K-NH_2:** ε260 = 115900 L·mol^{-1}·cm^{-1}, 180 nmol, 9 %, tR (HPLC): 1.46 min (3 − 30 % B in 2 min). $C_{144}H_{190}N_{70}O_{41}S$. ESI-MS: m/z = 1197.3 ([M+3H]$^{3+}$, $^{+}$, calcd.: 1197.5), 897.9 ([M+4H]$^{4+}$,calcd.: 898.4), 718.8 ([M+5H]$^{5+}$, calcd.: 718.9)

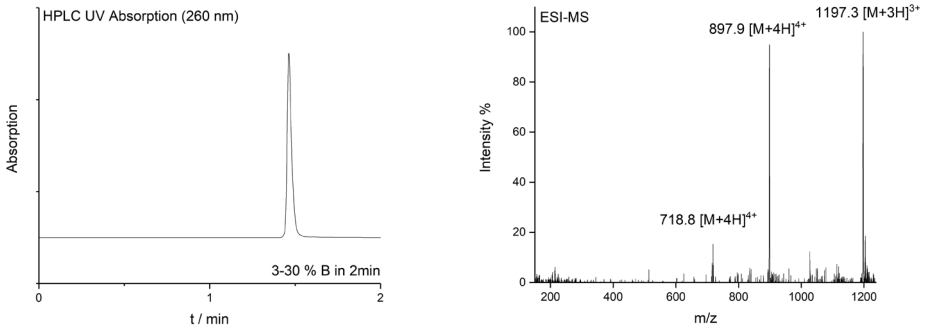

S5 **H-DDatac at(~CH_2SH)cc aacacK -NH_2:** ε_{260} = 132800 L·mol^{-1}·cm^{-1}, 500 nmol, 25 %, tR (HPLC): 1.60 min (3 − 30 % B in 2 min). $C_{154}H_{200}N_{80}O_{42}S$. ESI-MS: m/z = 966.9 ([M+4H]$^{4+}$, calcd.: 965.9), 773.4 ([M+5H]$^{5+}$, calcd.: 772.9), 644.9 ([M+6H]$^{6+}$, calcd.: 644.3)

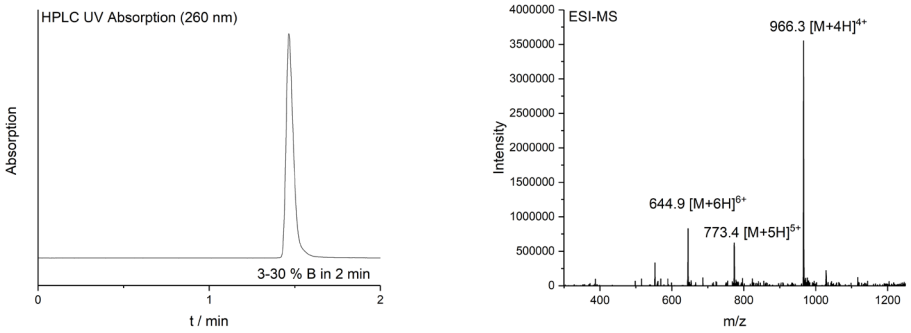

S6 **H-DDtcat(~CH_2SH)tcact(~CH_2SH)cggcK-NH2:** ε_{260} = 119000 L·mol^{-1}·cm^{-1}, 260 nmol, 13 %, t_R (HPLC): 1.60 min (3 − 30 % B in 2 min). $C_{154}H_{202}N_{74}O_{48}S_2$. ESI-MS: m/z = 981.5 ([M+4H]$^{4+}$, calcd.: 981.4), 785.5 ([M+5H]$^{5+}$, calcd.: 785.3), 654.8([M+6H]$^{6+}$, calcd.: 654.6)

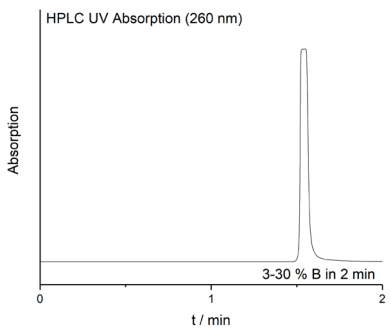

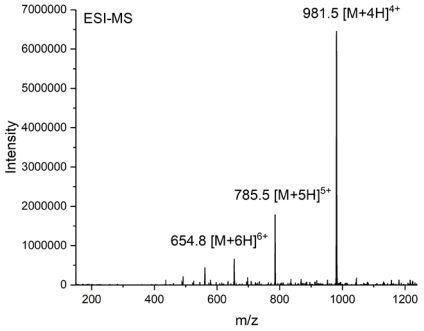

Glc2NTs-PNA conjugates

P2 **H-DD acct(CH_2S~Glc2NTs)atggactt tK-NH_2 (P3):** ε_{260} = 128300 L·mol^{-1}·cm^{-1}; 200 nmol, 50 %, tR (HPLC): 1.69 min (3 − 30 % B in 2 min). $C_{177}H_{230}N_{78}O_{58}S_2$. ESI-MS: m/z = 1111.4 ([M+4H]$^{4+}$, calcd.: 1111.7), 889.3 ([M+5H]$^{5+}$, calcd.: 889.5), 741.4 ([M+6H]$^{6+}$, calcd.: 741.5)

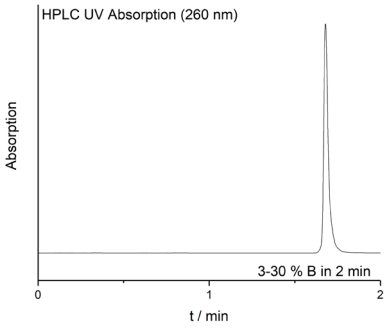

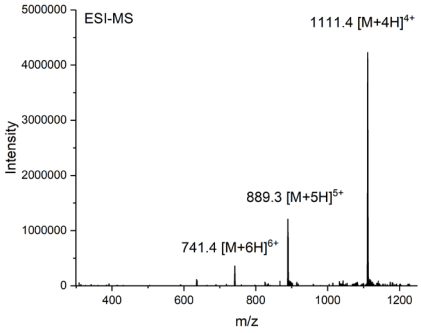

P3 **H- actt(CH_2S~Glc2NTs) acttcacgc K-NH_2:** ε_{260} = 121000 L·mol^{-1}·cm^{-1}, 82 nmol, 41 %, tR (HPLC): 1.72 min (3 − 30 % B in 2 min). $C_{167}H_{219}N_{75}O_{51}S_2$. ESI-MS: m/z = 1040.5 ([M+4H]$^{4+}$, calcd.: 1040.2), 832.6 ([M+5H]$^{5+}$, calcd.: 832.3), 694.0 ([M+6H]$^{6+}$, calcd.: 693.7)

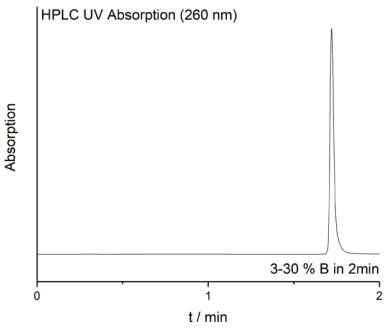

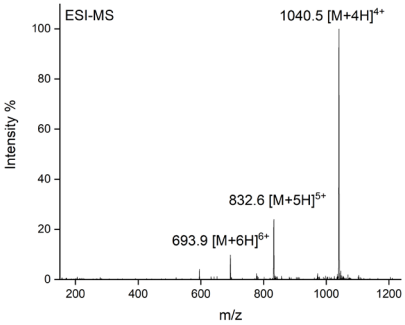

P4 **H-DDatgctacgtt(CH$_2$S~Glc2NTs)gacK-NH$_2$ (P5):**: ε_{260} = 131200 L·mol^{-1}·cm^{-1}, 316 nmol, 79 %, tR (HPLC): 1.51 min (3 − 30 % B in 2 min). $C_{178}H_{229}N_{81}O_{57}S_2$. ESI-MS: m/z = 1117.6 ([M+4H]$^{4+}$, calcd.: 1117.9), 894.5 ([M+5H]$^{5+}$, calcd.: 894.4), 745.2 ([M+6H]$^{6+}$, calcd.: 745.6)

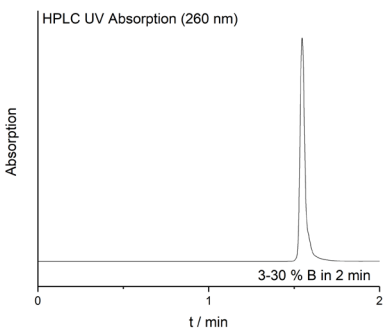

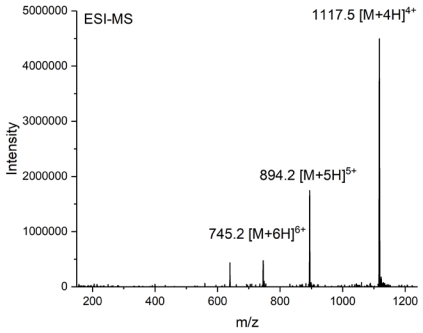

P5 **H-aactcctact(CH$_2$S~Glc2NTs)cctK-NH$_2$:** ε_{260} = 115900 L·mol^{-1}·cm^{-1}, 158 nmol, 37 %, tR (HPLC): 1.53 min (3 − 30 % B in 2 min). $C_{166}H_{219}N_{73}O_{51}S_2$. ESI-MS: m/z = 1030.2 ([M+4H]$^{4+}$, calcd.: 1030.2), 824.6 ([M+5H]$^{5+}$, calcd.: 824.3), 687.3 ([M+6H]$^{6+}$, calcd.: 687.1)

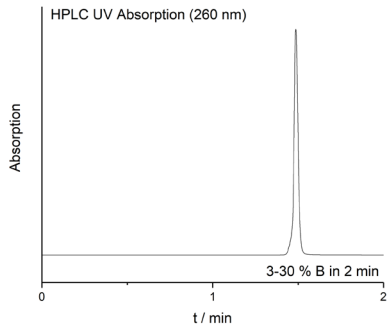

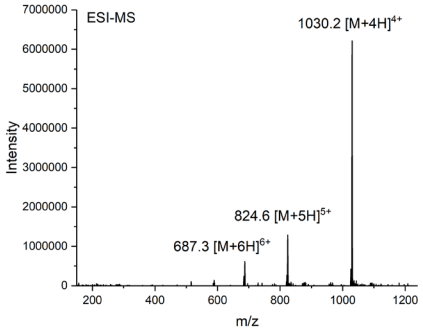

P6 **H-DDatacat(CH$_2$S~Glc2NTs)ccaacac -NH$_2$:** ε_{260} = 132800 L·mol^{-1}·cm^{-1}, 110 nmol, 55 %, tR (HPLC): 1.39 min (3 − 30 % B in 2 min). $C_{154}H_{200}N_{80}O_{42}S$. ESI-MS: m/z = 1098.1 ([M+4H]$^{4+}$, calcd.: 1097.9), 878.7 ([M+5H]$^{5+}$, calcd.: 878.5), 732.7 ([M+6H]$^{6+}$, calcd.: 732.3)

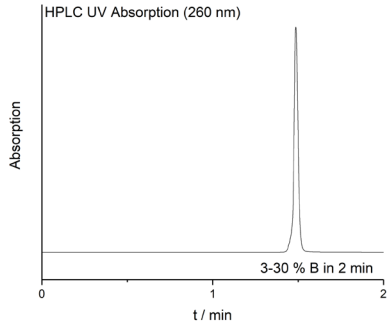

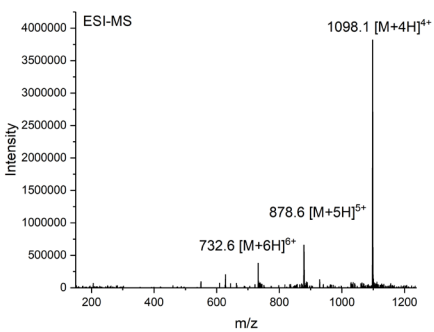

P7 **H-DDtcat(CH$_2$S~Glc2NTs)tcact(CH$_2$S~Glc2NTs)cggcK-NH$_2$:** ε_{260} = 119000 L·mol^{-1}·cm^{-1}, 86 nmol, 43 %, tR (HPLC): 1.77 min (3 − 30 % B in 2 min). $C_{176}H_{231}N_{77}O_{58}S_4$. ESI-MS: m/z = 996.5 ([M+5H]$^{5+}$, calcd.: 996.1), 830.5([M+6H]$^{6+}$, calcd.: 830.3)

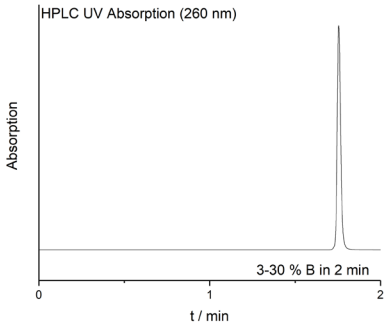

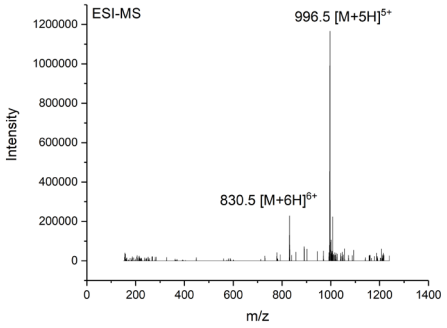

Mannose-PNA-conjugates

P8 **H-actt(CH$_2$S~Man) acttcacgcK-NH2:** Yield: (ε260 = 121000 L·mol-1·cm-1), 66 nmol, 33 %, tR (HPLC): 1.46 min (3 - 30 % B in 2 min). C_{160} H_{212} N_{74} $O_{50}S_1$.ESI-MS: m/z = 1001.6 ([M+4H]$^{4+}$, calcd.:1001.9)

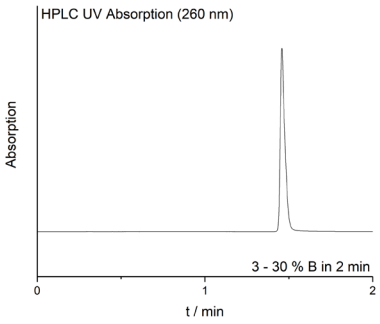

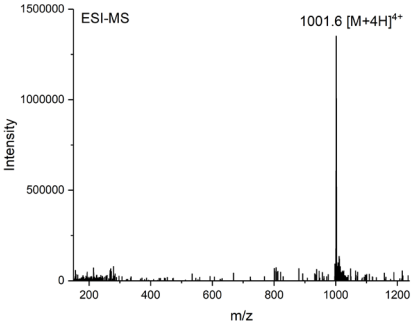

P9 **H-aactcctact(CH2S~Man)cctK-NH2:** (ε260 = 115900 L·mol-1·cm-1), 112 nmol, 56 %, tR (HPLC): 1.48 min (3 - 30 % B in 2 min). C_{159} H_{212} N_{72} $O_{50}S_1$. ESI-MS: m/z = 992.3 ([M+4H]$^{4+}$, calcd.: 992.0), 793.7 ([M+H]$^{5+}$, calcd.: 793.8), 661.7 ([M+H]$^{6+}$, calcd.: 661.6)

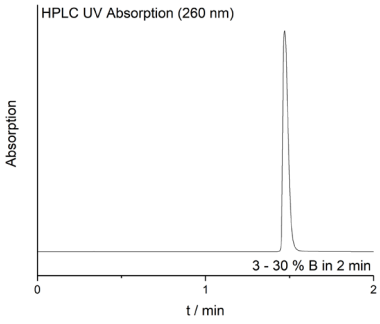

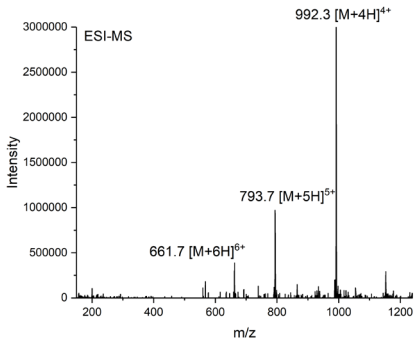

BiPhMan-PNA-conjugates

P-10 **H-DDacct(CH2S~BiphMan)atggactttK-NH2:** Yield: (ε260 = 140550 L·mol-1·cm-1), 156 nmol, 39 %, tR (HPLC): 2.29 min (3 - 40 % B in 4 min). C_{184} H_{231} $FN_{78}O_{60}S_2$. ESI-MS: m/z = 1154.7 ([M+4H]$^{4+}$, calcd.: 1155.1), 923.9 ([M+H]$^{5+}$, calcd.: 924.3), 770.7 ([M+H]$^{6+}$, calcd.: 770.4)

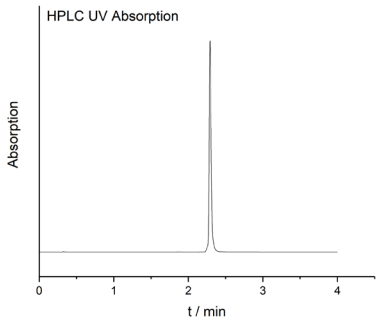

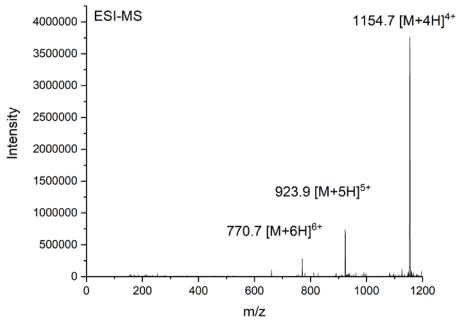

P-11 **H-DDatgctacgtt(CH2S~BiphMan)gacK-NH2:** Yield: (ε260 = 143450 L·mol-1·cm-1), 180 nmol, 45 %, tR (HPLC): 1.9 min (3 - 30 % B in 2 min). C_{184} H_{230} F_3N_{81} $O_{59}S_2$. ESI-MS: m/z = 1160.8 ([M+4H]$^{4+}$, calcd.: 1161.3), 929.4 ([M+H]$^{5+}$, calcd.: 929.3), 774.4 ([M+H] $^{6+}$, calcd.: 774.6)

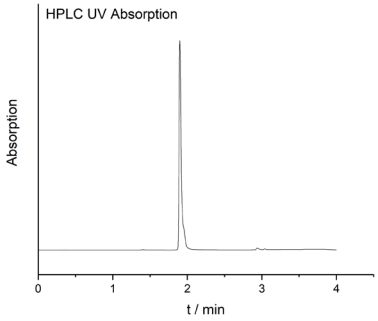

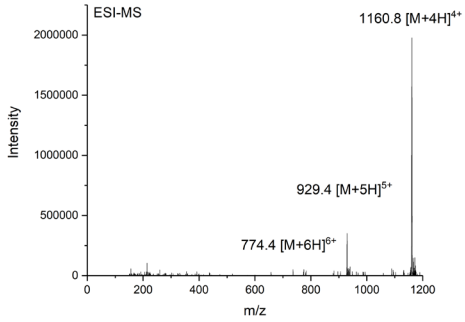

Glc2NHTs(triazole)-PNA conjugates

P12 **H-DDacct(triazole~Glc2NHTs)atggactt tK-NH2 (P3):** Yield: (ε260 = 128300 L·mol-1·cm-1), 160 nmol, 8 %, tR (HPLC): 1.67 min (3 - 30 % B in 2 min). C_{174} H_{227} N_{79} $O_{55}S_1$. ESI-MS: m/z = 1085.6 ([M+4H]$^{4+}$, calcd.: 1085.3), 868.4 ([M+H]$^{5+}$, calcd.: 868.4), 723.7 ([M+H]$^{6+}$, calcd.: 723.8)

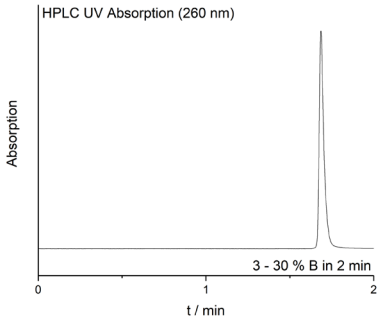

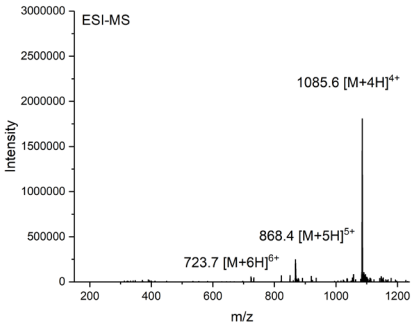

P13 **H-DDtcat(N3~Glc2NHTs)tcact(N3~Glc2NHTs)cggcK-NH2:** Yield: (ε260 = 119000 L·mol-1·cm-1), 140 nmol, 7 %, tR (HPLC): 1.84 min (3 - 30 % B in 2 min). C_{192} H_{256} N_{82} $O_{62}S_2$. ESI-MS: m/z = 1192.5 ([M+4H]$^{4+}$, calcd.: 1192.4), 954,5 ([M+H]$^{5+}$, calcd.: 954.2), 795.1 ([M+H]$^{6+}$, calcd.: 795.3)

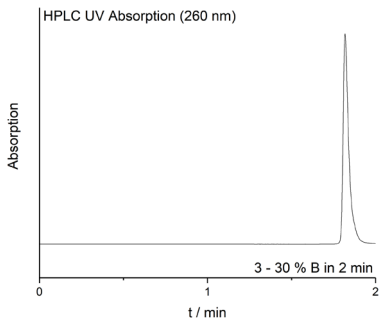

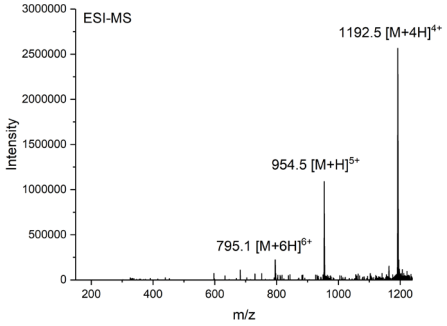

TriGlc2NTs-PNA-conjugates

P14 **H-DDacc t(CH_2S~TriGlc2NTs)atggactttK-NH_2:** ε_{260} = 128300 L·mol^{-1}·cm^{-1}, 236 nmol, 59 %, tR (HPLC): 2.15 min (3 − 30 % B in 4 min). $C_{220}H_{289}N_{89}O_{75}S_4$. ESI-MS: m/z = 1102.6 ([M+5H]$^{5+}$, calcd.: 1102.7), 919.3 ([M+6H]$^{6+}$, calcd.: 919.1), 788.3 ([M+7H]$^{7+}$, calcd.: 787.9)

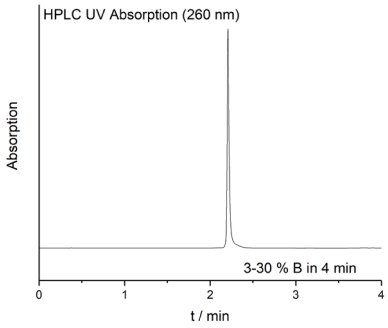

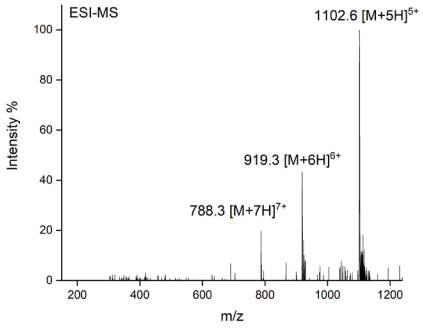

P15 **H-DDatgctacgtt(CH_2S~TriGlc2NTs)gacK-NH_2:** ε_{260} = 131200 L·mol^{-1}·cm^{-1}, 176 nmol, 44 %, tR (HPLC): 2.0 min (3 − 30 % B in 4 min). $C_{220}H_{229}N_{92}O_{74}S_4$. ESI-MS: m/z = 1107.5 ([M+5H]$^{5+}$, calcd.: 1107.7), 923.6 ([M+6H]$^{6+}$, calcd.: 923.2), 792.6 ([M+7H]$^{7+}$, calcd.: 791.5)

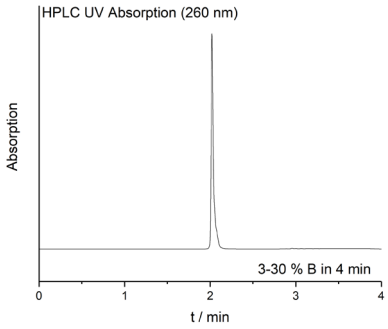

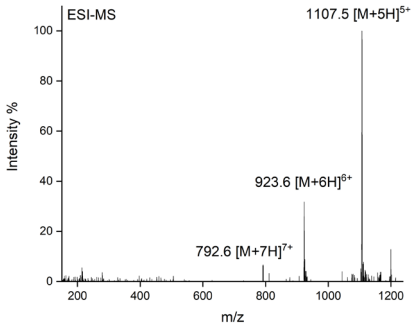

P16 **H-DDacct(CH2S~ Trimannose)atggactttK-NH2:** Yield: (ε260 = 128300 L·mol-1·cm-1), 268 nmol, 67 %, tR (HPLC): 1.28 min (3 - 30 % B in 2 min). C_{199} H_{268} N_{86} $O_{72}S$. ESI-MS: m/z = 1010.9 ($[M+H]^{5+}$, calcd.: 1010.8), 842.4($[M+H]^{6+}$, calcd.: 842.5), 722.7 ($[M+H]^{7+}$, calcd.: 722.3)

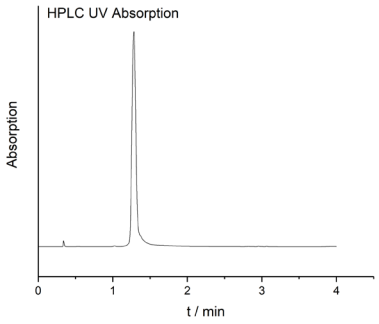

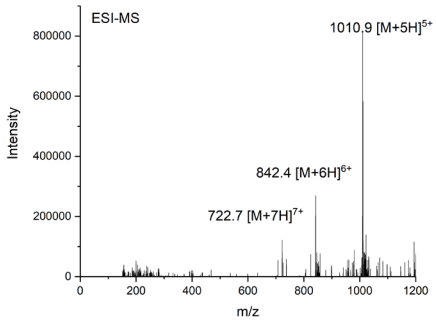

P-17 **H-DDatgctacgtt(CH2S~ Trimannose)gacK-NH2:** Yield: (ε260 = 131200 L·mol-1·cm-1), 216 nmol, 54 %, tR (HPLC): 1.18 min (3 - 30 % B in 2 min). C_{199} H_{267} N_{89} $O_{71}S$. ESI-MS: m/z = 1015.8 ($[M+H]^{5+}$, calcd.: 1015.8), 846.9 ($[M+H]^{6+}$, calcd.: 846.6), 726.2($[M+H]^{7+}$, calcd.: 725.8)

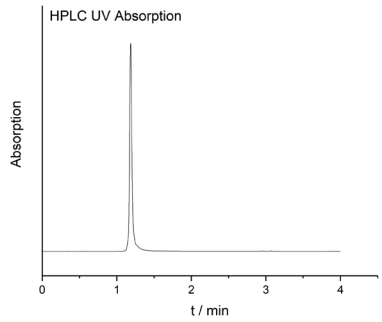

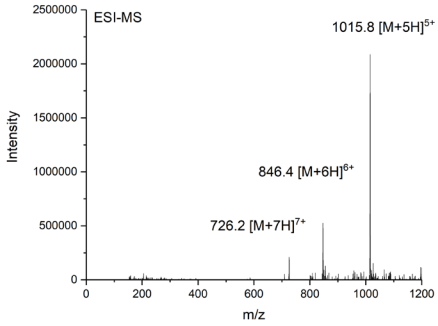

P18- **H-DDacct(CH2S~TriBiphMan)atggactttK-NH2:** Yield: (ε260 = 165050 L·mol-1·cm-1), 142 nmol, 71 %, tR (HPLC): 2.73 min (3 - 30 % B in 4 min). C_{241} H_{292} $F_9N_{89}O_{81}S_4$. ESI-MS: m/z = 1207.1 ($[M+H]^{5+}$, calcd.: 1207.2), 1006.2($[M+H]^{6+}$, calcd.: 1006.1), 862.4($[M+H]^{7+}$, calcd.: 862.5)

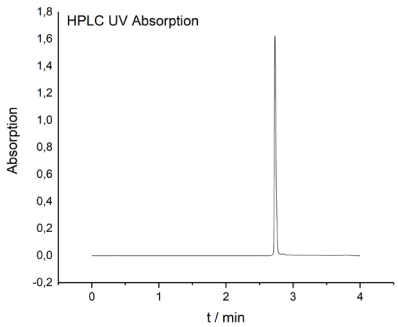

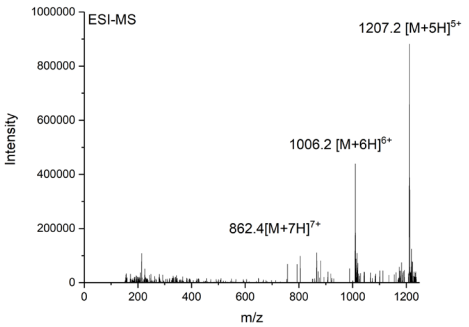

P19 **H-DDatgctacgtt(CH2S~TriBiPhMan)gacK-NH2:** Yield: (ε260 = 167950 L·mol-1·cm-1) , 96 nmol, 48 %, tR (HPLC): 2.71 min (3 - 30 % B in 4 min). C_{241} H_{287} F_9N_{92} $O_{80}S_4$. ESI-MS: m/z = 1211.8 ([M+H]$^{5+}$, calcd.: 1212.1), 1010.3 ([M+H]$^{6+}$, calcd.: 1010.3), 865.7 ([M+H]$^{7+}$, calcd.: 866.1)

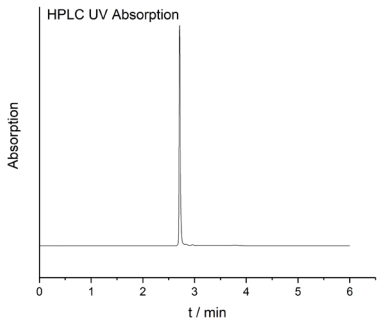

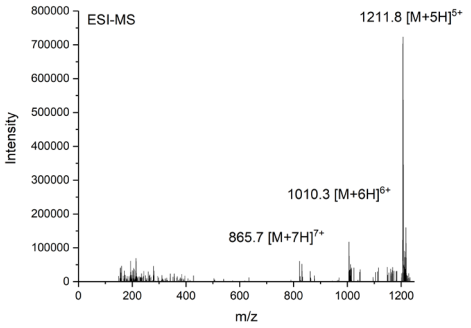

6.3 Ligand-PNA-DNA Duplex Composition

6.3.1 DNA templates

Cy5 - 5'- TAG AAG GCG ATG ATA GAA GGC GAT GAT AGA AGG CGA TGA -3' (**T01**)

5'- AGG AGT AGG AGT TTA GAA GGC GAT GAT AGA AGG CGA TGA -3' (**T02**)

5'- GTC AAC GTA GCA TTA GAA GGC GAT GAT AGA AGG CGA TGA -3' (**T03**)

5'- TAG AAG GCG ATG ATA GAA GGC GAT GAG CCG AGT GAA TGA -3' (**T04**)

5'- TAG AAG GCG ATG AAA AGT CCA TAG GTG TCA ACG TAG CAT -3' (**T05**)

5'- TAG AAG GCG ATG AGT GTT GGA TGT ATG TCA ACG TAG CAT -3' (**T06**)

5'- TAG AAG GCG ATG AGC GTG AAG TAA GTG CGT GAA GTA AGT -3' (**T07**)

5'- TAG AAG GCG ATG AAA AGT CCA TAG GTA AAG TCC ATA GGT -3' (**T08**)

Cy5 - 5'- TAG AAG GCG ATG AAA AGT CCA TAG GTA AAG TCC ATA GGT -3' (**T9**)

Atto647- 5'- TAG AAG GCG ATG AAA AGT CCA TAG GTA AAG TCC ATA GGT -3' (**T10**)

5'- TAG AAG GCG ATG AGT GTT GGA TGT ATA AAG TCC ATA GGT -3' (**T11**)

5'- TAG AAG GCG ATG AAG GAG TAG GAG TTG CGT GAA GTA AGT -3' (**T12**)

5'- AGG AGT AGG AGT TTA GAA GGC GAT GAA GGA GTA GGA GTT -3' (**T13**)

5'- GTC AAC GTA GCA TTA GAA GGC GAT GAG TCA ACG TAG CAT -3' (**T14**)

5'- GTC AAC GTA GCA TTA GAA GGC GAT GAA AAG TCC ATA GGT -3' (**T15**)

5'- TAGAAG GCG ATG AAA AGT CCA TAG GTT AAA GTC CAT AGG T -3' (**T16**)

5'- TAG AAG GCG ATG AAA AGT CCA TAG GTT TTA AAG TCC ATA GGT -3' (**T17**)

5'- TAG AAG GCG ATG AAA AGT CCA TAG GTT TTT TAA AGT CCA TAG GT -3' (**T18**)

5'- TAG AAG GCG ATG AGT GTT GGA TGT ATA GTC AAC GTA GCA T -3' (**T19**)

5'- TAG AAG GCG ATG AGT GTT GGA TGT ATA AAG TCA ACG TAG CAT -3' (**T20**)

5'- TAG AAG GCG ATG AGT GTT GGA TGT ATA AAA AGT CAA CGT AGC AT -3' (**T21**)

5'- AGG AGT AGG AGT TTA GAA GGC GAT GAG CGT GAA GTA AGT -3' (**T22**)

6.3.2 Ligand-PNA-DNA Duplex Composition

Table 22. Composition of the Ligand-PNA•DNA complexes. To a DNA template (T01 – T22) appropriate equivalents of a PNA oligomers (P1 – P19) were added. For complex hybridization, the mixture was heated to 80°C in a thermo shaker for 5 min and slowly left to cool down to rt.

Complex	nt	d [Å]	template	PNAs
nL-Cy5	-	-	T01	3xP1
G-Mono	-	-	T02	2xP1; P4
G-Mono	-	-	T03	2xP1; P3
G-16	5	16	T04	2xP1; P7
G-16-S	5	16	T04	2xP1; P13
G-23	7	23	T05	P1; P2; P4
G-29	9	29	T06	P1; P6; P4
G-42	13	42	T07	P1; 2xP3
G-42	13	42	T08	P1, 2xP2
G-42-S	13	42	T08	P1; 2xP12
G-42-Cy5	13	42	T09	P1, 2xP2
G-42-Atto647	13	42	T10	P1, 2xP2
G-49	15	49	T11	P1, P2, P6
G-62	19	62	T12	P1; P3; P5
G-84	26	84	T13	P1; 2xP5
G-84	26	84	T14	P1; 2xP4
G-104	32	104	T15	P1; P2; P4
G-42-F1	13	42	T16	P1, 2xP2
G-42-F3	13	42	T17	P1, 2xP2
G-42-F4	13	42	T18	P1, 2xP2
G-29-F1	9	29	T19	P1; P6; P4
G-29-F3	9	29	T20	P1; P6; P4
G-29-F5	9	29	T21	P1; P6; P4
Complex	nt	d [Å]	template	PNAs
TG-Mono	-	-	T03	2xP1. P15
TG-23	7	23	T05	P1; P14; P15
TG-42	13	42	T08	P1, 2xP14
TG-84	26	84	T14	P1; 2xP15
TG-104	32	104	T15	P1; P14; P15

M-Mono	-			2xP1; P9
M-42	13	42	T07	P1; 2xP8
M-62	19	62	T12	P1, P8; P9
M-84	26	84	T13	P1; 2xP9
M-104	32	104	T22	P1; P8; P9
TM-Mono	-	-	T03	2xP1;P17
TM-23	7	23	T05	P1; P16; P17
TM-42	13	42	T08	P1; 2xP16
TM-84	26	84	T14	P1; 2xP17
TM-104	32	104	T15	P1; P16, P17
B-Mono	-	-	T03	2xP1; P11
B-42	13	42	T08	P1; 2xP10
B-104	32	104	T15	P1; P10; P11
TB-Mono	-	-	T03	2xP1; P19
TB-23	7	23	T05	P1; P18; P19
TB-42	13	42	T08	P1; 2xP18
TB-104	32	104	T15	P1; P18; P19

6.4 Langerin ECD and CRD Receptor Expression and Purification

The expression and purification of the proteins langerin and DC-SIGN was kindly conducted by the Rademacher group (MPIKG) as previously published.[47]

Langerin extracellular domain. Expression and purification were conducted by the Rademacher group as previously published.[103] Briefly, the trimeric langerin extracellular domain (ECD) was expressed insolubly in *E. coli* BL21* (DE3) (Invitrogen). Following enzymatic cell lysis, inclusion bodies were harvested and subsequently solubilized. The sample was centrifuged and the langerin ECD was refolded overnight via rapid dilution. Next, the sample was dialyzed overnight, centrifuged and purified via mannan-agarose affinity chromatography (Sigma Aldrich). For ^{19}F R2-filtered NMR experiments, the buffer was exchanged to 25 mM Tris, 150 mM NaCl, 5 mM $CaCl_2$, pH 7.8. For SPR experiments, the buffer was exchanged to 20 mM HEPES, 150 mM NaCl, 1 mM $CaCl_2$, pH 7.4. The concentration of langerin ECD was determined via UV spectroscopy (ε_{280} = 56.170 mol^{-1} cm^{-1}).

Purity and monodispersity of langerin ECD samples were analyzed via SDS PAGE and DLS.

Langerin and DC-SIGN carbohydrate recognition domain. Expression and purification were conducted by the Rademacher group as previously published.[103] Briefly, the monomeric ^{15}N-labeled langerin and DC-SIGN carbohydrate recognition domain (CRD) was expressed insolubly in *E. coli* BL21* (DE3) (Invitrogen). Following enzymatic cell lysis, inclusion bodies were harvested and subsequently solubilized. The sample was centrifuged and the langerin CRDs were refolded overnight via rapid dilution. Next, the sample was dialyzed overnight, centrifuged and purified via StrepTactin affinity chromatography (Iba). After an additional dialysis step overnight, the sample was centrifuged and the buffer was exchanged to 25 mM HEPES, 150 mM NaCl , pH 7.0. The concentration of langerin and DC-SIGN CRDs was determined via UV spectroscopy (ε_{280} = 56.170 mol^{-1} cm^{-1*}, ε_{280} = 70 400 mol^{-1} cm^{-1}). Purity and monodispersity of langerin CRD samples were analyzed via SDS PAGE and DLS

6.5 Affinity Assays

6.5.1 ^{19}F-NMR Assay

The ^{19}F-NMR Assay was conducted and evaluated by Eike Wamhoff, Nina-Loiusa Efrém, Hannes Baukmann, Hengxi Zhang (all AG Rademacher, MPIKG Potsdam) and myself according to a previously described method.[93] Langerin ECD and CRD were obtained as described above.

Experiments with the langerin ECD were performed at a receptor concentration of 50 µM or 25 µM in 25 mM Tris with 10 % DMSO, 10% D_2O, 150 mM NaCl and 5 mM $CaCl_2$ at pH 7.8 and 25° C. Apparent relaxation rates $R2_{,obs}$ for the reporter ligand were determined using the CPMG pulse sequence as previously published. [93]

Experiments with the langerin CRD were performed at a receptor concentration of 50 µM in 25 mM HEPES with 10% DMSO, 10% D_2O, 150 mM NaCl and 5 mM $CaCl_2$ at pH 7.0 and 25°C.

TFA served as an internal reference at a concentration of 50 μM. Apparent relaxation rates R2, obs for the reporter ligand were determined using the CPMG pulse sequence as previously published.[93, 124-125]

Experiments with the DC-SIGN CRD were performed at a receptor concentration of 50 μM in 25 mM HEPES with 10% D2O, 150 mM NaCl and 5 mM CaCl2 at pH 7.0 and 25°C. TFA served as an internal reference at a concentration of 50 μM. Apparent relaxation rates $R2,_{obs}$ for the reporter ligand were determined using the CPMG pulse sequence as previously published [93, 124-125]

K_I determination. K_I values were determined as previously published for langerin.[93] Briefly, titration experiments were conducted at a concentration of 0.1 mM of reporter ligand (2-deoxy-2-trifluoroacetamido-α-mannoside)[93] at five competitor concentrations [I]T. Samples were prepared via serial dilution. **IC_{50} determination for Multivalent Glycomimetics.** Due to the complex equilibria and cooperativity effects present in competitive binding experiments with multivalent glycomimetics, IC_{50} values rather than K_I values were utilized to quantify affinities. IC_{50} values were determined in competitive binding experiments *via* the detection of binding of 0.1 mM reporter ligand (2-deoxy-2-trifluoroacetamido-α-mannoside)[93] to either the langerin ECD or CRD at six competitor concentrations. Samples were prepared *via* serial dilution. Equation 1 served to derive IC_{50} values and Hills factors p from R2, obs values in a two parameter fit. (Standard errors were derived directly from the fitting procedures). R2, max represents the relaxation rate at 0.1 mM reporter ligand **(**2-deoxy-2-trifluoroacetamido-α-mannoside**)** in presence of receptor and in absence of competitor. R2, min represents the relaxation rate at 0.1 mM reporter ligand in absence of the protein.

Equation 1 : $R2,=R2,f+(R2,max-R2,f1+(IC50[I]T)p)$

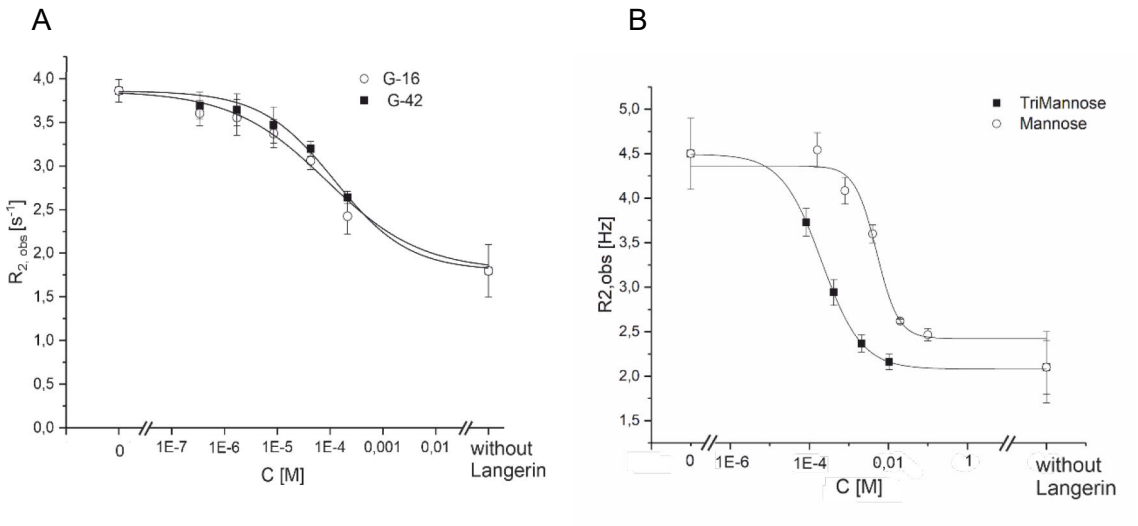

Figure 32 ^{19}F-NMR Assay: Concentration dependent inhibition of the langerin ECD by A) Glc2NHTs and TriGlc2NHTs B) Glc2NHTs-PNA-DNA duplexes (G-Mono, G-42, G-52, G-84 Å) [Protein] = 50 µM C) Glc2NHTs-PNA-DNA duplexes (G-16, G-23, G-29, G-42, G-49) [Protein] = 25 µM D) Glc2NHTs-PNA-DNA duplexes (G-16-S, G-42-S) [Protein] = 25 µM), E) Glc2NHTs-PNA-DNA duplexes (G-42, G-42-F1, G-42-F3, G-42-F) [Protein] = 25 µM), Glc2NHTs-PNA-DNA duplexes (G-30, G-30-F1, G-30-F3, G-30-F5) [Protein] = 25 µM). Errors are the SEM from the fit for one titration.

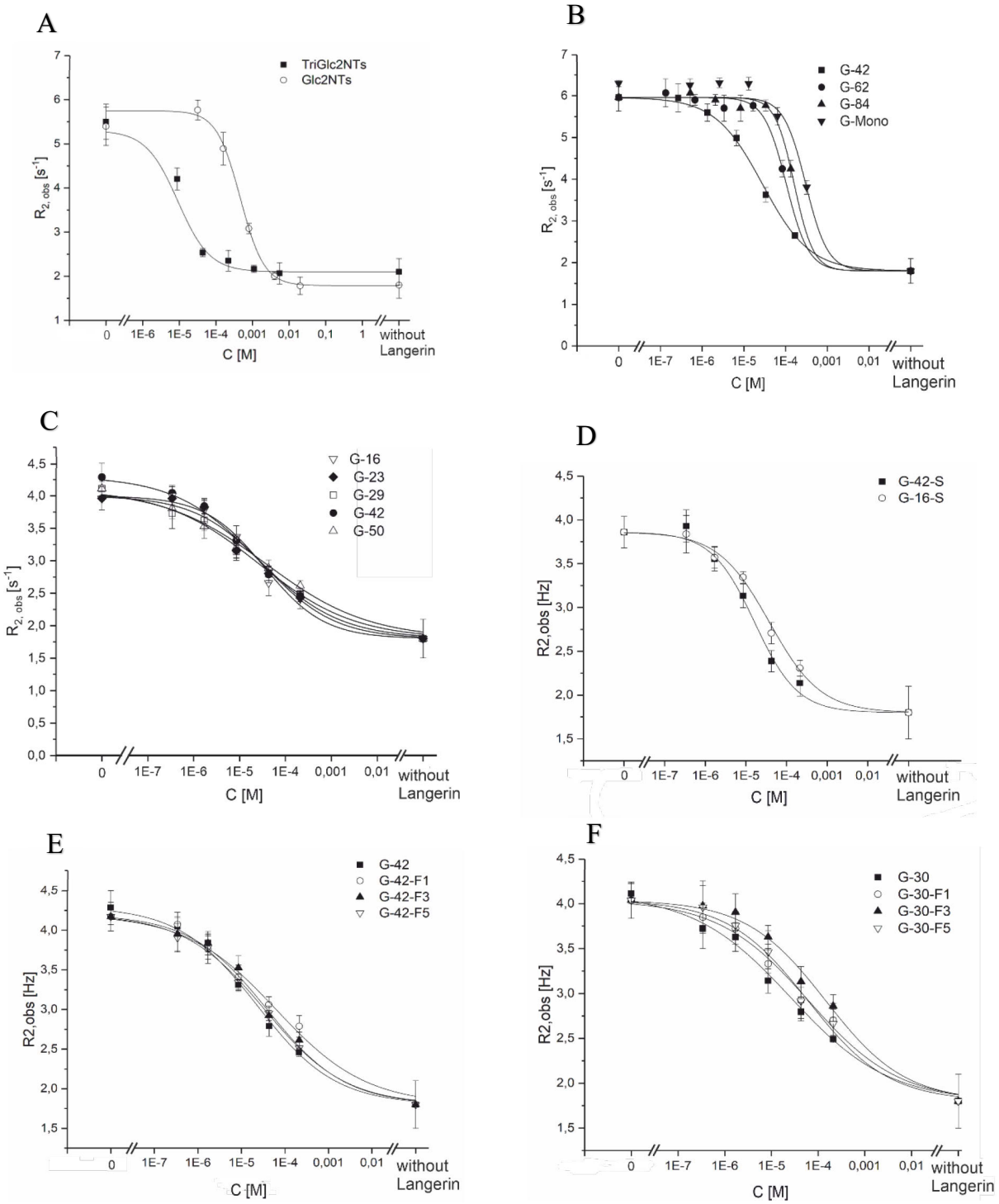

Figure 33 ^{19}F-NMR Assay: Concentration dependent inhibition of the langerin ECD by A) Glc2NHTs and TriGlc2NHTs B) Glc2NHTs-PNA-DNA duplexes (G-Mono, G-42, G-52, G-84 Å) [Protein] = 50 µM C) Glc2NHTs-PNA-DNA duplexes (G-16, G-23, G-29, G-42, G-49) [Protein] = 25 µM D) Glc2NHTs-PNA-DNA duplexes (G-16-S, G-42-S) [Protein] = 25 µM), E) Glc2NHTs-PNA-DNA duplexes (G-42, G-42-F1, G-42-F3, G-42-F) [Protein] = 25 µM), Glc2NHTs-PNA-DNA duplexes (G-30, G-30-F1, G-30-F3, G-30-F5) [Protein] = 25 µM). Errors are the SEM from the fit for one titration.

6.5.2 SPR Competitive Inhibition Experiments

The SPR assay was conducted by Kim Silberreis (Dernedde group, Charité) on a Biacore X100 instrument (GE Healthcare Europe GmbH Uppsala, Sweden) at 25°C and evaluated by myself. For immobilization of biotinylated α-D-mannose–PAA, the HBS-EP buffer (10 mM HEPES, 150 mM NaCl, 3 mM EDTA, pH 7.4 and 0.005% surfactant P 20) from GE Healthcare Europe GmbH was used. The sensor chip was initially conditioned with three consecutive 1 min injections of 1M NaCl in 50 mM NaOH before starting immobilization. Biotinylated α-D-mannose–PAA (20 mol %; Lectinity Holdings, Russia) was immobilized on the measuring channel of a streptavidin coated sensor chip (Sensor Chip SA, GE Healthcare Europe GmbH). On the reference channel of the same sensor chip, biotinylated α-D-galactose–PAA (Lectinity, Moscow, Russia) was immobilized. Running buffer during the assays was 20 mM HEPES, 150 mM NaCl, 1mM $CaCl_2$, pH 7.4, (all Carl Roth GmbH & Co. KG). For testing the experimental set up, single cycle kinetics were performed at five concentrations of langerin, ranging from 62 nM to 5000 nM, and finally a K_D value of 1.5 µM was determined. This study also confirmed the used protein contact times of 120 s, the dissociation time of 300 s and a flow rate of 20 µl/min. The chip surfaces were regenerated at 30 µl/min with 10 mM EDTA pH 8 and a contact time of 60 s. In the **dose response experiment** before injection, each protein sample ([langerin]=500 nM) and a serial dilution of the complexes (dissolved in 20 mM HEPES, 150 mM NaCl, 1mM $CaCl_2$, pH 7.4) were incubated for a minimum of 5 min at rt. The samples were injected over the reference and measuring channel. For evaluation the reference channel data were subtracted from the measuring channel data. The langerin control was measured before and after every dose response series. By calculating the regression between both values an individual langerin baseline drift was calculated for every dose response measurement. Corrected response values were calculated by dividing the RU of the dose response experiment by the individual langerin baseline RU. The corrected response values were used for curve creation and IC_{50} fitting procedure. Responses of the sample injections were extracted between report points set at the start of the injection (0 s) and at the end of the dissociation phase (250 s). Each data point

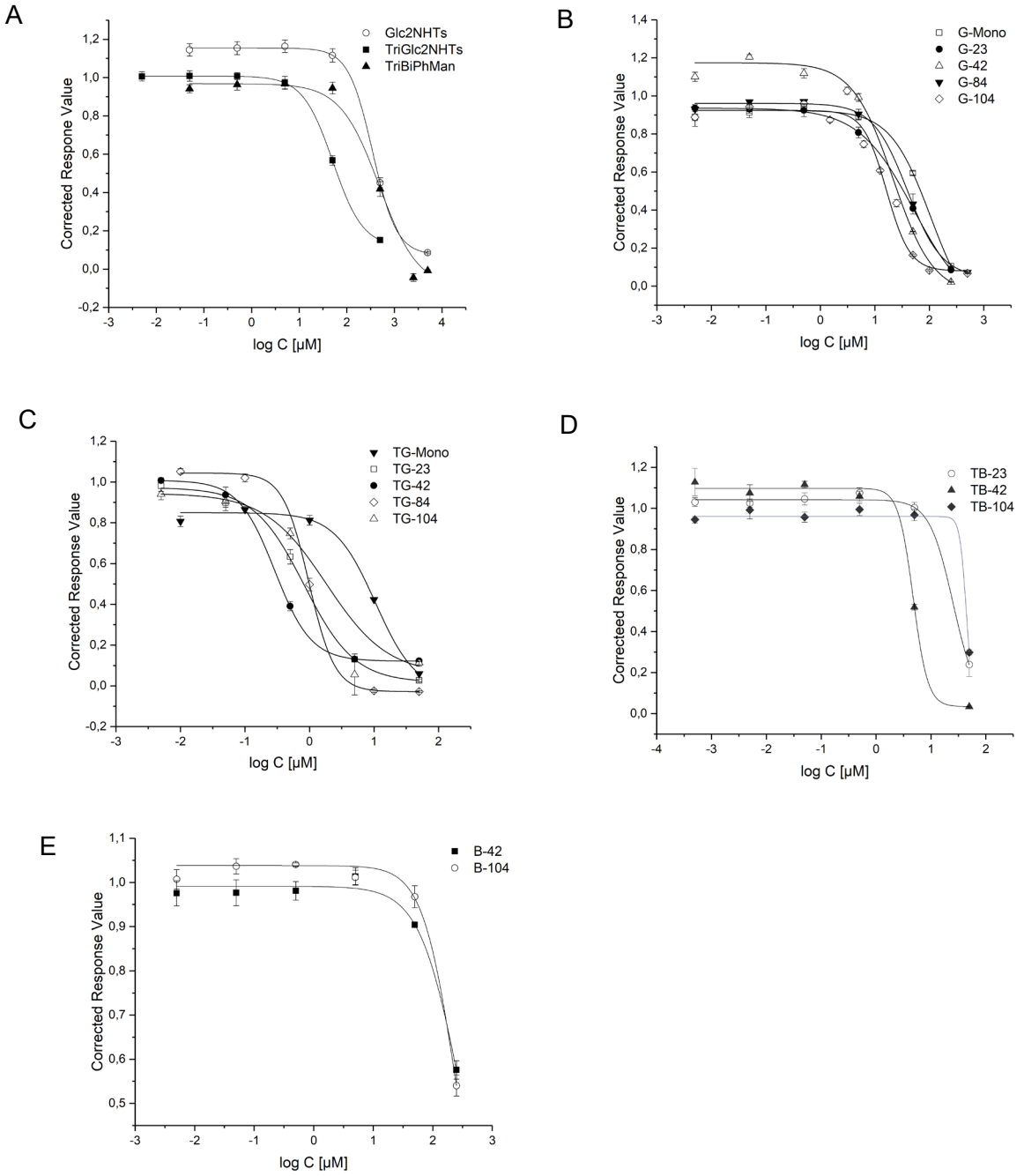

Figure 34 SPR Assay: Concentration dependent inhibition of the langerin ECD by A) mono ligands Glc2NHTs **72**, TriGlc2NHTs **31** and BiPhMan **49** B) Glc2NHTs-PNA-DNA duplexes (G-Mono, 23, 42, 84, 104) C) TriGlc2NHTs-PNA-DNA duplexes (TG-Mono, 23, 42, 84, 104) D) TriBiPhMan-PNA-DNA duplexes (TB-23, 42, 104), E) BiPhMan-PNA-DNA duplexes (B-42, 104). Errors are the SD of duplicates

represents the mean value (SEM) of 2 measurements (duplicates). In the **single concentration experiment** the protein sample [langerin]=500 nM) and the [complexes] = 10 µM (dissolved in 20 mM HEPES, 150 mM NaCl, 1mM $CaCl_2$, pH 7.4) were incubated for a minimum of 5 min at rt. The samples were injected over the

reference and measuring channel. For evaluation the reference channel data were subtracted from the measuring channel data.

6.5.3 Affinity Cell Assay

6.5.3.1 C-Type Lectin+ Model Cells

Wild type, langerin- and DC-SIGN-overexpressing Raji were kindly provided by the Rademacher group. The model cells were produced by a previously described method.[103] Raji cells were cultured in RPMI1640 medium (Sigma Aldrich) containing 10% FCS (Biochrom), 100 U*mL^{-1} penicillin and streptomycin (Life Technologies) and GlutaMax-I (Life Technologies). COS-7 cells (ATCC) were cultured in DMEM supplemented with 10% FCS (Pan-Biotech). All cell lines were maintained at 5% CO2 and 37°C.

6.5.3.2 Affinity Cell Assay Ligand-PNA-DNA duplexes.

Raji cells, suspended in cell culture medium (RPMI1640 (Sigma Aldrich)), were counted, centrifuged at 500 g for 3 min, aspirated, incubated with blocking buffer (0.2 mg/mL Salmon Sperm DNA, 0.2 % BSA in PBS) centrifuged at 500 g for 3 min, aspirated resuspended in culture medium at 37° C and 5% CO2. 50,000 cells were added to the 96 well microtiter plates (Nunc) to obtain a volume of 100 µl. To monitor internalization and binding, Biv-Glc2NTs-12 or Biv-TriGlc2NTs-13 in HBS (20 mM HEPES, 150 mM NaCl, 1mM $CaCl_2$, pH 7.4) were added to the cells at a final concentration of either 660 nM (Method I) or 66 nM (Method II). In case of control experiment 250 µg·mL^{-1} mannan in PBS was added to the cells and constructs. The cells and constructs were incubated for 45 min at 4° C and subsequently centrifuged at 500 g for 3 min. Cells were aspirated and resuspended in cell media for 60 min at 37° C and 5% CO2. Afterwards, the cells were resuspended in fresh cell culture medium before analyzing (Method I) or directly analysed without fresh medium (Method II). Internalization and binding of fluorophore marked complexes was evaluated by flow cytometry on an BA Accuri C6 Plus Flow Cytometer equipped with an autosampler by detecting the conjugated dye Cyanine5 with a 640 nm laser and > 670 filter set. 5000 events were measured for every well. The data was analysed with

CFlow Plus. For normalization the Mean Fluorescent Intensity (MFI) of the Raji cells (autofluorescence) was subtracted from the measured MFI of cells with ligands.

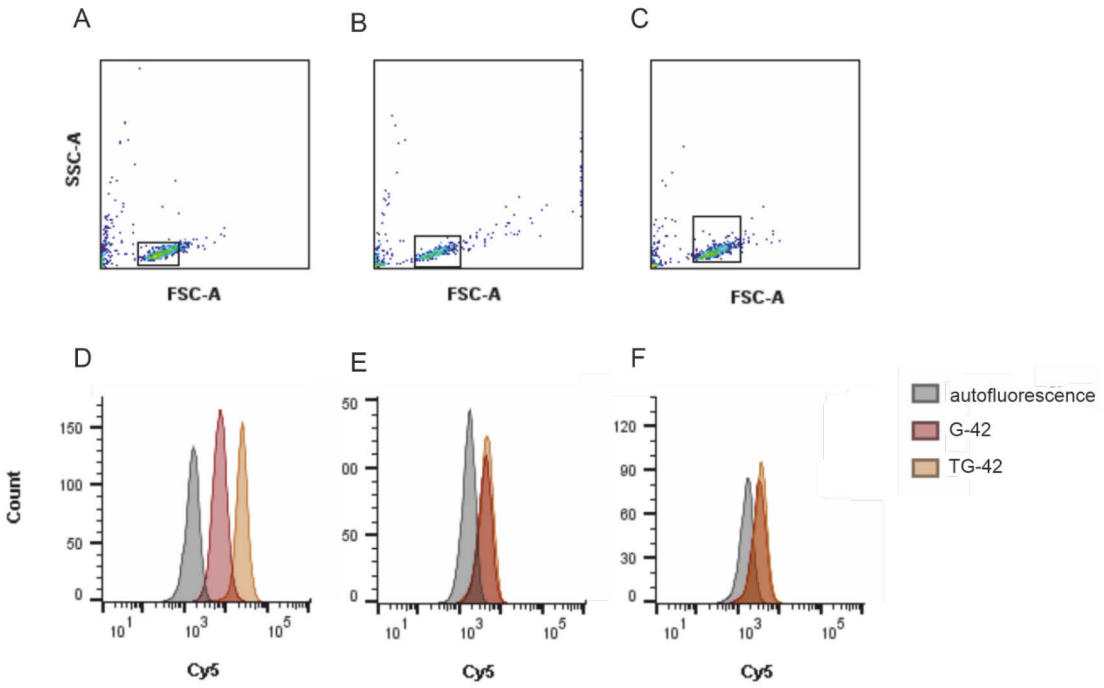

Figure 35. Example of gating strategy A)langerin$^+$, B) wild type, C) DC-SIGN$^+$ Raji cells; Example of histograms Raji cells (grey), Raji cells + G-42-Cy5 (red), and Raji cells + TG-42-Cy5 (orange) D) langerin$^+$, E) wild type, F) DC-SIGN$^+$.(Method I)

6.5.3.3 Liposomal binding assay

This assay was conducted and evaluated by Mareike Rentzsch (Rademacher group, MPIKG) as previously described.[47, 60] 50.000 cells per well were plated in 100 µl ice-cold full growth medium in a 96-well round bottom plate. Liposomes were added to a final total lipid concentration of 16 µM and incubated for 1 h on ice. After washing and resuspension in full growth medium, liposomal binding was evaluated on an Attune NxT Flow Cytometer (Life Technologies) by detecting the co-formulated dye Alexa647 with a 638 nm laser and 670/14 filter set analyzed in FlowJo.

6.5.4 Competitive Cell Assay

6.5.4.1 Assay with constructs with DNA overlap.

This assay was conducted by Felix Fuchsberger and me and evaluated by myself. 50,000 Raji cells (12.5 µl cell media, 4 % DMSO) were added to the 96 well microtiter plates (Nunc). To monitor inhibition, a serial dilution of ligands, dissolved in HBBS (4% DMSO), and FITC-dextran (2000kDa, 0.025 mg/mL) were added to the cells to a total volume 45 µl. The cells and constructs were incubated for 60 min at 4° C and subsequently centrifuged at 500 g for 3 min.

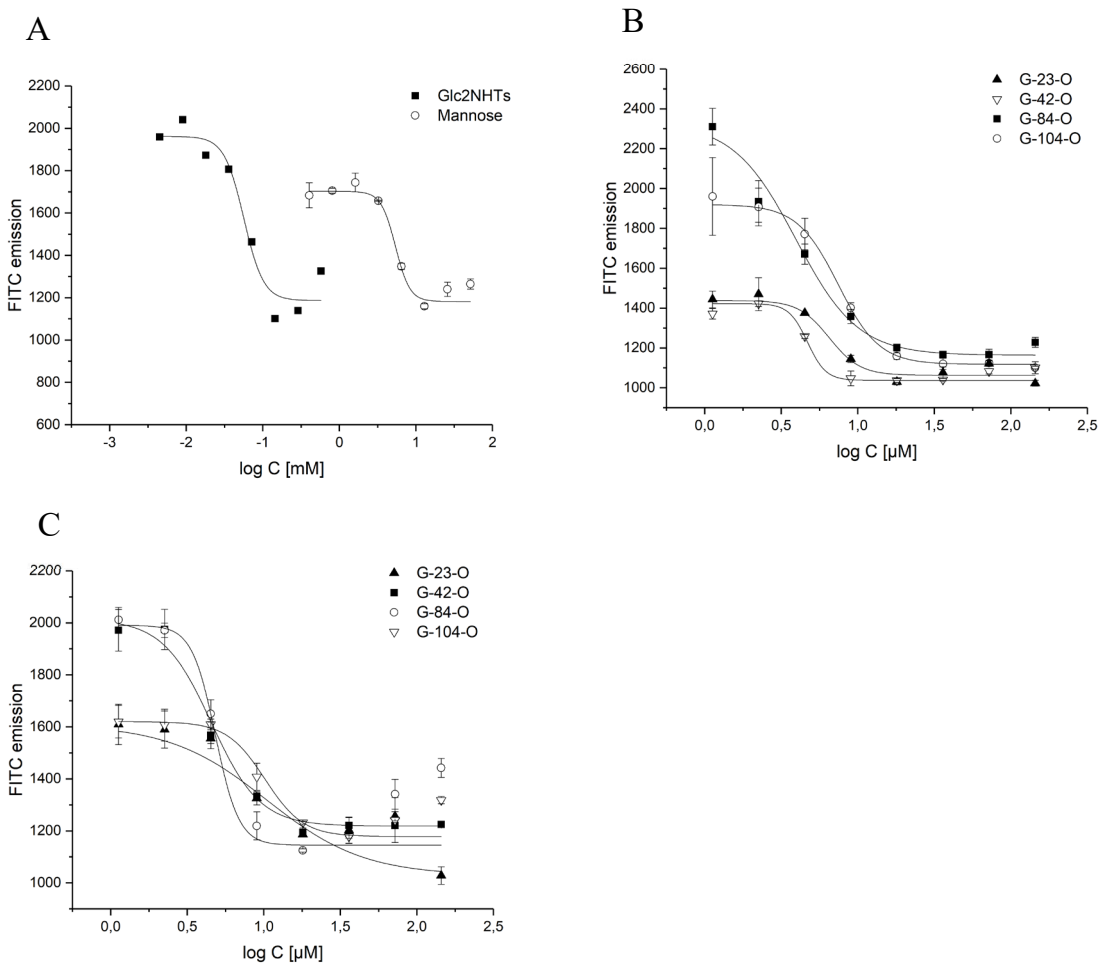

Figure 36 Competitive Cell Assay: Concentration dependent inhibition of the langerin expressing Raji cells by A) Mono-ligands Glc2NHTs **72** and mannose **33** B) Glc2NHTs-PNA-DNA duplexes (G-23-O, 42-O, 84-O, 104-O) Replicate 2 C) Glc2NHTs-PNA-DNA duplexes (G-23-O, 42-O, 84-O, 104-O) Replicate 3. Errors are the SD of technical triplicates

Cells were aspirated and resuspended in cell media before adding 4 % PFA for cell fixation. The cells were resuspended in fresh cell media and evaluated by flow

cytometry on an Attune Nxt Flow Cytometer equipped with an autosampler (Life Technologies) by detecting the conjugated dye FITC. The Mean Fluorescent Intensity (MFI) of 10,000 cells per well was measured. The MFI was plotted against the ligand concentrations. Each data point represents the mean value (SEM) of 3 measurements. The IC_{50} values were calculated via a dose response fitting procedure with Origin.

6.5.4.2 Assay with constructs without DNA overlap

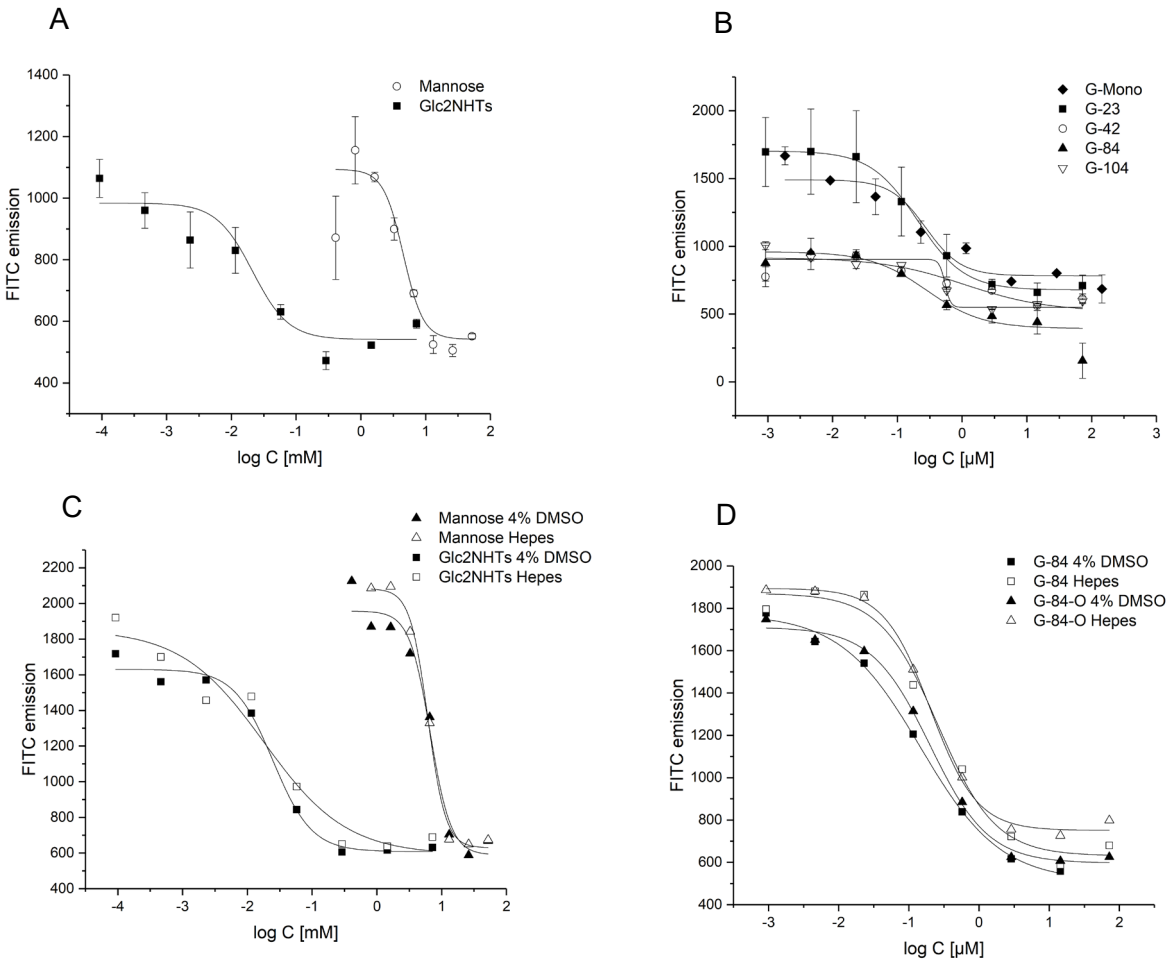

Figure 37 Competitive Cell Assay: Concentration dependent inhibition of the langerin expressing Raji cells by A) Mono-ligands Glc2NHTs **72** and mannose **33** B) Glc2NHTs-PNA-DNA duplexes (G-23, 42, 84, 104) C/D) Comparison of mannose and G-84 at different conditions. Errors are the SD of technical triplicates. Errors are from the SD of technical triplicates.

This assay was conducted by Felix Fuchsberger and evaluated by myself. 50,000 Raji cells (12.5 µl cell media) were added to the 96 well microtiter plates (Nunc). To monitor inhibition, a serial dilution of ligands, dissolved in 32.5 µl buffer (10 mM HEPES, 150 mM NaCl, 3 mM EDTA, pH 7.4), and FITC-dextran (2000kDa, 0.025 mg/mL) were added to the cells to a total volume 45 µl.

The cells and constructs were incubated for 60 min at 4° C and subsequently centrifuged at 500 g for 3 min. The Mean Fluorescent Intensity (MFI) of 10,000 cells per well was measured. The MFI was plotted against the ligand concentrations. Each data point represents the mean value (SEM) of 3 measurements. The IC_{50} values were calculated via a dose response fitting procedure with Origin.

.

7 List of Abbreviations

DNA (A, C, G, T) and PNA (a, c, g, t) nucleotides are noted by their common one letter code abbreviations.

Ac	Acetyl
Boc	*Tert*-butyloxycarbonyl
Bhoc	Benzhydryloxycarbonyl
BSA	*Bovine serum albumin*
Cbz	Carboxybenzyl
C_{eff}	Effective concentration
ConA	Concanavalin A
CTL	C-type lectin
CRD	Carbohydrate recognition domain
Cy5	Cyanine 5
D	Aspartate
DC	Dendritic cell
DCM	Dichloromethane
DC-SIGN	Dendritic Cell-Specific Intercellular adhesion molecule-3-Grabbing Non-integrin
DMF	Dimethylformamide
DMTST	Dimethyl(methylthio)sulfoniumtri-fluormethansulfonate
DNA	Deoxyribonucleic acid
ECD	Extracellular domain
EDT	1,2-Ethanedithiol
Ella	Enzyme linked lectin assay
EM	Effective molarity
F	Phenylalanine
Fmoc	Fluorenylmethoxycarbonyl
Gal	Galactose
Glc	Glucose
GlcNAc	N-Acetylglucosamine
Glc2NHTs	Tosylated glucosamine
Gp120	Glycoprotein 120
HATU	O-N, N, N′, N′-tetramethyluronium-hexafluorphosphat
HCTU	(2-(6-Chlor-1H-benzotriazol-1-yl)-1,1,3,3-tetramethylaminium-hexafluorophosphat)
HoBt	1-Hydroxybenzotriazol
HIV	Human immunodeficiency virus
HPLC	High pressure liquid chromatographie
K	Lysine

Man	Mannose
ManNAc	N-Acetylmannosamine
MFI	Mean fluorescence intensity
MPIKG	Max Planck Insitut für Kolloid- und Grenzflächenforschung
NHS	N-Hydroxysuccinimid
NMM	N-Methyl morpholine
nL	No ligand
NMP	N-Methyl-2-pyrrolidone
NMR	Nuclear magnetic resonance
P	Proline
PNA	Peptide nucleic acid
PyBop	Benzotriazol-1-yl-oxytripyrrolidinophosphonium-hexafluorophosphat
RU	Response unit
SPR	Surface Plasmon resonance
TCEP	tris(2-carboxyethyl)phosphine
TFA	Trifluoro acetic acid
TIS	Triisopropyl silan
THF	Tetra hydro furan
TLC	Thin layour chromatography
T_M	Melting temperature
Trt	Trityl
Ts	Tosyl
UV	Ultra violet
Z	Carboxybenzyl

8 References

1. Menchise, V.; De Simone, G.; Tedeschi, T.; Corradini, R.; Sforza, S.; Marchelli, R.; Capasso, D.; Saviano, M.; Pedone, C., *PNAS* **2003,** *100* (21), 12021.
2. Lees, W. J.; Spaltenstein, A.; Kingery-Wood, J. E.; Whitesides, G. M., *J. Med. Chem.* **1994,** *37* (20), 3419-3433.
3. Kingery-Wood, J. E.; Williams, K. W.; Sigal, G. B.; Whitesides, G. M., *J. Am. Chem. Soc.* **1992,** *114* (18), 7303-7305.
4. Weissleder, R.; Kelly, K.; Sun, E. Y.; Shtatland, T.; Josephson, L., *Nat. Biotechnol.* **2005,** *23* (11), 1418-23.
5. Gu, L.; Elkin, T.; Jiang, X.; Li, H.; Lin, Y.; Qu, L.; Tzeng, T.-R. J.; Joseph, R.; Sun, Y.-P., *ChemComm* **2005,** (7), 874-876.
6. Chen, Y.; Star, A.; Vidal, S., *Chem. Soc. Rev.* **2013,** *42* (11), 4532-42.
7. Roy, R.; Zanini, D.; Meunier, S. J.; Romanowska, A., *J. Chem. Soc. Chem. Comm.* **1993,** (24), 1869-1872.
8. Sansone, F.; Casnati, A., *Chem. Soc. Rev.* **2013,** *42* (11), 4623-39.
9. Kieburg, C.; Dubber, M.; Lindhorst, T. K., *Synlett* **1997,** *12* (12), 1447-1449.
10. Martinez, A.; Ortiz Mellet, C.; Garcia Fernandez, J. M., *Chem. Soc. Rev.* **2013,** *42* (11), 4746-73.
11. Lee, R. T.; Lee, Y. C., *Glycoconj.J.* **1987,** *4* (4), 317-328.
12. Sprengard, U.; Kretzschmar, G.; Bartnik, E.; Hüls, C.; Kunz, H., *Angew. Chem. Int. Ed.* **1995,** *34* (9), 990-993.
13. Diezmann, F.; Seitz, O., *Chem. Soc. Rev.* **2011,** *40* (12), 5789-801.
14. Lu, Y.; Weers, B.; Stellwagen, N. C., *Biopolymers* **2002,** *61* (4), 261-275.
15. Scheibe, C.; Bujotzek, A.; Dernedde, J.; Weber, M.; Seitz, O., *Chem. Sci.* **2011,** *2* (4).
16. Scheibe, C.; Wedepohl, S.; Riese, S. B.; Dernedde, J.; Seitz, O., *Chembiochem* **2013,** *14* (2), 236-50.
17. Bandlow, V.; Liese, S.; Lauster, D.; Ludwig, K.; Netz, R. R.; Herrmann, A.; Seitz, O., *J. Am. Chem. Soc.* **2017,** *139* (45), 16389-16397.
18. Abendroth, F.; Bujotzek, A.; Shan, M.; Haag, R.; Weber, M.; Seitz, O., *Angew. Chem. Int. Ed.* **2011,** *50* (37), 8592-6.
19. Marczynke, M.; Groger, K.; Seitz, O., *Bioconjug. Chem.* **2017,** *28* (9), 2384-2392.
20. Diezmann, F.; von Kleist, L.; Haucke, V.; Seitz, O., *Org. Biomol. Chem.* **2015,** *13* (29), 8008-15.
21. Eberhard, H.; Diezmann, F.; Seitz, O., *Angew. Chem. Int. Ed.* **2011,** *50* (18), 4146-50.
22. Stoitzner, P.; Sparber, F.; Tripp, C. H., *Immunol. Cell. Biol.* **2010,** *88* (4), 431-7.
23. Bhatia, S.; Camacho, L. C.; Haag, R., *J. Am. Chem. Soc.* **2016,** *138* (28), 8654-66.
24. Pieters, R. J., *Org. Biomol. Chem.* **2009,** *7* (10), 2013-25.
25. Mammen, M.; Choi, S.-K.; Whitesides, G. M., *Angew. Chem. Int. Ed.* **1998,** *37* (20), 2754-2794.

26. Fasting, C.; Schalley, C. A.; Weber, M.; Seitz, O.; Hecht, S.; Koksch, B.; Dernedde, J.; Graf, C.; Knapp, E. W.; Haag, R., *Angew. Chem. Int. Ed.* **2012,** *51* (42), 10472-98.
27. Ciaccio, C.; Coletta, A.; De Sanctis, G.; Marini, S.; Coletta, M., *IUBMB Life* **2008,** *60* (2), 112-23.
28. Karulin, A. Y.; Dzantiev, B. B., *Mol. Immunol.* **1990,** *27* (10), 965-971.
29. Kitov, P. I.; Bundle, D. R., *J. Am. Chem. Soc.* **2003,** *125* (52), 16271-16284.
30. Weber, M.; Bujotzek, A.; Haag, R., *J. Chem. Phys.* **2012,** *137* (5), 054111.
31. Liese, S.; Netz, R. R., *Beilstein J. Org. Chem.* **2015,** *11*, 804-16.
32. Liese, S.; Netz, R. R., *ACS Nano* **2018,** *12* (5), 4140-4147.
33. Krishnamurthy, V. M.; Semetey, V.; Bracher, P. J.; Shen, N.; Whitesides, G. M., *J. Am. Chem. Soc.* **2007,** *129* (5), 1312-1320.
34. von Krbek, L. K.; Achazi, A. J.; Schoder, S.; Gaedke, M.; Biberger, T.; Paulus, B.; Schalley, C. A., *Chem. Eur. J.* **2017,** *23* (12), 2877-2883.
35. Cecioni, S.; Imberty, A.; Vidal, S., *Chem. Rev.* **2015,** *115* (1), 525-61.
36. Dubel, N.; Liese, S.; Scherz, F.; Seitz, O., *Angew. Chem. Int. Ed.* **2019,** *58* (3), 907-911.
37. Rohse, P.; Wittmann, V., *Chem. Eur. J.* **2016,** *22* (28), 9724-33.
38. Gestwicki, J. E.; Cairo, C. W.; Strong, L. E.; Oetjen, K. A.; Kiessling, L. L., *J. Am. Chem. Soc.* **2002,** *124* (50), 14922-14933.
39. de Bakker, B. I.; de Lange, F.; Cambi, A.; Korterik, J. P.; van Dijk, E. M.; van Hulst, N. F.; Figdor, C. G.; Garcia-Parajo, M. F., *Chemphyschem* **2007,** *8* (10), 1473-80.
40. Mahajan, A.; Barua, D.; Cutler, P.; Lidke, D. S.; Espinoza, F. A.; Pehlke, C.; Grattan, R.; Kawakami, Y.; Tung, C. S.; Bradbury, A. R.; Hlavacek, W. S.; Wilson, B. S., *ACS Chem. Biol.* **2014,** *9* (7), 1508-19.
41. Mangold, S. L.; Cloninger, M. J., *Org. Biomol. Chem.* **2006,** *4* (12), 2458-65.
42. Vonnemann, J.; Liese, S.; Kuehne, C.; Ludwig, K.; Dernedde, J.; Bottcher, C.; Netz, R. R.; Haag, R., *J. Am. Chem. Soc.* **2015,** *137* (7), 2572-9.
43. van der Vlist, M.; Geijtenbeek, T. B., *Immunol. Cell. Biol.* **2010,** *88* (4), 410-5.
44. Drickamer, K.; Taylor, M. E., *Curr. Opin. Struct. Biol.* **2015,** *34*, 26-34.
45. Brown, G. D.; Willment, J. A.; Whitehead, L., *Nat. Rev. Immunol.* **2018,** *18* (6), 374-389.
46. Taylor, M. E.; Drickamer, K., In *Glycoscience: Biology and Medicine*, 2015; pp 1015-1020.
47. Wamhoff, E. C.; Schulze, J.; Bellmann, L.; Rentzsch, M.; Bachem, G.; Fuchsberger, F. F.; Rademacher, J.; Hermann, M.; Del Frari, B.; van Dalen, R.; Hartmann, D.; van Sorge, N. M.; Seitz, O.; Stoitzner, P.; Rademacher, C., *ACS Cent. Sci.* **2019,** *5* (5), 808-820.
48. Figdor, C. G.; van Kooyk, Y.; Adema, G. J., *Nat. Rev. Immunol.* **2002,** *2*, 77.
49. Romani, N.; Thurnher, M.; Idoyaga, J.; Steinman, R. M.; Flacher, V., *Immunol. Cell. Biol.* **2010,** *88* (4), 424-30.
50. Stambach, N. S.; Taylor, M. E., *Glycobiology* **2003,** *13* (5), 401-10.
51. Feinberg, H.; Powlesland, A. S.; Taylor, M. E.; Weis, W. I., *J. Biol. Chem.* **2010,** *285* (17), 13285-93.
52. Feinberg, H.; Taylor, M. E.; Razi, N.; McBride, R.; Knirel, Y. A.; Graham, S. A.; Drickamer, K.; Weis, W. I., *J. Mol. Biol.* **2011,** *405* (4), 1027-39.
53. Chatwell, L.; Holla, A.; Kaufer, B. B.; Skerra, A., *Mol. Immunol.* **2008,** *45* (7), 1981-94.
54. Holla, A.; Skerra, A., *Protein Eng. Des. Sel.* **2011,** *24* (9), 659-69.

55. Munoz-Garcia, J. C.; Chabrol, E.; Vives, R. R.; Thomas, A.; de Paz, J. L.; Rojo, J.; Imberty, A.; Fieschi, F.; Nieto, P. M.; Angulo, J., *J. Am. Chem. Soc.* **2015,** *137* (12), 4100-10.
56. Hanske, J.; Wawrzinek, R.; Geissner, A.; Wamhoff, E. C.; Sellrie, K.; Schmidt, H.; Seeberger, P. H.; Rademacher, C., *Chembiochem* **2017,** *18* (13), 1183-1187.
57. Steinman, R. M., *Annu. Rev. Immunol.* **2012,** *30*, 1-22.
58. Fehres, C. M.; Duinkerken, S.; Bruijns, S. C.; Kalay, H.; van Vliet, S. J.; Ambrosini, M.; de Gruijl, T. D.; Unger, W. W.; Garcia-Vallejo, J. J.; van Kooyk, Y., *Cell. Mol. Immunol.* **2017,** *14* (4), 360-370.
59. Fehres, C. M.; van Beelen, A. J.; Bruijns, S. C. M.; Ambrosini, M.; Kalay, H.; Bloois, L. V.; Unger, W. W. J.; Garcia-Vallejo, J. J.; Storm, G.; de Gruijl, T. D.; Kooyk, Y. V., *J. Invest. Dermatol.* **2015,** *135* (9), 2228-2236.
60. Schulze, J.; Rentzsch, M.; Kim, D.; Bellmann, L.; Stoitzner, P.; Rademacher, C., *Biochemistry* **2019,** *58* (21), 2576-2580.
61. Ota, F.; Hirayama, T.; Kizuka, Y.; Yamaguchi, Y.; Fujinawa, R.; Nagata, M.; Ismanto, H. S.; Lepenies, B.; Aretz, J.; Rademacher, C.; Seeberger, P. H.; Angata, T.; Kitazume, S.; Yoshida, K.; Betsuyaku, T.; Kida, K.; Yamasaki, S.; Taniguchi, N., *Biochim. Biophys. Acta* **2018,** *1862* (7), 1592-1601.
62. Feinberg, H.; Guo, Y.; Mitchell, D. A.; Drickamer, K.; Weis, W. I., *J. Biol. Chem.* **2005,** *280* (2), 1327-35.
63. Mitchell, D. A.; Fadden, A. J.; Drickamer, K., *J. Biol. Chem.* **2001,** *276* (31), 28939-45.
64. de Witte, L.; Nabatov, A.; Pion, M.; Fluitsma, D.; de Jong, M. A.; de Gruijl, T.; Piguet, V.; van Kooyk, Y.; Geijtenbeek, T. B., *Nat. Med.* **2007,** *13* (3), 367-71.
65. Porkolab, V.; Chabrol, E.; Varga, N.; Ordanini, S.; Sutkeviciu Te, I.; Thepaut, M.; Garcia-Jimenez, M. J.; Girard, E.; Nieto, P. M.; Bernardi, A.; Fieschi, F., *ACS Chem. Biol.* **2018,** *13* (3), 600-608.
66. Andreini, M.; Doknic, D.; Sutkeviciute, I.; Reina, J. J.; Duan, J.; Chabrol, E.; Thepaut, M.; Moroni, E.; Doro, F.; Belvisi, L.; Weiser, J.; Rojo, J.; Fieschi, F.; Bernardi, A., *Org. Biomol. Chem.* **2011,** *9* (16), 5778-86.
67. Zaric, M.; Lyubomska, O.; Poux, C.; Hanna, M. L.; McCrudden, M. T.; Malissen, B.; Ingram, R. J.; Power, U. F.; Scott, C. J.; Donnelly, R. F.; Kissenpfennig, A., *J. Invest. Dermatol.* **2015,** *135* (2), 425-434.
68. Lauster, D.; Klenk, S.; Ludwig, K.; Nojoumi, S.; Behren, S.; Adam, L.; Stadtmuller, M.; Saenger, S.; Zimmler, S.; Honzke, K.; Yao, L.; Hoffmann, U.; Bardua, M.; Hamann, A.; Witzenrath, M.; Sander, L. E.; Wolff, T.; Hocke, A. C.; Hippenstiel, S.; De Carlo, S.; Neudecker, J.; Osterrieder, K.; Budisa, N.; Netz, R. R.; Bottcher, C.; Liese, S.; Herrmann, A.; Hackenberger, C. P. R., *Nat. Nanotechnol.* **2020**.
69. Cecioni, S.; Oerthel, V.; Iehl, J.; Holler, M.; Goyard, D.; Praly, J. P.; Imberty, A.; Nierengarten, J. F.; Vidal, S., *Chem. Eur. J.* **2011,** *17* (11), 3252-61.
70. Luczkowiak, J.; Munoz, A.; Sanchez-Navarro, M.; Ribeiro-Viana, R.; Ginieis, A.; Illescas, B. M.; Martin, N.; Delgado, R.; Rojo, J., *Biomacromolecules* **2013,** *14* (2), 431-7.
71. Becer, C. R.; Gibson, M. I.; Geng, J.; Ilyas, R.; Wallis, R.; Mitchell, D. A.; Haddleton, D. M., *J. Am. Chem. Soc.* **2010,** *132* (43), 15130-15132.
72. Seitz, O., *J. Pept. Sci.* **2019,** *25* (7), e3198.

73. Wittmann, V.; Pieters, R. J., *Chem. Soc. Rev.* **2013,** *42* (10), 4492-503.
74. Tabarani, G.; Reina, J. J.; Ebel, C.; Vives, C.; Lortat-Jacob, H.; Rojo, J.; Fieschi, F., *FEBS Lett.* **2006,** *580* (10), 2402-8.
75. Martinez-Avila, O.; Hijazi, K.; Marradi, M.; Clavel, C.; Campion, C.; Kelly, C.; Penades, S., *Chem. Eur. J.* **2009,** *15* (38), 9874-88.
76. Lasala, F.; Arce, E.; Otero, J. R.; Rojo, J.; Delgado, R., *Antimicrob. Agents Chemother.* **2003,** *47* (12), 3970-2.
77. Varga, N.; Sutkeviciute, I.; Ribeiro-Viana, R.; Berzi, A.; Ramdasi, R.; Daghetti, A.; Vettoretti, G.; Amara, A.; Clerici, M.; Rojo, J.; Fieschi, F.; Bernardi, A., *Biomaterials* **2014,** *35* (13), 4175-84.
78. Neuhaus, K.; Wamhoff, E. C.; Freichel, T.; Grafmueller, A.; Rademacher, C.; Hartmann, L., *Biomacromolecules* **2019**.
79. Morbioli, I.; Porkolab, V.; Magini, A.; Casnati, A.; Fieschi, F.; Sansone, F., *Carbohydr. Res.* **2017,** *453-454*, 36-43.
80. Ordanini, S.; Varga, N.; Porkolab, V.; Thepaut, M.; Belvisi, L.; Bertaglia, A.; Palmioli, A.; Berzi, A.; Trabattoni, D.; Clerici, M.; Fieschi, F.; Bernardi, A., *Chem. Commun. (Camb)* **2015,** *51* (18), 3816-9.
81. Artner, L. M.; Merkel, L.; Bohlke, N.; Beceren-Braun, F.; Weise, C.; Dernedde, J.; Budisa, N.; Hackenberger, C. P., *Chem. Commun. (Camb)* **2012,** *48* (4), 522-4.
82. Eriksson, M.; Nielsen, P. E., *Nat. Struct. Biol* **1996,** *3* (5), 410-413.
83. Rasmussen, H.; Kastrup, J. S.; Nielsen, J. N.; Nielsen, J. M.; Nielsen, P. E., *Nat. Struct. Biol* **1997,** *4* (2), 98-101.
84. Zhan, Y.; Zocchi, G., *EPL Europhys. Lett.* **2017,** *119* (4).
85. Manicardi, A.; Corradini, R., *Artif. DNA PNA XNA* **2014,** *5* (3), e1131801.
86. Dragulescu-Andrasi, A.; Rapireddy, S.; Frezza, B. M.; Gayathri, C.; Gil, R. R.; Ly, D. H., *J. Am. Chem. Soc.* **2006,** *128* (31), 10258-10267.
87. Matsuura, K.; Hibino, M.; Ikeda, T.; Yamada, Y.; Kobayashi, K., *Chem. Eur. J.* **2004,** *10* (2), 352-9.
88. Gorska, K.; Huang, K. T.; Chaloin, O.; Winssinger, N., *Angew. Chem. Int. Ed.* **2009,** *48* (41), 7695-700.
89. Matsui, M.; Ebara, Y., *Bioorg. Med. Chem. Lett.* **2012,** *22* (19), 6139-43.
90. Yamabe, M.; Kaihatsu, K.; Ebara, Y., *Bioconjug. Chem.* **2018,** *29* (5), 1490-1494.
91. Machida, T.; Novoa, A.; Gillon, E.; Zheng, S.; Claudinon, J.; Eierhoff, T.; Imberty, A.; Romer, W.; Winssinger, N., *Angew. Chem. Int. Ed.* **2017,** *56* (24), 6762-6766.
92. Wamhoff, E.-C. Glycomimetic Langerin Ligands for Langerhans Cell Targeting. 2017.
93. Wamhoff, E. C.; Hanske, J.; Schnirch, L.; Aretz, J.; Grube, M.; Varon Silva, D.; Rademacher, C., *ACS Chem. Biol.* **2016,** *11* (9), 2407-13.
94. Garber, K. C.; Wangkanont, K.; Carlson, E. E.; Kiessling, L. L., *Chem. Commun. (Camb)* **2010,** *46* (36), 6747-9.
95. Luczkowiak, J.; Sattin, S.; Sutkeviciute, I.; Reina, J. J.; Sanchez-Navarro, M.; Thepaut, M.; Martinez-Prats, L.; Daghetti, A.; Fieschi, F.; Delgado, R.; Bernardi, A.; Rojo, J., *Bioconjug. Chem.* **2011,** *22* (7), 1354-65.

96. Sutkeviciute, I.; Thepaut, M.; Sattin, S.; Berzi, A.; McGeagh, J.; Grudinin, S.; Weiser, J.; Le Roy, A.; Reina, J. J.; Rojo, J.; Clerici, M.; Bernardi, A.; Ebel, C.; Fieschi, F., *ACS Chem. Biol.* **2014,** *9* (6), 1377-85.
97. Bandlow, V.; Lauster, D.; Ludwig, K.; Hilsch, M.; Reiter-Scherer, V.; Rabe, J. P.; Bottcher, C.; Herrmann, A.; Seitz, O., *Chembiochem* **2019,** *20* (2), 159-165.
98. Sharma, C.; Awasthi, S. K., *Chem. Biol. Drug Des.* **2017,** *89* (1), 16-37.
99. Tomasic, T.; Hajsek, D.; Svajger, U.; Luzar, J.; Obermajer, N.; Petit-Haertlein, I.; Fieschi, F.; Anderluh, M., *Eur. J. Med. Chem.* **2014,** *75*, 308-26.
100. Scheibe, C. Multivalente Präsentation von Kohlenhydraten via PNA•DNA-Hybridisierung. Doctoral Dissertation, Humboldt Universität zu Berlin, 2012.
101. Merkel, M.; Peewasan, K.; Arndt, S.; Ploschik, D.; Wagenknecht, H. A., *Chembiochem* **2015,** *16* (11), 1541-53.
102. Jensen, K. K.; Ørum, H.; Nielsen, P. E.; Nordén, B., *Biochemistry* **1997,** *36* (16), 5072-5077.
103. Aretz, J.; Wamhoff, E. C.; Hanske, J.; Heymann, D.; Rademacher, C., *Front. Immunol.* **2014,** *5*, 323.
104. Ponader, D.; Maffre, P.; Aretz, J.; Pussak, D.; Ninnemann, N. M.; Schmidt, S.; Seeberger, P. H.; Rademacher, C.; Nienhaus, G. U.; Hartmann, L., *J. Am. Chem. Soc.* **2014,** *136* (5), 2008-16.
105. Wamhoff, E. C. Glycomimetic Langerin Ligands for Langerhans Cell Targeting. Doctoral Dissertation, Freie Universität, Berlin, Germany, 2017.
106. Duinkerken, S.; Horrevorts, S. K.; Kalay, H.; Ambrosini, M.; Rutte, L.; de Gruijl, T. D.; Garcia-Vallejo, J. J.; van Kooyk, Y., *Theranostics* **2019,** *9* (20), 5797-5809.
107. Lepenies, B.; Lee, J.; Sonkaria, S., *Adv. Drug Deliv. Rev.* **2013,** *65* (9), 1271-81.
108. Micheel, F.; Michaelis, E., *Chem. Ber.* **1958,** *91* (1), 188-194.
109. Bergmann, M.; Zervas, L., *Ber. Dtsch. Chem. Ges.* **1931,** *64* (5), 975-980.
110. Kyas, A.; Feigel, M., *Helv. Chim. Acta* **2005,** *88* (9), 2375-2396.
111. Ellervik, U.; Magnusson, G., *Carbohydr. Res.* **1996,** *280* (2), 251-260.
112. Martinez-Bailen, M.; Jimenez-Ortega, E.; Carmona, A. T.; Robina, I.; Sanz-Aparicio, J.; Talens-Perales, D.; Polaina, J.; Matassini, C.; Cardona, F.; Moreno-Vargas, A. J., *Bioorg. Chem.* **2019,** *89*, 103026.
113. Hasegawa, T.; Numata, M.; Okumura, S.; Kimura, T.; Sakurai, K.; Shinkai, S., *Org. Biomol. Chem.* **2007,** *5* (15), 2404-12.
114. Bukowski, R.; Morris, Laura M.; Woods, Robert J.; Weimar, T., *Eur. J. Org. Chem.* **2001,** *2001* (14), 2697-2705.
115. Hayes, W.; Osborn, H. M. I.; Osborne, S. D.; Rastall, R. A.; Romagnoli, B., *Tetrahedron* **2003,** *59* (40), 7983-7996.
116. Lindhorst, T. K.; Kötter, S.; Krallmann-Wenzel, U.; Ehlers, S., *J. Chem. Soc. Perkin Trans. 1* **2001,** (8), 823-831.
117. Martin, A. L.; Li, B.; Gillies, E. R., *J. Am. Chem. Soc.* **2009,** *131* (2), 734-741.
118. Maunier, V.; Boullanger, P.; Lafont, D.; Chevalier, Y., *Carbohydr. Res.* **1997,** *299* (1), 49-57.
119. Yu, H.; Chen, X., *Org. Lett.* **2006,** *8* (11), 2393-2396.
120. Combemale, S.; Assam-Evoung, J. N.; Houaidji, S.; Bibi, R.; Barragan-Montero, V., *Molecules* **2014,** *19* (1), 1120-49.

121. Han, Z.; Pinkner, J. S.; Ford, B.; Chorell, E.; Crowley, J. M.; Cusumano, C. K.; Campbell, S.; Henderson, J. P.; Hultgren, S. J.; Janetka, J. W., *J. Med. Chem.* **2012,** *55* (8), 3945-59.
122. Englund, E. A.; Appella, D. H., *Org. Lett.* **2005,** *7* (16), 3465-3467.
123. Totsingan, F.; Tedeschi, T.; Sforza, S.; Corradini, R.; Marchelli, R., *Chirality* **2009,** *21* (1), 245-253.
124. Carr, H. Y.; Purcell, E. M., *Phys. Rev.* **1954,** *94* (3), 630-638.
125. Meiboom, S.; Gill, D., *Rev. Sci. Instrum.* **1958,** *29* (8), 688-691.

9 Appendix

NMR spectra of ligands

2-Acetamidoethyl- α-D-mannoside (74)

^{1}H-NMR (400 MHz, D_2O)

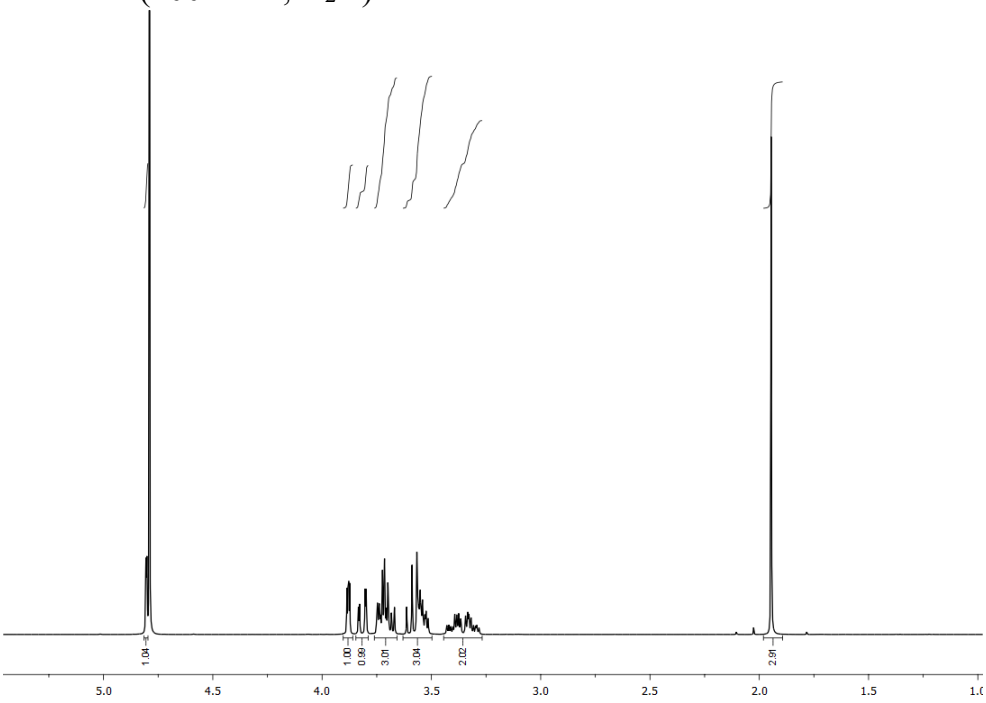

^{13}C-NMR (100.6 MHz, D_2O)

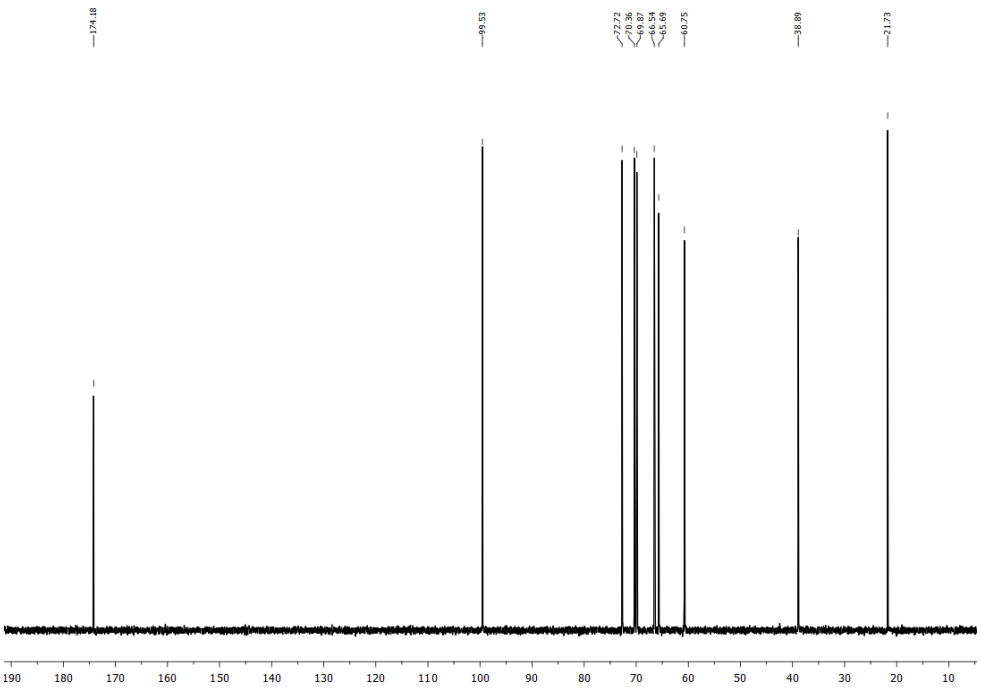

TriMan (40)

^{1}H-NMR (500 MHz, MeOD)

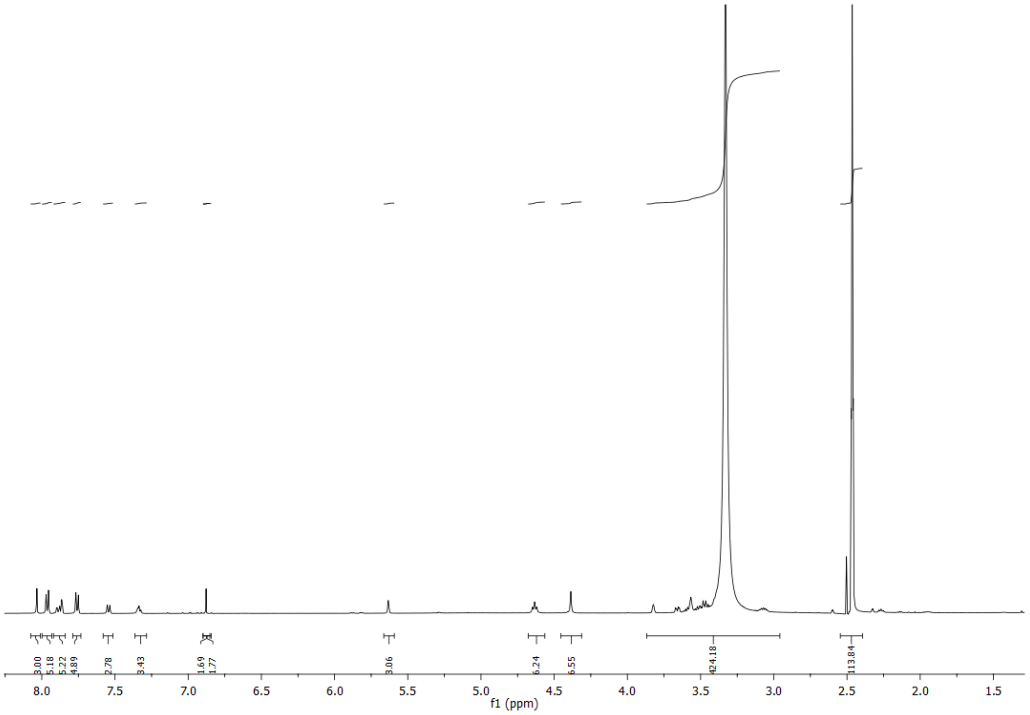

^{13}C-NMR (100.6 MHz, MeOD)

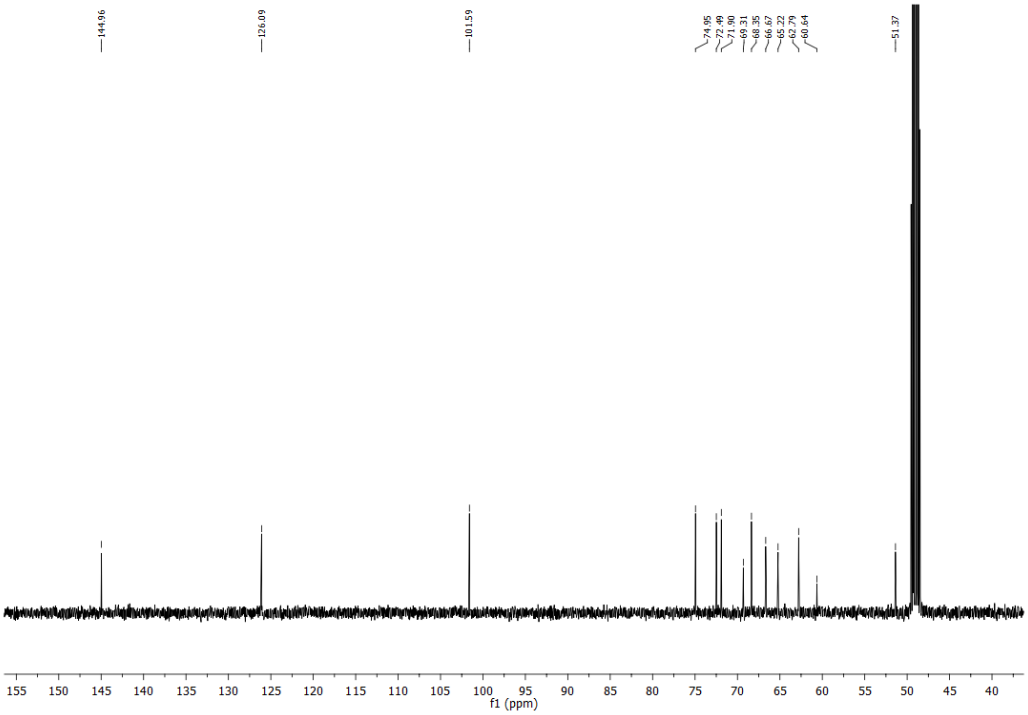

1-(2-Trifluoromethyl-4-carboxylate-phenyl) phenoxy -6-(2-azido)ethylsulfonamido -mannoside (49)

^{1}H-NMR (500 MHz, MeOD)

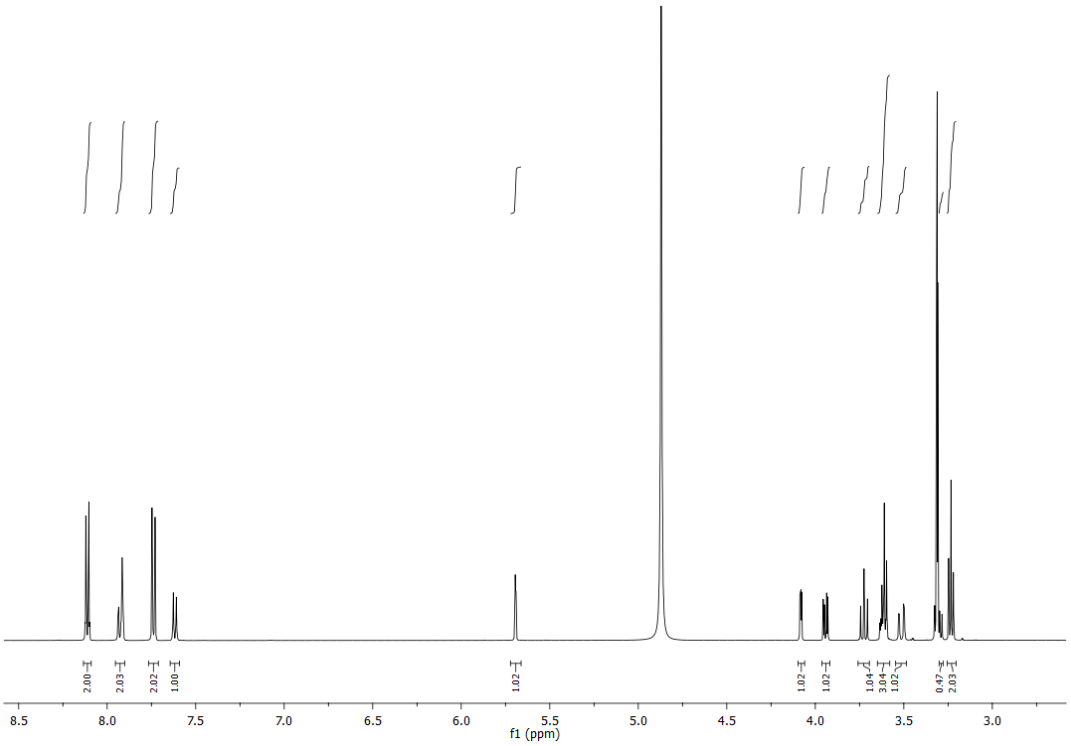

^{13}C-NMR (100.6 MHz, D_2O)

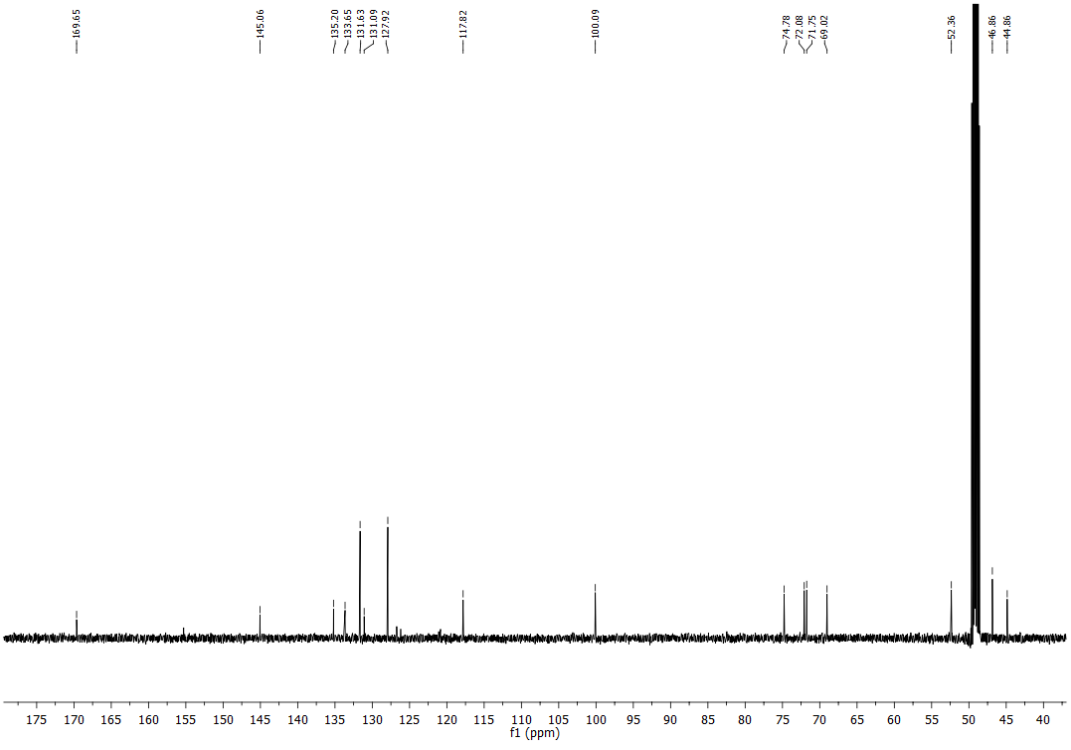

Maleimido-TriBiPhMan (51)

^{1}H-NMR (500 MHz, DMSO)

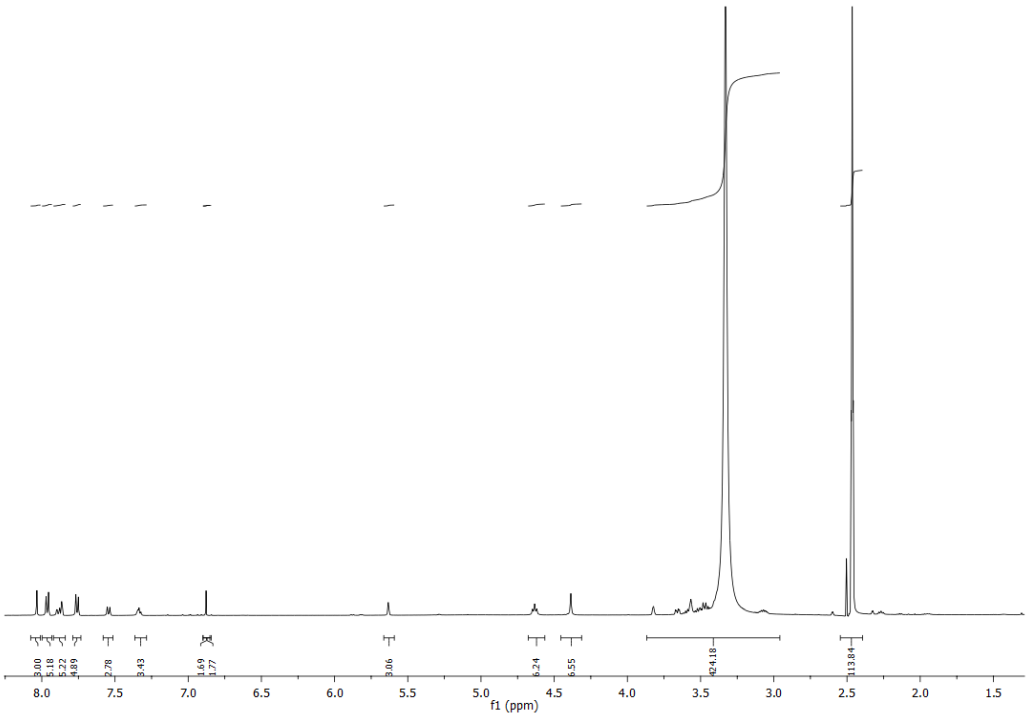

TriGlc2NHTs (31)

^{1}H-NMR (500 MHz, MeOD)

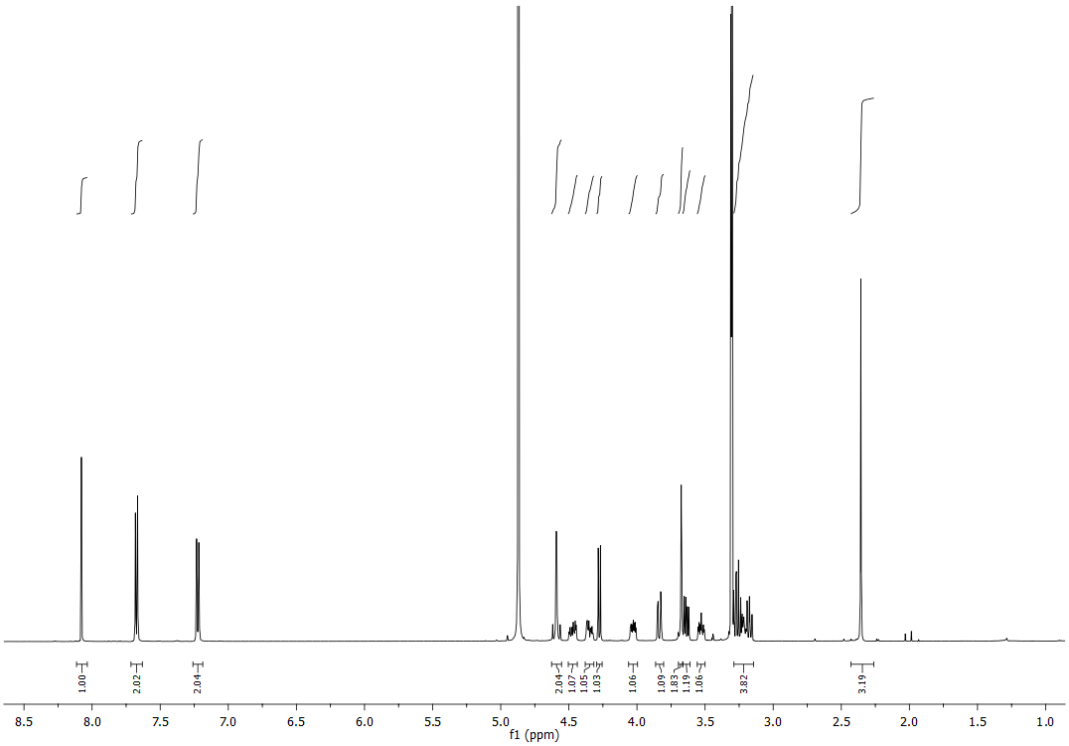

^{13}C-NMR (100.6 MHz, D_2O)

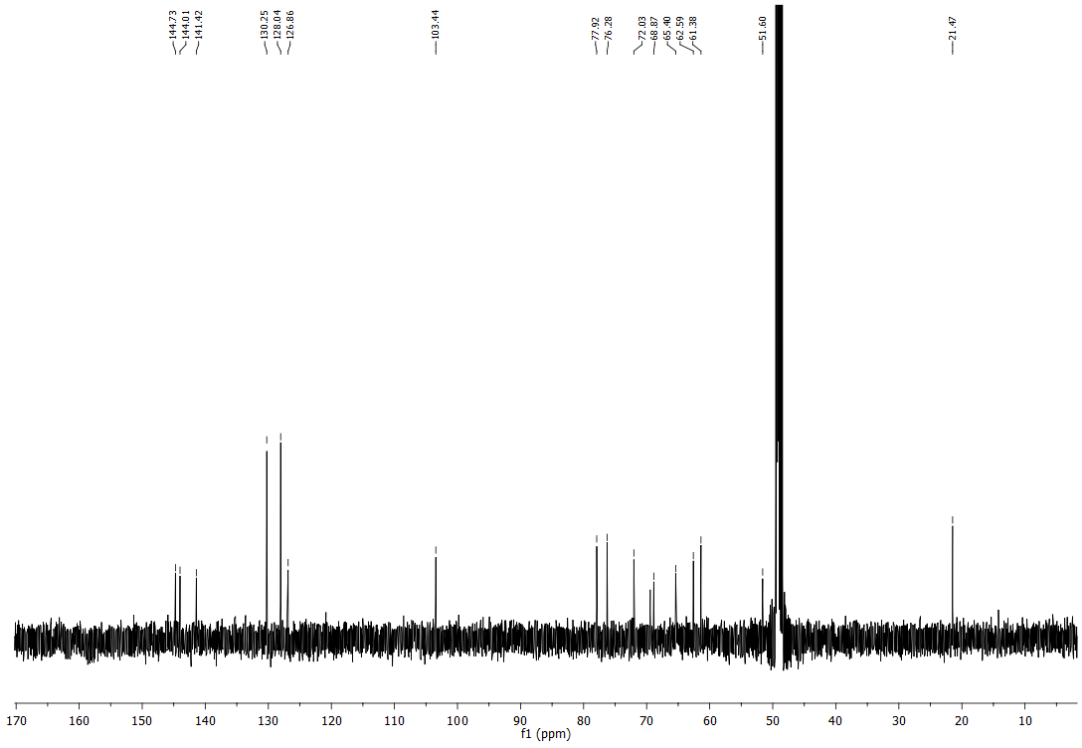

2'-Acetamidoethyl 2-deoxy-2-(*p*-toluenesulfonylamido) - β-D –glucoside (75)

^{1}H-NMR (400 MHz, D_20)

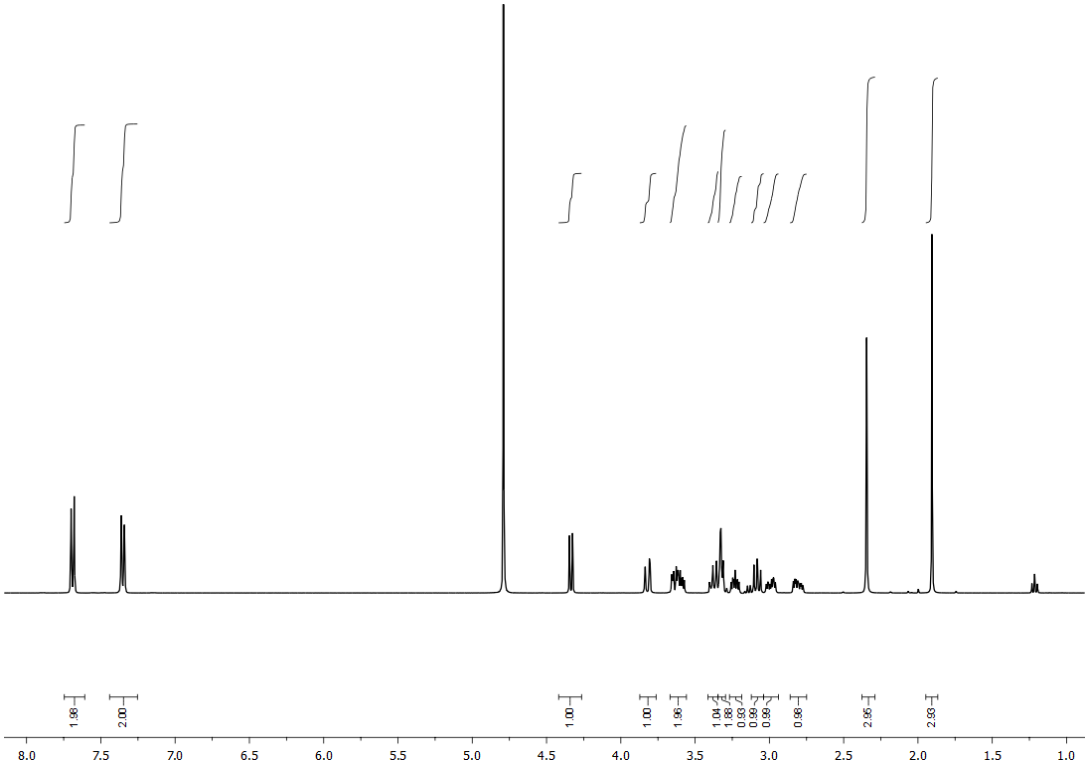

^{13}C-NMR (100.6 MHz, D_2O)

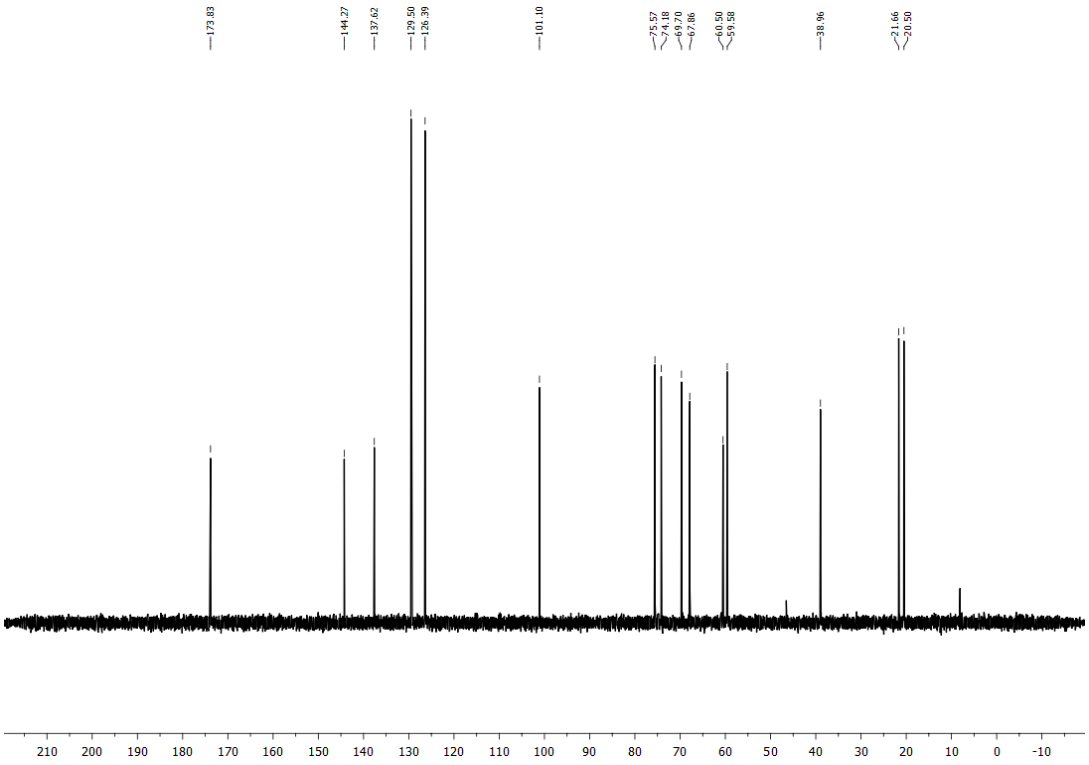

Selbständigkeitserklärung

„Ich erkläre, dass ich die Dissertation selbständig und nur unter Verwendung der von mir gemäß § 7 Abs. 3 der Promotionsordnung der Mathematisch-Naturwissenschaftlichen Fakultät, veröffentlicht im Amtlichen Mitteilungsblatt der Humboldt-Universität zu Berlin Nr. 42/2018 am 11.07.2018 angegebenen Hilfsmittel angefertigt habe."

_____

Datum, Unterschrift